Exohedral Functionalization and Applications of the Trimetallic Nitride Endohedral Metallofullerenes

Erick Barton Iezzi

Dissertation submitted to the Faculty of Virginia Polytechnic Institute and State University in partial fulfillment of the requirements for the degree of

Doctor of Philosophy
in
Chemistry

Harry C. Dorn, Chair
James M. Tanko
Brian E. Hanson
Paul A. Deck
Timothy E. Long

October 14, 2003
Blacksburg, Virginia

Keywords: Metallofullerene, endohedral, functionalization, X-ray contrast, scandium nitride

Exohedral Functionalization and Applications of the Trimetallic Nitride Endohedral Metallofullerenes

Erick B. Iezzi

(ABSTRACT)

This dissertation addresses the exohedral cage functionalization and potential applications of the $Sc_3N@C_{80}$ and $Sc_3N@C_{78}$ trimetallic nitride endohedral metallofullerenes. In addition, this dissertation discusses miscellaneous research that is relevant to the aformentioned metallofullerenes and their applications, such as the discovery of a new cage isomer (D_{5h}) of $Sc_3N@C_{80}$, the synthesis of $Lu_3N@C_{80}$ as a novel X-ray contrasting agent, and the synthesis of $Sc_3{}^{15}N@C_{80}$ with $^{15}N_2$ gas.

The first derivative of $Sc_3N@C_{80}$ was synthesized by functionalizing the exterior of the cage via a [4 + 2] cycloaddition reaction with a ^{13}C-labeled intermediate. Addition occurred across the [5,6] ring-juncture of the cage to form a mono-adduct, which has a mirror plane of symmetry as observed from the time-averaged ^{13}C NMR spectrum. The structure of the mono-adduct was confirmed by X-ray crystallography. Diethyl and dibenzyl malonate adducts of $Sc_3N@C_{80}$ were synthesized, in addition to a ^{15}N-labeled terminal amine derivative. Water-soluble metallofullerenols, $Sc_3N@C_{80}(OH)_{\sim 10}(O)_{\sim 10}$, were synthesized from polyanionic intermediates.

The $Sc_3N@C_{78}$ metallofullerene was derivatized with a ^{13}C-labeled reagent to afford mono-, di- and tri-adducts. A single structural isomer of the mono-adduct was found, while several isomers of the di- and tri-adducts were observed by HPLC. ^{13}C and ^{1}H NMR data of the mono-adduct support a structure that results from addend addition to an asymmetric site on the C_{78} carbon cage.

The HPLC isolation and characterization of $Lu_3N@C_{80}$ is discussed. When irradiated with X-rays, $Lu_3N@C_{80}$ provided a small level of contrast that can only be attributed to the large atomic number (Z) of the lutetium atoms. Mixed-metal species that contains gadolinium and lutetium or holmium and lutetium could be employed as multifunctional contrasting agents for X-ray, MRI and radiopharmaceuticals, thereby eliminating the need for three separate agents.

A new cage isomer of the $Sc_3N@C_{80}$ metallofullerene was synthesized and partially isolated by HPLC. This carbon cage possesses D_{5h} symmetry, as indicated by the time-averaged six line ^{13}C NMR spectrum with a 1:2:2:1:1:1 ratio.

The internal metal-nitride cluster of $Sc_3N@C_{80}$ was synthesized with a ^{15}N-label for studying the motion(s) of the cluster (within the carbon cage) at various temperatures using ^{15}N NMR spectroscopy.

Acknowledgements

I would like to thank my Ph.D. advisor, Dr. Harry C. Dorn, for his guidance, friendship and support during my tenure as a graduate student at Virginia Tech. We met under the most unusual of circumstances (during lunch at Burger King), and I am grateful that he accepted me as a student when I was contemplating leaving Virginia Tech. I thank him for allowing me to develop a project that has enabled me to achieve publications and accolades that I never thought possible. Furthermore, I thank him for his empathy during the periods when I was extremely frustrated with my project and/or the lack of starting materials. I am glad we were able to accomplish all the goals of the project, and I hope that metallofullerene research grants him luck and prosperity.

There are several faculty members in the chemistry department that I would like to acknowledge. First of all, I thank the members of my Ph.D. committee (Dr. James Tanko, Dr. Paul Deck, Dr. Brian Hanson and Dr. Tim Long) for the help and guidance they gave over the past four years. I especially thank Dr. Tanko for his guidance with departmental policies (i.e., literature review) when there seemed to be a lack of structure in the graduate curriculum, along with the several letters of recommendation that he was kind enough to write for me over the last two years. I thank Dr. Paul Carlier for a letter of recommendation and for helping with the essay that facilitated me winning an ACS Division of Organic Chemistry Graduate Fellowship. I thank Dr. Richard Gandour for his guidance and help with the proposal section of the NIH postdoctoral fellowship that I hope to win, and I thank him for writing a letter of recommendation. In addition, I thank Dr. Alan Esker for all his helpful advice, for writing a letter of recommendation for the ACS fellowship, and for giving me a place to live during the final months of my graduate career.

I would like to thank Tom Glass in Analytical Services for help with running numerous NMR samples. Without Tom, several portions of my Ph.D. project would not have been successful. I also thank my colleague, Dr. James Duchamp (Emory and Henry College), for all his work and helpful discussions over the past few years. Jim was a great friend and basically my only lab mate at Virginia Tech.

Finally, and most importantly, I would like to thank both God and my parents. I thank God for answering my prayers and helping me through the tough times, and I hope that I am continually blessed with good fortune throughout my life. As for my parents, I could not have achieved this degree without them. They were always there for me when I needed them, and they are the most loving and caring parents that a son could have.

Table of Contents

Page

CHAPTER 1 – Introduction and Background……..……..…..……1
1.1. Historical overview……..……1
1.1.1. C_{60} and empty-cage fullerenes…….……...1
1.1.2. Endohedral metallofullerenes…….……2
1.1.2.1. Traditional metallofullerenes…….……..2
1.1.2.2. Trimetallic nitride endohedral metallofullerenes…….……3
1.2. Synthesis, isolation, purification and mechanistic formation…….……6
1.2.1. Synthesis of fullerenes and metallofullerenes……..……6
1.2.2. Extraction from soot…….……...8
1.2.3. Purification by liquid chromatography…….……...9
1.2.4. Mechanistic formation of fullerenes and metallofullerenes…….……..11
1.3. Structure and cage stability…….……...12
1.3.1. Isolated-pentagon rule (IPR)…….……12
1.3.2. Icosahedral symmetry and charge transfer……13
1.3.3. Internal motion and electrostatic potential…….……16
1.4. Organic functionalization of C_{60} and traditional metallofullerenes…….……..18
1.4.1. Reactivity of the C_{60} fullerene……...18
1.4.1.1. Hydroxylation of C_{60} ...…….……19
1.4.1.2. C_{60} anions and the addition of nucleophiles……..20
1.4.1.3. Cycloaddition reactions with C_{60} ...……...24
1.4.1.4. Radical additions to C_{60} ...……26
1.4.2. Reactivity of traditional metallofullerenes…….28
1.4.2.1. Radical addition with traditional metallofullerenes……...28
1.4.2.2. Electrophilic and nucleophilic additions……30
1.4.2.3. Hydroxylation of traditional metallofullerenes……..30
1.5. Electronic properties of traditional and trimetallic nitride metallofullerenes……31
1.5.1. Electrochemistry……31
1.5.2. UV-Vis-NIR absorption……32
1.6. Fullerene and metallofullerene-based materials……33
1.6.1. Fullerene-containing polymers……..33
1.6.2. Films, mono-layers, supramolecular assemblies and nanodevices……38
1.6.3. Medicinal applications of fullerenes and metallofullerenes……..42
1.6.3.1. Medicinal applications with C_{60} fullerene……42
1.6.3.1.1. Toxicity studies……..42
1.6.3.1.2. Antiviral activity……43
1.6.3.1.3. Neuroprotective ability……..45
1.6.3.2. Medicinal applications of metallofullerenes……..45
1.6.3.2.1. MRI contrast agents and biodistribution……45
1.6.3.3. Radiopharmaceuticals and biodistribution……48

CHAPTER 2 – Project Overview……...……50

CHAPTER 3 – Functionalization of $Sc_3N@C_{80}$ ……..……..…..53
3.1. Introduction……...53
3.2. Results and Discussion……..55
3.2.1. The first derivative of $Sc_3N@C_{80}$ ……..……55
3.2.2. X-ray crystal structure of the first $Sc_3N@C_{80}$ derivative……..….62
3.2.3. Malonate derivatives of $Sc_3N@C_{80}$ ……..65
3.2.4. A ^{15}N-labeled terminal amine derivative of $Sc_3N@C_{80}$ for addend attachment……..…..68
3.2.4.1. 1,3-Dihydrobenzo[c]thiophene (**10**)……..……..69
3.2.4.2. 1,3-Dihydrobenzo[c]thiophene-2,2-dioxide (**11**)……...71
3.2.4.3. 1,3-Dihydro-5-nitrobenzo[c]thiophene-2,2-dioxide (^{15}N-labeled) (**12**)……...71
3.2.4.4. 5-Amino-1,3-dihydrobenzo[c]thiophene-2,2-dioxide (^{15}N-labeled) (**13**)……...73
3.2.4.5. Terminal amine derivative of $Sc_3N@C_{80}$ (^{15}N-labeled) (**14**)…….....74
3.2.5. Water-soluble metallofullerenols from $Sc_3N@C_{80}$ (**15**)……76
3.3. Experimental……..81
3.3.1. Materials and purification……..81
3.3.2. Analytical methods……82
3.3.3. Synthesis of ^{13}C-labeled 6,7-dimethoxyisochroman-3-one (**2**)……84
3.3.4. Synthesis of ^{13}C-labeled $Sc_3N@C_{80}$–$C_{10}H_{12}O_2$ cycloadduct (**4**)……...87
3.3.5. Synthesis of ^{13}C-labeled diethyl malonate adduct of $Sc_3N@C_{80}$ (**6**)…….95
3.3.6. Synthesis of dibenzyl malonate adduct of $Sc_3N@C_{80}$ (**8**)……97
3.3.7. Synthesis of 1,3-dihydrobenzo[c]thiophene (**10**)……...99
3.3.8. Synthesis of 1,3-dihydrobenzo[c]thiophene-2,2-dioxide (**11**)…….102
3.3.9. Synthesis of ^{15}N-labeled 1,3-dihydro-5-nitrobenzo[c]thiophene-2,2-dioxide (**12**)……105
3.3.10. Synthesis of ^{15}N-labeled 5-amino-1,3-dihydrobenzo[c]thiophene-2,2-dioxide (**13**)……..108
3.3.11. Synthesis of a ^{15}N-labeled $Sc_3N@C_{80}$–terminal amine derivative (**14**)….112
3.3.12. Synthesis of $Sc_3N@C_{80}(OH)_{\sim 10}(O)_{\sim 10}$ metallofullerenols (**15**)……..114

CHAPTER 4 – Functionalization of $Sc_3N@C_{78}$ ……..…...117
4.1. Introduction……..117
4.2. Results and Discussion……..119
4.2.1. ^{13}C-labeled cycloadducts of the $Sc_3N@C_{78}$ metallofullerene (**3**)……119
4.3. Experimental……128
4.3.1. Materials and purification……128
4.3.2. Analytical methods……..129
4.3.3. Synthesis of ^{13}C-labeled $Sc_3N@C_{78}$–$(C_{10}H_{12}O_2)_n$ cycloadducts (**3**)……130

CHAPTER 5 – X-ray Contrast, a D_{5h} Isomer and ^{15}N-labeling of the Internal Metal-Nitride Cluster……..…..…..……133
5.1. Introduction……..133
5.2. Results and Discussion……..139

5.2.1. A lutetium-based contrast agent……...139
5.2.2. A D_{5h} isomer of the $Sc_3N@C_{80}$ metallofullerene……144
5.2.3. ^{15}N-labeling of internal cluster in the $Sc_3N@C_{80}$ metallofullerene…….146
5.3. Experimental……151
5.3.1. Materials and purification……151
5.3.2. Analytical methods……..151
5.3.3. Synthesis of $Lu_3N@C_{80}$ ……..…153
5.3.4. Synthesis of D_{5h} $Sc_3N@C_{80}$ ……..……...155
5.3.5. Synthesis of $Sc_3{}^{15}N@C_{80}$ ……..……..…..157

CHAPTER 6 – Summary, Conclusions and Future Work……..…….……159
6.1. Summary and conclusions……...159
6.2. Future work…...……..162

Appendix I. Schlegel diagram of $Sc_3N@C_{80}$ carbon cage……...164
Appendix II. Schlegel diagrams of $Sc_3N@C_{78}$ carbon cage....……165
Appendix III. How to operate the Krätschmer-Huffman generator
at Virginia Tech…….....166
Appendix IV. Determination of symmetry……..169
Appendix V. X-ray crystal structure coordinates of
4,5-dimethoxy-*o*-quinodimethane–$Sc_3N@C_{80}$ (**4**)……..170
Appendix VI. Cover of Science News magazine (July 13, 2002)……..……189

Vita……...190

List of Figures and Tables

Page

Figure 1.1. A generic structure of $A_3N@C_{80}$ ……...4
Figure 1.2. A generic structure of $A_3N@C_{68}$ ……....5
Figure 1.3. A generic structure of $A_3N@C_{78}$ ……...5
Figure 1.4. Drawing of a typical Krätschmer-Huffman generator…….....7
Figure 1.5. Schematic diagram of laser furnace……....8
Figure 1.6. 3-[(pentabromobenzyl)oxy]propylsilyl (PBB) stationary phase……...10
Figure 1.7. Tripodal 2,4-dinitrophenyl (DNP) ether stationary phase…….10
Figure 1.8. Computer generated structure of $Sc_3N@C_{68}$ with highlighted pentalenes……13
Figure 1.9. Rapid circular motion of two La^{+3} atoms (blue) inside the I_h C_{80} cage……16
Figure 1.10. Electrostatic potential map of I_h $[C_{80}]^{-6}$ ……..17
Figure 1.11. Reduction of C_{60} in CH_3CN/toluene at –10 °C using (a) cyclic voltammetry at a 100 mV/s scan rate and (b) differential pulse voltammetry (50-mV pulse, 50-ms pulse width, 300-ms period, 25 mV/s scan rate). $TBAPF_6$, 0.1 M, was used as the supporting electrolyte……..21
Figure 1.12. Reactivity of the pyracylene-type unit on C_{60} ……..……..22
Figure 1.13. Various types of C_{60} fullerene-containing polymers……...34
Figure 1.14. Polyoxyethylene arms on C_{60} ……37
Figure 1.15. Self-assembled phen-C_{60} monolayer on Au (111)……...38
Figure 1.16. $La_2@C_{80}$ 'peapods'……..42
Figure 1.17. ^{14}C-labeled C_{60} derivative……43
Figure 1.18. (a) Molecular model (side view) of HIVP inhibition with a C_{60} fullerene derivative, and (b) top view of HIVP inhibition……44
Figure 1.19. Biodistribution data for $^{166}Ho@C_{82}(OH)_x$ in BALB/c mice……...49

Figure 3.1. Numbering scheme for 6,7-dimethoxyisochroman-3-one **2**……..56
Figure 3.2. HPLC chromatogram of $Sc_3N@C_{80}$ **3** (31% conc.) and mono-adduct **4** (41% conc.) (x = mono-adduct of D_{5h} isomer?)……....58
Figure 3.3. MALDI-TOF MS of the mono-adduct **4** (*m/z* 1274) and $Sc_3N@C_{80}$ (*m/z* 1109) using a 9-nitroanthracene matrix……...59
Figure 3.4. Motifs of reactive sites on the I_h $Sc_3N@C_{80}$ **3** cage that yield a mirror plane of symmetry: (a) 1,3 position on a five-membered ring, (b) 1,2 position at a [5,6] juncture on a five-membered ring, (c) 1,4 position on a six-membered ring, and (d) Gauss View structure (non-optimized) of mono-adduct **4** from addend addition at a [5,6] bond-juncture (site "b") on the $Sc_3N@C_{80}$ cage……....62
Figure 3.5. X-ray crystal structure of mono-adduct **4** at 91K……..63
Figure 3.6. A close-up view of mono-adduct **4** crystal structure……....63
Figure 3.7. Crystal unit cell of mono-adduct **4** showing: (a) bipyramidal shape and (b) head-to-tail pi-stacking between adducts (benzenes omitted)…….....64

Figure 3.8. HPLC chromatogram of $Sc_3N@C_{80}$–dibenzyl malonate adducts **8** and unreacted $Sc_3N@C_{80}$ **3**……...67
Figure 3.9. HPLC chromatogram of $Sc_3N@C_{80}$–terminal amine derivatives (^{15}N-labeled) **14** and unreacted $Sc_3N@C_{80}$ **3**……75
Figure 3.10. Carbon XPS of water-soluble metallofullerenols **15** on gold……..78
Figure 3.11. LD-TOF mass spectrum of decomposed metallofullerenols **15**……..79
Figure 3.12. Conceptual drawing of adduct **4** when polyhydroxylated……...80
Figure 3.13. 400 MHz ^1H NMR spectrum of ^{13}C-labeled 6,7-dimethoxyisochroman-3-one **2**……..85
Figure 3.14. 100 MHz ^{13}C NMR spectrum of ^{13}C-labeled 6,7-dimethoxyisochroman-3-one **2**……...86
Figure 3.15. 400 MHz ^1H NMR spectrum of ^{13}C-labeled $Sc_3N@C_{80}$ mono-adduct **4** at room temperature (23 ºC)……88
Figure 3.16. 100 MHz ^{13}C NMR spectrum of ^{13}C-labeled $Sc_3N@C_{80}$ mono-adduct **4**……..89
Figure 3.17. 500 MHz COSY spectrum of ^{13}C-labeled $Sc_3N@C_{80}$ mono-adduct **4**……..90
Figure 3.18. 400 MHz ^1H NMR spectrum at 90 ºC of ^{13}C-labeled $Sc_3N@C_{80}$ mono-adduct **4** in 1,1,2,2-tetrachloroethane-d_2 ……91
Figure 3.19. 500 MHz HMQC spectrum of ^{13}C-labeled $Sc_3N@C_{80}$ mono-adduct **4**……..92
Figure 3.20. 500 MHz HMBC spectrum of ^{13}C-labeled $Sc_3N@C_{80}$ mono-adduct **4**……..93
Figure 3.21. UV-Visible spectrum of ^{13}C-labeled $Sc_3N@C_{80}$ mono-adduct **4**……..94
Figure 3.22. 100 MHz ^{13}C NMR spectrum of ^{13}C-labeled diethyl malonate adduct of $Sc_3N@C_{80}$ **6**……..96
Figure 3.23. 500 MHz ^1H NMR spectrum of dibenzyl malonate adduct of $Sc_3N@C_{80}$ **8**……..98
Figure 3.24. 400 MHz ^1H NMR spectrum of 1,3-dihydrobenzo[c]thiophene **10**……..100
Figure 3.25. 100 MHz ^{13}C NMR spectrum of 1,3-dihydrobenzo[c]thiophene **10**…….101
Figure 3.26. 500 MHz ^1H NMR spectrum of 1,3-dihydrobenzo[c]thiophene-2,2-dioxide **11**……103
Figure 3.27. 100 MHz ^1H NMR spectrum of 1,3-dihydrobenzo[c]thiophene-2,2-dioxide **11**……104
Figure 3.28. 500 MHz ^1H NMR spectrum of ^{15}N-labeled 1,3-dihydro-5-nitrobenzo[c]thiophene-2,2-dioxide **12** (x = impurity)……...106
Figure 3.29. 100 MHz ^{13}C NMR spectrum of ^{15}N-labeled 1,3-dihydro-5-nitrobenzo[c]thiophene-2,2-dioxide **12** (x = impurity)……...107
Figure 3.30. 400 MHz ^1H NMR spectrum of ^{15}N-labeled 5-amino-1,3-dihydrobenzo[c]thiophene-2,2-dioxide **13**……..109
Figure 3.31. 100 MHz ^{13}C NMR spectrum of ^{15}N-labeled 5-amino-1,3-dihydrobenzo[c]thiophene-2,2-dioxide **13** (x = impurity)……..110
Figure 3.32. 50 MHz ^{15}N NMR spectrum of ^{15}N-labeled 5-amino-1,3-dihydrobenzo[c]thiophene-2,2-dioxide **13**……..111

Figure 3.33. 400 MHz ^{1}H NMR spectrum of ^{15}N-labeled $Sc_3N@C_{80}$–terminal amine **14**……113
Figure 3.34. FT-IR spectrum of $Sc_3N@C_{80}(OH)_{\sim 10}(O)_{\sim 10}$ metallofullerenols **15** on a 3M™ polyethylene card……...115
Figure 3.35. FT-IR spectrum of 3M™ polyethylene card (blank)……..116

Figure 4.1. MALDI-TOF MS of tri-adduct **3** showing decomposition to mono-, di- and parent. Small amounts of the oxide and C_{88} adducts are also present……121
Figure 4.2. Non-coalescence of peaks in the ^{1}H NMR spectra of mono-adduct **3** with variation of temperature……...123
Figure 4.3. An example of an asymmetric mono-adduct **3** when addition has occurred across a [6,6] bond-juncture and the internal cluster is localized……124
Figure 4.4. Plausible reactive sites (dark bonds) on $Sc_3N@C_{78}$ ($D_{3h'}$ (78:5)) that yield a symmetric or asymmetric mono-adduct when internal cluster is dynamic……...124
Figure 4.5. 125 MHz ^{13}C NMR spectrum (5x12, 3x6) of $Sc_3N@C_{78}$ ……..125
Figure 4.6. 500 MHz ^{1}H NMR spectrum at 60 ºC of ^{13}C-labeled $Sc_3N@C_{78}$–$(C_{10}H_{12}O_2)_1$ adduct **3**……...131
Figure 4.7. 125 MHz ^{13}C NMR spectrum of ^{13}C-labeled $Sc_3N@C_{78}$–$(C_{10}H_{12}O_2)_1$ adduct **3** (x = impuity)..……...132

Figure 5.1. Iohexol (a commercially available X-ray contrast agent)……...135
Figure 5.2. A simple representation of metal-nitride cluster and carbon cage motions……...136
Figure 5.3. (a) HPLC trace (Buckyclutcher column, toluene, 2 ml/min. flow rate) and (b) Neg-DCI mass spectrum of pure $Lu_3N@C_{80}$ ……139
Figure 5.4. Gauss View structure of $Lu_3N@C_{80}$ ……...140
Figure 5.5. UV-Visible spectra comparison between $Lu_3N@C_{80}$ (top) and $Sc_3N@C_{80}$ (bottom)……141
Figure 5.6. Negative DCI mass spectrum showing $Lu_3N@C_{80}$ (*m/z* = 1499), $GdLu_2N@C_{80}$ (*m/z* = 1481) and $Gd_2LuN@C_{80}$ (*m/z* = 1463). $Lu_2@C_{82}$ (*m/z* = 1335) and $LuGd@C_{82}$ (*m/z* = 1316) are also present……...142
Figure 5.7. Negative DCI mass spectrum showing $Lu_3N@C_{80}$ (*m/z* = 1499), $HoLu_2N@C_{80}$ (*m/z* = 1489) and $Ho_2LuN@C_{80}$ (*m/z* = 1479). $Lu_2@C_{82}$ (*m/z* = 1335) and $LuHo@C_{82}$ (*m/z* = 1325) are also present……...142
Figure 5.8. Yields for $Ho_nLu_{3-n}@C_{80}$ soluble extracts (carbon disulfide) relative to $Lu_2@C_{84}$ based on negative DCI mass spectroscopy……143
Figure 5.9. X-ray photograph of: (a) contrast (arrows point to bright areas) provided by $Lu_3N@C_{80}$ on a Teflon block, (b) C_{60} fullerene on a Teflon block and (c) a blank Teflon block. The samples were exposed for 3.5 minutes at 30 kV……...…..143

Figure 5.10. HPLC chromatogram and mass spectrum of $Sc_3N@C_{80}$ (both isomers, *ca.* 9% ^{13}C- labeled). Top: HPLC peak with shoulder (toluene, 1 ml/min, 28.3 min. retention time) on a Trident Tri-DNP (Buckyclutcher) column. Bottom: Neg-DCI mass spectrum with highest peak at *m/z* = 1117……..144
Figure 5.11. $Sc_3N@C_{80}$ structures (Gauss View) of the I_h isomer (left) and the D_{5h} isomer (right). The top and bottom views are rotated 90˚ from each other. All five-membered rings are colored green……145
Figure 5.12. HPLC chromatographic purification of $Sc_3{}^{15}N@C_{80}$ (38% conc.) at 0.5 ml/min. flow rate in toluene……..……..……....147
Figure 5.13. Neg-DCI mass spectrum of pure $Sc_3{}^{15}N@C_{80}$ …….147
Figure 5.14. Neg-DCI mass spectra of fullerene extract from vaporization under (a) a static environment of $^{15}N_2$ and He gas, (b) a static environment of $^{14}N_2$ and He gas, and (c) a dynamic environment of $^{15}N_2$ and He gas……149
Figure 5.15. 125 MHz ^{13}C NMR spectrum of $Lu_3N@C_{80}$ ……154
Figure 5.16. 100 MHz ^{13}C NMR spectrum of D_{5h} (◆) and I_h (∗) isomers of $Sc_3N@C_{80}$ ……..156
Figure 5.17. 100 MHz ^{13}C NMR spectrum of $Sc_3{}^{15}N@C_{80}$ …….158

Figure 6.1. Conceptual drawing of a metallofullerene derivative that is coupled to a human epidermal growth factor (EGF) peptide. The EGF peptide binds to the epidermal growth factor receptor (EGFR) that is overexpressed in certain types of cancer cells (i.e., breast cancer)…….162

Page

Table 3.1. ^1H and ^{13}C NMR signal comparisons (ppm) between $Sc_3N@C_{80}$ mono-adduct **4** and the C_{60} mono-adduct…….……61

CHAPTER 1 – Introduction and Background

1.1. Historical overview

1.1.1. C_{60} and empty-cage fullerenes

In 1985, Smalley and co-workers[1] discovered the first fullerene molecule, C_{60}, during their mass spectrometric studies of carbon clusters that were generated from the laser vaporization of graphite in a high-pressure supersonic nozzle. 0.7 nm in diameter, the C_{60} molecule is an empty soccer-ball-shaped cage composed of 12 pentagons and 20 hexagons. The stable and highly symmetric structure of C_{60} is reminiscent of the geodesic domes (architectural structures of great stability) developed by the famed architect Richard Buckminster Fuller. The relationships between the two generated what has become the generic term "fullerenes", and the term "buckyballs" has evolved as a playful designation of the carbon molecules.[2] In addition to graphite, diamonds and nanotubes, fullerenes are one of only four known allotropes of carbon.

The discovery of the novel carbon-based structure (C_{60}) had attracted the attention of scientists throughout the world, yet all fullerene research in the early stage was limited to theoretical studies due to the small quantities of material produced.[3] However, in 1990, Krätschmer and Huffman[4] reported a simple procedure that allowed for the generation of macroscopic quantities of fullerenes (C_{60}, C_{70}, and other empty-cages) by arc vaporization of inexpensive graphite rods. To date, C_{60} remains the most abundant member of the fullerene family.

---

[1] Kroto, H. W.; Heath, J. R.; O'Brien, S. C.; Curl, R. F.; Smalley, R. E. C_{60}: Buckminsterfullerene. *Nature* **1985**, *318*, 162–163.

[2] Hammond, G. S. The Fullerenes: Overview 1991. In *Fullerenes: Synthesis, Properties, and Chemistry of Large Carbon Clusters;* Hammond, G. S., Kuck, V. J., Eds.; ACS Symposium Series 481; American Chemical Society: Washington, DC, 1992; p ix.

[3] Withers, J. C.; Pan, C.; Loutfy, R. O. Fullerene Prices: How Low Will They Be? In *Fullerenes: Recent Advances in the Chemistry and Physics of Fullerenes and Related Materials*. Kadish, K. M., Ruoff, R. S., Eds.; The Electrochemical Society, Inc.: Pennington, NJ, 1994; p 23.

[4] Kratschmer, W.; Lamb, L. D.; Fostiropoulos, K.; Huffman, D. R. Solid C_{60}: A New Form of Carbon. *Nature* **1990**, *347*, 354–358.

The I_h symmetry of C_{60} was originally identified by its four-band IR spectrum,[4] and soon afterwards by its one-line ^{13}C NMR spectrum.[5] The latter paper also reported the separation of C_{70} from the products of the carbon-arc synthesis by column chromatography on alumina. This was the first time that elemental allotropes had been separated using this technique.[6] The ^{13}C NMR for C_{70} consisted of five lines, providing evidence that the molecule possessed D_{5h} symmetry.[5] A number of empty-cage fullerenes, such as C_{76},[7] C_{78},[8,9] C_{84}[9,10] and higher, have also been isolated and characterized.

1.1.2. Endohedral metallofullerenes

1.1.2.1. Traditional metallofullerenes

Several days after the discovery of C_{60}, the same group found that LaC_{60} was formed via laser vaporization of $LaCl_3$–impregnated graphite rods.[7] They observed, by mass spectrometry, a series of C_n^+ and LaC_n^+ ions along with LaC_{60}^+ and $La_2C_{60}^+$, and proposed that the lanthanide atom(s) had been encapsulated inside the carbon shell. A few years later, Chai and co-workers[8] reported the first macroscopic amount of metallofullerenes by laser vaporization of a La_2O_3/graphite composite rod in a helium-filled tube-oven at high temperatures. Although La@C_{60}, La@C_{70} and La@C_{82} were observed in the mass spectra of the toluene extract, only the La@C_{82} molecule was air stable.

The ability to place metal atoms inside carbon cages has led to the synthesis of novel molecules that are now called "endohedral metallofullerenes". For naming purposes, the "@" symbol is used to indicate that atoms to the left are encapsulated within the carbon

---

[5] Taylor, R.; Hare, J. P.; Abdul-Sada, A. K.; Kroto, H. W. Isolation, Separation and Characterization of the Fullerenes C_{60} and C_{70}: The Third Form of Carbon. *J. Chem. Soc., Chem. Commun*. **1990**, *20*, 1423–1425.

[6] Fowler, P. W.; Manolopoulos, D. E. *An Atlas of Fullerenes*; International Series of Monographs on Chemistry 30; Clarendon Press: Oxford, 1995; p 6.

[7] Heath, J. R.; O'Brien, S. C.; Zhang, Q.; Liu, Y.; Curl, R. F.; Kroto, H. W.; Tittel, F. K.; Smalley, R. E. Lanthanum Complexes of Spheroidal Carbon Shells. *J. Am. Chem. Soc.* **1985**, *107*, 7779–7780.

[8] Chai, Y.; Guo, T.; Jin, C.; Haufler, R. E.; Chibante, L. P. F.; Fure, J.; Wang, L.; Alford, J. M.; Smalley, R. E. Fullerenes with Metals Inside. *J. Phys. Chem.* **1991**, *95*, 7564–7568.

cage on the right.[8] However, the corresponding IUPAC nomenclature is different from the M@C_n nomenclature that is conventionally used. The IUPAC recommends,[9] for example, that La@C_{82} be called [82-C_{3v}(II)]fullerene-*incar*-lanthanum, and the formula be written as *i*LaC_{82}{C_{3v}(II)}.

To date, Group 2 metals (Ca, Sr, Ba), Group 3 metals (Sc, Y, La), alkali metals (Li, Na, K, Cs), tetravalent metals (U, Zr, Hf), and most of the lanthanide metals have been successfully encapsulated into fullerene cages to produce mono-, di-, tri-, or tetrametallofullerenes.[10] These are all known as "traditional" metallofullerenes. The endohedral metal(s) have been confirmed by synchrotron X-ray powder diffraction, while information on the electronic structures and properties are obtained by spectroscopic methods such as EPR, UV-Vis-NIR, XPS and CV. Theoretical studies have helped to understand symmetry, thermal stability, and charge transfer effects that occur within the metallofullerene molecules. Unfortunately, the difficulty in producing over a few milligrams of material has hampered the ability to fully investigate the physical and chemical properties of countless traditional metallofullerenes.

1.1.2.2. Trimetallic nitride endohedral metallofullerenes

In 1999, a novel family of endohedral metallofullerenes were discovered at Virginia Tech by inducing dinitrogen gas into the generator during arc vaporization of composite (metal oxide/graphite) rods.[11] The most abundant of this family, $Sc_3N@C_{80}$, is a C_{80} cage that encapsulates a planar cluster of three metal atoms and a central nitrogen atom. The molecule was found to have a mass-to-charge ratio (*m/z*) of 1109, and the two-line ^{13}C NMR spectrum (time-averaged) of a 10% ^{13}C-labeled sample provided evidence that the cage possessed icosahedral (I_h) symmetry.[11] However, this icosahedral cage is different

[9] Godly, E. W.; Taylor, R. Nomenclature and terminology of fullerenes: A preliminary survey. *Pure App. Chem.* **1997**, 69, 1412–1434.

[10] Liu, S.; Sun, S. Recent progress in the studies of endohedral metallofullerenes. *J. Organomet. Chem.* **2000**, *599*, 74–86.

[11] Stevenson, S.; Rice, G.; Glass, T.; Harich, K.; Cromer, F.; Jordan, M. R.; Craft, J.; Hadju, E.; Bible, R.; Olmstead, M. M.; Maltra, K.; Fisher, A. J.; Balch, A. L.; Dorn, H. C. Small-bandgap endohedral metallofullerenes in high yield and purity. *Nature* **1999**, *401*, 55–57.

from that of C_{60}, because the C_{80} cage is composed of both corannulene-type carbon atoms (intersection of one five-membered and two six-membered rings) and pyrene-type carbons atoms (intersection of three six-membered rings), as opposed to solely corannulene-type. The I_h C_{80} cage contains 60 corannulene and 20 pyrene-type carbons, and the cage possesses 20 pentagons and 30 hexagons.

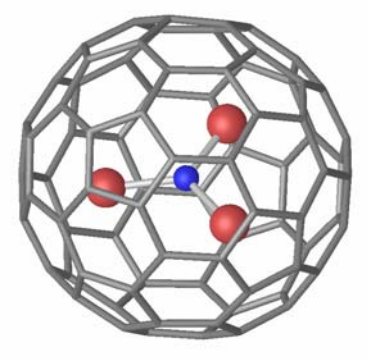

Figure 1.1. A generic structure of $A_3N@C_{80}$.

The internal cluster is dynamic at room temperature, as indicated by the single line in the ^{45}Sc NMR spectrum. These molecules are designated with the general symbol $A_3N@C_{80}$ (Figure 1.1), and species may contain either Group 3 or lanthanide metals, or a combination of both. Yields have been found to vary tremendously depending on the metal(s) of choice. Currently, $Sc_3N@C_{80}$ is the third most abundant fullerene species after C_{60} and C_{70}.

Another molecule in the trimetallic nitride family was discovered when a mass of 965 was observed in the mass spectra of metallofullerene extract.[12] This trimetallic nitride endohedral, $Sc_3N@C_{68}$, is a non-classical endohedral (lacks isolated pentagons) whose structure yielded twelve-line ^{13}C NMR and single-line ^{45}Sc NMR spectrum, which are consistent for a cage with D_3 symmetry (Figure 1.2). Interestingly, the planar scandium nitride cluster in this species is not dynamic, but rather it is localized over the three C_2

[12] Stevenson, S.; Fowler, P. W.; Heine, T.; Duchamp, J. C.; Rice, G.; Glass, T.; Harich, K.; Hajdu, E.; Bible, R.; Dorn, H. C. A stable non-classical metallofullerene family. *Nature* **2000**, *408*, 427–428.

axes of the cage (Figure 1.2, areas highlighted in blue). These are sites of fused pentagons, which are also known as pentalenes.

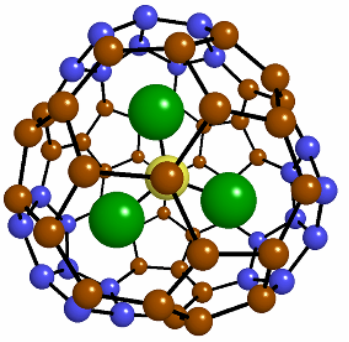

Figure 1.2. A generic structure of $A_3N@C_{68}$.

Yields of $Sc_3N@C_{68}$ molecules are significantly less (*ca.* $1/10^{th}$) than those of the $Sc_3N@C_{80}$ species.

The third and final species of the trimetallic nitride endohedral metallofullerene family is $A_3N@C_{78}$ (Figure 1.3).[13] When three scandium atoms are encapsulated the molecule has a mass of 1085. The carbon cage of this species exhibited $D_{3h'}$ symmetry, one of five possible isomers for the empty C_{78} cage. This was confirmed by an eight line ^{13}C NMR spectrum, and later by X-ray crystallography.[14]

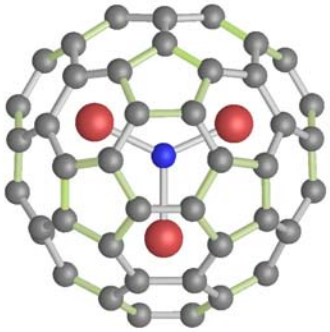

Figure 1.3. A generic structure of $A_3N@C_{78}$.

---

[13] Olmstead, M. M.; de Bettencourt-Dias, A.; Duchamp, J. C.; Stevenson, S.; Marciu, D.; Dorn, H. C.; Balch, A. L. Isolation and Structural Characterization of the Endohedral Fullerene $Sc_3N@C_{78}$. *Angew. Chem. Int. Ed.* **2001**, *40*, 1223–1225.

[14] Campanera, J. M.; Bo, C.; Olmstead, M. M.; Balch, A. L.; Poblet, J. M. Bonding within the Endohedral Fullerenes $Sc_3N@C_{78}$ and $Sc_3N@C_{80}$ as Determined by Density Functional Calculations and Reexamination of the Crystal Structure of $\{\{Sc_3N@C_{78}\}\cdot Co(OEP)\}\cdot 1.5(C_6H_6)\cdot 0.3(CHCl_3)$. *J. Phys. Chem. A* **2002**, *106*, 12356–12364.

Density functional theory (DFT) calculations[14] were employed to corroborate the X-ray crystal structure data that depicts a cage structure of $Sc_3N@C_{80}$ with the scandium metals located over the three C_3 axes. These axes are sites of two fused hexagons with abutted pentagons (pyracylene-type units). As with $A_3N@C_{68}$, the $A_3N@C_{78}$ species are produced in significantly smaller quantities than $A_3N@C_{80}$.

The trimetallic nitride endohedral metallofullerenes are produced in higher yields than many of the traditional metallofullerenes; however, numerous composite rods must be vaporized in order to acquire just a few milligrams of product.

1.2. Synthesis, isolation, purification and mechanistic formation

1.2.1. Synthesis of fullerenes and metallofullerenes

C_{60} and empty-cage fullerenes can be synthesized by numerous methods; however, only two methods are currently known for synthesizing traditional metallofullerenes, and only one for the trimetallic nitride endohedral metallofullerenes.

The most common method of synthesizing all fullerenes and metallofullerenes is through the use of a Krätschmer-Huffman generator (Figure 1.4).[15] Originally developed for the large-scale synthesis of C_{60}, an alternating or direct current (AC or DC) is used to arc-vaporize a graphite rod under a dynamic helium atmosphere at over 3000 ºC. For traditional metallofullerene production, a hollowed graphite rod is packed with a metal-oxide/graphite mix, then arc-vaporized in the same manner used to produce the empty-cages. A dynamic environment of both nitrogen gas and helium is needed for the synthesis of the trimetallic nitride endohedral metallofullerenes. Once a rod is burned, the resulting carbon soot is collected from the bottom of the generator. Prior to arc vaporization, the composite rods are normally subjected to heat treatment (1000 ºC) in a high vacuum. Although not completely understood, it is believed that the heating process converts the metal oxides into metal carbides.[10]

---

[15] Krätschmer, W.; Fostiropoulos, K.; Huffman, D. R. The infrared and ultraviolet absorption spectra of laboratory-produced carbon dust: evidence for the presence of the C_{60} molecule. *Chem. Phys. Lett.* **1990**, *170*, 167–171.

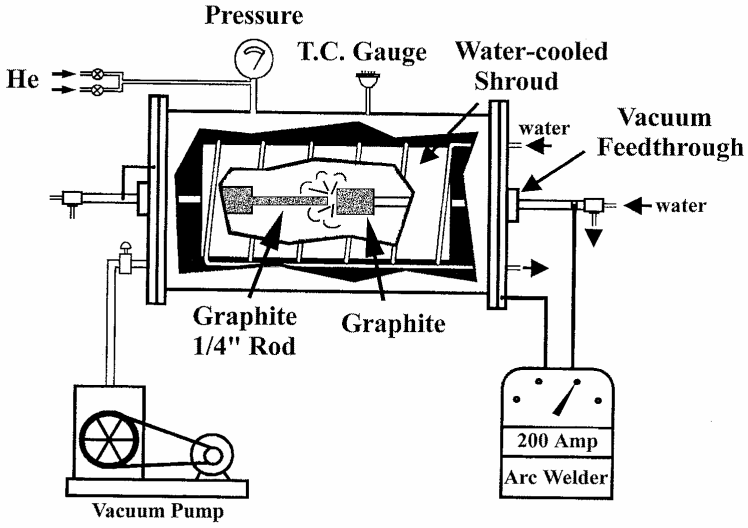

Figure 1.4. Drawing of a typical Krätschmer-Huffman generator.

The less common method of traditional metallofullerene synthesis involves a high-temperature laser vaporization of the composite rods.[8,16,17] First, a rod is placed in the laser furnace and heated to 1200 °C. Once the temperature is reached, a Nd:YAG laser doubled into the green (532 nm, 300 mJ per pulse at 10 Hz) is focused onto the target rod. The rod is rotating under an argon gas flow (500 Torr) to ensure a fresh surface (Figure 1.5).[18,19]

---

[16] Haufler, R. E.; Chai, Y.; Chibante, L. P. F.; Conceicao, J.; Jin, C.; Wang, L. S.; Maruyama, S.; Smalley, R. E. Cage Arc Generation of C_{60}. In *Clusters and Cluster-Assembled Materials.* Averback, R. S., Bernhoc, J., Nelson, D. L., Eds.; Materials Research Society: Pittsburgh, PA, 1991; Vol. 206, pp 627−637.

[17] Ying, Z. C.; Jin, C.; Hettich, R. L.; Puretzky, A. A.; Haufler, R. E.; Compton, R. N. Production and Characterization of Metallofullerene "Superatoms". In *Fullerenes: Recent Advances in the Chemistry and Physics of Fullerenes and Related Materials.* Kadish, K., Ruoff, R., Eds.; The Electrochemical Society, Inc.: Pennington, NJ, 1994; Vol. 1, pp 1402−1412.

[18] Shinohara, H. Endohedral Metallofullerenes. *Rep. Prog. Phys.* **2000**, *63*, 843−892.

[19] Smalley, R. E. Self-Assembly of the Fullerenes. *Acc. Chem. Res.* **1992**, *25*, 98−105.

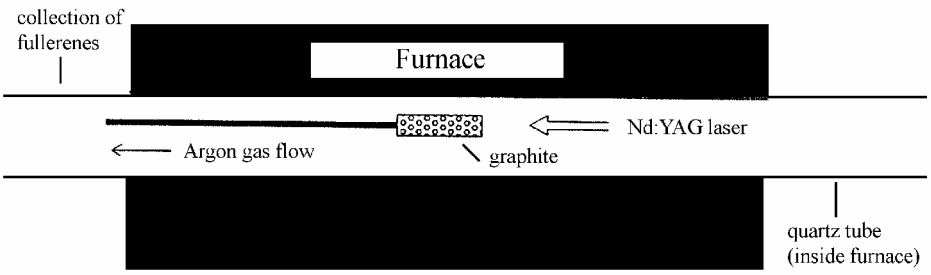

Figure 1.5. Schematic diagram of laser furnace.

Once the rod is burned, the metallofullerenes flow down a tube with the argon gas carrier, and are finally trapped on a quartz tube wall near the end of the furnace. A similar method is used for the production of single-walled carbon nanotubes.[20]

1.2.2. Extraction from soot

Separation of metallofullerenes (traditional and trimetallic nitrides) and empty-cages from the primary soot is usually performed by carbon disulfide extraction through a porous cellulose thimble. Khemani and colleagues[21] discovered that Soxhlet extraction with hot solvent normally increases the extraction efficiency of empty-cages such as C_{60} and C_{70}. Frequently, only half of the metallofullerene are extracted from the primary soot with these solvents, and additional extractions with pyridine or 1,2,4-trichlorobenzene is needed to recover all material.[22,23] Non-soluble materials which

[20] Thess, A.; Lee, R.; Nikolaev, P.; Dai, H.; Petit, P.; Robert, J.; Xu, C.; Lee, Y. H.; Kim, S. G.; Rinzler, A. G.; Colbert, D. T.; Scuseria, G. E.; Tomanek, D.; Fischer, J. E.; Smalley, R. E. Crystalline Ropes of Metallic Carbon Nanotubes. *Science* **1996**, *273*, 483–487.

[21] Khemani, K. C.; Prato, M.; Wudl, F. A Simple Soxhlet Chromatographic Method for the Isolation of Pure C_{60} and C_{70}. *J. Org. Chem.* **1992**, *57*, 3254–3256.

[22] Inakuma, M.; Ohno, M.; Shinohara, H. ESR Studies of Endohedral Mono-Metallo-Fullerenes. In *Fullerenes: Recent Advances in the Chemistry and Physics of Fullerenes and Related Materials.* Kadish, K., Ruoff, R., Eds.; The Electrochemical Society, Inc.: Pennington, NJ, 1995; Vol. 2, pp 330–342.

[23] Yamamoto, K.; Funasaka, H.; Takahashi, T.; Akasaka, T. Isolation of an ESR-Active Metallofullerene of La@C_{82}. *J. Phys. Chem.* **1994**, *98*, 2008–2011.

remain in the thimble include graphite, amorphous carbon and a small amount of carbon nanotubes.

1.2.3. Purification by liquid chromatography

High performance liquid chromatography (HPLC) is the standard technique for separating metallofullerenes, empty-cage fullerenes, and structural isomers of both species.[24-27] For all metallofullerene purifications, a two- or three-phase sequence of HPLC columns with different absorption mechanisms must be utilized. The typical purification of the $A_3N@C_{80}$ metallofullerenes is discussed in the following paragraphs.

In the first stage of the HPLC separation, metallofullerene extract is separated with a 5-PBB (5 μm, pentabromobenzyl) column (Figure 1.6) using carbon disulfide as the eluent. The column separates the empty-cages and metallofullerenes based on the size of their respective carbon cage. Thus, C_{60} elutes before the C_{70} fullerene. Consequently, empty-cage C_{84} and the $A_3N@C_{80}$ metallofullerene elute at the same time. The mechanism of separation is believed to occur due to the interaction between the polarizable bromine atoms of the stationary phase and the pi-electron density on the carbon cages.

---

[24] Kikuchi, K.; Nakahara, H.; Honda, M.; Suzuki, S.; Saito, K.; Shiromaru, H.; Yamauchi, K.; Ikemoto, I.; Kuramochi, T.; Hino, S.; Achiba, Y. Separation, Detection, and UV/Visible Absorption-Spectra of Fullerenes – C-76, C-78, C-84. *Chem. Lett.* **1991**, 1607–1610.

[25] Klute, R. C.; Dorn, H. C.; McNair, H. M. HPLC Separation of Higher (C_{84+}) Fullerenes. *J. Chromatogr. Sci.* **1992**, *30*, 438–442.

[26] Meier, M. S.; Selegue, J. P. Efficient Preparative Separation of C60 and C70. Gel Permeation Chromatography of Fullerenes Using 100% Toluene as Mobile Phase. *J. Org. Chem.* **1992**, *57*, 1924–1926.

[27] Jinno, K.; Saito, Y. Separation of Fullerenes by Liquid Chromatography: Molecular Recognition Mechanisms in Liquid Chromatographic Separation. In *Advances in Chromatography;* Brown, P. R., Grushka, E., Eds.; Marcel Dekker, Inc.: New York, 1996, Vol. 36, pp 65–125.

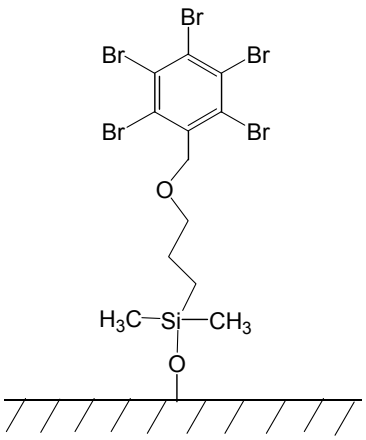

Figure 1.6. 3-[(pentabromobenzyl)oxy]propylsilyl (PBB) stationary phase.[28]

The solution containing C_{84} and $A_3N@C_{80}$ must then undergo an additional HPLC separation to afford the pure trimetallic nitride endohedral metallofullerene. This separation is achieved using a Trident-Tri-DNP (Buckyclutcher) column (Figure 1.7) with toluene as the eluent. With the second column, $A_3N@C_{80}$ elutes at a longer time

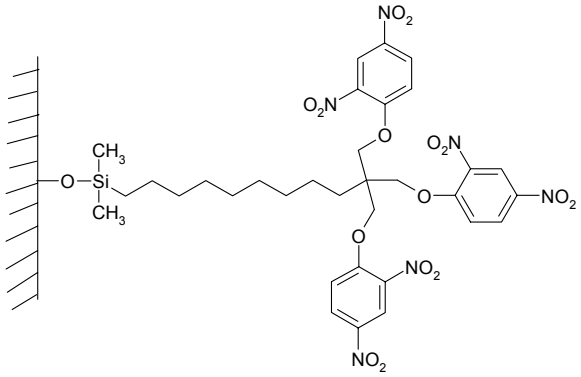

Figure 1.7. Tripodal 2,4-dinitrophenyl (DNP) ether stationary phase.[29]

than the C_{84} fullerene. The mechanism of separation is believed to result from an interaction of the polar stationary phase with: 1) an induced dipole moment that the

[28] Kimata, K.; Hirose, T.; Moriuchi, K.; Hosoya, K.; Araki, T.; Tanaka, N. High-Capacity Stationary Phases Containing Heavy Atoms for HPLC Separation of Fullerenes. *Anal. Chem.* **1995**, *67*, 2556–2561.

[29] Welch, C. J.; Pirkle, W. H. Progress in the design of selectors for buckminsterfullerene. *J. Chromatogr.* **1992**, *609*, 89–101.

metal-nitride cluster creates inside the cage or 2) an induced dipole moment on the exterior of the cage due to a change in the electronic nature (polarizability) of the cage.

Purified samples are confirmed by either matrix-assisted laser desorption time-of-flight (MALDI-TOF) mass spectrometry or negative-ion desorption chemical ionization (Neg-DCI) mass spectrometry.

1.2.4. Mechanistic formation of fullerenes and metallofullerenes

The mechanistic of fullerene formation via the arc vaporization of graphite rods is believed to be a stepwise growth process.[30] Initially, the planar sheets of graphite are vaporized into cationic carbon clusters (C_n^+) of only a few atoms. These clusters begin to grow as they diffuse out of hot plasma and into the cooler periphery, forming linear (C_5^+ and C_6^+), monocyclic (C_{11}^+- C_{20}^+), mono- and bicyclic planar clusters (C_{21}^+- C_{28}^+), and eventually three-dimensional (C_{29}^+) cationic systems. The free valences on carbon ("dangling bonds") combine to form closed spherical surfaces,[31] and therefore the first fullerene species arises at C_{30}^+, with C_{60} forming through continual cluster growth or the collision of smaller clusters.

Strout and Scuseria[32] proposed that the aforementioned clusters may undergo various cycloadditions (i.e., [2+4] and [4+6]) and 1,2-carbon shifts in order to form hoops that contain five- and six-membered rings, eventually leading to the closed shell fullerenes. Initially, these closed fullerenes may not correspond to a stable structure, although they can isomerize during the annealing process to form the most stable species. The process of fullerene formation is highly exothermic. Helium is used as a buffer gas in the process, and a specific pressure level (helium concentration) is essential for controlling the rate of cluster diffusion and eventual fullerene growth.

---

[30] Schwartz, H. The Mechanism of Fullerene Formation. *Angew. Chem. Int. Ed. Engl.* **1993**, *32*, 1412–1415.

[31] Haufler, R. E.; Chai, Y.; Chibante, L. P. F.; Conceicao, J.; Jin, C.; Wang, L.-S.; Maruyama, S.; Smalley, R. E. Carbon-arc Generation of Carbon Sixty-atom Molecules. *Mater. Res. Soc. Symp. Proc.* **1991,** *206*, 627–637.

[32] Strout, D. L.; Scuseria, G. E. A Cycloaddition Model for Fullerene Formation. *J. Phys. Chem.* **1996**, *100*, 6492–6498.

The mechanism of formation of traditional and trimetallic nitride endohedral metallofullerenes is unknown. However, it is believed that at sometime during the growth process the metal atoms or metal-nitride cluster (A_3N) are coordinated to a cationic cluster(s) or hoop, which subsequently grow around them to form the respective carbon cage. On the other hand, it is possible, though less likely, that the cages open to insert the metal atoms or cluster during the cooling process. The selective formation of an A_3N cluster (i.e., Sc_3N) in the trimetallic nitride endohedral metallofullerenes gives rise to a stable carbon cage. This stabilization will be discussed in the next section. A series of ring opening reactions with fullerene cages have been investigated by Rubin and co-workers in effort to insert metal atoms and produce large-scale amounts of endohedral metallofullerenes.[33]

1.3. Structure and cage stability

1.3.1. Isolated-pentagon rule (IPR)

The carbon cages of fullerenes and metallofullerenes have structural isomers with different five- and six-membered ring patterns. Kroto[34]and Schmalz[35] theorized that the stability of the curved fullerene cages is a result of released steric strain in the isolated pentagons. The isolated pentagon rule (IPR), considered the essential rule governing the geometry of fullerenes, states that stable fullerenes are those in which all pentagons on the cage are surrounded by five hexagons.

---

[33] Rubin, Y. Ring Opening Reactions of Fullerenes: Designed Approaches to Endohedral Metallofullerenes. In *Fullerenes and Related Structures.* Hirsch, A., Ed. Topics in Current Chemistry; Springer-Verlag: New York, 1999; 199, pp 67–91.

[34] Kroto, H. W. The stability of the fullerenes C_n, with n = 24, 28, 32, 36, 50, 60, and 70. *Nature* **1987**, *329*, 529–531.

[35] Schmalz, T. G.; Seitz, W. A.; Klein, D. J.; Hite, G. E. Elemental Carbon Cages. *J. Am. Chem. Soc.* **1988**, *110*, 1113–1127.

The discoveries of $Sc_3N@C_{68}$[12] (Figure 1.8) and $Sc_2@C_{66}$[36] in recent years have provided evidence that not all stable fullerene cages are not governed by the isolated pentagon rule.

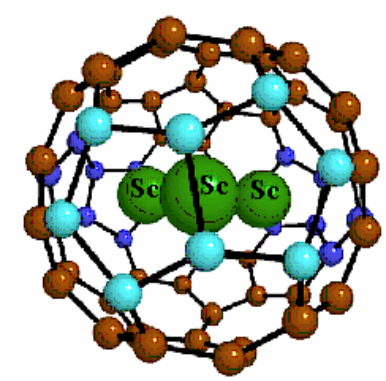

Figure 1.8. Computer generated structure of $Sc_3N@C_{68}$ with highlighted pentalenes.

These IPR-violating cages possess different arrangements of fused five-membered rings (pentalenes). The spiral algorithm predicted 6,332 possible isomers $Sc_3N@C_{68}$. Of these, the rounded D_3-symmetric cage of $Sc_3N@C_{68}$ (isomer 6,140) was the most stable isomer that also supported the ^{13}C NMR data.[12] Recent X-ray crystallographic data has verified that the symmetry is correct.[37] Charge transfer from the encapsulated metal atoms to the carbon cage is the reason for stabilization of the otherwise extremely unstable C_{68} and C_{66} cages, which cannot be isolated as empty-cage species.

1.3.2. Icosahedral symmetry and charge transfer

Empty-cage C_{80} has seven distinct structures (D_2, D_{5d}, C_{2v}, $C_{2v'}$, D_3, D_{5h} and I_h) that satisfy the so-called isolated pentagon rule (IPR). Theoretical calculations (ab initio and DFT) by Kobayashi and coworkers[38-41] determined that the most thermodynamically

---

[36] Wang, C.-R.; Kai, T.; Tomiyama, T.; Yoshida, T.; Kobayashi, Y.; Nishibori, E.; Takata, M.; Sakata, M.; Shinohara, H. C_{66} fullerene encaging a scandium dimer. *Nature* **2000**, *408*, 426.

[37] Olmstead, M. M.; Lee, H. M.; Duchamp, J. C.; Stevenson, S.; Marciu, D.; Dorn, H. C.; Balch, A. L. $Sc_3N@C_{68}$: Folded Pentalene Coordination in an Endohedral Fullerene that Does Not Obey the Isolated Pentagon Rule. *Angew. Chem. Int. Ed.* **2003**, *42*, 900–903.

[38] Kobayashi, K.; Nagase, S. Structures and Electron States of Endohedral Dimetallofullerenes: $M_2@C_{80}$ (M = Sc, Y, La, Ce, Pr, Eu, Gd, Yb and Lu). *Chem. Phys. Lett.* **1996**, *262*, 227–232.

stable isomers of empty-cage C_{80} are those with D_2 and D_{5d} symmetries, while the I_h isomer is the least stable by *ca.* 52 kcal/mol. The HOMO-LUMO gaps suggested that the D_2 symmetry isomer was slightly less reactive (greater air stability) than the D_{5d}, and the former was eventually isolated and characterized.[42] Furthermore, semi-empirical and ab initio calculations have shown that the I_h isomer can distort, due to the Jahn-Teller effect, to form the more stable D_2 isomer.[43]

The I_h C_{80} cage has only two electrons in its fourfold degenerate highest occupied molecular orbital (HOMO). Upon accommodation of six electrons, the I_h isomer forms a closed-shell electronic state and becomes the most thermodynamically stable of all seven isomers. The lanthanide atoms of $La_2@C_{80}$ and the metal-nitride cluster of the $A_3N@C_{80}$ species (where A = Group 3 or lanthanide) both provide stability by formally donating six electrons to the cage.[11,38-41,44] The resulting electronic states can be described as $[La^{+3}]_2@[C_{80}]^{-6}$ and $[A_3N]^{+6}@[C_{80}]^{-6}$.

In the dimetallofullerene case ($M_2@C_{80}$), calculations of the I_h C_{80} cage with scandium and yttrium (lighter members of Group 3) showed that three valence electrons were transferred from each yttrium atom to form a closed-shell electronic state, yet only two from each scandium atom, thereby leaving the HOMO of the cage unfilled in the $Sc_2@C_{80}$ case.[38,40] The inability to transfer six electrons from the two scandium atoms could be the reason why $Sc_2@C_{84}$, which requires the transfer of only four electrons to stabilize the cage, is a commonly isolated species as opposed to $Sc_2@C_{80}$.

Density functional theory (DFT) calculations of $Sc_3N@C_{80}$ have shown that the formal electronic state ($[Sc_3N]^{+6}@[C_{80}]^{-6}$) is not an accurate description of charge transfer

---

[39] Akasaka, T.; Nagase, S.; Kobayashi, K.; Walchli, M.; Yamamoto, K.; Funasaka, H.; Kako, M.; Hoshino, T.; Erata, T. ^{13}C and ^{139}La NMR Studies of $La_2@C_{80}$: First Evidence for Circular Motion of Metal Atoms in Endohedral Dimetallofullerenes. *Angew. Chem., Int. Ed. Engl.* **1997**, *36*, 1643–1645.

[40] Nagase, S.; Kobayashi, K.; Akasaka, T. Recent Progress in Endohedral Dimetallofullerenes. *J. Mol. Struct. (Theochem)* **1997**, *398–399*, 221–227.

[41] Nagase, S.; Kobayashi, K.; Akasaka, T. Recent Advances in the Structural Determination of Endohedral Metallofullerenes. *J. Comput. Chem.* **1998**, *19*, 232–239.

[42] Hennrich, F. H.; Michel, R. H.; Fisher, A.; Richard-Schneider, S.; Gilb, S.; Kappes, M. M.; Fuchs, D.; Bürk, M.; Kobayashi, K.; Nagase, S. Isolation and Characterization of C_{80}. *Angew. Chem. Int. Ed. Engl.* **1996**, *35*, 1732–1734.

[43] Kobayashi, K.; Nagase, S.; Akasaka, T. A Theoretical Study of C_{80} and $La_2@C_{80}$. *Chem. Phys. Lett.* **1995,** *245*, 230–236.

within the molecule.[45,46] If each Sc atom possessed a +3 charge and the central nitrogen a -3, then the highly ionic Sc_3N cluster should appear as a pyramidal ammonia-like structure within the cage; however, severe electrostatic repulsions between the scandium atoms are minimized by the cluster assuming a planar configuration. As a result, significant p_Π-d_Π covalent bonding ("back bonding") occurs between the nitrogen and scandium atoms, which allows for shorter Sc-N bond distances and an increase in electron density on the Sc atoms. From the Mulliken analysis,[45] the charge (q) on the central nitrogen was –0.9 ($s^{1.7}p^{4.2}$), meaning that only *ca.* 0.3 electrons, and not a full electron, were transferred from each Sc atom. In addition, each scandium atom donated nearly one s electron to the carbon cage (q = +1.2, $s^{0.2}p^{0.2}d^{1.4}$).

The aforementioned computational results were corroborated by experimental X-ray absorption spectroscopy (XAS) results from the Sc $L_{2,3}$ edge of a $Sc_3N@C_{80}$ sample.[47] The Sc atoms were found to have a 3d electron count of 0.6 ($3d^{0.6}$), thereby yielding an effective Sc valence count of 2.4. An additional 0.3 electrons are transferred from each scandium atom to nitrogen, which leaves a total of 6.3 electrons [(3 x 2.4) – (3 x 0.3) = 6.3)] that are transferred to the C_{80} cage to stabilize the I_h symmetry.

Unlike the planar Sc_3N cluster, DFT calculations demonstrate that when La_3N is placed inside the I_h C_{80} cage it assumes a pyramidal structure.[46] The removal of electrons is easier from the larger La atoms, and the La_3N cluster donates two more electrons to the cage than does Sc_3N. As a result, the molecule adopts a formal charge state of $[La_3N]^{+8}@[C_{80}]^{-8}$, and the two electrons fill the four-fold degenerate LUMO of the icosahedral cage to create an open-shell electronic state, which is presumably more reactive than the closed-shell structure of $Sc_3N@C_{80}$. The La atoms possess a larger positive charge than the Sc atoms, but in this case the severe electrostatic repulsions

---

[44] Kobayashi, K.; Nagase, S.; Akasaka, T. Endohedral Dimetallofullerenes $Sc_2@C_{84}$ and $La_2@C_{80}$. Are the Metal Atoms Still Inside the Fullerene Cages? *Chem. Phys. Lett.* **1996**, *261*, 502–506.

[45] Krause, K.; Kuzmany, H.; Georgi, P.; Dunsch, L.; Vietze, K.; Seifert, G. Structure and Stability of Endohedral Fullerene $Sc_3N@C_{80}$: A Raman, Infrared, and Theoretical Analysis. *J. Chem. Phys.* **2001**, *115*, 6596–6605.

[46] Kobayashi, K. Sano, Y.; Nagase, S. Theoretical Study of Endohedral Metallofullerenes: $Sc_{3-n}La_nN@C_{80}$ (n = 0–3). *J. Comp. Chem*. **2001**, *22*, 1353–1358.

[47] Alvarez, L.; Pichler, T.; Georgi, P.; Schwieger, T.; Peisert, H.; Dunsch, L.; Hu, Z.; Knupfer, M.; Fink, J.; Bressler, P.; Mast, M.; Golden, M. S. Electronic Structure of Pristine and Intercalated $Sc_3N@C_{80}$ Metallofullerene. *Phys. Rev. B* **2002**, *66*, 035107/1–035107/7.

between the La atoms cannot be minimized (cannot form a planar structure) due to the longer La-N bond distances and cage size-restrictions. Furthermore, the overall molecule is destabilized due electrostatic repulsions between the negatively charge nitrogen (at the cluster vertex) and the $[C_{80}]^{-8}$ cage. Calculations show that stabilization of the Sc_3N cluster inside the I_h C_{80} cage decreases as Sc atoms are replaced with La, which may be why mass spectrometric yields of $La_3N@C_{80}$ appear to be significantly less (*ca.* 10% $Sc_2@C_{84}$) than $Sc_3N@C_{80}$.[48]

Although not C_{80} cages, the D_{3h} cage of $Sc_3N@C_{78}$ and the D_3 cage of $Sc_3N@C_{68}$ are formally stabilized by transfer of six electrons from the internal clusters.[12,13,14]

1.3.3. Internal motion and electrostatic potential

The room temperature (296 K) ^{139}La NMR spectrum of an isolated $La_2@C_{80}$ (^{13}C-enriched) sample exhibited a single line, suggesting that the two La^{+3} atoms inside the cage are equivalent. Accordingly, the ^{13}C NMR spectrum (300 K) showed a single broad resonance, indicating that the equivalency of these La^{+3} atoms arises due to their rapid circular motion inside the negatively charged cage (Figure 1.9).[39] The electrostatic

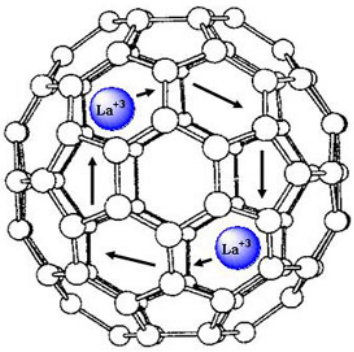

Figure 1.9. Rapid circular motion of two La^{+3} atoms (blue) inside the I_h C_{80} cage.

[48] Dorn, H. C.; Stevenson, S.; Craft, J.; Cromer, F.; Duchamp, J.; Rice, G.; Glass, T.; Harich, K.; Fowler, P. W.; Heine, T.; Hajdu, E.; Bible, R.; Olmstead, M. M.; Maitra, K.; Fisher, A. J.; Balch, A. L. Endohedrals. In *Electronic Properties of Novel Materials – Molecular Nanostructures*; Kuzmany, H., Fink, J., Mehring, M., Roth, S., Eds.; AIP Conference Proceedings; American Institute of Physics: Melville, NY, 2000; 544, pp 135–141.

potential map of I_h $[C_{80}]^{-6}$ is almost circular with no clear minima, thus reflecting the round structure of the cage (Figure 1.10).[41,44] In addition, calculations revealed that due to the electrostatic potential the barrier of rotation inside the I_h C_{80} cage is extremely small (*ca.* 5 kcal/mol). Therefore, by lowering the temperature to 258 K, the La atoms became localized within the cage and yielded a thirteen line ^{13}C NMR spectrum that is consistent for a cage with D_{2h} symmetry. Furthermore, the geometry optimized structure of $La_2@C_{80}$ results in a endohedral metallofullerene with D_{2h} symmetry.

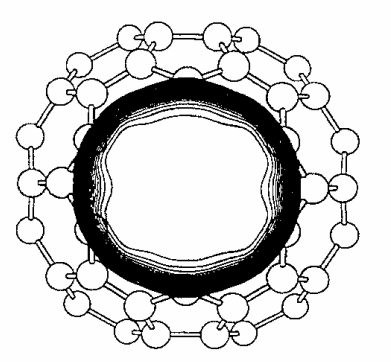

Figure 1.10. Electrostatic potential map of I_h $[C_{80}]^{-6}$. Reprinted from reference 44 with permission from Elsevier.

Contrary to the findings for $La_2@C_{80}$, the room temperature ^{13}C NMR spectrum (time averaged) of $Sc_3N@C_{80}$, acquired by Dorn and co-workers,[11] showed two resonances in a 3:1 ratio. The $[Sc_3N]^{+6}$ cluster is rapidly rotating (dynamic) inside the C_{80} cage, which therefore preserves the overall I_h symmetry of the cage on the NMR timescale. The observed NMR signals are in conjunction with the predicted (calculated) structure of an I_h C_{80} cage.[49] However, it should be noted that IR and Raman measurements by Krause and colleagues[45] support a carbon cage structure of $Sc_3N@C_{80}$ that has C_3 symmetry and not I_h symmetry.

At room temperature, the $[Sc_3N]^{+6}$ cluster inside $Sc_3N@C_{78}$ is presumably dynamic along the belt of the cage, thereby leading to an eight line ^{13}C NMR spectrum for the cage.[13] However, DFT calculations have predicted that the position of lowest energy for

[49] Fowler, P. W.; Manolopoulos, D. E. *An Atlas of Fullerenes*; International Series of Monographs on Chemistry 30; Clarendon Press: Oxford, 1995; p 6.

the cluster is when the Sc atoms of the cluster are static and located over the three pyracylene patches ([6,6] ring-junctures) of the $D_{3h'}$ (78:5) C_{78} cage.[14] Extremely high energies were generated when the Sc atoms were moved to other sites within the molecule. Furthermore, there is an in-plane bonding interaction between the cage orbitals and the d_{xy}-type orbitals of Sc when the metal atoms reside over the [6,6] junctures of the cage. The $[Sc_3N]^{+6}$ cluster is planar when this occurs.

For $Sc_3N@C_{68}$, the internal cluster is presumably static due to a lack of room for rotation inside the cage. This hypothesis is bolstered by the experimentally observed twelve line ^{13}C NMR and single line ^{45}Sc NMR spectra. It is also worth mentioning that the X-ray crystal structure of the molecule at low temperature (91 K) shows the Sc atoms located over the sites of three fused pentagons (pentalenes).[50]

1.4. Organic functionalizations of C_{60} and traditional metallofullerenes

1.4.1. Reactivity of the C_{60} fullerene

The reactivity of C_{60} can be described as a strained, electron-deficient polyalkene with localized double bonds.[51] The chemistry is governed largely by a combination of steric effects, a drive to increase aromaticity of the cage, electron withdrawal by the cage, and an increase in localization of pi-electrons following a first addition.[52] It forms adducts readily with radicals, carbenes, nucleophiles, and participates as the electron-deficient dienophile in a large variety of thermal and photochemical cycloadditions.[53] In addition, C_{60} is readily hydrogenated, fluorinated, and forms complexes with many transition metals. Once the fullerene carbon atoms become functionalized, the hybridization is changed from a strained trigonal-planar (sp^2) to a less strained tetrahedral (sp^3) state.

---

[50] Olmstead, M. M.; Lee, H. M.; Duchamp, J. C.; Stevenson, S.; Marciu, D.; Dorn, H. C.; Balch, A. L. $Sc_3N@C_{68}$: Folded Pentalene Coordination in an Endohedral Fullerene that Does Not Obey the Isolated Pentagon Rule. *Angew. Chem. Int. Ed.* **2003**, *42*, 900–903.

[51] Haddon, R. C. Chemistry of the Fullerenes: The Manifestation of Strain in a Class of Continuous Aromatic Molecules. *Science* **1993**, *261*, 1545–1550.

[52] Taylor, R. Surprise, Serendipity, and Symmetry in Fullerene Chemistry. *Synlett* **2000**, 776–793.

1.4.1.1. Hydroxylation of C_{60}

Hydroxyfullerenes, or fullerenols, are highly water-soluble fullerene derivatives. One method of synthesizing fullerenols was performed by the reaction of C_{60} with BH_3/THF followed by H_2O_2/NaOH under a nitrogen environment.[54] This produced pairs of adjacent hydroxyl groups and protons on the fullerenes. Molecular oxygen was then introduced to the hydroborated molecules to form completely hydroxylated adducts (Scheme 1.1).

Scheme 1.1

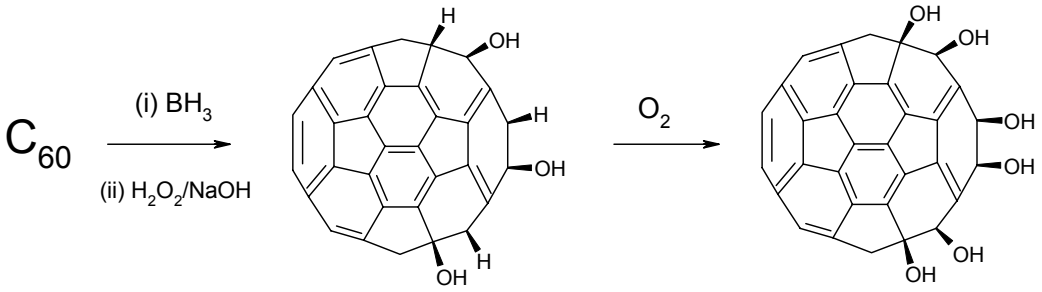

A different method of hydroxylation, reported by Chiang et al.,[55] involved the reaction of C_{60} with nitrogen dioxide (NO_2) in solution to produce an insoluble polynitrofullerene. The radicals were generated by reaction of sodium nitrite with concentrated HNO_3 in benzene, under a nitrogen atmosphere. The polynitrofullerenes were then hydrolyzed in an aqueous NaOH solution to afford a polyhydroxylated fullerene. The mass spectrum, obtained by fast atom bombardment (FAB), showed an exponential decay of masses ranging from sixteen to one hydroxyl groups.

A simple method of hydroxylation, proposed by Li et al.,[56] used tetrabutylammonium hydroxide (TBAOH) as a phase-transfer catalyst, along with a 50 wt% NaOH solution, to

---

[53] Diederich, F.; Thilgen, C. Covalent Fullerene Chemistry. *Science* **1996**, *271*, 317–323.

[54] Schneider, N. S.; Darwish, A. D.; Kroto, H. W.; Taylor, R.; Walton, D. R. M. Formation of Fullerols via Hydroboration of Fullerene–C_{60}. *J. Chem. Soc., Chem. Commun.* **1994**, 463–464.

[55] Chiang, L. Y.; Bhonsle, J. B; Wang, L.; Shu, S. F.; Chang, T. M.; Hwu, J. R. Efficient One-Flask Synthesis of Water-soluble [60]Fullerenols. *Tetrahedron* **1996**, *52*, 4963–4972.

[56] Li, J.; Takeuchi, A.; Ozawa, M.; Li, X.; Saigo, K.; Kitazawa, K. C_{60} Fullerol Formation catalyzed by Quaternary Ammonium Hydroxides. *J. Chem. Soc., Chem. Commun.* **1993**, 1784–1785.

achieve water-soluble C_{60} derivatives. The presence of molecular oxygen was necessary during the reaction to ensure high reaction efficiency. Although the authors were unable to produce mass spectral data, the elemental analysis illustrated that the products possessed an average of twenty-four hydroxyl groups. To date, the mechanism of hydroxylation is not fully understood.

Water-soluble fullerene derivatives with polar hydroxyl groups have potential applications in aqueous solution chemistry, biochemistry and electrochemistry, as well as in the synthesis of novel fullerene derivatives.[56]

1.4.1.2. C_{60} anions and the addition of nucleophiles

Molecular orbital calculations of C_{60} indicate that the LUMOs (lowest unoccupied molecular orbitals) exhibit relatively low energy and are triply degenerate.[57-62] Because of this, C_{60} was predicted to be a fairly electronegative molecule that could be reduced up to its hexa-anion (C_{60}^{-6}). Initially, cyclic voltammetry studies had demonstrated reductions with only two[63] and three[64] electrons; however, once the expansion of the

---

[57] Haymet, A. D. J. C_{120} and C_{60}: Archimedean Solids Constructed from sp^2 Hybridized Carbon Atoms. *Chem. Phys. Lett.* **1985**, *122*, 421–424.

[58] Haddon, R. C.; Brus, L. E.; Raghavachari, K. Electronic Structure and Bonding in Icosahedral C_{60}. *Chem. Phys. Lett.* **1986**, *125*, 459–464.

[59] Satpathy, S. Electronic Structure of the Truncated-Icosahedral C_{60} Cluster. *Chem. Phys. Lett.* **1986**, *130*, 545–550.

[60] Hale, P. D. Discrete-Variational-Xα Electronic Structure Studies of the Spherical C_{60} Cluster: Prediction of Ionization Potential and Electronic Transition Energy. *J. Am. Chem. Soc.* **1986**, *108*, 6087–6088.

[61] Larsson, S.; Volosov, A.; Rosen, A. Optical-Spectrum of the icosahedral C_{60}-Follene-60. *Chem. Phys. Lett.* **1987**, *137*, 501–504.

[62] Rosen, A.; Wastberg, B. Calculations of the ionization thresholds and electron affinities of the neutral, positively and negatively charged C_{60}–"follene-60". *J. Chem. Phys.* **1989**, *90*, 2525–2526.

[63] Haufler, R. E.; Conceicao, J.; Chibante, L. P. F.; Chai, Y.; Byrne, N. E.; Flanagan, S.; Haley, M. M.; O'Brien, S. C.; Pan, C.; Xiao, Z.; Billups, W. E.; Ciufolini, M. A.; Hauge, R. H.; Margrave, J. L.; Wilson, L. J.; Curl, R. F.; Smalley, R. E. Efficient Production of C_{60} (Buckminsterfullerene), $C_{60}H_{36}$, and the Solvated Buckide Ion. *J. Phys. Chem.* **1990**, *94*, 8634–8636.

[64] Allemand, P.-M.; Koch, A.; Wudl, F.; Rubin, Y.; Diederich, F.; Alvarez, M. M.; Anz, S. J.; Whetten, R. L. Two Different Fullerenes Have the Same Cyclic Voltammetry. *J. Am. Chem. Soc.* **1991**, *113*, 1050–1051.

available solvent potential window was increased, reductions with four,[65] five,[66] and six[67-69] (Figure 1.11) electrons were realized.

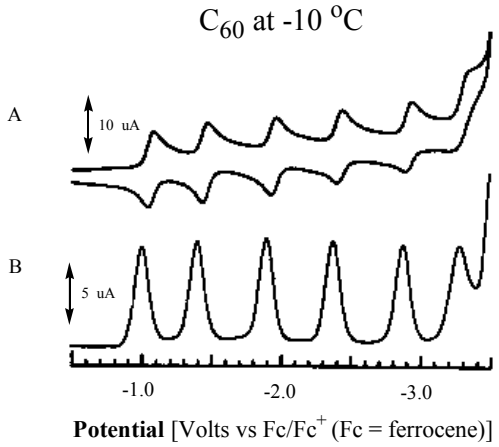

Figure 1.11. Reduction of C_{60} in CH_3CN/toluene at –10 °C using (a) cyclic voltammetry at a 100 mV/s scan rate and (b) differential pulse voltammetry (50-mV pulse, 50-ms pulse width, 300-ms period, 25 mV/s scan rate). $TBAPF_6$, 0.1 M, was used as the supporting electrolyte. Reprinted with permission from reference 67. Copyright 1992 American Chemical Society.

A close examination of a C_{60} model revealed that the cage possessed *six* pyracylene-type units (fused six-membered rings with abutted pentagons), and that the external pi-electrons of these pyracylene units create a non-aromatic (4n) system on the cage.[70] Therefore, it was hypothesized that each unit would provide the driving force for the capture of up to two electrons, either by direct electron transfer to give aromatic (4n + 2)

---

[65] Dubois, D.; Kadish, K. M.; Flanagan, S.; Haufler, R. E.; Chibante, L. P. F.; Wilson, L. J. Spectroelectrochemical Study of the C_{60} and C_{70} Fullerenes and Their Mono-, Di-, Tri-, and Tetraanions. *J. Am. Chem. Soc.* **1991**, *113*, 4364–4366.

[66] Dubois, D.; Kadish, K. M.; Flanagan, S.; Wilson, L. J. Electrochemical Detection of Fulleronium and Highly Reduced Fulleride (C_{60}^{5-}) Ions in Solution. *J. Am. Chem. Soc.* **1991**, *113*, 7773–7774.

[67] Xie, Q.; Perez-Cordero, E.; Echegoyen, L. Electrochemical Detection of C_{60}^{6-} and C_{70}^{6-}: Enhanced Stability of Fullerides in Solution. *J. Am. Chem. Soc.* **1992**, *114*, 3978–3980.

[68] Ohsawa, Y.; Saji, T. Electrochemical Detection of C_{60}^{6-} at Low Temperature. *J. Chem. Soc., Chem. Commun.* **1992**, 781–782.

[69] Zhou, F.; Jehoulet, C.; Bard, A. J. Reduction and Elecrochemistry of C_{60} in Liquid Ammonia. *J. Am. Chem. Soc.* **1992**, *114*, 11004–11006.

[70] Trost, B. M.; Bright, G. M.; Frihart, C.; Brittelli, D. Perturbed [12]Annulenes. The Synthesis of Pyracylene. *J. Am. Chem. Soc.* **1971**, *93*, 737–745.

dianions, or in the form of a lone pair (nucleophile) to give a "cyclopentadienide" mono-adduct (Figure 1.12).[71]

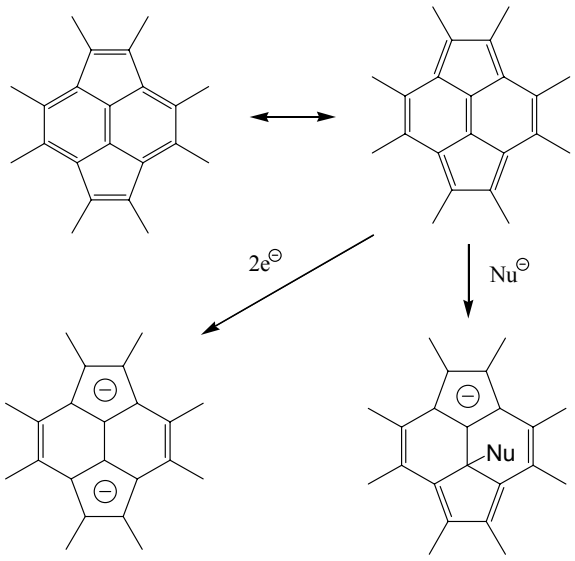

Figure 1.12. Reactivity of the pyracylene-type unit on C_{60}.

To test this hypothesis, a number of carbon and nitrogen nucleophiles were reacted with C_{60}. For instance, organolithium and Grignard reagents were found to react rapidly with C_{60} to form RC_{60}^- anions.[72-74] When the reactions were carried out in toluene, the salts immediately precipitated out of solution upon addition of the nucleophile. Electrophilic sources, such as strong acids and methyl iodide, were then added to cap the "cyclopentadienide" anion and form the 1,2-addition product (Scheme 1.2). Unlike the milder Grignard reagents, organolithium reagents gave high product yields.[75] The 'R' in Scheme 1.2 represents groups such as methyl, allyl, isopropyl, t-butyl and phenyl.

---

[71] Wudl, F. The Chemical Properties of Buckminsterfullerene (C_{60}) and the Birth and Infancy of Fulleroids. *Acc. Chem. Res.* **1992**, *25*, 157–161.

[72] Hirsch, A.; Soi, A.; Karfunkel, H. R. Titration of C_{60}: A Method for the Synthesis of Organofullerenes. *Angew. Chem., Int. Ed. Engl.* **1992**, *31*, 766–768.

[73] Hirsch, A.; Grosser, T.; Skiebe, A.; Soi, A. Synthesis of Isomerically Pure Organodihydrofullerenes. *Chem. Ber.* **1993**, *126*, 1061–1067.

[74] Fagan, P. J.; Krusic, P. J.; Evans, D. H.; Lerke, S. A.; Johnston, E. Synthesis, Chemistry, and Properties of a Monoalkylated Buckminsterfullerene Derivative, *t*-Bu60 Anion. *J. Am. Chem. Soc.* **1992**, *114*, 9697–9699.

[75] Hirsch, A. Nucleophilic Additions. *The Chemistry of the Fullerenes;* Thieme Medical Publishers, Inc.: New York, 1994; p 58.

Scheme 1.2

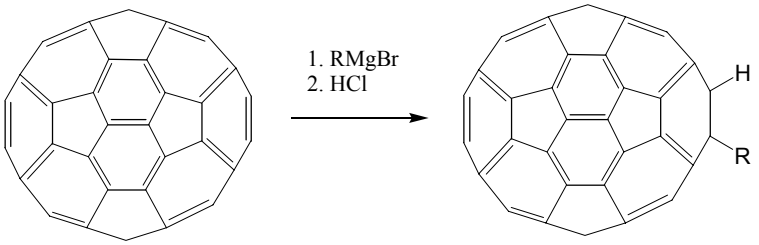

Cyclopropanation reactions were found to readily occur with the C_{60} fullerene. An example of the latter, which was developed by Bingel,[76] shows that a clean cyclopropanation with C_{60} occurs with carbon nucleophiles (carbanions) of α-halo esters and α-halo ketones (Scheme 1.3). Sodium hydride (NaH) deprotonates the diethyl bromomalonate, which adds to the pyracylene site of C_{60} to form the adjacent stabilized anion. The cyclopropyl ring on the mono-adduct is formed by an S_N2 displacement of bromine. This reaction was performed at room temperature.

Scheme 1.3

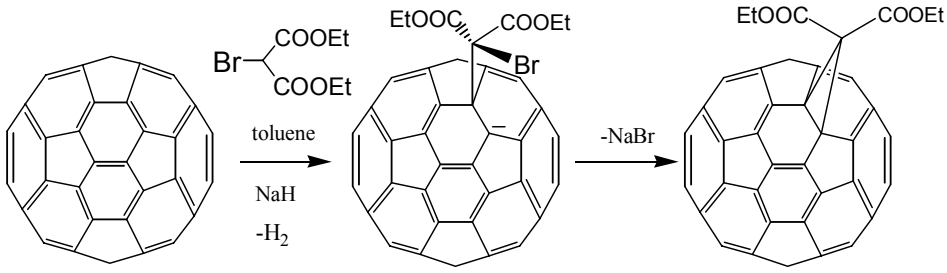

Highly nucleophilic primary and secondary aliphatic amines were found to undergo facile additions to C_{60}.[77-79] When C_{60} was treated with a primary amine, such as propylamine or ethylenediamine, the magenta-colored C_{60} solution quickly became a

---

[76] Bingel, C. Cyclopropanierung von Fullerenen. *Chem. Ber.* **1993**, *126*, 1957–1959.

[77] Hirsch, A.; Li, Q.; Wudl, F. Globe-trotting Hydrogens on the Surface of the Fullerene Compound $C_{60}H_6(N(CH_2CH_2)_2O)_6$. *Angew. Chem., Int. Ed. Engl.* **1991**, *30*, 1309–1310.

[78] Seshadri, R.; Govindaraj, A.; Nagarajan, R.; Pradeep, T.; Rao, C. N. R. Addition of Amines and Halogens to Fullerene C_{60} and C_{70}. *Tetrahedron Lett.* **1992**, *33*, 2069–2070.

[79] Skiebe, A.; Hirsch, A.; Klos, H.; Gotschy, B. [DBU]C_{60}. Spin pairing in a fullerene salt. *Chem. Phys. Lett.* **1994**, *220*, 138–140.

green color. After about 15 hours the solution turned a brownish color. ESR analysis showed that radicals of C_{60} and amino radicals were present, thus yielding evidence that the addition mechanism was stepwise. The brownish product was diamagnetic, while the green colored intermediate is typical for anionic complexes of C_{60} (Scheme 1.4). In the first step of the reaction, a single-electron is transferred to the cage to form the "cyclopentadienide" anion. The positively charged amino radical and the C_{60} radical

Scheme 1.4

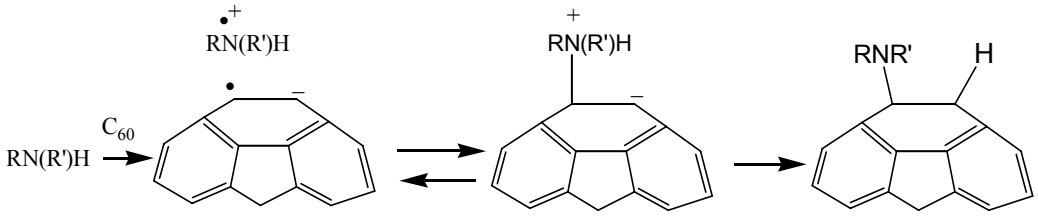

recombine to give a green intermediate. Proton transfer from the covalently bonded amino group yields the neutral brown product.

Secondary amines, such as piperazine, *N,N*'-dimethylethylenediamine or homopiperazine, add smoothly to C_{60}.[80] In dilute solutions of the reactants, mono- and bisadducts are predominantly formed, even if a large excess of the diamine is added.

1.4.1.3. Cycloaddition reactions with C_{60}

Empty-cage fullerenes are strong dieno/dipolarophiles that readily undergo cycloaddition reactions across the [6,6] bond-junctures of their pyracylene-type units. The ability of C_{60} to undergo these reactions has enabled almost any functional group to be covalently linked to the molecule. Conditions for the reactions are strongly dependent on the reactivity of the dienes.

A variety of endocyclic and exocyclic dienes have been attached to C_{60} using Diels-Alder [4+2] cycloadditions. Scheme 1.5 illustrates how cyclopentadiene[81,82] and

[80] Kampe, K.-D.; Egger, N.; Vogel, M. Diamino and Tetraamino Derivatives of Buckminsterfullerene C_{60}. *Angew. Chem., Int. Ed. Engl.* **1993**, *32*, 1175–1176.

anthracene,[82,83,84] both endocyclic, react with C_{60} to produce mono-adducts. The addition of cyclopentadiene (*ca.* 1.5 equiv.) to C_{60} afforded high product yields, whereas a ten-fold equivalence of anthracene promoted only a small amount (*ca.* 25%) of adduct formation.

Scheme 1.5

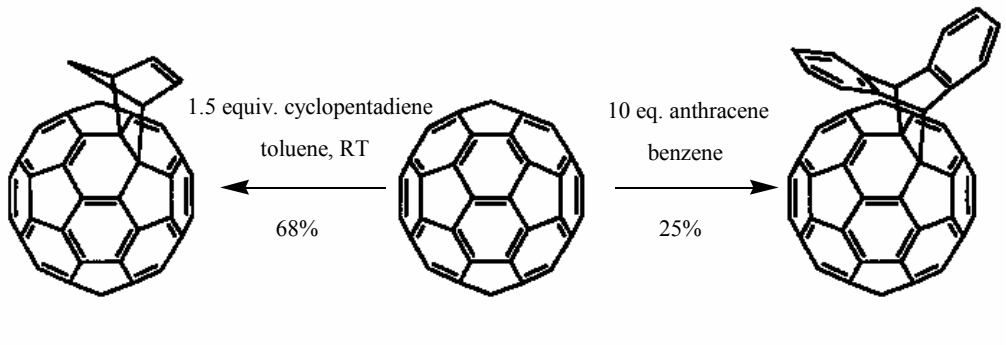

The adducts were heated to demonstrate the ease of the retro-Diels-Alder reaction. However, this thermal reversibility led to problems when obtaining mass spectrometry data. To combat the problem, pentamethylcyclopentadiene, an electron donating diene, was employed to promote thermally stabile mono-adducts.[85]

For exocyclic [4+2] cycloadditions, the reaction between C_{60} and 2,3-dimethylbutadiene led to a three dimensional hexa-adduct with T_h symmetry (Scheme 1.6).[86,87] This adduct resembled the skeletal structure of the radiolarian *Hexacontium asteracanthion* (virus), and was stable under nitrogen for 12 hours at room temperature.

---

[81] Rotello, V. M.; Howard, J. B.; Yadav, T.; Conn, M. M.; Viani, E.; Giovane, L. M.; Lafleur, A. L. Isolation of Fullerene Products from Flames: Structure and Synthesis of the C_{60}-Cyclopentadiene Adduct. *Tetrahedron Lett.* **1993**, *34*, 1561–1562.

[82] Tsuda, M.; Ishida, T.; Nogami, T.; Kurono, S.; Ohashi, M. Isolation and Characterization of Diels-Alder Adducts of C_{60} with Anthracene and Cyclopentadiene. *J. Chem. Soc., Chem. Commun.* **1993**, 1296–1298.

[83] Schlueter, J. A.; Seaman, J. M.; Taha, S.; Cohen, H.; Lykke, K. R.; Wang, H. H.; Williams, J. M. Synthesis, Purification, and Characterization of the 1:1 Addition Product of C_{60} and Anthracene. *J. Chem. Soc., Chem. Commun.* **1993**, 972–974.

[84] Rubin, Y.; Khan, S.; Freedberg, D. I.; Yeretzian, C. Synthesis and X-ray Structure of a Diels-Alder Adduct of C_{60}. *J. Am. Chem. Soc.* **1993**, *115*, 344–345.

[85] Meidine, M. F.; Avent, A. G.; Darwish, A. D.; Kroto, H. W.; Ohashi, O.; Taylor, R.; Walton, D. R. M. Pentamethylcyclopentadiene Adducts of [60]- and [70]- Fullerene. *J. Chem. Soc., Perkin Trans. 2* **1994**, 1189–1193.

[86] Krautler, B.; Maynollo, J. A Highly Symmetric Sixfold Cycloaddition Product of Fullerene C_{60}. *Angew. Chem., Int. Ed. Engl.* **1995**, *34*, 87–88.

[87] Maynollo, J.; Krautler, B. Diels-Alder Reaction of the [60]fullerene: From regularly functionalized carbon spheres to cyclophanes. *Fullerene Sci. Techn.* **1996**, *4*, 213–226.

Scheme 1.6

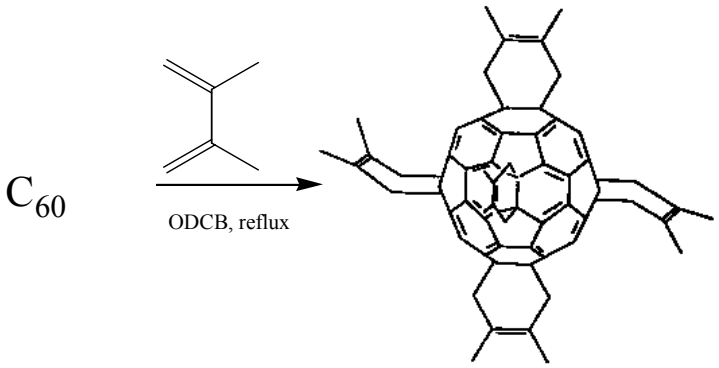

Although Diels-Alder [4+2] adducts of C_{60} represent the majority of cycloaddition functionalizations, other cycloaddition reactions, such as [2+1], [2+2] and [3+2], have been thoroughly documented over the last 10-12 years.

1.4.1.4. Radical additions to C_{60}

Thermally and photochemically initiated radical additions to C_{60} take place with a variety of precursor molecules. Similar to nucleophiles, a large variety of radicals easily add to C_{60}, forming both paramagnetic and diamagnetic adducts. When radicals add across the [6,6] ring-juncture (pyracylene-type units), unpaired electrons become highly localized on the C_{60} surface. Because of its tremendous reactivity towards radicals, McEwen co-workers[88] have suggested that C_{60} is a "radical sponge".

Mono-radical adducts of C_{60} have been produced using a variety of methods. In one case, Yoshida and colleagues[89] used fluoroalkyl halides and Bu_3SnH with a radical initiator to conveniently prepare fluoroalkyl-modified C_{60} adducts (Scheme 1.7).

---

[88] McEwen, C. N.; McKay, R. G.; Larsen, B. S. C_{60} as a Radical Sponge. *J. Am. Chem. Soc.* **1992**, *114*, 4412–4414.

[89] Yoshida, M.; Suzuki, D.; Iyoda, M. Convenient Synthesis of 1-Fluoroalkyl-2-hydro[60]fullerene Using Fluoroalkyl Halide with Tributyltin Hydride under Radical Conditions. *Chem. Lett.* **1996**, 1097−1098.

Scheme 1.7

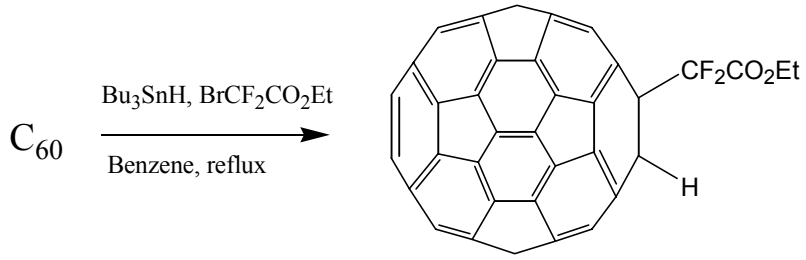

It is worth noting that fluoroalkyl analogues of C_{60} were thermally stable and did not undergo α- or β-eliminations, as opposed to additions with nucleophilic alkyl reagents.

Multiple radical additions arose when C_{60} solutions were irradiated for a prolonged period of time in the presence of excess radical precursors. Krusic et al.[90] demonstrated that photochemically generated benzyl radicals react with C_{60} to provide radical and non-radical adducts, $(C_6H_5CH_2)_nC_{60}$, with n=1 to at least 15. Radical adducts have been identified by ESR spectroscopy as allylic $(C_6H_5CH_2)_3C_{60}$ and cyclopentadienyl $(C_6H_5CH_2)_5C_{60}$ radicals (Scheme 1.8). The stability of the fourth intermediate is restricted due to the two unfavorable [5,6] double-bonds on the fullerene cage. However, addition of a fifth benzyl radical ('R' in Scheme 1.8) is favored in order to form the resonance stabilized intermediate.

[90] Krusic, P. J.; Wasserman, E.; Keizer, P. N.; Morton, J. R.; Preston, K. F. Radical Reactions of C_{60}. *Science* **1991**, *254*, 1183–1185.

Scheme 1.8

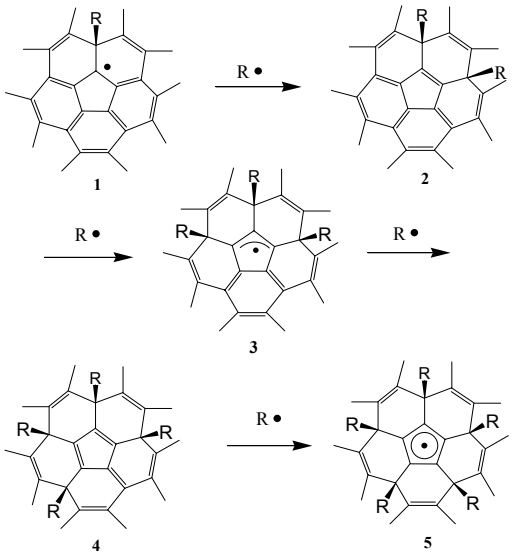

1.4.2. Reactivity of traditional metallofullerenes

Derivatives of traditional metallofullerenes are of great interest due to the novel properties they may provide. However, the chemical properties of metallofullerenes will undoubtedly be altered, with respect to their corresponding empty cage, as a result of encapsulating metal atoms and acquiring addition charge on the carbon cage. Efforts to discover the chemical properties of these materials remain hampered by their limited availability, their difficult purification, and the stability of the molecules towards oxygen.

1.4.2.1. Radical addition with traditional metallofullerenes

Akasaka and colleagues[91,92,93] were the first individuals to chemically functionalize a mono- and dimetallofullerene species. Using only small amounts of material (0.1 – 1

[91] Akasaka, T.; Kato, T.; Kobayashi, K.; Nagase, S.; Yamamoto, K.; Funasaka, H.; Takahashi, T. Exohedral adducts of La@C_{82}. *Nature* **1995**, *374*, 600–601.

[92] Akasaka, T.; Nagase, S.; Kobayashi, K.; Suzuki, T.; Kato, T.; Yamamoto, K.; Funasaka, H.; Takahashi, T. Exohedral Derivatization of an Endohedral Metallofullerene Gd@C_{82}. *J. Chem. Soc., Chem. Commun.* **1995**, 1343–1344.

[93] Akasaka, T.; Nagase, S.; Kobayashi, K.; Suzuki, T.; Kato, T.; Kikuchi, K.; Achiba, Y.; Yamamoto, K.; Funasaka, H.; Takahashi, T. Synthesis of the First Adducts of the Dimetallofullerenes La_2@C_{80} and Sc_2@C_{84} by Additon of a Disilirane. *Angew. Chem., Int. Ed. Engl.* **1995**, *34*, 2139–2141.

mg), they found that La@C_{82}, Gd@C_{82} and La_2@C_{80} reacted both thermally and photochemically with an excess of 1,1,2,2-tetrakis(2,4,6-trimethylphenyl)-1,2-disilirane (Mes = 2,4,6-trimethylphenyl) (Scheme 1.9), whereas the empty-caged fullerenes

Scheme 1.9

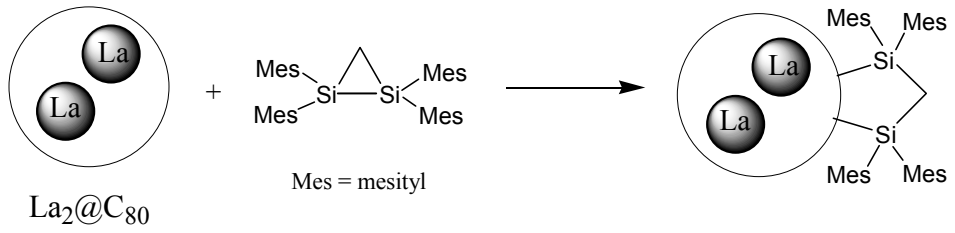

La_2@C_{80}

(i.e., C_{60}, C_{70}, C_{76}, C_{82}) were only reactive under the photochemical conditions. The mass spectrometry analysis showed that only 1:1 adducts were formed in each case.

All three metallofullerenes had lower reduction potentials (i.e., -0.31V for La_2@C_{80} vs. -1.12V for C_{60})[93] than the previously noted empty-cage fullerenes. Therefore, when the reactions occur under thermal conditions, exclusive radical addition to the metallofullerenes is due to their stronger electron-accepting character. However, while the reduction potential of Sc_2@C_{84} is only slightly higher than La_2@C_{80}, the thermal addition is suppressed, as in the case with the empty-cages. These results suggest that thermal addition is initiated by electron transfer from 1,1,2,2-tetrakis(2,4,6-trimethylphenyl)-1,2-disilirane to the metallofullerene cages. Adducts with multiple additions were not observed, and a fully characterized structure of the 1:1 adducts remains unresolved at the present time.

1.4.2.2. Electrophilic and nucleophilic additions

The paramagnetic nature of La@C_{82} and Y@C_{82} allows one to monitor chemical

reactivity by ESR spectroscopy. Tumanskii et al.[94-96] studied the reactivity of La@C_{82} (isomers I and II) in a mixture with C_{60} and C_{70}, versus L_2Pt^o (RHg-Pt(PPh_3)$_2$-Br), a phosphoryl radical (•P(O)(O*i*Pr)$_2$) and trifluoroacetic acid (TFA). The reaction was then monitored with electron spin resonance (ESR) spectroscopy. Whereas the first two reagents did not change the ESR spectra of lanthanum in La@C_{82}, an excess of the TFA produced new signals for isomer II that were attributed to the formation of a protonated metallofullerene, $[La@C_{82}H]^+•(OCOCF_3)^-$. Multiplets of isomer I did not change. The same reactivity was also found for Y@C_{82}. These results demonstrated the nucleophilic character of the metallofullerene carbon cages, and the ability to selectively distinguish between two isomers.

In a different experiment, Suzuki and co-workers[97] showed that the chemical reaction of La@C_{82} (1 mg) and an excess of diphenyldiazomethane (Ph_2CN_2) at 60 ºC gave adducts with one to three additions. All products were characterized using ESR spectroscopy and fast atom bombardment mass spectrometry (FAB MS).

1.4.2.3. Hydroxylation of traditional metallofullerenes

Water-soluble metallofullerenols have been synthesized from procedures that are similar to those used for C_{60} hydroxylations. Kato and co-workers[98] recently synthesized a multi-hydroxylated fullerene, Gd@$C_{82}(OH)_n$ (n = 30-40), using the transfer agent (TBAOH) procedure developed by Li et al.[56] (section *1.4.1.1.*). On the other hand, Sun

---

[94] Tumanskii, B. L.; Bashilov, V. V.; Solodovnikov, S. P. Sokolov, V. I.; Bubnov, V. P.; Laukhina, E. E.; Estrin, Y. I.; Kol'tover, V. K.; Yagubskii, E. B. EPR Study of reactivity of endohedral metallofullerene La@C_{82} and Y@C_{82}. *Fullerene Sci. Techn.* **1998**, *6*, 445–451.

[95] Bashilov, V. V.; Tumanskii, B. L.; Petrovoskii, P. V.; Sokolov, V. I. Heterometallic binuclear complexes involving the mercury–platinum bond as a source of a platinum carbenoid in reactions with fullerene-60. *Russ. Chem. Bull., Eng. Trans.* **1994**, *43*, 1069–1072.

[96] Tumanskii, B. L.; Bashilov, V. V.; Solodovnikov, S. P.; Sokolov, V. I. EPR Investigation of the Adducts of Element-Centered Radicals with Polyhedral Carbon Clusters (Fullerenes). *Russ. Chem. Bull., Eng. Trans.* **1992**, *41*, 1140–1141.

[97] Suzuki, T.; Maruyama, Y.; Kato, T. Chemical Reactivity of a Metallofullerene: EPR Study of Diphenylmethano-La@C_{82} Radicals. *J. Am. Chem. Soc.* **1995**, *117*, 9606–9607.

[98] Kato, H.; Suenaga, K.; Mikawa, M.; Okumura, M.; Miwa, N.; Yashiro, A.; Fujimura, H.; Mizuno, A.; Nishida, Y.; Kobayashi, K.; Shinohara, H. Syntheses and EELS characterization of water-soluble multi-hydroxyl Gd@C_{82} fullerenols. *Chem. Phys. Lett.* **2000**, *324*, 255–259.

and co-workers[99] synthesized $Pr@C_{82}O_m(OH)_n$ ($m \approx 10$ and $n \approx 10$) using NO_2 under an oxygen environment. Both polyhydroxylated species were found to be extremely difficult to characterize by mass spectrometry and elemental analysis.

1.5. Electronic properties of traditional and trimetallic nitride metallofullerenes

1.5.1. Electrochemistry

The reductive/oxidative (redox) properties of a few traditional metallofullerenes have been investigated using cyclic voltammetry (CV). Suzuki et al.[100] measured the cyclic voltammograms of $La@C_{82}$, and discovered that the redox properties are different than many of the empty-cage fullerenes (i.e., C_{60}, C_{70} and C_{84}). Not only was $La@C_{82}$ a moderate electron-donor, but it was also a stronger electron-acceptor than C_{60}, C_{70} and C_{84}. Interestingly, when one electron was transferred to the paramagnetic C_{82} cage of $La@C_{82}$, the resulting charged species was a diamagnetic metallofullerene with a closed-shell electronic state of $(La^{+3}@[C_{82}]^{-4})^{-1}$. The added electron had filled the singly occupied HOMO, thereby maintaining the +3 charge on the encapsulated La atom.[100,101] Cationic species resulted from the one electron oxidation of $La@C_{82}$, which once again forms a closed-shell electronic state. Similar redox properties were discovered for the $Y@C_{82}$, $Ce@C_{82}$, $Gd@C_{82}$ and $Sc@C_{82}$ mono-metallofullerenes,[102-104] and $Sc_3@C_{82}$.[105]

---

[99] Sun, D.; Huang, H.; Yang, S. Synthesis and Characterization of a Water-Soluble Endohedral Metallofullerol. *Chem. Mater.* **1990**, *11*, 1003–1006.

[100] Suzuki, T.; Maruyama, Y.; Kato, T. Electrochemical Properties of $La@C_{82}$. *J. Am. Chem. Soc.* **1993**, *115*, 11006–11007.

[101] Akasaka, T.; Wakahara, T.; Nagase, S.; Kobayashi, K.; Waelchli, M.; Yamamoto, K.; Kondo, M.; Shirakura, S.; Okubo, S.; Maeda, Y.; Kato, T.; Kako, M.; Nakadaira, Y.; Nagahata, R.; Gao, X.; Van Caemelbecke, E.; Kadish, K. M. $La@C_{82}$ Anion. An Unusually Stable Metallofullerene. *J. Am. Chem. Soc.* **2000**, *122*, 9316–9317.

[102] Suzuki, T.; Kikuchi, K.; Oguri, F.; Nakao, Y.; Suzuki, S.; Achiba, Y.; Yamamoto, K.; Funasaka, H.; Takahashi, T. Electrochemical Properties of Fullerenolanthanides. *Tetrahedron* **1996**, *52*, 4973–4982.

[103] Anderson, M. R.; Dorn, H. C.; Burbank, P. M.; Gibson, J. R. Voltammetric Studies of $M_n@C_{82}$. In *Fullerenes: Recent Advances in the Chemistry and Physics of Fullerenes and Related Materials.* Kadish, K., Ruoff, R., Eds.; The Electrochemical Society, Inc.: Pennington, NJ, 1997; Vol. 4, pp 448–456.

[104] Rübsam, M.; Schweitzer, P.; Dinse, K.-P. Rotational Dynamics of Metallo-endofullerenes in Solution. *J. Phys. Chem.* **1996**, *100*, 19310–19314.

Currently, little is known of the electrochemical properties of the trimetallic nitride endohedrals. Recent results suggest that $Sc_3N@C_{80}$ reacts much differently than the traditional species.[106] Upon a one electron reduction at room temperature the $Sc_3N@C_{80}$ solution changed color, and an ESR signal was detected. However, the electron was not accepted by the cage, but instead was donated back into the Sc_3N cluster, as evident by the fifteen line ESR signal of the Sc (I = 7/2) atoms with a large hyperfine coupling. No coupling was observed to nitrogen (I = 1).

The closed-shell electronic state of highly stable $Sc_3N@C_{80}$ is formally described as $[Sc_3N]^{+6}@[C_{80}]^{-6}$. Thus, to remain an overall stable species, the electron must not be accepted by the LUMO of the diamagnetic I_h C_{80} cage. The newly formed anionic species is presumed to have an electronic configuration of $([Sc_3N]^{+5}@[C_{80}]^{-6})^{-1}$.

1.5.2. UV-Vis-NIR absorption

The UV-Vis-NIR absorption spectra of metallofullerenes are very different from those of the empty-cages. Normally, mono-metallofullerenes show absorbances out to *ca.* 1500 nm, due to their lower energy HOMO–LUMO gaps (band-gaps). The absorption spectra for the major isomers (C_2, C_{2V} and C_{3V}) of mono-metallofullerenes, such as $M@C_{82}$ (M = Sc, Y, La),[22,107,108] are all well represented by a sharp peak around 1000 nm and broad peak around 1400 nm. A 1.3 eV (1000 nm) band-gap has been observed for $La_2@C_{80}$.[11]

Dorn and colleagues[11] observed similar data for $Sc_3N@C_{80}$, which illustrated a maximum absorbance around 1560 nm, and corresponds to a band-gap of 0.8 eV. However, DFT calculations[45-47] and electron affinity measurements[109] have shown that

---

105 Shinohara, H.; Sato, H.; Ohkohchi, M.; Ando, Y.; Kodama, T.; Shida, T.; Kato, T.; Saito, Y. Encapsulation of a Scandium Trimer in C_{82}. *Nature* **1992**, *357*, 52–54.

106 Jakes, P.; Dinse, K.-P. Chemically Induced Spin Transfer to an Encased Molecular Cluster: An EPR Study of Sc3N@C80 Radical Anions. *J. Am. Chem. Soc.* **2001**, *123*, 8854–8855.

107 Kikuchi, K.; Suzuki, S.; Nakao, Y.; Nakahara, N.; Wakabayashi, T.; Shiromaru, H.; Saito, K.; Ikemoto, I.; Achiba, Y. Isolation and characterization of the metallofullerene LaC_{82}. *Chem. Phys. Lett.* **1993**, *216*, 67–71.

108 Kikuchi, K.; Nakao, Y.; Suzuki, S.; Achiba, Y. Characterization of the Isolated $Y@C_{82}$. *J. Am. Chem. Soc.* **1994**, *116*, 9367–9368.

109 Ioffe, I. N.; Ievlev, A. S.; Boltalina, O. V.; Sidorov, L. N.; Dorn, H. C.; Stevenson, S.; Rice, G. Electron Affinity of some Trimetallic Nitride and Conventional Metallofullerenes. *Int. J. Mass Spectrom.* **2002**, *213*, 183–189.

the true band-gap is much larger (2–6.5 eV), which supports the reason for the lower reactivity and higher abundance of $Sc_3N@C_{80}$. The observed small band-gap may have resulted from the recently discovered D_{5h} isomer of $Sc_3N@C_{80}$ (Chapter 5).

1.6. Fullerene and metallofullerene-based materials

1.6.1. Fullerene-containing polymers

At the present time, fullerene-containing polymers have been synthesized with C_{60} and C_{70} fullerenes, albeit the majority of the work has been with the former. When fullerenes are incorporated into a polymer, the individual properties of each fullerene are transferred to the bulk. As a result, this enables the preparation of novel electroactive, photoactive and non-linear optical polymers.

The incorporation of C_{60} with polymers has produced basically five types of structural combinations.[110-113] These combinations include: 1) fullerenes in the backbone of the polymer chain (pearl necklace or in-chain); 2) polymers bearing pendant fullerenes (pendant charm bracelet or on-chain); 3) random polymers irradiating from a fullerene spheroid (starburst type or cross-link type); 4) polymers terminated by a fullerene unit (end-chain type); 5) dendrimers (Figure 1.13).[110]

---

[110] Prato, M. Fullerene Materials. In *Fullerenes and Related Structures*. Hirsch, A., Ed.; Springer: New York, 1999; Vol. 199, pp 173–187; Prato, M. [60] Fullerene chemistry for materials science applications. *J. Mater. Chem.* **1997**, *7*, 1097–1109.

[110] Mirkin, C. A.; Caldwell, W. B. Thin Film, Fullerene-Based Materials. *Tetrahedron* **1996**, *52*, 5113–5130.

[111] Hirsch, A. Fullerene Polymers. *Adv. Mater.* **1993**, *5*, 859–861.

[112] Okamura, H.; Terauchi, T.; Minoda, M.; Fukada, T.; Komatsu, K. Synthesis of 1,4-Dipolystyryldihydro[60]fullerenes by Using 2,2,6,6-Tetramethyl-1-polystyroxypiperidine as a Radical Source. *Macromolecules* **1997**, *30*, 5279–5284.

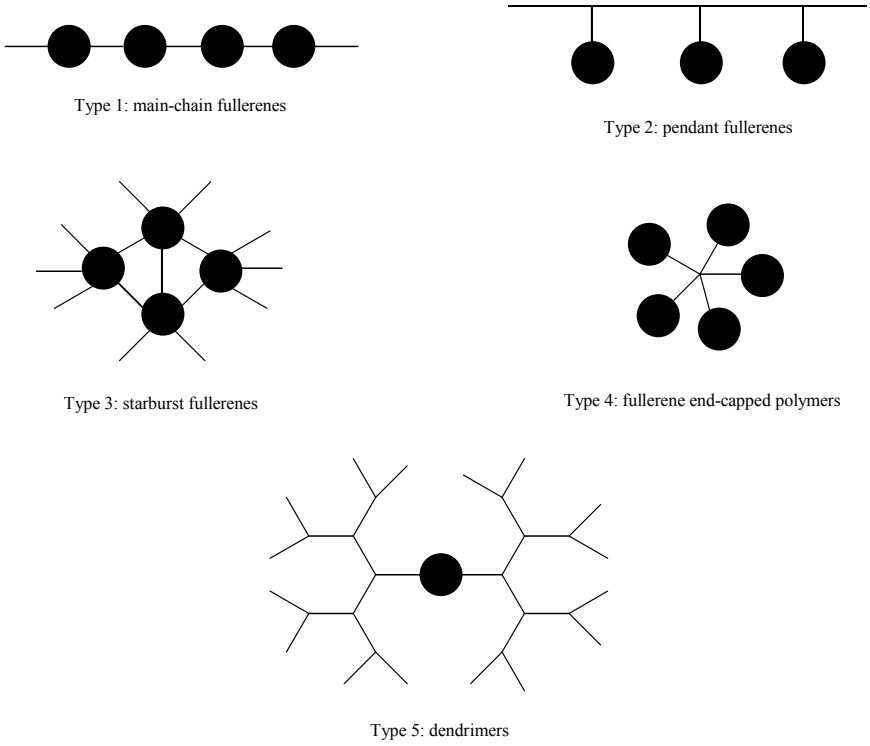

Figure 1.13. Various types of C_{60} fullerene-containing polymers.

Fullerenes have been incorporated into polymers by methods such as thermal and photochemical cycloadditions, free radical polymerizations, anionic addition of living polymerizations, and electrochemical polymerizations.

Tajima and co-workers[113] produced a cross-linked polymer through the photochemical cycloaddition of C_{60} with furan units on the polymer side chain. The polymer chain was a radical synthesized poly(2-hydroxyethylmethacrylate) (PHMA), and the furan group of the side chain was attached by reaction with 2-furoyl chloride (Scheme 1.10).

[113] Tajima, Y.; Tezuka, Y.; Yajima, H.; Ishii, T.; Takeuchi, K. Photo-crosslinking polymers by fullerene. *Polymer* **1997**, *38*, 5255–5257.

Scheme 1.10

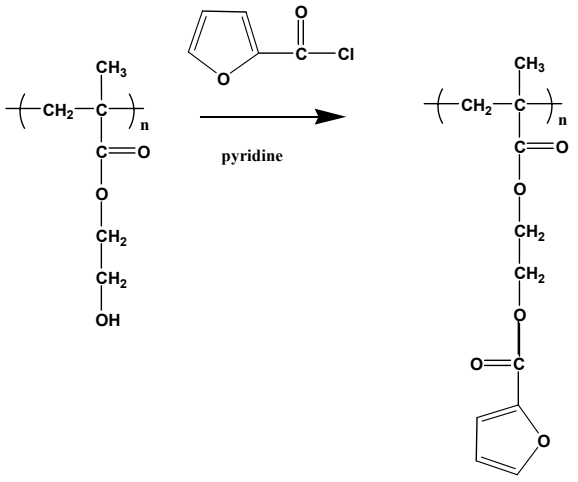

When excited by UV or visible light, C_{60} binds to one furan unit of a PHMA chain to yield a C_{60}-containing polymer. The C_{60} moiety in the C_{60}-containing polymer then binds to furan units of other PHMA chains to construct the fullerene-polymer network.

Under radical conditions, Cao and Webber[114] were able to copolymerize C_{60} and styrene into star-like structures with C_{60} at the core. These materials are known as "flagellenes". The copolymerization was performed in both the bulk and when co-dissolved in an aromatic solvent. Absorption by the copolymer was strongly modified from that of the parent fullerene. Furthermore, the fluorescence of the polymer was blue-shifted and much stronger. Ford and collaborators[115] reported a comparison between poly(methyl methacrylate) (PMMA)/C_{60} and polystyrene (PS)/C_{60} systems that were generated via radical-chain polymerization. Whereas the high molecular weight polystyrene contained from ten to one hundred fullerene units, the high molecular weight PMMA contained an average of only one C_{60} unit per polymer chain.

---

[114] Cao, T.; Webber, S. E. Free-Radical Copolymerization of Fullerenes with Styrene. *Macromolecules* **1995**, *28*, 3741–3743.

[115] Ford, W. T.; Graham, T. D.; Mourey, T. H. Incorporation of C_{60} into Poly(methyl methacrylate) and Polystyrene by Radical Chain Polymerization Produces Branched Structures. *Macromolecules* **1997**, *30*, 6422–6429.

An anionic living polymerization of polystyrene and C_{60} was also used to synthesize flagellene-type adducts.[116] The adducts were given this name because they are comprised of flexible polymeric chains covalently attached to a fullerene "sphere", thus having a resemblance to the snake-like appendages of the Flagellata-unicellular protozoa. Additions of the polystyrene anions occurred across the [6,6] bond-junctures of the pyracylene-type units on C_{60}, and the fullerene anions were then capped with iodomethane (Scheme 1.11). The number of polymeric arms ranged from 1 to ~10.

Scheme 1.11

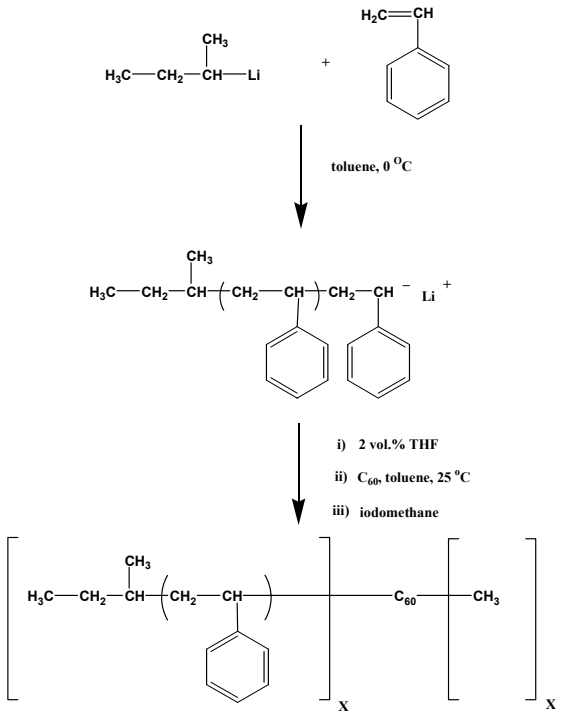

Alternatively, the fullerene anions were capped with protons.[117]

Amphiphilic star-like polymers with a fullerene core were prepared by Delpeux and colleagues (Figure 1.14).[118a] To accomplished this, monomethyl ethers of oligomeric

[116] Samulski, E. T.; DeSimone, J. M.; Hunt, M. O., Jr.; Menceloglu, Y. Z.; Jarnagin, R. C.; York, G. A.; Labat, K. B.; Wang, H. Flagellenes: Nanophase-Separated, Polymer-Substituted Fullerenes. *Chem. Mater.* **1992**, *4*, 1153–1157.

[117] Wignall, G. D.; Affholter, K. A.; Bunick, G. J.; Hunt, M. O., Jr.; Menceloglu, Y. Z.; DeSimone, J. M.; Samulski, E. T. Synthesis and SANS Structural Characterization of Polymer-Substituted Fullerenes (Flagellenes). *Macromolecules* **1995**, *28*, 6000–6006.

polyoxyethylenes having azide end-groups [$CH_3O(CH_2CH_2O)_nCH_2CH_2N_3$] were treated with C_{60}. A water-soluble fullerene-containing polymer was achieved when the number

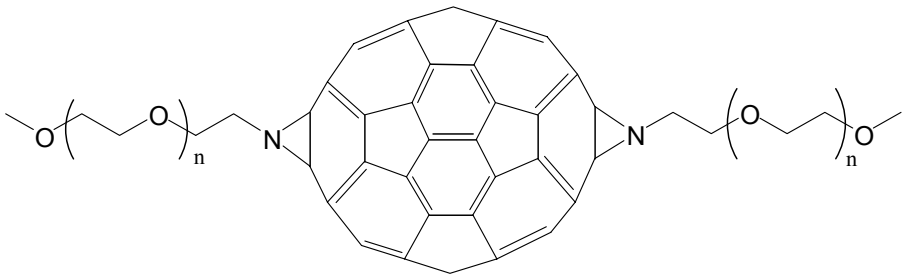

Figure 1.14. Poly(oxyethylene) arms on C_{60}.

and length of the hydrophilic arms became large enough. In similar work, hydrophilic monoaminopolyethers (crown ethers) of various sizes were attached to C_{60} fullerene to evaluate the water solubility of the joint complex.[118b] Some of the crown ethers used include: 2-(aminomethyl)-15-crown-5, 2-(aminomethyl)-18-crown-6, and 1-aza-18-crown. As the size of the polymeric crown ether became larger, the solubility of the complex increased. Star-like fullerene-polymers with extremely long chains have been employed as surface activating agents (surfactants) during emulsion polymerizations. The long ether-based chains act as the hydrophilic ends, while the fullerene cores form a hydrophobic shell on the outside.[118b]

In forthcoming years, metallofullerenes may fashion polymeric networks that exhibit novel chemical and physical properties which are otherwise unattainable with C_{60} and empty-cage fullerenes. Potential applications include photovoltaics, quantum computing and semiconductors.

---

[118] (a) Delpeux, S.; Beguin, F.; Benoit, R.; Erre, R.; Manolova, N.; Rashkov, I. Fullerene Core Star-like Polymers—1. Preparation from Fullerenes and Monoazidopolyethers. *Eur. Polym. J.* **1998**, *34*, 905–915. (b) Delpeux, S.; Beguin, F.; Manolova, N.; Rashkov, I. Fullerene core star-like polymers. 2. Preparation from fullerenes and linear or cyclic monoaminopolyethers. *Eur. Polym. J.* **1999**, *35*, 1619–1628.

1.6.2. Films, mono-layers, supramolecular assemblies and nanodevices

Fullerenes and metallofullerenes are interesting molecules due to their unique photophysical, photoelectric and photo-electrochemical properties. Self-assembled monolayers (SAM) and Langmuir–Blodgett (LB) films are two methods for controlling structure at the molecular level, thereby allowing one to tailor design a nanodevice which meets a specific application.

Dominguez and co-workers[119] formed a self-assembled monolayer on a gold surface using a phenanthroline[C_{60}]fullerene (phen-C_{60}) adduct (Figure 1.15). Spontaneous self-

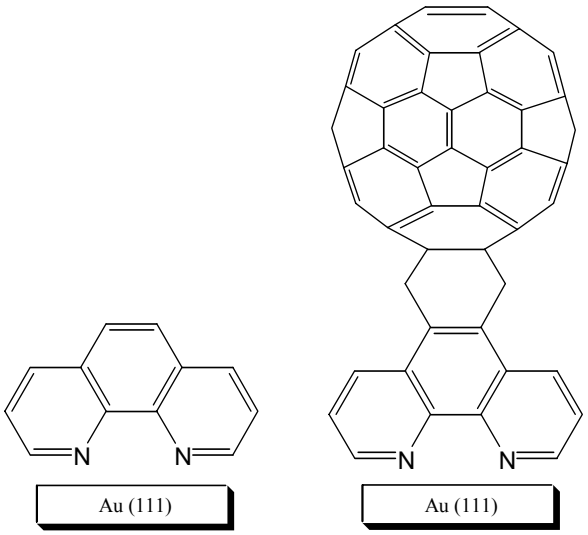

Figure 1.15. Self-assembled phen-C_{60} monolayer on Au (111).

assembly of 1,10-phenanthroline on the Au(111) surface resulted in the formation of well-ordered monolayers; however, addition of phen-C_{60} resulted in the intercalation of the phenanthrolyl group directly into the stacks. Self-assembly from a solution of phen-C_{60}, which contained a small amount of 1,10-phenanthroline, resulted in the formation of a secondary layer of fullerene moieties.[119] The geometry of the packing appeared to be controlled by the dimensions of the two partners, as the fullerene diameter is about 0.1

[119] Dominguez, O.; Echegoyen, L.; Cunha, F.; Tao, N. Self-Assembled Fullerene-Derivative Monolayers on a Gold Substrate Using Phenanthroline-Au Interactions. *Langmuir* **1998**, *14*, 821–824.

nm and the phenanthrolin-phenanthroline distances are approximately 1/3 (0.33 nm). Thiol-functionalized C_{60} fullerenes have also been utilized to prepare self-assembled monolayers.[110,120,121]

The preparation of Langmuir-Blodgett films is difficult due to the highly hydrophobic nature of fullerene and metallofullerene cages, which tend to aggregation on the water surface almost immediately after the solvent evaporates. This problem was reconciled for C_{60} by preparing derivatives with hydrophilic side chains.[122,123]

A novel amphiphilic C_{60} derivative for Langmuir-Blodgett (LB) films, C_{60}-AOOA, was prepared using a thermally reversible Diels-Alder reaction between C_{60} and an anthracene derivative that possessed a terminal carboxylic acid side chain (Scheme 1.12).[124] The temporary introduction of the carboxylic acid functionality provided

Scheme 1.12

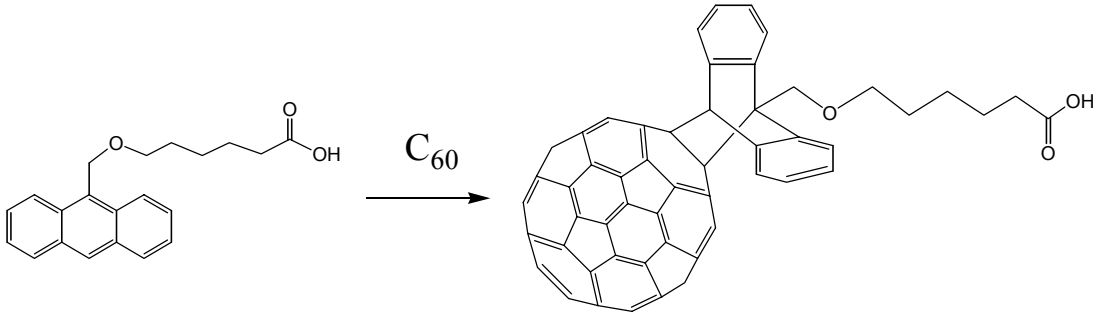

sufficient interaction with the water layer, thereby allowing for a successfully transfer of fullerenes onto a solid substrate to form the LB films (monolayers and/or multi-layers). Upon heating, the C_{60}-AOOA decomposed to yield a C_{60} layer and/or C_{60}/C_{60}-AOOA

---

120 Shi, X.; Caldwell, W. B.; Chen, K.; Mirkin, C. A. A Well-Defined Surface-Confinable Fullerene: Monolayer Self-Assembly on Au(111). *J. Am. Chem. Soc.* **1994**, *116*, 11598–11599.

121 Akiyama, T.; Imahori, H.; Ajawakom, A.; Sakata, Y. Synthesis and Self-Assembly of Porphyrin-linked Fullerene on Gold Surface Using S-Au Linkage. *Chem. Lett.***1996**, 907–910.

122 Cardullo, F.; Diederich, F.; Echegoyen, L.; Habicher, T.; Jayaraman, N.; Leblanc, R. M.; Stoddart, J. F.; Wang, S. Stable Langmuir and Langmuir-Blodgett Films of Fullerene-Glycodendron Conjugates. *Langmuir* **1998**, *14*, 1955–1959.

123 Guldi, D. M.; Tian, Y.; Fendler, J. H.; Hungerbuhler, H.; Asmus, K.-D. Stable Monolayers and Langmuir-Blodgett Films of Functionalized Fullerenes. *J. Phys. Chem.* **1995**, *99*, 17673–17676.

124 Kawai, T.; Scheib, S.; Cava, M. P.; Metzger, R. M. Langmuir-Blodgett Films of a Thermally Labile 1:1 Adduct of C60 Fullerene and 8-(9-Anthryl)-7-oxaoctanoic Acid. *Langmuir* **1997**, *13*, 5627–5633.

mixed layers. Metallofullerene derivatives for Langmuir-Blodgett film preparation have not yet been realized.

LB films were readily prepared using various mixtures of Dy@C_{82} and arachidic acid (AA).[125] Films were fabricated with the vertical dipping method with mixtures (AA/Dy@C_{82}) that were doped with cadmium (Cd^{+2}), as opposed to the molecular aggregates that formed with pure Dy@C_{82}. Ordered layer structures were formed when the molar ratios of the mixture exceeded 2:1. Photoelectrochemical measurements of mixtures without Cd^{+2} demonstrated that the low reduction potential of Dy@C_{82} afforded a photoactive film.[126a]

A novel supramolecular assembly of Dy@C_{82} and *p-tert*-butylcalix[8]arene (C8A) was prepared in order to study the formation of a novel LB film using host-guest complexes.[126b] These [Dy@C_{82}–C8A] complexes, and the resulting LB films, were more difficult to form than those with C_{60} ([C_{60}–C8A]) due to the higher activation barrier for encapsulation of the metallofullerene. The higher barrier was a result of the larger size and loss of rotational freedom (entropy effect) of the cage upon complexation with the calixarene. On the other hand, the resulting complex had a higher stability than [C_{60}–C8A] due to the interaction between the electron rich cage of Dy@C_{82} and the pi-electron system of the calixarene.

Conducting polymers with extended pi-conjugated systems are interesting electronic and optoelectronic materials with potential applications in devices such as photodiodes and solar cells. Based on previous C_{60}/polymer composite work, Fujii and co-workers mixed La@C_{82} and poly(3-hexylthiophene) (PAT-6) into a composite solution and measured the properties of the resulting spin-coated thin film.[127] The photoluminescence

---

[125] Li, X.; Yang, S.; Yang, S.; Xu, Y.; Liu, Y.; Zhu, D. Formation and Structural Characteristics of Langmuir-Blodgett Films of the Endohedral Metallofullerene Dy@C_{82} mixed with Cadmium Arachidate. *Thin Film Solids* **2002,** *413*, 231–236.

[126] (a) Yang, S.; Yang, S. Photoelectrochemistry of Langmuir-Blodgett Films of the Endohedral Metallofullerene Dy@C_{82} on ITO Electrodes. *J. Phys. Chem. B* **2001**, *105*, 9406–9412. (b) Yang, S. Yang, S. Preparation and Film Formation Behavior of the Supramolecular Complex of the Endohedral Metallofullerene Dy@C_{82} with Calix[8]arene. *Langmuir* **2002**, *18*, 8488–8495.

[127] Fujii, A.; Umeda, T.; Shirakawa, T.; Akasaka, T.; Yoshino, K. Photocurrent Enhancement in Conducting Polymer Device by Doping with Endohedral Metallofullerene La@C_{82}. *Jpn. J. Appl. Phys.* **2002**, *41*, 2254–2255.

of the polymer was suppressed by the electron accepting character of La@C_{82}, while the photocurrent intensity of the polymer (PAT-6) was significantly enhanced as the concentration of metallofullerene increased.

Novel supramolecular assemblies, for potential nano-electronic[128] and nano-optoelectronic[129] devices (i.e., quantum computers), have been formed by impregnating single-walled nanotubes (SWNTs) with metallofullerenes. Lee and colleagues[130] demonstrate that the properties of a semi-conducting SWNT could be modified by inserting Gd@C_{82} metallofullerenes. Local elastic strain and a charge transfer effect between the metallofullerene cages and sidewalls of the SWNT caused a decrease (*ca.* 0.5 eV to 0.1 eV) in the SWNT band-gap at sites where Gd@C_{82} was inserted, thereby creating multiple one-dimensional quantum dots of about 10 nm along the length of the tube. These assemblies are known as "peapods".

Luzzi and co-workers[131a] impregnated SWNTs with La_2@C_{80} metallofullerenes (Figure 1.16), and studied sections of the peapod with high-resolution transmission electron microscopy (HR-TEM). The molecules appeared spheroidal, which corroborated the calculations for the geometry optimized structure (D_{2h}) of the I_h C_{80} cage when two La atoms are encapsulated.[43] The authors also concluded that the La–La actual bond distance is slightly larger than predicted by theory. Trimetallic nitride endohedral metallofullerenes, $Er_xSc_{3-x}N$@C_{80} (x = 0-3), have also been placed inside SWNTs to generate peapod systems.

---

[128] Toth, G.; Lent, C. S. Quantum Computing with Quantum-dot Cellular Automata. *Phys. Rev. A* **2001**, *63*, 052315–052323.

[129] Faist, J.; Capasso, F.; Sirtori, C.; Sivco, D. L.; Hutchinson, A. L.; Cho, A. Y. Continuous Wave Operation of a Vertical Transition Quantum Cascade Laser above T = 80 K. *Appl. Phys. Lett.* **1995**, *67*, 3057–3059.

[130] (a) Lee, J.; Kim, H.; Kahng, S.-J.; Kim, G.; Son, Y.-M.; Ihm, J.; Kato, H.; Wang, Z. W.; Okazaki, T.; Shinohara, H.; Kuk, Y. Bandgap Modulation of Carbon Nanotubes by Encapsulated Metallofullerenes. *Nature* **2002**, *415*, 1005–1008. (b) Okazaki, T.; Shimada, T.; Suenaga, K.; Ohno, Y.; Mizutani, T.; Lee, J.; Kuk, Y.; Shinohara, H. Electronic Properties of Gd@C_{82} metallofullerene peapods: $(Gd@C_{82})_n$@SWNTs. *Appl. Phys. A* **2003**, *76*, 475–478.

[131] (a) Smith, B. W.; Luzzi, D. E.; Achiba, Y. Tumbling Atoms and Evidence for Charge Transfer in La_2@C_{80}@SWNT. *Chem. Phys. Lett.* **2000**, *331*, 137–142. (b) Russo, R.; Smith, B. W.; Satishkumar, B. C.; Luzzi, D. E.; Dorn, H. C. Encapsulated molecules in carbon nanotubes. Structure and properties. In *Materials Research Society Symposium Proceedings*; 2001; 675, pp W1.3.1.–W1.3.7.

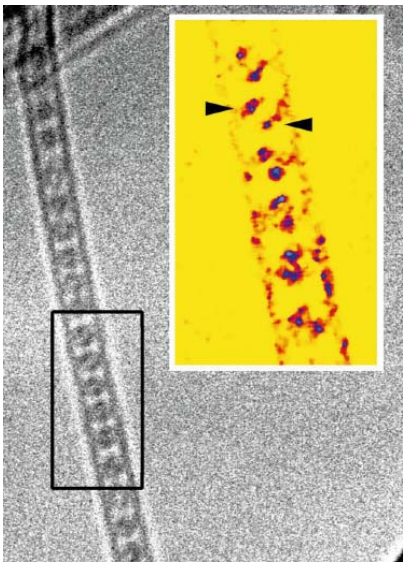

Figure 1.16. $La_2@C_{80}$ 'peapods'. Reprinted from reference 131 with permission from Elsevier.

1.6.3. Medical applications of fullerenes and metallofullerenes

Water-soluble fullerene and metallofullerene derivatives have a potentially large number of applications in medicine. Currently, only a limited number of biodistribution, toxicity and metabolic studies with fullerene derivatives have been conducted. However, even less is known for metallofullerenes due to their extremely limited quantities and unknown functionalization methods.

1.6.3.1. Medicinal applications with C_{60} fullerene

1.6.3.1.1. Toxicity studies

A ^{14}C-labeled pyrrolidinium salt of C_{60} was synthesized and administered to rats intravenously.[132] The compound was observed to accumulate rapidly in the liver, and up to 95% was found localized in the liver after five days. No traces were found in the feces or urine. In a different example, a more hydrophilic ^{14}C-labeled derivative of C_{60} (Figure 1.17), when administered intravenously, was found to accumulate rapidly in various

[132] Bullard-Dillard, R.; Creek, K. E.; Scrivens, W. A.; Tour, J. M. Tissue Sites of Uptake of ^{14}C-lableled C_{60}. *Bioorg. Chem.* **1996**, *24*, 376–385.

tissues, penetrate the blood-brain barrier, and remain in the body after one week.[133] However, when orally administered to rats, the derivative was not effectively absorbed and was excreted in the feces. Acute toxicity of the latter derivative was discovered to be quite low.

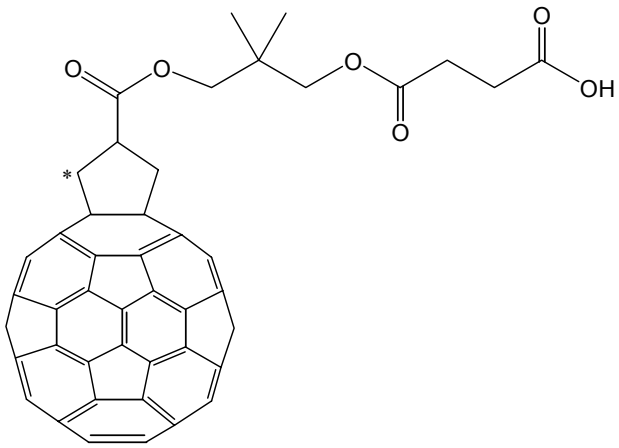

Figure 1.17. ^{14}C-labeled C_{60} derivative.

In vivo studies of fullerenols have demonstrated the ability to suppress the microsomial enzyme levels and decrease the activities of P450-dependent mono-oxygenase, in addition to a concentration dependent inhibition of mitochondrial Mg^{2+}-ATPase activity.[134]

1.6.3.1.2. Antiviral activity

The protease of the human immunodeficiency virus 1 (HIVP) is a viable target for inhibition with C_{60} derivatives, because the cavity of the protease is both cylindrical and lined primarily with hydrophobic amino acids.

---

[133] Yamago, S.; Tokuyama, H.; Nakamura, E.; Kikuchi, K.; Kananishi, S.; Sueki, K.; Nakahara, H.; Enomoto, S.; Ambe, F. *In vivo* biological behavior of a water-miscible fullerene: ^{14}C labeling, absorption, distribution, excretion and acute toxicity. *Chem. Biol.* **1995**, *2*, 385–389.

[134] Ueng, T. H.; Kang, J. J.; Wang, H. W.; Cheng, Y. W.; Chiang, L. Y. Suppression of Microsomal Cytochrome P450-dependent Monooxygenases and Mitochondrial Oxidative Phosphorylation by Fullerenol, a Polyhydroxylated Fullerene C_{60}. *Toxicol. Lett.* **1997**, *93*, 29–37.

Friedman and co-workers used molecular modeling to demonstrate how a functionalized C_{60} molecules would fit into the cavity of the protease.[135] The hydrophobic end (the cage) of the molecule must fit snuggly into the active site, while the water-soluble arms extend out of the active site and into the solvent (Figure 1.18).

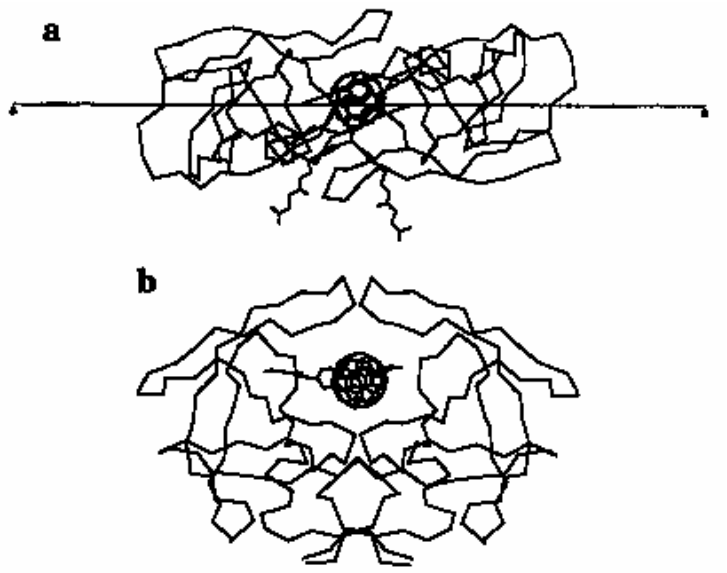

Figure 1.18. (a) Molecular model (side view) of HIVP inhibition with a C_{60} fullerene derivative, and (b) top view of HIVP inhibition. Reprinted with permission from reference 135a. Copyright 1993 American Chemical Society.

In vitro studies, with a "first generation" water-soluble derivative, showed inhibition of acutely and chronically affected peripheral blood mononuclear cells (PBMC) with an EC_{50} of 7 μm.[136,137] No cytotoxic effects were recorded for non-infected PBMC.

---

[135] (a) Friedman, S. H.; DeCamp, D. L.; Sijbesma, R. P.; Srdanov, G.; Wudl, F.; Kenyon, G. L. Inhibition of the HIV-1 Protease by Fullerene Derivatives: Model Building Studies and Experimental Verification. *J. Am. Chem. Soc.* **1993**, *115*, 6506–6509. (b) Friedman, S. H.; Ganapathi, P. S.; Rubin, Y.; Kenyon, G. L. Optimizing the Binding of Fullerene Inhibitors of the HIV-1 Protease through Predicted Increases in Hydrophobic Desolvation. *J. Med. Chem.* **1998**, *41*, 2424–2429.

[136] Sijbesma, R.; Srdanov, G.; Wudl, F.; Castoro, J. A.; Wilkins, C.; Friedman, S. H.; DeCamp, D. L.; Kenyon, *G. L. Synthesis of a Fullerene Derivative for the Inhibition of HIV Enzymes. J. Am. Chem. Soc.* ***1993,*** 115, 6510–6512.

[137] Schinazi, R. F.; Sijbesma, R. P.; Srdanov, G.; Hill, C. L.; Wudl, F. Synthesis and Virucidal Activity of a Water-soluble, Configurationally Stable, Derivatized C_{60} Fullerene. *Antimicrob. Agents Chemother.* **1993**, *37*, 1707–1710.

1.6.3.1.3. Neuroprotective ability

Many neurodegenerative diseases originate from an excess production of superoxidase and nitric oxide radicals, whose origin may be the result of overexcitation of glutamic acid receptors.[138] Molecules that strongly absorb radicals have been shown to inhibit cell death, and because C_{60} is probably the world's most efficient radical sponge, it is being considered as a possible biological antioxidant. For example, carboxylfullerene derivatives have extended the lives of transgenic mice that carry a defective copy of the gene encoding for human superoxide dismutase (SOD1), which is usually found in cases of amyotrophic lateral sclerosis (ALS). ALS is commonly known as Lou Gehrig's disease.[139]

Additional medicinal applications of C_{60} derivatives include: DNA cleavage and photodynamic therapy, antiapoptotic and antibacterial activity, and antiproliferative agents.[138,140]

1.6.3.2. Medicinal applications of metallofullerenes

1.6.3.2.1. MRI contrast agents and biodistribution

Magnetic resonance imaging (MRI) is one of the main diagnostic tools used in the medical field. The images produced are based on the relaxation of radio-frequency irradiated protons in water, and therefore a brighter image indicates that a greater density of water is present in the sample (i.e., human tissue). However, in the case of small tumors, only a small amount of water is present, and the corresponding image is not adequate for a definitive diagnosis. To correct the problem, MRI contrasting agents are administered to aid in the relaxation of the water protons and provide a sharper image. The most popular of these agents is the commercially available gadolinium(III) chelate of

---

[138] Da Ros, T.; Prato, M. Medicinal Chemistry with Fullerenes and Fullerene Derivatives. *Chem. Comm.* **1999**, 663–669.

[139] Dugan, L. L.; Turetsky, D. M.; Du, C.; Lobner, D.; Wheeler, M.; Almli, C. R.; Shen, K.-F.; Luh, T.-Y.; Choi, D. W.; Lin, T.-S. Carboxyfullerenes as Neuroprotective Agents. *Proc. Natl. Acad. Sci. USA* **1997**, *94*, 9434–9439.

diethylenetriaminepentaacetate ($DTPA^{-5}$), otherwise known as Magnevist. This agent, [Gd-$DTPA^{-2}$], is highly water-soluble, and utilizes the paramagnetic nature of Gd^{+3} (S = *7/2*) to relax the nearby water protons. The occurrence of a direct Gd^{+3}-H_2O bond is responsible for the relaxation; therefore, the faster the rate of exchange with the nearby water molecules, the brighter the resulting image will be (Scheme 1.13). Unfortunately,

Scheme 1.13

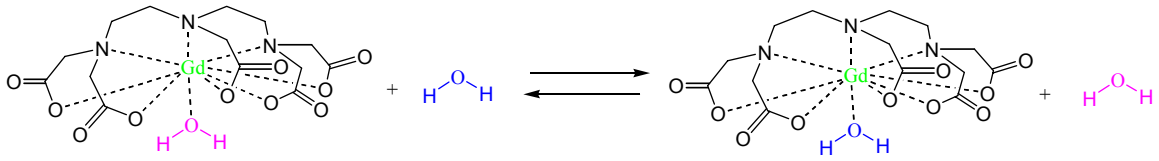

there are problems with these chelated compounds. The gadolinium chelates can dissociate, thereby releasing toxic Gd^{+3} ions that become embedded in the surrounding tissue. Furthermore, $[Gd(DTPA)(H_2O)]^{-2}$ is unstable to acidic conditions, such as the that found in the gastrointestinal track.[141]

Water-soluble metallofullerenes are potential replacements for the commercial MRI contrast agents, because the metal atom and carbon cage do not possess a dissociation constant, and a low toxicity has been demonstrated with the C_{60} fullerene cage and its derivatives. Shinohara and colleagues,[142] in addition to Cagle and co-workers,[141] have evaluated the use of a gadolinum metallofullerene, $Gd@C_{82}$, as a potential magnetic resonance imaging (MRI) contrast agent. This molecule was rendered water-soluble via a polyhydroxylation procedure, and the new metallofullerenols, $Gd@C_{82}(OH)_x$, demonstrated a lower rate of relaxivity than the commercial contrast agent (Magnevist).

---

[140] Wilson, L. J. Medicinal Applications of Fullerene and Metallofullerenes. *Electrochem. Soc. Interface* **1999**, *8*, 24–28.

[141] Cagle, D. W.; Alford, J. M.; Tien, J.; Wilson, L. J. Gadolinium-Containing Fullerenes for MRI Contrast Agent Applications. In *Fullerenes: Recent Advances in the Chemistry and Physics of Fullerenes and Related Materials*. Kadish, K., Ruoff, R., Eds.; The Electrochemical Society, Inc.: Pennington, NJ, 1997; Vol. 4, pp 361–368.

[142] Shinohara, H.; Yagi, K.; Nakamura, E. Japanese Patent 143,478, 1996.

However, gadolinium metallofullerenols that were synthesized by Zhang et al.,[143] with a different procedure, demonstrated a proton magnetic relaxivity rate (T_1) (a.k.a. spin-lattice relaxivity) of 47.0 ± 1.0 $mM^{-1}s^{-1}$, which is nearly ten times the commercial compound's rate of 4.3 $mM^{-1}s^{-1}$.

The surrounding water molecules cannot directly interact with the Gd^{+3} ion inside the cage, and therefore relaxation is hypothesized to occur from an electronic interaction between the water molecules and the paramagnetic (*S = 1/2*) cage (due to the hydroxylation procedure) of the metallofullerenol. The paramagnetic cage has a large surface area (220 $Å^2$), and numerous water molecules can interact with cage simultaneously via hydrogen bonding with the hydroxyl groups.[140]

Recently, mono-metallofullerenes ($M@C_{82}$) that contained La, Ce, Dy, Gd and Er were converted into water-soluble polyhyroxylated species and their subsequent relaxitivity rates measured.[144] Rates ranged from 0.8–73 $sec^{-1}mM^{-1}$ at 0.47 T, with the gadolinium species ($Gd@C_{82}(OH)_x$) providing the fastest rate, which is nearly 20 times greater than Magnevist.

The main problem with polyhydroxylated metallofullerenes is that they tend to form aggregates in solution that localize in the reticuloendothelial system (RES) of rodents, and for fullerene-based pharmaceuticals to be successful, sufficient water-solubility without RES localization must be achieved. Recently, Bolskar and colleagues[145] synthesized a water-soluble derivative of $Gd@C_{60}$ that is not polyhydroxylated. Instead, the derivative is functionalized with terminal acid groups that impart water-solubility to the molecule, but also allow for interactions between the cage and nearby water molecules so that relaxivity can be achieved. This unique adduct is $Gd@C_{60}[C(COOH)_2]_{10}$, and has been found to behave much like the commercially available Gd chelate-based (i.e., Magnevist) MRI contrast agents. The agent moved

---

[143] Zhang, S.; Sun, D.; Li, X.; Pei, F.; Liu, S. Synthesis and Solvent Enhanced Relaxation Property of Water-soluble Endohedral Metallofullerenes. *Fullerene Sci. Techn.* **1997**, *5*, 1635–1643.

[144] Kato, H.; Kanazawa, Y.; Okumura, M.; Taninaka, A.; Yokawa, T.; Shinohara, H. Lanthanoid Endohedral Metallofullerenes for MRI Contrast Agents. *J. Am. Chem. Soc.* **2003**, *125*, 4391–4397.

[145] Bolskar, R. D.; Benedetto, A. F.; Husebo, L. O.; Price, R. E.; Jackson, E. F.; Wallace, S.; Wilson, L. J.; Alford, J. M. First Soluble $M@C_{60}$ Derivatives Provide Enhanced Access to Metallofullerenes and Permit in Vivo Evaluation of $Gd@C_{60}[C(COOH)_2]_{10}$ as a MRI Contrast Agent. *J. Am. Chem. Soc.* **2003**, *125*, 5471–5478.

rapidly to the kidneys, with only minimal uptake into the liver. Excretion of the agent, via the bladder, occurred within 1 hour of injection. This behavior is a striking contrast to polyhydroxylated metallofullerenes, which have rapid uptake into the liver. Relaxivity measurements of $Gd@C_{60}[C(COOH)_2]_{10}$ reveal a rate (4.6 mM^{-1} at 20 MHz and 40 °C) that is comparable to the commercial MRI contrast agents.

1.6.3.3. Radiopharmaceuticals and biodistribution

Holmium metallofullerenes have been evaluated as potential radio-tracers in nuclear medicine. For instance, Wilson and co-workers[146] have studied the neutron-bombardment of a holmium metallofullerene, $^{165}Ho@C_{82}$, and its water-soluble metallofullerenol, $^{165}Ho@C_{82}(OH)_x$ (x = 24-26), from a highly thermal neutron source. When neutron activated, ^{165}Ho is converted to ^{166}Ho, which then emits a beta particle to become ^{166}Er. The metallofullerene's survival is maximized (30%) under highly thermal irradiation conditions, and the survival rate remains nearly constant with time.[146]

Biodistribution studies (Figure 1.19) of the radioactive metallofullerenol, $^{166}Ho@C_{82}(OH)_x$, were conducted using BALB/c mice. The results showed that the tracer is localized primarily in the liver, with slow clearance over 48 hours. However, localization in bone had gradually increased over the 48 hour time period. These results contrast with the control compound, $Na_2[^{166}Ho(DPTA)•(H_2O)]$, which was excreted within 1 hour after administration. In addition, metabolic studies indicated that the fullerenol cage was not likely degraded under biological conditions.

[146] Wilson, L. J.; Cagle, D. W.; Thrash, T. P.; Kennel, S. J.; Mirzadeh, S.; Alford, J. M.; Ehrhardt, G. J. Metallofullerene Drug Design. *Coord. Chem. Rev.* **1999**, *190–192*, 199–207.

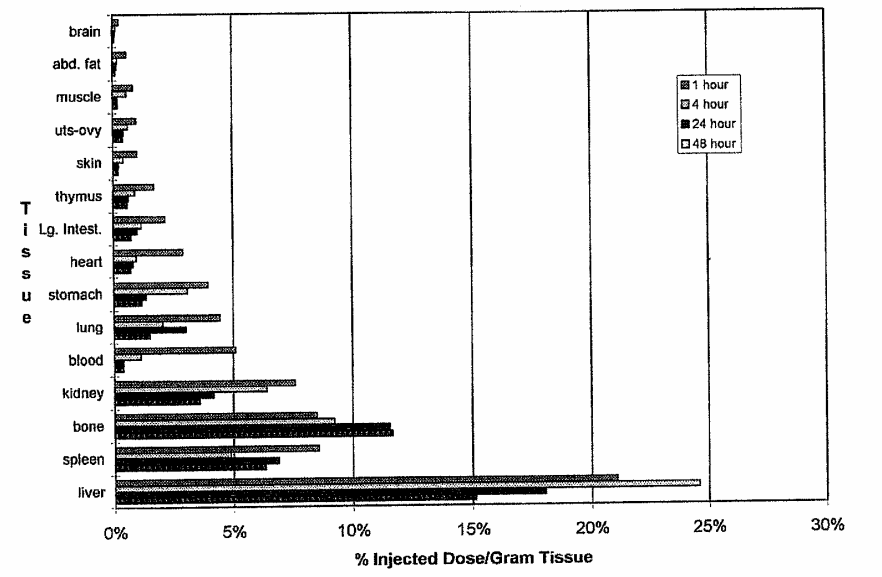

Figure 1.19. Biodistribution data for $^{166}Ho@C_{82}(OH)_x$ in BALB/c mice. Reprinted from reference 146 with permission from Elsevier.

The effects of β^- decay on the stability of ^{155}Sm, ^{161}Gd and ^{177}Yb metallofullerenes was also investigated.[147]

[147] Sueki, K.; Akiyama, K.; Kikuchi, K.; Nakahara, H.; Tomura, K. Stability of Radio-metallofullerenes against Beta-decay. *J. Radioanal. Nucl. Chem.* **1999**, *239*, 179–185.

CHAPTER 2 – Project Overview

The majority of this dissertation research concerns the functionalization of the recently discovered trimetallic nitride endohedral metallofullerenes. As discussed in Chapter 1, these novel materials are composed of an all carbon cage that encapsulates a cluster of three metal atoms (Group 3 or lanthanides) and a central nitrogen atom. Currently, there are three known species ($A_3N@C_{80}$, $A_3N@C_{78}$ and $A_3N@C_{68}$) in this interesting family of molecules, and the $A_3N@C_{80}$ species is the most abundantly produced of the three.

The $Sc_3N@C_{80}$ metallofullerene species and the ubiquitous C_{60} fullerene both contain cages of I_h symmetry (see Appendix IV, Determination of symmetry), although C_{80} does not contain the reactive [6,6] ring-junctures (pyracylene-type units) that are commonly used to functionalize C_{60}. Hence, the reactivity of the $Sc_3N@C_{80}$ molecule was initially unknown, and numerous highly regarded individuals in the field of fullerene chemistry had hypothesized that either a novel method would be needed to functionalize the molecule, or that the molecule would be completely unreactive. To complicate problems, only small amounts (*ca.* 1-5 mgs) of material were available to perform chemical reactions, and the material was available on an irregular basis.

The majority of the functionalization work that occurred throughout this project was performed with the $Sc_3N@C_{80}$ metallofullerene. At the beginning of the project, commercially available Diels-Alder cycloaddition reagents, such as pentamethylcyclopentadiene and anthracene, were added to room temperature and refluxing toluene solutions containing *ca.* 1 mg of the metallofullerene, respectively. A change of solution color was not observed for either $Sc_3N@C_{80}$ reaction, whereas addition of these same reagents to a C_{60} solution provides a rapid color change, thereby visually signifying that the molecule has reacted. Furthermore, mass spectral analysis on several instruments showed that only the parent metallofullerene and no reaction products were present, while the small quantities of material prevented structural characterization by NMR methods. Therefore, we concluded that a reaction had not occurred, and that

achieving a functionalization of $Sc_3N@C_{80}$ would be more difficult than just having to work with small amounts of material. Other commonly used organic functionalization methods, such as radical and nucleophilic reagents, were also attempted with the $Sc_3N@C_{80}$ metallofullerene, although none of these methods were successful.

I finally discovered that $Sc_3N@C_{80}$ (*ca.* 6.5 mg) could be functionalized with a highly reactive Diels-Alder cycloaddition reagent. To our surprise, only a mono-adduct of the molecule was formed, unlike the C_{60} fullerene that can add up to 6 addends. However, reaction yields of the C_{60} mono-adduct are nearly 40%, whereas those of $Sc_3N@C_{80}$ were only slightly greater than 10% when a ten-fold excess or reagent was employed. This proved that the C_{60} molecule is more reactive.

The cycloaddition reagent was synthesized with a ^{13}C label so structural data from the small amount of reaction product could be achieved. A single resonance was observed by ^{13}C NMR spectroscopy, which meant that the mono-adduct of $Sc_3N@C_{80}$ possessed a mirror plane of symmetry. Utilizing a ball and stick model to deduce the possible reactive sites on the cage, we were therefore able to propose a structure for the novel mono-adduct. Obtaining sufficient mass spectral data of the metallofullerene adduct was an additional difficulty, although I eventually discovered that only one technique and one specific matrix could be used to achieve results.

A few months later, an X-ray crystal structure of the mono-adduct verified that our proposed structure was correct. This adduct represented the first functionalized and fully characterized derivative of a trimetallic nitride metallofullerene, and an article highlighting the work was published in Chemical and Engineering News (**2002**, *80 (4)*, p.15). The same magazine also sited the work as one of the year's most important developments in chemistry (*Chem. Eng. News* **2002**, *80 (50)*, p.45), while the cover of Science News magazine (Appendix VI) pictured the molecule as a 'conceptual model' of future fullerene drugs.

Additional functionalization works in this Ph.D. dissertation include: 1) the synthesis of a water-soluble polyhydroxylated $Sc_3N@C_{80}$, 2) the synthesis of diethyl and dibenzyl malonate derivatives of $Sc_3N@C_{80}$, 3) an asymmetric cycloaddition adduct of $Sc_3N@C_{78}$, and 4) a ^{15}N-labeled derivative of $Sc_3N@C_{80}$ for potential solid phase peptide attachment.

It is worth noting that the inability to work with greater than 10-20 milligrams of material ultimately hampered my ability to perform multi-step chemical reactions.

Contrasting agents are just one of the several proposed medicinal applications for metallofullerenes. With this in mind, lutetium-based metallofullerenes were synthesized for utilization as X-ray contrasting agents. A CS_2 solution containing only 3 mg of pure $Lu_3N@C_{80}$ was evaporated onto a Teflon block. By irradiating with X-rays, we observed that the sample provided a small level of contrast. The high atomic number of the lutetium atoms are responsible for this contrast. Mixed metallofullerenes (i.e., $GdLu_2@C_{80}$ and $HoLu_2@C_{80}$) species were synthesized as potential multi-purpose contrasting agents.

An internal ^{15}N-labeling experiment of $Sc_3N@C_{80}$ was performed to understand: 1) the charge transfer, 2) the possible metal-nitride cluster pyramidalization issues within the cage and 3) the overall cluster motion within the cage.

All project works will be thoroughly discussed in the subsequent chapters of this dissertation.

CHAPTER 3 – Functionalization of $Sc_3N@C_{80}$

3.1. Introduction

The organic functionalization chemistry of the empty-cage C_{60} fullerene has grown exponentially since the molecule was discovered to possess reactive double bonds at the [6,6] ring-junctures of the cage, otherwise known as pyracylene-type units.[1-5] Each C_{60} molecular cage contains six of these reactive units; however, the [6,6] bond-junctures of larger empty cages (i.e., C_{70} and C_{78}) are not necessarily as reactive as C_{60} due to cage shape and strain.[6,7] Although novel derivatives of empty-cages have been synthesized, functionalized endohedral metallofullerenes hold a greater promise for creating unique molecules with extraordinary properties due to the wide variety of metals and metal clusters that can be encapsulated inside the carbon cages.[8-12] Unfortunately, little is

---

1 Trost, B. M.; Bright, G. M.; Frihart, C.; Brittelli, D. Perturbed [12]annulenes. Synthesis of Pyracylenes. *J. Am. Chem. Soc.* **1971**, *93*, 737–745.

2 Fagan, P. J.; Calabrese, J. C.; Malone, B. A Multiply-substituted Buckminsterfullerene (C60) with an Octahedral Array of Platinum. *J. Am. Chem. Soc.* **1991**, *113*, 9408–9409.

3 Olah, G. A.; Bucsi, I.; Lambert, C.; Aniszfeld, R.; Trivedi, N. J.; Sensharma, D. K.; Prakash, G. K. S. Chlorination and bromination of fullerenes. Nucleophilic methoxylation of polychlorofullerenes and their aluminum trichloride catalyzed Friedel-Crafts reaction with aromatics to polyarylfullerenes. *J. Am. Chem. Soc.* **1991**, *113*, 9385–9387; Polyarenefullerenes, C60(H-Ar)n, obtained by acid-catalyzed fullerenation of aromatics. *J. Am. Chem. Soc.* **1991**, *113*, 9387–9388.

4 Suzuki, T.; Li, Q.; Khemani, K. C.; Wudl, F.; Almarsson, O. Systematic Inflation of Buckminsterfullerene C60 – Synthesis of Diphenyl Fulleroids C61 to C66. *Science* **1991**, *254*, 1186–1188.

5 Wudl, F. The Chemical Properties of Buckminsterfullerene (C-60) and the Birth and Infancy of Fulleroids. *Acc. Chem. Res.* **1992**, *25*, 157–161.

6 Meier, M. S.; Wang, G.-W.; Haddon, R. C.; Brock, C. P.; Lloyd, M. A.; Selegue, J. P. Benzyne Adds Across a Closed 5-6 Ring Fusion in C70: Evidence for Bond Delocalization in Fullerenes. *J. Am. Chem. Soc.* **1998**, *120*, 2337–2342.

7 Taylor, R. C-60, C-70, C-76, C-78 and C-84 - Numbering, Pi-bond Order Calculations and Addition Pattern Considerations. *J. Chem. Soc., Perkin Trans. 2* **1993**, 813–824.

8 Yannoni, C. S.; Hoinkis, M.; deVries, M. S.; Bethune, D. S.; Salem, J. R.; Crowder, M. S.; Johnson, R. D. Scandium Clusters in Fullerene Cages. *Science* **1992**, *256*, 1191–1192.

9 Guo, T.; Diener, M. D.; Chai, Y.; Alford, M. J.; Haufler, R. E.; McClure, S. M.; Ohno, T.; Weaver, J. H.; Scuseria, G. E.; Smalley, R. E. Uranium Stabilization of C_{28} – A Tetravalent Fullerene. *Science* **1992**, *257*, 1661–1664.

10 Kikuchi, K.; Kobayashi, K.; Sueki, K.; Suzuki, S.; Nakahara, H.; Achiba, Y.; Tomura, K.; Katada, M. Encapsulation of Radioactive 159Gd and 161Tb Atoms in Fullerene Cages. *J. Am. Chem. Soc.* **1994**, *116*, 9775–9776.

11 Suzuki, S.; Torishu, H.; Kubota, H.; Wakabayashi, T.; Shiromaru, H.; Achiba, Y. Formation and Stability of Small Metallocarbon Clusters – What is the Specificity for the Formation of Stable Metallofullerenes. *Int. J. Mass Spectr. Ion Process.* **1994**, *138*, 297–306.

known of cage structure and reactivity for most endohedral metallofullerenes, which are produced in much smaller quantities than most empty-cage fullerenes.

In 1999, the novel endohedral metallofullerene[13], $Sc_3N@C_{80}$ (Chapter 1, Figure 1.1), was produced by introducing nitrogen gas into a Krätschmer-Huffman generator when vaporizing graphite rods that are packed with a metal oxide. This method of synthesis is known as the trimetallic nitride template (TNT) process. The most abundant of three known trimetallic nitrides, $Sc_3N@C_{80}$ can be formally viewed as a positively charged planar cluster of atoms inside a negatively charged icosahedral (I_h) carbon cage, $[Sc_3N]^{+6}@[C_{80}]^{-6}$. Although both C_{60} and the C_{80} carbon cage of $Sc_3N@C_{80}$ have icosahedral symmetry (I_h),[14,15] C_{60} consists of a single pyracylene-type carbon, whereas the $Sc_3N@C_{80}$ cage is composed to two types of carbon atoms; a pyrene-type carbon (intersection of three six-membered rings) and a corannulene-type carbon (intersection of a five-membered ring and two six-membered rings).[13] The I_h C_{80} cage does not possess pyracylene-type reactive sites; therefore, other reactive sites must be present on the molecule for derivatization to occur. Furthermore, the pi-bond sketch of the $Sc_3N@C_{80}$ cage is unknown, because the C_{80} cage of the molecule possesses additional electrons ($[C_{80}]^{-6}$).

As discussed in Chapter 2, numerous initial attempts to functionalize the novel $Sc_3N@C_{80}$ metallofullerene were unsuccessful, even though a variety of organic reagents were employed that are commonly used to derivatize the C_{60} fullerene.

---

[12] Ding, J. Q.; Lin, N.; Weng, L. T.; Cue, N.; Yang, S. H. Isolation and Characterization of a New Metallofullerene, $Nd@C_{82}$. *Chem. Phys. Lett.* **1996**, *261*, 92–97.

[13] Stevenson, S.; Rice, G.; Glass, T.; Harich, K.; Cromer, F.; Jordan, M. R.; Craft, J.; Hadju, E.; Bible, R.; Olmstead, M. M.; Maltra, K.; Fisher, A. J.; Balch, A. L.; Dorn, H. C. Small-bandgap Endohedral Metallofullerenes in High Yield and Purity. *Nature* **1999**, *401*, 55–57.

[14] Krätschmer, W.; Lamb, L. D.; Fostiropoulos, K.; Huffman, D. R. Solid C_{60} – A New Form of Carbon. *Nature* **1990**, *347*, 354–358.

[15] Taylor, R.; Hare, J. P.; Abdul-Sada, A. K.; Kroto, H. W. Isolation, Separation and Characterization of the Fullerenes C_{60} and C_{70} – The 3rd Form of Carbon. *J. Chem. Soc., Chem. Commun.* **1990**, *20*, 1423–1424.

3.2. Results and Discussion

3.2.1. The first derivative of $Sc_3N@C_{80}$

The first derivative of $Sc_3N@C_{80}$ was synthesized by reacting the metallofullerene with a Diels-Alder cycloaddition precursor. However, because only milligram amounts (*ca.* 5 mgs) of metallofullerene were available for functionalization, it was decided that a NMR active label should be present on the adduct if structural data was to be acquired.

The cycloaddition precursor, 6,7-dimethoxyisochroman-3-one (^{13}C-labeled) **2**, was synthesized by following a procedure by Pandey and co-workers,[16] and using ^{13}C-labeled formaldehyde (99% ^{13}C) to label the precursor **2** at the 1-position. The reaction (Scheme 3.1) proceeded within 1 hour via an electrophilic aromatic substitution (EAS) reaction

Scheme 3.1

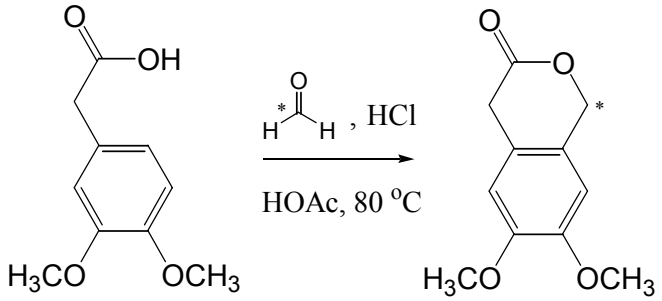

between ^{13}C-labeled formaldehyde and (3,4-dimethoxyphenyl)acetic acid **1**, under acidic conditions, with subsequent displacement of water. The yield of **2** was *ca.* 31%, most likely due to lactone hydrolysis under the acidic conditions. A further decrease in the yield of **2** occurred when the time was increase by only 0.5 hours.

The ^{1}H NMR spectrum of 6,7-dimethoxyisochroman-3-one **2** (Figure 3.13) shows resonances that are consistent with the structure of a labeled compound. The two protons

[16] Pandey, G. D.; Tiwari, K. P. Synthesis of 2-Hydroxy-3,10, 11-trimethoxy-5,6,13, 13a-tetrahdro-8*H*-dibenzo[*a,g*]quinolizine (Govanine). *Indian J. Chem.* **1980**, *19B*, 66–68.

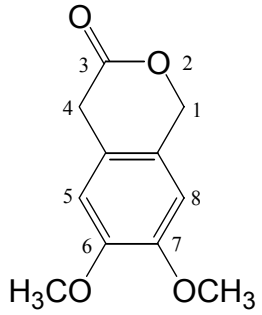

Figure 3.1. Numbering scheme for 6,7-dimethoxyisochroman-3-one **2**.

of the ^{13}C-labeled methylene carbon are split into doublet ($^{1}J_{CH}$ = 149.2 Hz) that is centered at 5.25 ppm. A splitting of *ca.* 150 Hz is consistent for a ^{13}C–^{1}H bond. An aromatic proton (8-position) (Figure 3.1) is also split into a doublet by the addition of a ^{13}C atom to the methylene group (1-position), even though the coupling is long range (3 bonds). The coupling is 8 Hz, and the aromatic proton is found at 6.74 ppm. The methylene protons at the 3-position are found 3.63 ppm, while the other aromatic proton and the six methoxy protons are found at 6.70 and 3.88 ppm, respectively.

The ^{13}C NMR spectrum of **2** (Figure 3.14) depicts resonances that correspond to all 11 carbon atoms in the structure. The ^{13}C methylene atom is found at 70.24 ppm, while the non-labeled methylene carbon is found at 35.81 ppm. The signals for the two methoxy carbons are found at 56.36 and 56.39 ppm. Aromatic carbons of the structure are found at 108.24, 110.36, 123.17, 123.79, 149.64 and 148.53, with signals at 108.24 and 110.36 ppm corresponding to the carbons with attached protons. The carbonyl carbon is located at 171.06 ppm.

To synthesize the first trimetallic nitride endohedral metallofullerene adduct **4** (4,5-dimethoxy-*o*-quinodimethane–$Sc_3N@C_{80}$), a 1,2,4-trichlorobenzene (TCB) solution containing *ca.* 6.5 mg of $Sc_3N@C_{80}$ (99%) **3** was refluxed (214 °C) with a ten-fold excess of **2**. During the high temperature reflux, carbon dioxide was thermally extruded from **2** to generate a highly reactive *o*-quinodimethane intermediate that reacted with the $Sc_3N@C_{80}$ in a [4 + 2] cycloaddition fashion (Scheme 3.2).[17] Metallofullerene **3** is less

[17] Belik, P.; Gügel, A.; Kraus, A.; Spickermann, J.; Enkelmann, V.; Frank, G.; Müllen, K. The Diels-Alder Adduct of C_{60} and 4,5-Dimethoxy-*o*-quinodimethane Synthesis, Crystal Structure and Donor-acceptor Behavior. *Adv. Mater.* **1993**, *5*, 854–856; Reaction of Buckminsterfullerene with Ortho-

reactive than the C_{60} fullerene, and an excess of reagent **2** was used to improve the product yields. The crude reaction solution was purified by HPLC methods using the Trident-Tri-DNP (Buckyclutcher) column with chloroform as

Scheme 3.2

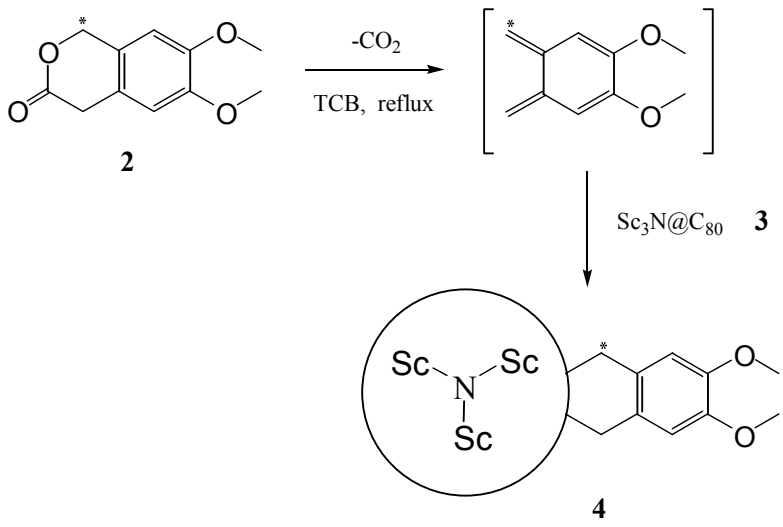

2 **4**

the eluent to reveal a single reaction product that dominated the solution. Injection sizes of the crude reaction solution ranged from 10 to 400 µl at a slow flow rate (1.25 ml/min.). From the HPLC chromatogram (Figure 3.2), the mono-adduct **4** had a retention time of 18.63 minutes, as opposed to a shorter time of 16.5 minutes for the unreacted metallofullerene **3**. The longer retention time of the product **4** is probably due to an increase in the dipole moment from the internal Sc_3N cluster of the metallofullerene when the cage is derivatized. The yield of mono-adduct **4** was *ca.* 2.5 milligrams. The peak in Figure 3.2 marked with an 'x' is assumed to be a mono-adduct of D_{5h} $Sc_3N@C_{80}$ (Chapter 5).

The matrix-assisted (9-nitroanthracene[18]) laser-desorption ionization time-of-flight mass spectrum (MALDI-TOF MS) of **3** (Figure 3.3) displayed a peak for the ^{13}C-labeled

---

quinodimethane – A New Access to Stable C_{60} Derivatives. *Angew. Chem. Intl. Ed. Engl.* **1993**, *32*, 78–80.

[18] Ballenweg, S.; Gleiter, R.; Krätschmer, W. Chemistry at cyclopentene addends on [60] fullerene. Matrix-assisted laser desorption ionization time-of-flight mass spectrometry (MALDI-TOF MS) as a quick and facile method for the characterization of fullerene derivatives. *Synth. Met.* **1996**, *77*, 209–212.

mono-adduct **4** at *m/z* = 1274, and a peak at *m/z* = 1109 for the parent metallofullerene **3**. Masses were not observed when this specific matrix was not employed. Furthermore, the synthesized adduct **4** yields a molecular ion peak at a higher abundance than the parent endohedral metallofullerene, which contrasts all previously reported mass spectra of functionalized endohedral metallofullerenes.[19] Adducts of higher mass were not observed within the spectrum.

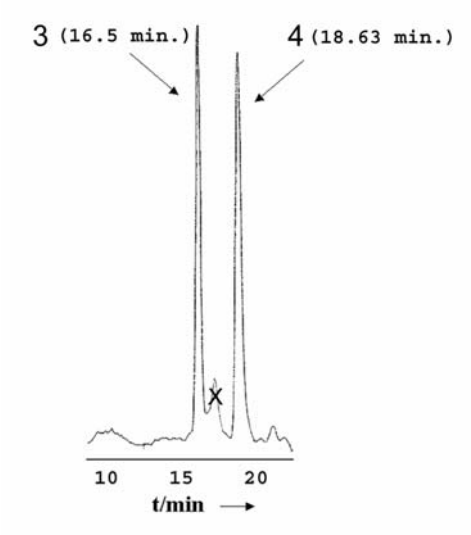

Figure 3.2. HPLC chromatogram of crude reaction solution showing unreacted $Sc_3N@C_{80}$ **3** (31% conc.) and mono-adduct **4** (41% conc.) (x = mono-adduct of D_{5h} isomer?).

[19] Akasaka, T.; Nagase, S.; Kobayashi, K.; Suzuki, T.; Kato, T.; Kikuchi, K.; Achiba, Y.;Yamamoto, K.; Funasaka, H.; Takahashi, T. Synthesis of the First Adducts of Dimetallofullerenes $La_2@C_{80}$ and $Sc_2@C_{84}$ by Addition of Disilirane. *Angew. Chem. Int. Ed. Engl.* **1995**, *34*, 2139–2141; Exohedral Adducts of $La@C_{82}$. *Nature* **1995**, *374*, 600–601.

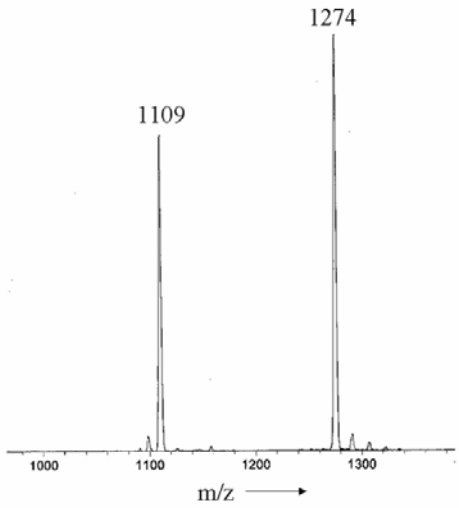

Figure 3.3. MALDI-TOF MS of the mono-adduct **4** (*m/z* 1274) and $Sc_3N@C_{80}$ (*m/z* 1109) using a 9-nitroanthracene matrix.

The metallofullerene mono-adduct **4** is not very soluble in chloroform-d, and therefore 1,1,2,2-tetrachloroethane-d_2 was needed to obtain sufficient NMR structural data. The ^{13}C-labeled carbon atom proved to be a valuable asset in that it provided an unequivocal interpretation of the ^{13}C NMR spectrum for **4** (Figure 3.16), which showed a single narrow signal at 42.25 ppm on the NMR timescale due to motion of the internal Sc_3N cluster. This finding indicated that the two methylene carbons of the adduct were equivalent, and that the mono-adduct possessed a mirror plane of symmetry.

In the ^1H NMR spectrum of the mono-adduct **4** (Figure 3.15), the resonances for the six methoxy protons of the adduct are found 3.98 ppm, while those for the two phenyl protons are found at 7.01 ppm. In addition, the signals that represent the methylene protons are shown as a broad multiplet in the range of 3.2-3.8 ppm. The latter region of the spectrum was difficult to interpret, and therefore 2D NMR techniques were implemented in order to provide a lucid understanding of the electronic environments for the hydrogen atoms in the mono-adduct **4**.

The two non-equivalent geminal hydrogens (A,B system) that are attached to the methylene carbons of the mono-adduct **4** are centered at 3.41 and 3.57 ppm, respectively. This was easily deduced from the 2D COSY (Correlation Spectroscopy) NMR spectrum (Figure 3.17) by showing that one methylene hydrogen is coupled to the other. The

downfield signal ("A") is clearly resolved into 6 lines with the area of the large central doublet integrating to one hydrogen atom. Here, coupling to hydrogen atom "B" is $^{1}J_{HH}$ = 14 Hz, because "A" is attached to the ^{12}C methylene atom. However, when attached to the ^{13}C-labeled methylene carbon atom, hydrogen atom "A" is observed to split into two symmetric doublets (centered at *ca.* 3.71 and 3.44 ppm) with a coupling constant $^{1}J_{CH}$ = 133 Hz. As for methylene hydrogen "B", the 6 lines are broadened and inadequately resolved as indicated by the outer doublet at *ca.* 3.27 ppm and the 4 lines that are buried under the signals from hydrogen atom "A". Explanations for these results may be due to different motions of the two methylene hydrogens, such as a ring inversion, or possible quadrupolar interactions with the encapsulated scandium atoms. It is important to note that similar adducts with C_{60} fullerene have demonstrated proton signal broadening.

The linewidths of the ^{1}H NMR spectrum can be sharpened if the NMR temperature is either raised or lowered. For instance, the spectrum of **4** at 90 °C (Figure 3.18) shows twelve well resolved signals that correspond to the four protons of the adduct when the entire region is integrated. Ring inversion within the addend occurs rapidly due to the high temperature, which causes the NMR to see an 'averaged' position for the methylene hydrogens, rather than a single 'frozen' position. Mono-adduct **4** has poor solubility in chloroform-d and methylene chloride-d_2, and thus the higher freezing point of 1,1,2,2-tetrachloroethane-d_2 (–43 ºC) prevented spectra from being obtained at lower temperatures.

2D HMQC (Heteronuclear Multiple Quantum Correlation) (Figure 3.19) verified that the two sets of non-equivalent methylene hydrogens were attached to equivalent carbon atoms of the symmetric adduct **4**, and also provided the ^{13}C NMR chemical shift of the methoxy carbons (55.93 ppm) on the adduct. The ^{13}C chemical shifts of adjacent carbon atoms to the methylene carbons were achieved using 2D HMBC (Heteronuclear Multiple Bond Coordination) (Figure 3.20). Hydrogens of the methylene groups are coupled, via 2-bond coupling ($^{2}J_{CH}$), to the sp^3-hybridized carbon atoms of the metallofullerene cage (52.30 ppm), which is the site where the reaction has occurred. In addition, the hydrogens are also coupled ($^{2}J_{CH}$) to the sp^2-hybridized carbons of the phenyl ring

(126.53 ppm). The ^{13}C NMR structural data comparison of the mono-adduct **4** and a previously synthesized C_{60} adduct are presented in Table 3.1.[20]

	$Sc_3N@C_{80}$ adduct	C_{60} adduct
methylene carbon	42.25	46.62
methylene protons	3.41 and 3.57	4.37 and 4.74
methoxy carbon	55.93	58.20
methoxy protons	3.98	4.01
sp^3 carbon on cage	52.30	67.94
phenyl protons	7.01	7.20

Table 3.1. ^1H and ^{13}C NMR signal comparisons (ppm) between $Sc_3N@C_{80}$ mono-adduct **4** and the C_{60} mono-adduct.

The mirror plane in 4,5-dimethoxy-*o*-quinodimethane–$Sc_3N@C_{80}$ **4** was engendered by reagent **2** addition to one of only three possible sites on the I_h cage of $Sc_3N@C_{80}$ **3**, as illustrated in Figure 3.4. The proposed mechanism of addition was via a [4 + 2] cycloaddition, thereby reacting with a localized double bond at a [5,6] ring-juncture on the I_h C_{80} cage of the metallofullerene. Additions to reactive sites "a" and "c" were less likely and would have led to highly strained adducts. Furthermore, addition at proposed site "b" (Figure 3.4) had conserved the symmetry plane within the cage of the mono-adduct **4**.

[20] Iezzi, E. B.; Duchamp, J. C.; Harich, K.; Glass, T. E.; Lee, H. M.; Olmstead, M. M.; Balch, A. L.; Dorn, H. C. A Symmetric Derivative of the Trimetallic Nitride Endohedral Metallofullerene, $Sc_3N@C_{80}$. *J. Am. Chem. Soc.* **2002**, *124*, 524–525.

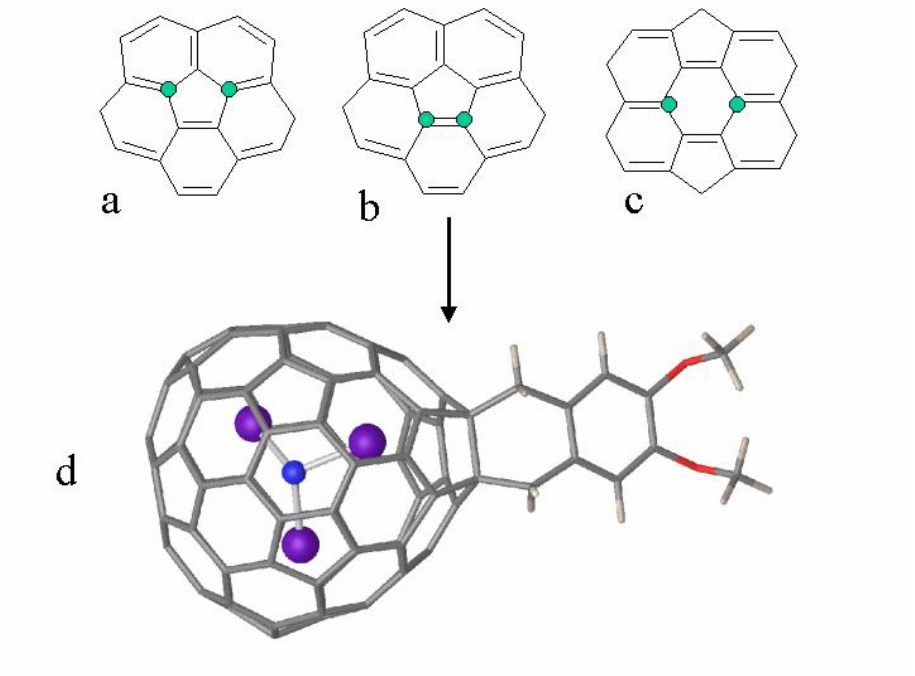

Figure 3.4. Motifs of reactive sites on the I_h $Sc_3N@C_{80}$ **3** cage that yield a mirror plane of symmetry: (a) 1,3 position on a five-membered ring, (b) 1,2 position at a [5,6] juncture on a five-membered ring, (c) 1,4 position on a six-membered ring, and (d) Gauss View structure (non-optimized) of mono-adduct **4** from addend addition at a [5,6] bond-juncture (site "b") on the $Sc_3N@C_{80}$ cage.

3.2.2. X-ray crystal structure of the first $Sc_3N@C_{80}$ derivative

The Gauss View structure of 4,5-dimethoxy-*o*-quinodimethane–$Sc_3N@C_{80}$ **4** (Figure 3.4d) was corroborated when the X-ray crystal structure of the adduct was finally achieved (Figure 3.5).[21] Grown from a benzene solution with a drop of methanol, the crystal structure of mono-adduct **4** shows that functionalization had indeed occurred at a [5,6] ring-juncture (corannulene-type site) of the I_h $Sc_3N@C_{80}$ **3** cage. This reactive site is known as carbons 1 and 2 from the numbering scheme of the I_h C_{80} cage (Appendix I, Schlegel diagram). As shown in Figure 3.6, the C1–C2 distance of adduct **4**, 1.626 Å, is substantially elongated when compared to a normal C–C distance (1.437 Å) at a [5,6]

[21] Lee, H. M.; Olmstead, M. M.; Iezzi, E.; Duchamp, J. C.; Dorn, H. C.; Balch, A. L. Crystallographic Characterization and Structrual Analysis of the First Organic Functionalization Product of the Endohedral Fullerene $Sc_3N@C_{80}$. *J. Am. Chem. Soc.* **2002**, *124*, 3494–3495.

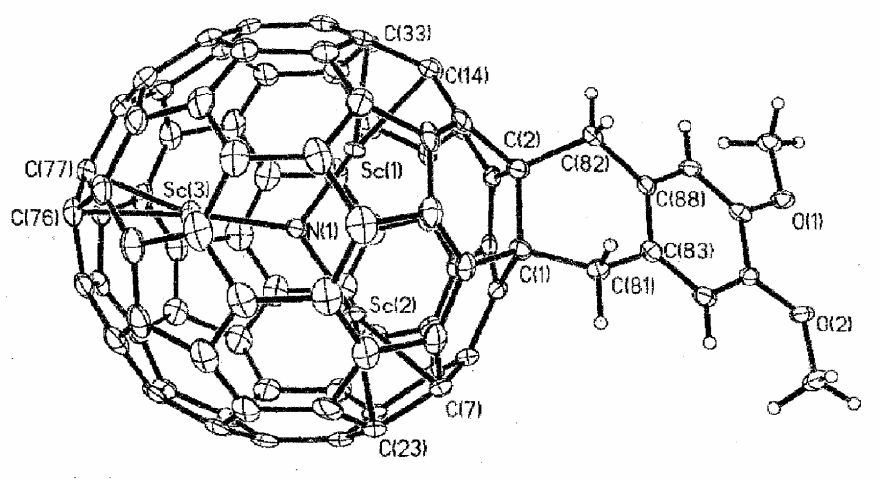

Figure 3.5. X-ray crystal structure of mono-adduct **4** at 91K.[21]

ring-juncture of the cage. Furthermore, the carbons of C1 and C2 are pulled towards the addend and away from the cage, while the bond distances between C9–C10 and C11–C12 have been shortened to 1.374 and 1.380 Å, respectively.

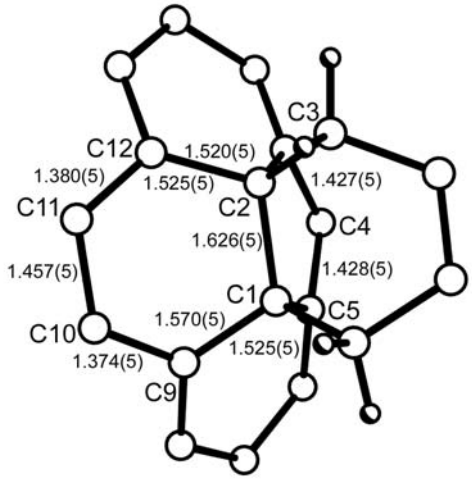

Figure 3.6. A close-up view of mono-adduct **4** crystal structure.[21]

The Sc_3N cluster of adduct **4** (Figure 3.7) remains planar inside the cage, although the Sc–N distances have increased from 2.011 and 1.966 Å (unfunctionalized $Sc_3N@C_{80}$) to 2.032, 2.020 and 2.029 Å.[21] In addition, the increased Sc–N distances have caused the cage to distort at the sites where the scandium atoms are localized. For instance, carbons

C7, C14 and C76 have pyramidalization angles of *ca.* 14°, whereas the majority of carbon atoms within the cage have angles of *ca.* 10°.[21] The X-ray crystal coordinates of 4,5-dimethoxy-*o*-quinodimethane–$Sc_3N@C_{80}$ **4** are provided in Appendix V. Although not commonly used, the IUPAC name of adduct **4** would be 1,2-(4,5-dimethoxy-*o*-quinodimethane)[80-I_h]fullerene-*incar*-scandium nitride.

The crystals of adduct **4** are black, bipyramidal, and small in size (0.06 mm x 0.11 mm x 0.10 mm).[21] Interestingly, the unit cell of the crystal (Figure 3.7) shows that the adduct is packed in a head-to-tail formation. This is most likely due to pi-stacking between the aromatic cage and the phenyl ring of the addend. It should also be noted that two scandium atoms of the internal cluster are directed towards the methoxy groups of the addend (Figure 3.7b), thereby implying that a dipole moment may exist between the positive head (scandium atoms in cluster) and the negative tail (methoxy groups) of mono-adduct **4**. This may explain why adduct **4** has a longer HPLC (Buckyclutcher column) retention time than the parent metallofullerene, $Sc_3N@C_{80}$ **3**.

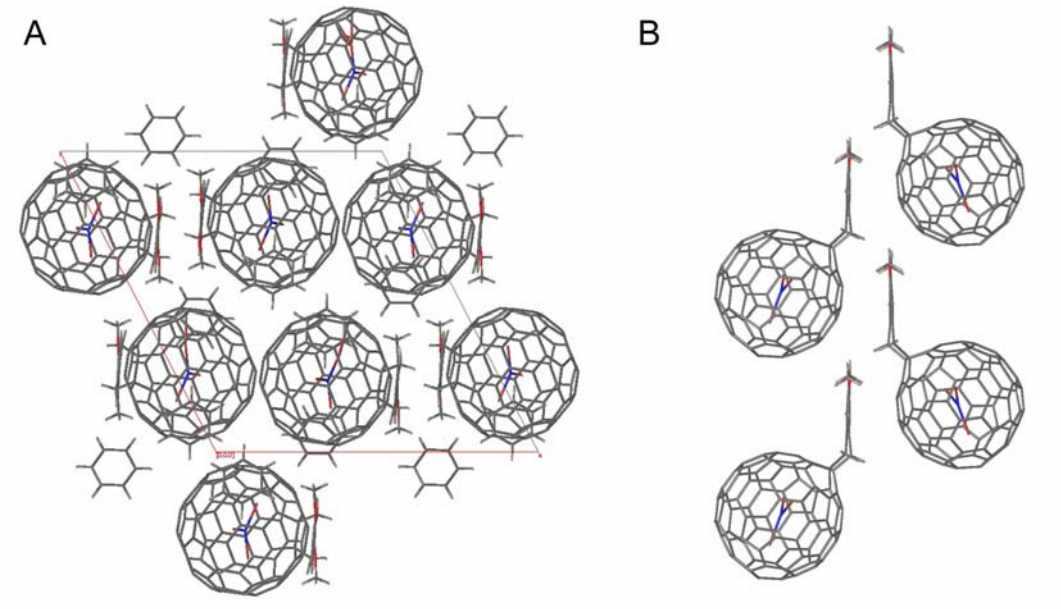

Figure 3.7. Crystal unit cell of mono-adduct **4** showing: (a) bipyramidal shape and (b) head-to-tail pi-stacking between adducts (benzenes omitted).

3.2.3. Malonate derivatives of $Sc_3N@C_{80}$

Derivatives of $Sc_3N@C_{80}$ that contained a cyclopropyl ring were achieved by reacting the metallofullerene with diethyl and dibenzyl malonate. The reagents were attached to the cage by the so-called Hirsch-Bingel method,[22] in which CBr_4 and DBU are used to remove the central protons (2-position) of the malonate in order to react with the fullerene cage. The mechanistic pathway is not fully understood, although it is belived to occur via a brominated malonate (at the 2-position) with subsequent carbanion formation, which then reacts with the cage via a cyclopropanation (Scheme 3.3). However, it should be noted that we believe that the mechanism of attachment to the I_h cage isomer of $Sc_3N@C_{80}$ (isomer lacks pyracylene-type units) occurs via an *in situ* generated carbene of the malonate.

Scheme 3.3

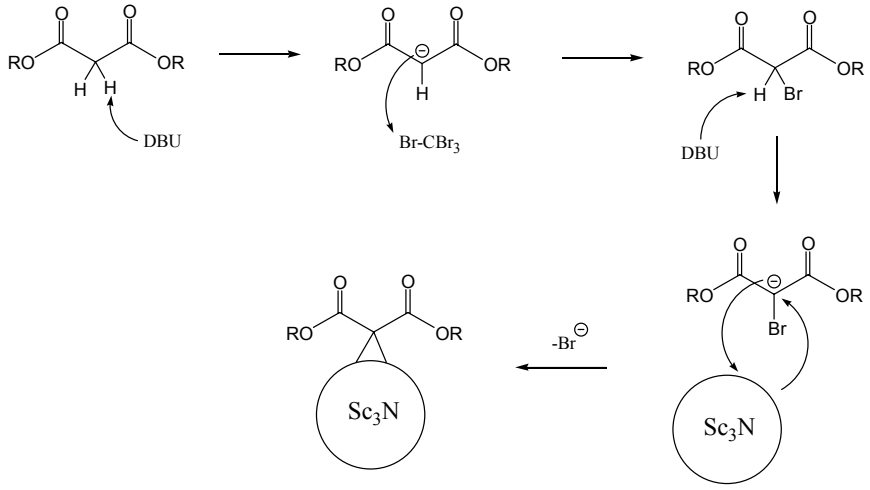

Diethyl malonate **5** was the first chosen malonate to be reacted with $Sc_3N@C_{80}$ because it was available with a ^{13}C-labeled at the 2-position. In addition, only milligram amounts (*ca.* 8 mgs) of the metallofullerene were available at the time, and adducts with

[22] (a) Bingel, C. Cyclopropylation of Fullerenes. *Chem. Ber.* **1993**, *126*, 1957–1959. (b) Camps, X.; Hirsch, A. Efficient cyclopropanation of C_{60} starting from malonates. *J. Chem. Soc., Perkin Trans. 1* 1997, 1595–1596.

a labeled atom were necessary for achieving structural data from the small amount of reactive products that might be formed. Adduct **6** of $Sc_3N@C_{80}$ **3** was synthesized as depicted in Scheme 3.4.

Scheme 3.4

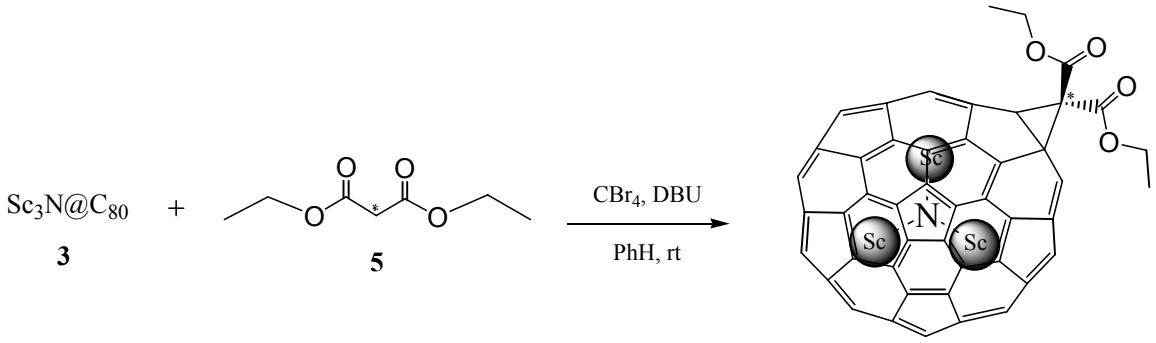

The yield of adduct **6** was extremely low (<0.5 mg) due to the low reactivity of $Sc_3N@C_{80}$, and achieving a mass spectrum of the product was unsuccessful. The latter may be attributed to a low stability of adduct **6**. Furthermore, the adduct did not elute when injected into the HPLC system.

The ^{13}C NMR spectrum (Figure 3.22) shows a single line (49.64 ppm) that represents the labeled position of adduct **6**, and this signal cannot be mistaken for a signal from unreacted diethyl malonate (2-^{13}C) (41.89 ppm). Furthermore, Scheme 3.4 illustrates that the addend is attached to a [5,6] ring-juncture of the cage, although this site has not been proven as the reactive site for cyclopropyl derivatives. Achieving a crystal of adduct **6** for X-ray structure elucidation has been unsuccessful thus far.

To improve the chances for growing a crystal of a $Sc_3N@C_{80}$–malonate adduct, a derivative that contained benzyl groups was synthesized with the idea that the aromatic rings would provide a means for pi-stacking with the cage. This dibenzyl malonate adduct (**8**) was synthesized using the previously discussed Hirsch-Bingel procedure (Scheme 3.5).

Peaks were observed at 12.77, 14.30 and 15.11 minutes in the HPLC chromatogram (Figure 3.8), although the third product peak was greater in concentration (*ca.* 3%) than

the other two. It is interesting that these three products elute at an earlier time than the parent $Sc_3N@C_{80}$ metallofullerene, which may be attributed to a decrease in the internal dipole moment of the cage and/or a decrease in the external polarization of the cage (from the pi-electrons) due to exohedral functionalization. The masses of all three

Scheme 3.5

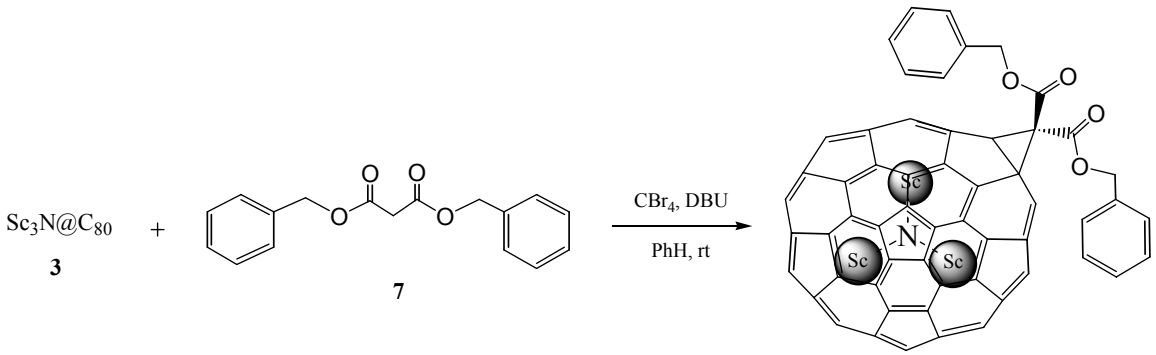

products were *ca.* 1391, which corresponds to the mass of the desired benzyl adduct **8**. The third product (peak 3) is believed to result from functionalization of the I_h $Sc_3N@C_{80}$ isomer, while the other two are possibly derivatives of the recently discovered D_{5h}

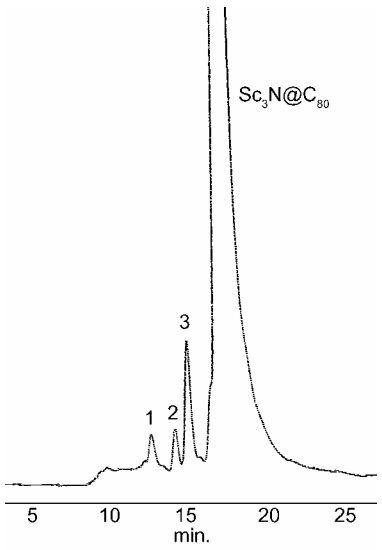

Figure 3.8. HPLC chromatogram of $Sc_3N@C_{80}$–dibenzyl malonate adducts **8** (peaks 1,2 and 3) and unreacted $Sc_3N@C_{80}$.

isomer.[23] The details of this latter isomer are discussed in Chapter 5. However, for the sake of visualization, adduct **8** (Scheme 3.5) is shown as a derivative of the I_h isomer.

Adduct **8** is not ^{13}C-labeled, and therefore a ^{13}C NMR spectra could not be achieved from the small amount of reaction products (*ca.* 0.5 mgs for peak 3, and <0.5 mgs for peaks 1 and 2). Nonetheless, from the obtained ^{1}H NMR spectrum (Figure 3.23), all three isomers show signals that correspond to the protons of adduct **8** (Scheme 3.5). The ten phenyl protons of the molecule are located at 7.31-7.36 ppm, while the four methylene protons are found at 5.32 ppm and close to the solvent peak. Deuterated methylene chloride was used as the NMR solvent, because chloroform-d, benzene-d6 and 1,1,2,2-tetrachloroethane-d2 all yielded solvent signals in the area of the benzyl proton signals of adduct **8**. No other solvents could be used to solubilize the adducts.

To date, crystal growth for all three isomers of adduct **8** has been unsuccessful, and therefore the site of addend attachment remains unknown.

3.2.4. A ^{15}N-labeled terminal amine derivative of $Sc_3N@C_{80}$ for addend attachment

A ^{15}N-labeled terminal amine derivative **14** of $Sc_3N@C_{80}$ was specifically synthesized for attaching various groups (i.e., peptides and water-soluble dendrimers) that would impart water-solubility to the highly hydrophobic metallofullerene. This task was accomplished through the five step synthesis that is depicted in Scheme 3.6. The ^{15}N-label would provide verification that an attached addend has indeed reacted at the site of the amine, as opposed to wrapping around the complex to impart the water-solubility.

[23] Duchamp, J. C.; Demortier, A.; Fletcher, K. R.; Dorn, D.; Iezzi, E. B.; Glass, T.; Dorn, H. C. An Isomer of the Endohedral Metallofullerene $Sc_3N@C_{80}$ with D_{5h} Symmetry. *Chem. Phys. Lett.* **2003**, *375*, 655–659.

Scheme 3.6

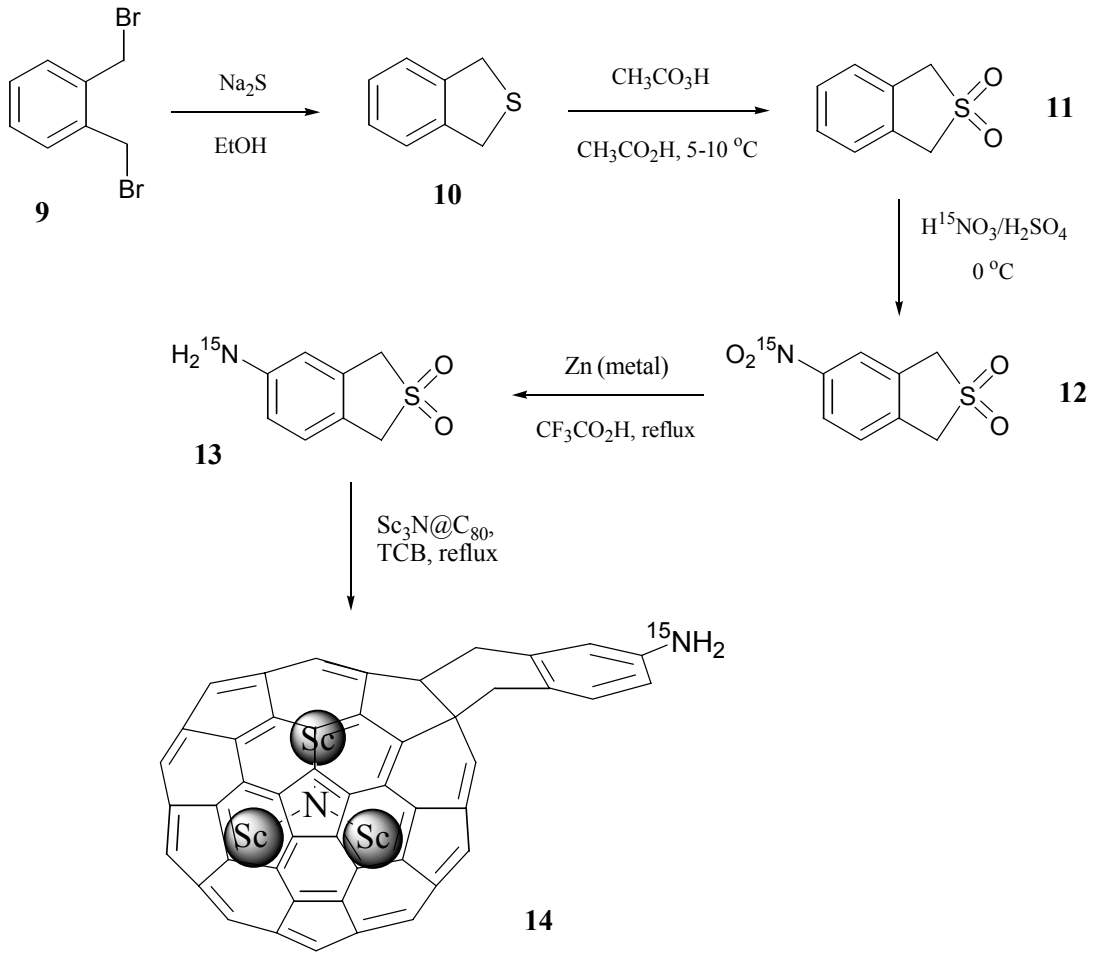

3.2.4.1. 1,3-Dihydrobenzo[c]thiophene (10)

The first stage of the synthesis was achieved by following a vaguely detailed procedure from Cava and colleagues.[24] Here, hydrogen sulfide (H_2S) was bubbled through an ethanolic sodium ethoxide solution to yield sodium sulfide (Na_2S), which

[24] Cava, M. A.; Deana, A. A. Condensed Cyclobutane Aromatic Compounds. VI. The Pyrolysis of 1,3-Dihydroisothianaphthene-2,2-dioxide: A New Synthesis of Benzocyclobutene *J. Am. Chem. Soc.* **1959**, *81*, 4266–4268.

subsequently reacted with α,α'-dibromo-*o*-xylene **9** to yield 1,3-dihydrobenzo[c]thiophene **10** (Scheme 3.7). The generation of ethanolic Na_2S (cloudy

Scheme 3.7

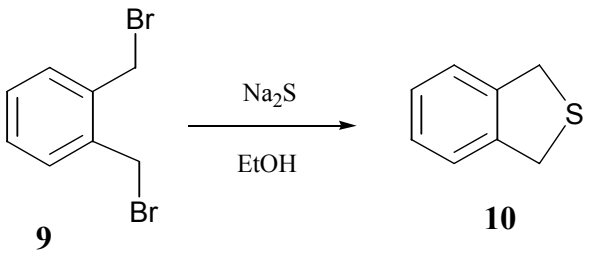

9 **10**

yellow-colored solution) in large amounts is crucial for achieving a good yield of **10**, although the solution may still not be saturated even after increasing the time of bubbling from 30 minutes (lit. ref.) to 1.5 hours. Furthermore, once reagent **9** is added, a S_N2 displacement of both bromine atoms by Na_2S must occur to form **10**. This may contribute to the low yield (*ca.* 23%) of **10**, because the addition of **9** to the ethanolic solution creates a viscous suspension that is difficult to stir. A gentle reflux of ethanol was observed on the sides of the flask upon addition of **9**, in addition to the liberation of heat from the bottom.

The distillation of pure **10** from the crude oil was performed until 10% crude material remained, and solidification occurred almost immediately upon placement of the pure material in the freezer. Product **10** decomposes to an unknown black material, presumably from oxidation, when left open to the air at room temperature for a few hours.

The NMR spectra of **10** were easily interpreted. In the ^{1}H NMR spectrum of **10** (Figure 3.24), the methylene protons are found at 4.28 ppm, while the aromatic protons are found as a multiplet (7.21-7.27 ppm) due to an AA'BB' splitting. The ^{13}C NMR spectrum of **10** (Figure 3.25) shows four resonances. The symmetric methylene carbons are located at 38.28 ppm, while the aromatic carbons are found at 124.92, 126.94 and 140.48 ppm.

3.2.4.2. 1,3-Dihydrobenzo[c]thiophene-2,2-dioxide (11)

This second stage of the five step synthesis (Scheme 3.6) was also achieved by following a procedure from Cava et al.[24] In this step, thiophene **10** was oxidized to sulfone **11** with peracetic acid at low temperatures (Scheme 3.8). The procedure is relatively simple, and high yields (>90%) are generated as long as the temperature is kept within the stated range. In addition, sulfone **11** precipitated as pure white crystals

Scheme 3.8

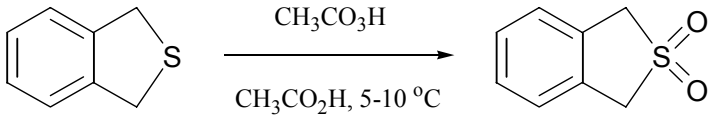

10 **11**

.

from the acetic acid solution, and therefore did not need to be recrystallized as stated in the procedure.[24]

In the ^{1}H NMR spectrum of **11** (Figure 3.26), all proton signals are shifted slightly downfield, with respect to **10**, due to the electron withdrawing nature of the oxygen atoms. The methylene protons are now located at 4.37 ppm, while the aromatic protons are once again found as a multiplet from 7.28-7.38 ppm, due to the AA'BB' splitting that occurs. The ^{13}C NMR spectrum (Figure 3.27) shows four resonances that are also shifted downfield. The signal representing the methylene carbons is now located at 57.16 ppm, while the aromatic carbons have shifted downfield to 126.28, 129.07 and 131.48 ppm.

3.2.4.3. 1,3-Dihydro-5-nitrobenzo[c]thiophene-2,2-dioxide (^{15}N-labeled) (12)

The third stage of the five step synthesis (Scheme 3.6) dealt with the inclusion of a ^{15}N-labeled atom via the nitration of 1,3-dihydrobenzo[c]thiophene-2,2-dioxide **11** in sulfuric acid. The procedure of converting **11** to **12** (Scheme 3.9) was adapted from

Walter and co-workers,[25] where ^{15}N nitric acid (65 wt.%, 99% ^{15}N) was substituted for the non-labeled acid. The starting material was not dissolved when the nitric acid solution was less than 65 wt.%. This is due to the high insolubility of **11** in water. Furthermore, the yield of **12** was markedly increased (from 81.5% to 93.8%) by stirring the solution at room temperature for an additional two hours (5 hrs. total). The product

Scheme 3.9

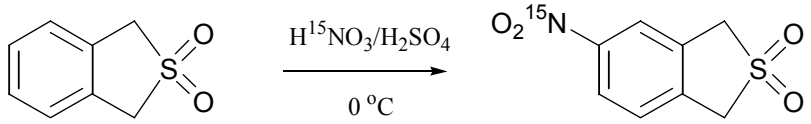

11 **12**

(**12**) was precipitated as a clumpy white material when poured over crushed ice in a beaker. A faint smell of sulfuric acid remained even after the product was washed numerous times with water. The product was *ca.* 98% pure from the ^{1}H NMR and was used without further purification.

In the ^{1}H NMR spectrum of **12** (Figure 3.28), the methylene protons are shifted downfield (compared to **11**) due to the addition of the electron withdrawing nitro group. These protons are now found at 4.46 and 4.48 ppm. In addition, the aromatic protons are no longer symmetric, and are now located at 7.54, 8.24 and 8.26 ppm.

The signals in the ^{13}C NMR spectrum (Figure 3.29) are also shifted downfield. Methylene carbons are found at 56.82 and 56.86 ppm, while the carbons with attached protons are located at 121.70, 124.23 and 127.50 ppm. The signals for the two carbon atoms of the aromatic ring that are adjacent to the methylene carbons are found at 133.32 and 138.50 ppm, respectively. Furthermore, the ^{15}N atom of the nitro group is coupled to the adjacent carbon of the aromatic ring to yield a doublet ($^{1}J_{NC}$ = 15.2 Hz) centered at 148.33 ppm.

---

[25] Walter, M.; Gügel, A.; Spickermann, J.; Belik, P.; Kraus, A.; Müllen, K. Synthesis and Chemical Transformations of the Diels-Alder Adduct of [60]Fullerene and 4-Amino-*o*-quinodimethane. *Fullerene Sci. Technol.* **1996**, *4*, 101−113.

3.2.4.4. 5-Amino-1,3-dihydrobenzo[c]thiophene-2,2-dioxide (^{15}N-labeled) (13)

The synthesis of 5-amino-1,3-dihydrobenzo[c]thiophene-2,2-dioxide (^{15}N-labeled) **13** was accomplished by reducing the nitro group of **12** with zinc metal in refluxing trifluoroacetic acid (Scheme 3.10). This procedure was not taken from the literature.

Scheme 3.10

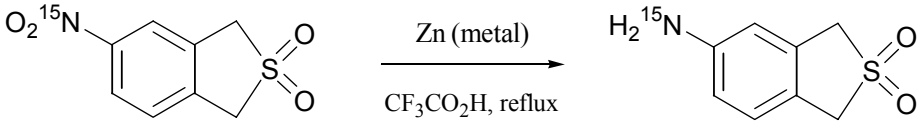

12 **13**

A few problems were encountered during this procedure. First of all, while the reduction of **12** proceeded quickly (<15 minutes), a side reaction with zinc produced a reddish-colored solution. As a result, neutralization of the solution with 25 wt.% NaOH (to precipitate **13**) produced a mustard-colored precipitate. The precipitate was not soluble in chloroform, benzene, methylene chloride, acetone, methanol or dimethyl sulfoxide, although sonication in DMSO-d_6 dissolved a sufficient amount material to acquire a ^{1}H NMR spectrum that showed the presence of solely **13**. It is unclear as to what the majority of the precipitate was, although zinc oxide and zinc acetate are possible explanations. Furthermore, additional signals were not present in the ^{1}H NMR spectrum of the crude product, because trifluoroacetic acid was used as the solvent instead of glacial acetic acid. The desired product (**13**) was extracted with hot water (100 °C), and gravity filtered to separate from the crude insoluble material. The bright yellow color of **13** could not be removed, and therefore was used without further purification. Attempts at utilizing concentrated HCl as the solvent or tin metal as the reducing agent were both unsuccessful at yielding **13**.

The ^{1}H NMR spectrum of **13** (Figure 3.30) shows signals at 4.22 and 4.28 ppm that correspond to the four methylene protons. The equivalent protons of the amine are split by the ^{15}N nitrogen atom, thereby yielding a doublet ($^1J_{HN}$ = 84 Hz) that is centered at

5.25 ppm. The three aromatic protons of the compound are found at 6.48, 6.52 and 6.96 ppm.

For the ^{13}C NMR spectrum of **13** (Figure 3.31), the methylene carbons are located at 56.39 and 57.03 ppm, while the aromatic carbons that are bound to hydrogen atoms are found at 110.94, 114.56, 118.79, 127.03, 133.29 and 149.43 ppm. A coupling between the adjacent aromatic carbon and the ^{15}N nitrogen atom was not observed.

A signal for the ^{15}N nitrogen atom was located at 57.30 ppm in the ^{15}N NMR spectrum of **13** (Figure 3.32).

3.2.4.5. Terminal amine derivative of $Sc_3N@C_{80}$ (^{15}N-labeled) (14)

The ^{15}N-labeled terminal amine derivative of $Sc_3N@C_{80}$ **14** was synthesized (Scheme 3.11) by refluxing a 1,2,4-trichlorobenzene (TCB) solution of $Sc_3N@C_{80}$ **3** with a ten-fold excess of 5-amino-1,3-dihydrobenzo[c]thiophene-2,2-dioxide (^{15}N-labeled) **13**. Sulfur dioxide (SO_2) is thermally extruded from **13** when heated at over 200 °C, forming a highly reactive *o*-quinodimethane intermediate that undergoes a [4 + 2] cycloaddition with the $Sc_3N@C_{80}$ **3** metallofullerene. This reaction is similar to the one depicted in Scheme 3.2. Failure to use an excess of reagent **13** results in extremely low yields of adduct **14**.

Scheme 3.11

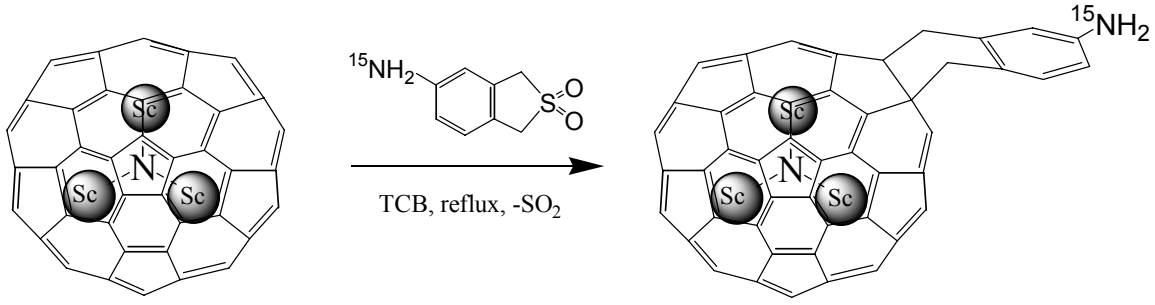

3 **14**

The HPLC chromatogram (Buckyclutcher column) of **14** in chloroform shows four peaks (Figure 3.9). Peaks labeled 2 (23.18 min.), 3 (25.67 min.) and 4 (27.88 min.)

correspond to adduct **14**, while the fourth (peak 1, 16.42 min.) is the parent metallofullerene **3**. Injection sizes were 200 µl at 1.25 ml/min. Flash chromatography on silica gel can also be used to separate the unfunctionalized $Sc_3N@C_{80}$ **3** (removed with toluene) from adduct **14** (removed with a toluene/methanol (4:1) mixture), although

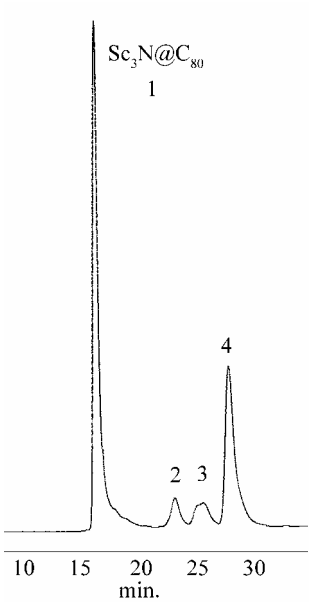

Figure 3.9. HPLC chromatogram of $Sc_3N@C_{80}$–terminal amine derivatives (^{15}N-labeled) **14** and unreacted $Sc_3N@C_{80}$ **3**.

HPLC purification of the latter fraction is still need to separate the three isomers of **14**. Concentrations of **14** from HPLC are *ca.* 5% for peaks 2 and 3, while peak 4 is more than five times those at 29%. Yield of peak 4 was *ca.* 16 milligrams. All products appear as brown/black in color. The longer retention times of the three products, with respect to the parent metallofullerene, are most likely due to the materials possessing a larger internal dipole moment (from to the metal-nitride cluster) and/or a more polarizable electronic configuration on the exterior of the cage as a result of the exohedral functionalization. Furthermore, because the HPLC solvent is chloroform, the amine of **14** could hydrogen bond with a nearby mono-adduct, thereby creating adducts that appear to be larger and even more polar.

A ^{1}H NMR spectrum of **14** (Figure 3.33) was only obtained from peak 4 of the three isomers, due to the likelihood that the product results from the I_h isomer of $Sc_3N@C_{80}$.

In addition, adduct **14** is even less soluble in 1,1,2,2-tetrachloroethane-d_2 than adduct **4** (section 3.3.1), due to the hydrogen bonding amine, which thereby decreased the ability to obtain a well resolved proton spectrum. Resonances that represent the methylene protons of **14** are located as a multiplet in the range of 3.33-3.56 ppm. As stated in section 3.3.1, motion (ring inversion) of the six-membered ring of the adduct is responsible for the broadening of the peaks. The amine protons are found as a broad doublet (3.65-4.00 ppm) due to hydrogen bonding between amine groups of neighboring adducts and small traces of water. Addition of D_2O to the NMR tube shows the disappearance of these signals due to proton exchange. The three phenyl protons are located in the range of 6.56-7.00 ppm. Raising the NMR temperature to 90 ºC will sharpen the linewidths by causing fast ring inversion of the adduct, in addition to less hydrogen bonding between the amine groups of neighboring adducts.

The other two products of **14** are probably derivatives of the D_{5h} isomer of $Sc_3N@C_{80}$ (Chapter 5). A ^{13}C NMR of spectrum was not obtained due to the lack of a ^{13}C-labeled atom and low product solubility. The low solubility of **14** in deuterated solvents prevented the attainment of a ^{15}N NMR spectrum; however, when $Sc_3N@C_{80}$ in Scheme 3.11 was replaced by C_{60} fullerene the resulting product had a greater solubility in 1,1,2,2-tetrachloroethane-d_2, and a signal for the ^{15}N nitrogen atom of the amine group was found at 51.34 ppm.

Although the yield of product **14** is low, the inability to acquire larger amounts of $Sc_3N@C_{80}$ (starting material) has prevented attempts to couple novel peptides and/or water-soluble groups to the ^{15}N-labeled terminal amine of **14**.

3.2.5. Water-soluble metallofullerenols from $Sc_3N@C_{80}$ (15)

Water-soluble $Sc_3N@C_{80}$ metallofullerenols **15** were achieved by employing a similar procedure used by Lu and co-workers[26] to synthesize C_{60} and C_{70} fullerenols. A toluene solution of pure $Sc_3N@C_{80}$ **3** (*ca.* 4 mg, 99%) was refluxed with sodium metal under an argon atmosphere to produce a black polyanionic species that precipitated from solution

[26] Lu, C.; Yao, S.; Wang, W.; Tong, Y.; Lin, W.; Rong, T.; Lin, N. Laser flash photolysis of fullerols of C-60 and of C-70 in aqueous solutions. *Sci. China, Ser. B* **1998**, *41*, 259–265.

(Scheme 3.12). Exposure of this mixture to water and air then oxidized the precipitate and produced a golden-colored aqueous solution that contained **15**. The addition of

Scheme 3.12

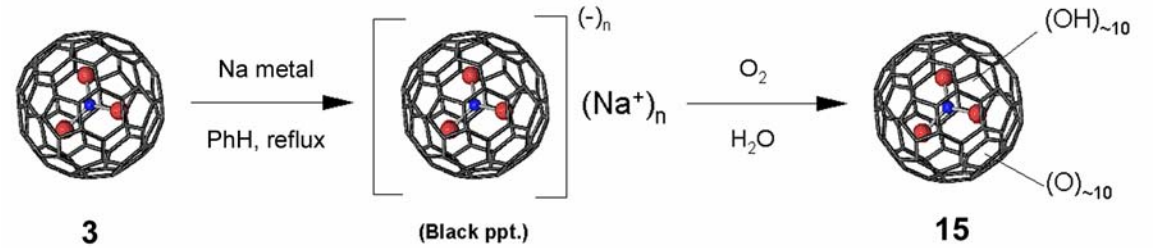

oxygen has been found to be important to the formation of water-soluble fullerene adducts.[27] The mechanism of hydroxyl group formation is unknown.

The FT-IR spectrum of the water-soluble polyhydroxylated adducts **15** (Figure 3.34) was measured on a polyethylene card. The spectrum shows a broad peak at 3384.6 cm^{-1} for the hydroxyl groups attached to the carbon cage. A strong peak at 1629.0 cm^{-1} yields evidence of remaining pi-bonded carbons (C=C), while an OH deformation stretch, 1323.1 cm^{-1}, and C–O stretching absorptions, 1107.7 cm^{-1} and 1028.1 cm^{-1}, both appear as strong and broad peaks. These results are consistent with previously reported FT-IR spectrum of fullerenols and metallofullerenols.[27,28,29] The broad band at 615.4 cm^{-1} is also consistent with the assignment for the internal Sc_3N cluster recently reported as 599, 621, and 577 cm^{-1}, for $Sc_3N@C_{80}$ (experimental), $[Sc_3N]^0$ (calculated), and $[Sc_3N]^{6+}$ (calculated), respectively.[30] Figure 3.35 shows the IR peaks that are attributed to the polyethylene card (blank).

---

[27] Li, J.; Takeuchi, A.; Ozawa, M.; Li, X.; Saigo, K.; Kitazawa, K. C_{60} Fullerol Formation Catalyzed by Quaternary Ammonium Hydroxides. *J. Chem. Soc., Chem. Commun.* **1993**, 1784–1785.

[28] Zhang, S.; Sun, D.; Li, X.; Pei, F. Liu, S. *Fullerene Sci. Technol.* **1997**, *5*, 1635.

[29] Kato, H.; Suenaga, K.; Mikawa, M.; Okumura, M.; Miwa, N.; Yashiro, A.; Fujimura, H.; Mizuno, A.; Nishida, Y.; Kobayashi, K.; Shinohara, H. Syntheses and EELS Characterization of Water-soluble Multi-hydroxyl $Gd@C_{82}$ Fullerenols. *Chem. Phys. Lett.* **2000**, *324*, 255–259.

[30] Krause, M.; Kuzmany, H.; Georgi, P.; Dunsch, L.; Vietze, K.; Seifert, G. Structure and Stability of Endohedral Fullerene $Sc_3N@C_{80}$: A Raman, Infrared, and Theoretical Analysis. *J. Chem. Phys.* **2001**, *115*, 6596–6605.

An X-ray Photoelectron Spectroscopy (XPS) spectrum of the metallofullerenols **15** on gold (Figure 3.10) demonstrates the different types of functionalized carbon atoms on the water-soluble cages. The asymmetric spectrum for the core level region of carbon

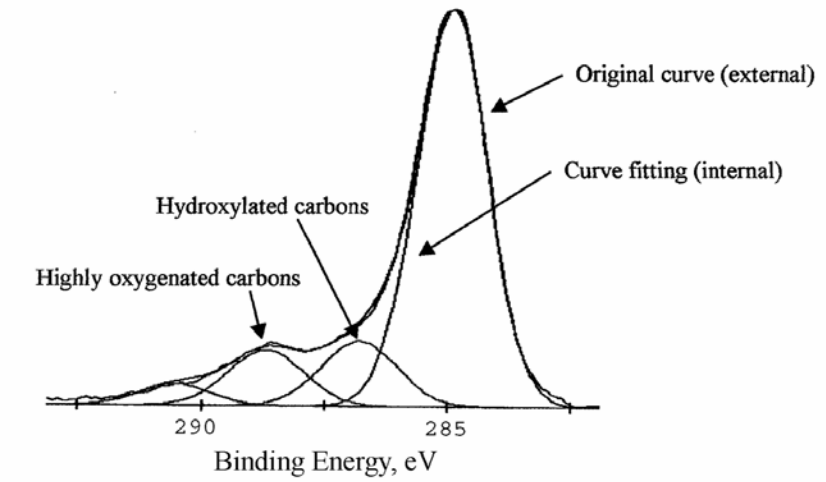

Figure 3.10. Carbon XPS of water-soluble metallofullerenols **15** on gold.

(C1s) indicates that oxidative cage functionalization has occurred, and a curve fitting of the region requires four distinct peaks to fit the asymmetric curve, as illustrated. The largest peak, 284.94 eV (73%), is consistent with sp^2 non-functionalized carbon atoms for the remaining pi-bonded carbons of the cage. Peaks at 286.80 eV (12.6%) and 288.69 eV (10.8%) are attributed to hydroxylated (–C–OH) and highly oxygenated carbon atoms (ether linkages or peroxides), respectively. Once again, this is similar to previously reported carbon XPS data for water-soluble metallofullerene adducts.[31] The corresponding areas of the oxygenated carbon (hydroxylated and highly oxygenated) peak areas suggest a metallofullerenol with the formula $Sc_3N@C_{80}(OH)_{\sim 10}(O)_{\sim 10}$. The small peak around 290.54 eV (3.6%) is a $\pi \rightarrow \pi^*$ transition, or shake-up.

The laser-desorption time-of-flight (LD-TOF) mass spectrum of **15** (Figure 3.11) shows a single peak at *m/z* = 1109, indicating the presence of the parent endohedral metallofullerene, $Sc_3N@C_{80}$ **3**. Similar to previous work on hydroxylated

[31] Sun, D.; Huang, H.; Yang, S. Synthesis and Characterization of a Water-soluble Endohedral Metallofullerol. *Chem. Mater.* **1999**, *11*, 1003–1006.

metallofullerenes, the water-soluble adducts decompose to the unsubstituted metallofullerene during heating/laser desorption.

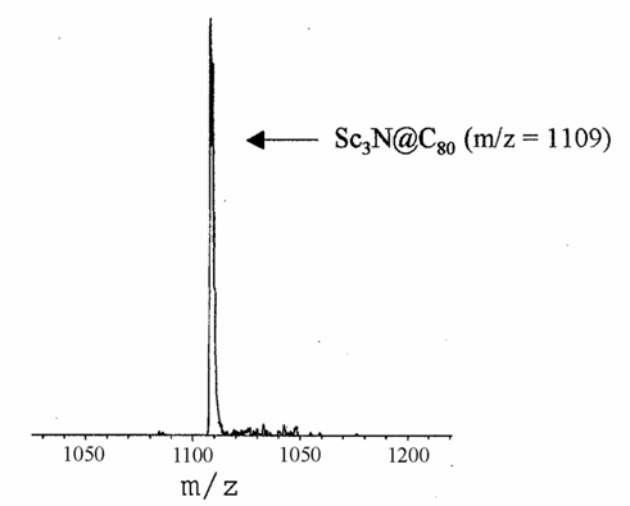

Figure 3.11. LD-TOF mass spectrum of decomposed metallofullerenols **15**.

This data represents the first synthesis of a water-soluble trimetallic nitride endohedral metallofullerene.[32] However, it is worth noting that these metallofullerenols can also be synthesized with a 50 wt.% NaOH solution and a few drops of tetrabutylammonium hydroxide (TBAOH) as a phase-transfer agent.

An attempt to synthesize a water-soluble polyhydroxylated derivative of 4,5-dimethoxy-*o*-quinodimethane–$Sc_3N@C_{80}$ **4**, via the phase-transfer method, was only *partially* successful. For instance, adduct **4** (*ca.* 16.5 mg) precipitated from a toluene solution upon addition of the TBAOH phase-transfer agent; however, when the precipitate was stirred in water, only a *small amount* of material dissolved to produce a golden-brown colored aqueous solution. Furthermore, a ^{13}C NMR spectrum of this water-soluble material in D_2O did not show the presence of the ^{13}C-labeled atom on **4**.

There are two explanations for why a ^{13}C NMR signal of the aforementioned water-soluble adduct was not observed. First of all, adduct **4** may not have been hydroxylated enough to provide a highly water-soluble sample, thereby preventing a signal from being

[32] Iezzi, E. B.; Cromer, F.; Stevenson, P.; Dorn, H. C. Synthesis of the First Water-soluble Trimetallic Nitride Endohedral Metallofullerols. *Synth. Met.* **2002**, *128*, 289–291.

observed due to a dearth of sample in the NMR tube. Second, the cage of adduct **4** may have been hydroxylated in random positions and may contained a wide range of hydroxyl groups. This would cause a large number of broadened and poorly resolved ^{13}C NMR signals to be present in the spectrum, rather than a single well resolved signal that represented a single product. Figure 3.12 is a conceptual drawing of adduct **4** with a

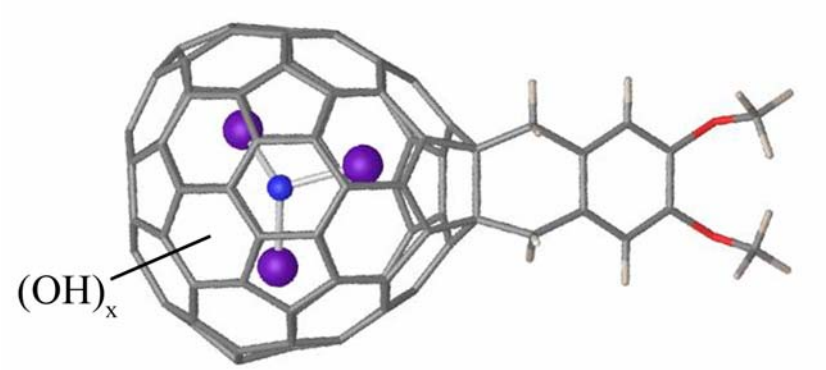

Figure 3.12. Conceptual drawing of adduct **4** when polyhydroxylated.

polyhydroxylated cage.

Water-soluble metallofullerene derivatives that contain specific metal atoms may have applications as MRI, X-ray and PET imaging agents.

3.3. Experimental

3.3.1. Materials and purification

HPLC grade solvents were used unless stated otherwise. Anhydrous solvents were obtained by distillation from appropriate drying agents. Toluene was refluxed with sodium metal and distilling at a reduced pressure. 1,2,4-trichlorobenzene (TCB) was obtained from Aldrich chemical company as anhydrous.

Solvents for extraction and chromatography were HPLC grade unless otherwise specified. All HPLC separations were performed using an Acuflow Series III pump and Applied Biosystems 757 Absorbance Detector (λ = 390 nm). Data was recorded on a Hitachi D-2500 Chromato-Integrator. The $Sc_3N@C_{80}$ metallofullerene was purified from soluble fullerene extract by employing a two-stage HPLC process. The first stage used a 5-PBB (pentabromobenzyl) column (5 μm, 250 mm x 20 mm ID: Phenomenex) with carbon disulfide (CS_2) as the eluent. The flow rate was 2 ml/min. The second stage used a Trident-Tri-DNP (Buckyclutcher) column (5 μm, 250 mm x 10 mm ID: Regis Chemical) with toluene as the eluent. The flow rate was 2 ml/min. HPLC purification of $Sc_3N@C_{80}$ adducts were performed using the Buckyclutcher column with chloroform as eluent (1.25 ml/min.), unless stated otherwise. Flash chromatography purification of functionalized $Sc_3N@C_{80}$ was performed using Silica gel (200–400 Mesh, 60Å) from Aldrich chemical company.

Chloroform-d and 1,1,2,2-tetrachloroethane-d_2 (both from Cambridge Isotope Laboratory) were dried with molecular sieves. All other deuterated solvents were used as received.

Suppliers of reagents were as follows: Luna nanoMaterials – $Sc_3N@C_{80}$ (*ca.* 97%); Aldrich – (3,4-dimethoxyphenyl)acetic acid (98%), 1,8-diazabicyclo[5.4.0]undec-7-ene (DBU, 98%), CBr_4 (99%), sodium (dry, stick), α,α'-dibromo-*o*-xylene (96%), hydrogen sulfide (99.5+%), peracetic acid (32 wt.% in AcOH), trifluoroacetic acid (TFA, 99%), petroleum ether (38-60 °C b.p.), dibenzyl malonate (99%), tetrabutylammonium hydroxyide (TBAOH, 40 wt.%), aqueous sodium hydroxide (50 wt.%), sodium metal (in kerosene); Cambridge Isotope Laboratory – Formaldehyde (20 wt.% in H_2O, ^{13}C 99%),

diethyl malonate (2-^{13}C 99%); Icon Isotopes – ^{15}N nitric acid (65 wt.%, ^{15}N 99%); VWR – Zinc metal.

Commercial reagents were purified as follows: (3,4-dimethoxyphenyl)acetic acid was recrystallized from H_2O; α,α'-dibromo-*o*-xylene was recrystallized from $CHCl_3$; zinc metal was ground with mortar and pestle, washed with conc. HCl for two minutes, washed with H_2O, washed with MeOH and allowed to dry. All other reagents were used as received from vendor.

3.3.2. Analytical methods

^{1}H and ^{13}C NMR spectra were obtained with either a JEOL Eclipse+ 500 spectrometer or a Varian Unity 400 spectrometer, unless stated otherwise. Tetramethylsilane (TMS) was used as the external standard. ^{1}H-^{13}C Heteronuclear Multiple Quantum Correlation (HMBC), ^{1}H-^{13}C Heteronuclear Multiple Bond Correlation (HMQC) ^{1}H-^{1}H Correlation Spectroscopy (COSY) and ^{15}N NMR spectra were obtained with a JEOL Eclipse+ 500 spectrometer. Nitromethane was used as the external standard for ^{15}N NMR spectra. The ^{13}C NMR spectra of the functionalized metallofullerenes were recorded using a 5 second delay between pulses, while an 8 second delay was used for obtaining ^{15}N NMR spectra of specific functionalized metallofullerenes.

Mass spectra of functionalized metallofullerenes were obtained with a Kratos Kompact SEQ matrix-assisted laser-desorption ionization time-of-flight (MALDI-TOF) mass spectrometer using 9-nitroanthracene as a matrix. Mass spectra of non-functionalized (parent) metallofullerenes were obtained with a Fisons VG Quattro mass spectrometer using a desorption chemical-ionization (DCI) probe and negative ionization. All other mass spectra were obtained with a JEOL HX-110 Dual Focusing mass spectrometer using high resolution fast atom bombardment (HR-FAB) or electron ionization (EI).

Infrared spectra were recorded with a Perkin Elmer 1615 Series FT-IR Spectrometer and disposable 3M™ polyethylene cards. Range of transmission was 4000–400 cm^{-1}. UV-Visible spectra were obtained using quartz cuvettes and a Spectronic GenSys 5

Spectrometer (Emory and Henry College). X-ray photoelectron spectra of samples were acquired with a Perkin Elmer 5400 XPS.

3.3.3. Synthesis of ^{13}C-labeled 6,7-dimethoxyisochroman-3-one (2)

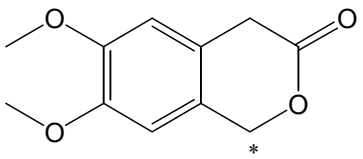

0.714 g (3.64 mmol) of (3,4-dimethoxyphenyl)acetic acid **1** (Aldrich) was added to a 25 ml round bottom flask with 2.12 ml of glacial acetic acid. The flask was placed in a hot water bath and stirred until all material was dissolved. 0.60 ml of conc. HCl (37 wt.%) and 1 ml (7.20 mmol) of a formaldehyde (99% ^{13}C) (Cambridge Isotope Laboratory, Inc.) solution were then added to the round bottom, and the entire solution was heated for 1 hour at *ca.* 83 °C. The solution turned a bright yellow color during that period. Once finished, the solution was cooled to room temperature, and 5 ml of H_2O and 10 ml of $CHCl_3$ were added to the flask. The flask was shaken, and the contents were poured into a 30 ml separatory funnel. The $CHCl_3$ layer (bottom) was added to a 125 ml separatory funnel and the aqueous solution was extracted again with 10 ml of $CHCl_3$. Small portions of a 5 wt.% $NaHCO_3$ solution (5 g in 95 ml H_2O) were added to the separatory funnel, with shaking and venting, until all the acetic acid was neutralized. 20 ml of H_2O was then added to the separatory funnel, and the $CHCl_3$ layer was added to a 25 ml round bottom flask. The pH of solution was tested to make sure it was neutral. A few spatula tips full of Na_2SO_4 were added to the round bottom, and the solution was poured into a 25 ml pear shaped flask. The solvent was removed via rotary evaporator to reveal a pale yellow material. The product was recrystallized with EtOH (200 proof) to yield white crystals. The product was air dried, then dried in an oven (*ca.* 110 ºC) for 30 minutes. Weight of product was 0.235 g (30.8% yield). ^{1}H NMR (400 MHz, $CDCl_3$): δ 3.63 (s, 2H), 3.88 (s, 6H, OCH_3), 5.25 (d, 2H, $^1J_{CH}$ = 149.2 Hz, CH_2), 6.70 (s, 1H, aromatic CH) and 6.74 (d, 1H, aromatic CH). ^{13}C NMR (100 MHz, $CDCl_3$, 1s delay, 44.7° pulse, 3000 scans): δ 35.81, 56.35, 56.39, 70.24, 108.24, 110.36, 123.17, 123.79, 149.63 and 171.06. HR-FAB MS (positive ionization): Calcd. mass is 209.100, and found 210.08386 [M + 1].

Figure 3.13. 400 MHz ^{1}H NMR spectrum of ^{13}C-labeled 6,7-dimethoxyisochroman-3-one **2**.

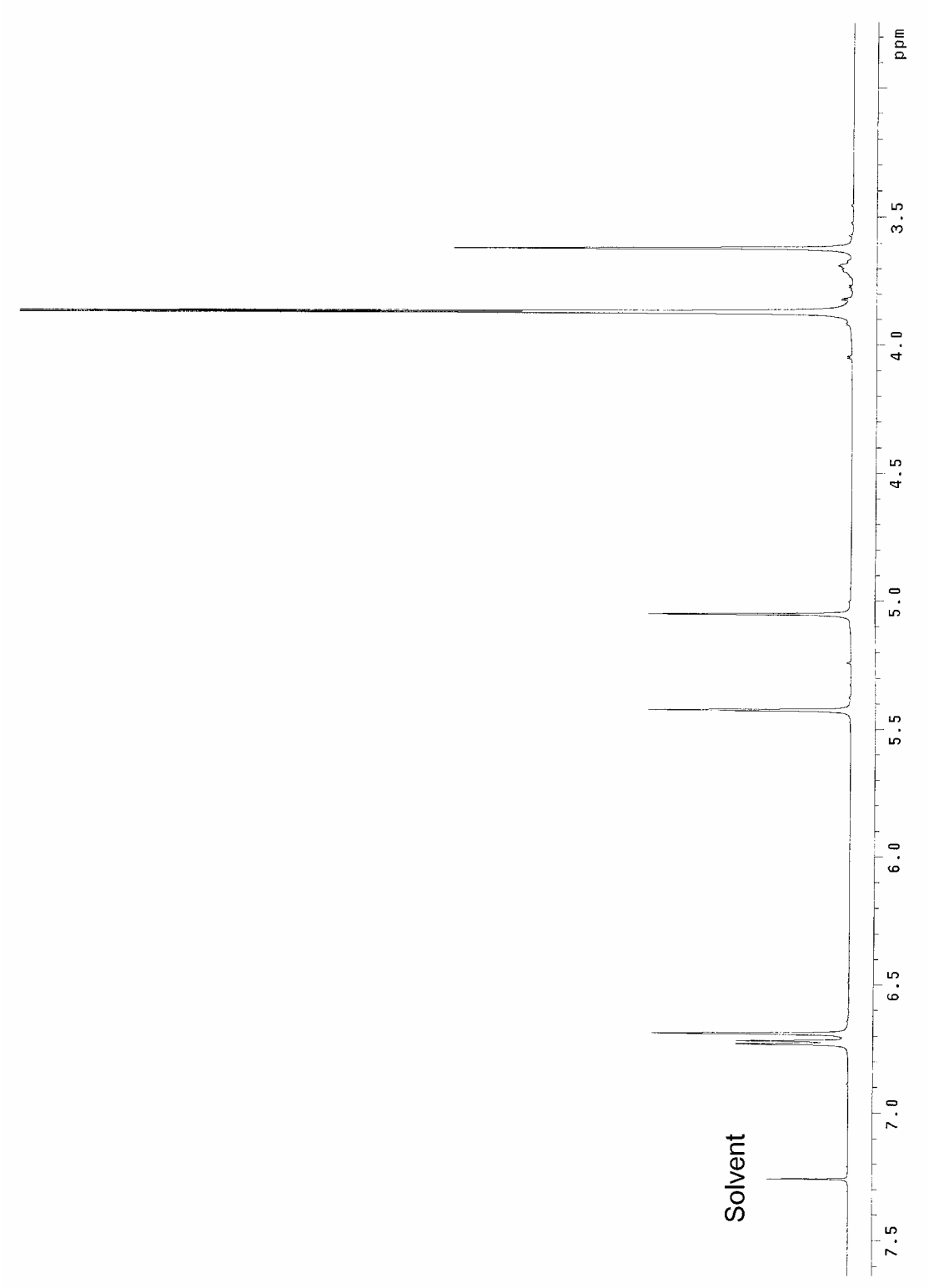

Figure 3.14. 100 MHz ^{13}C NMR spectrum of ^{13}C-labeled 6,7-dimethoxyisochroman-3-one **2**.

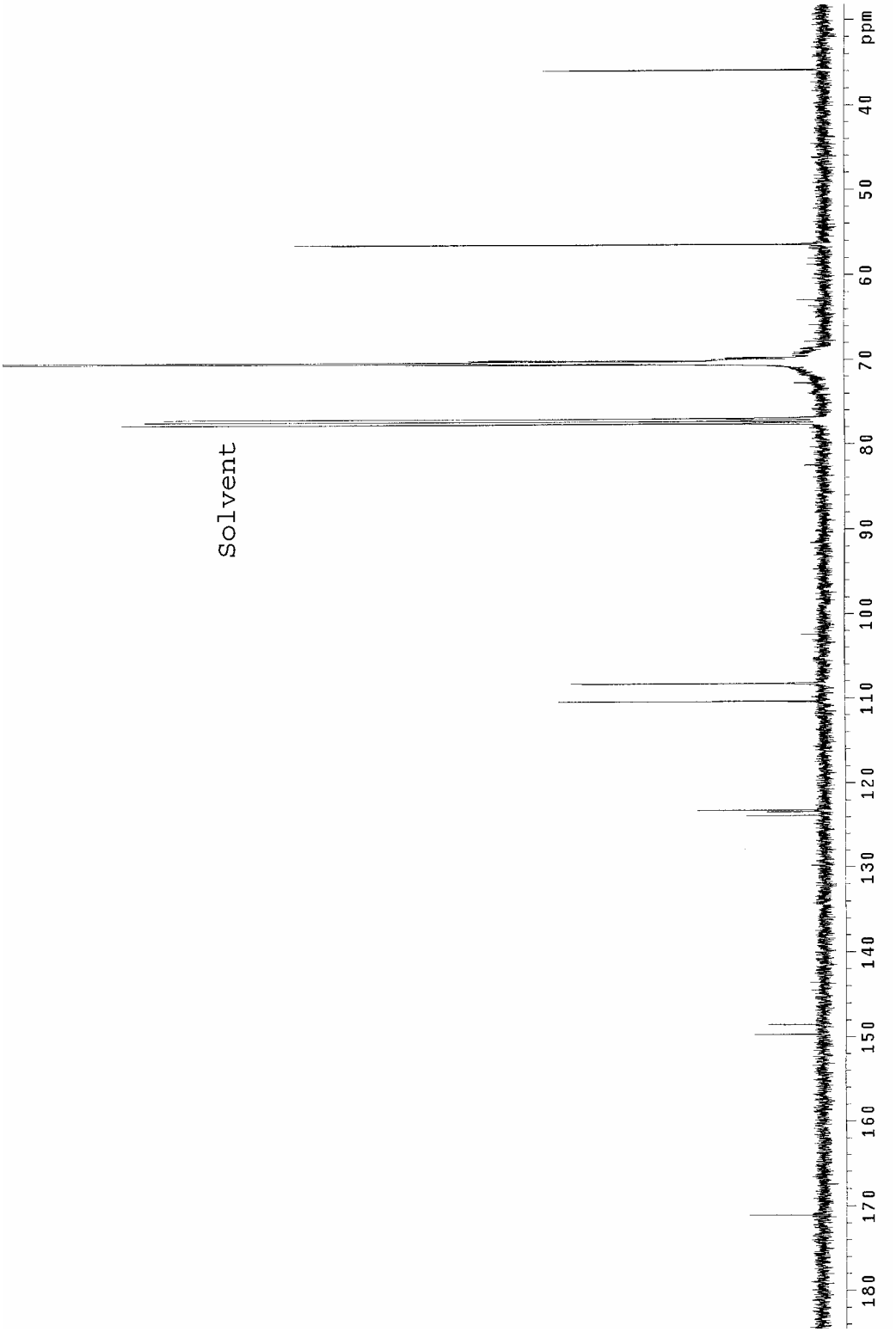

3.3.4. Synthesis of ^{13}C-labeled $Sc_3N@C_{80}$–$C_{10}H_{12}O_2$ cycloadduct (4)

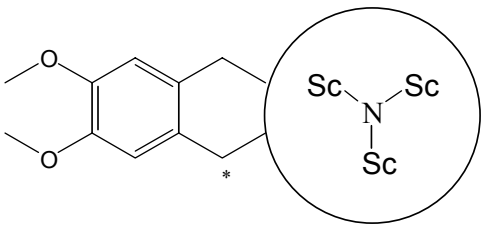

10 ml of 1,2,4-trichlorobenzene (TCB) was added to a 25 ml round bottom flask containing *ca.* 6.5 mg (0.59 μmol) of $Sc_3N@C_{80}$ **3** (99%) metallofullerene. While stirring, a 3 ml solution containing 12.25 mg (5.86 μmol) of 6,7-dimethoxyisochroman-3-one (^{13}C-labeled) **2** was added, and the solution was refluxed under a nitrogen atmosphere for 24 hours. The solution was allowed to cool to room temperature, and the solvent was removed via reduced pressure and low heat to obtain a brown colored product. The crude reaction product was separated by HPLC using the Buckyclutcher column with $CHCl_3$ as eluent. Adduct **4** elutes at 18.63 minutes. Weight of product was *ca.* 2.5 mgs (41% from HPLC). ^1H NMR (400 MHz, $C_2Cl_4D_2$, 23 ºC): δ 3.20-3.80 (m, br, 4H), 3.98 (s, 6H, OCH_3) and 7.01 (s, 2H, CH). ^{13}C NMR (90 MHz, $C_2Cl_4D_2$, 16 hour scan): δ 42.25 (s, CH_2). HMQC (500 MHz, $C_2Cl_4D_2$), HMBC (500 MHz, $C_2Cl_4D_2$), and COSY (500 MHz, $C_2Cl_4D_2$) spectra were also acquired. MALDI-TOF (negative ionization): masses found at 1274 for product and 1109 for $Sc_3N@C_{80}$. UV-Vis ($CHCl_3$): peak at 965 nm.

Figure 3.15. 400 MHz ^{1}H NMR spectrum of ^{13}C-labeled $Sc_3N@C_{80}$ mono-adduct **4** at room temperature (23 ºC).

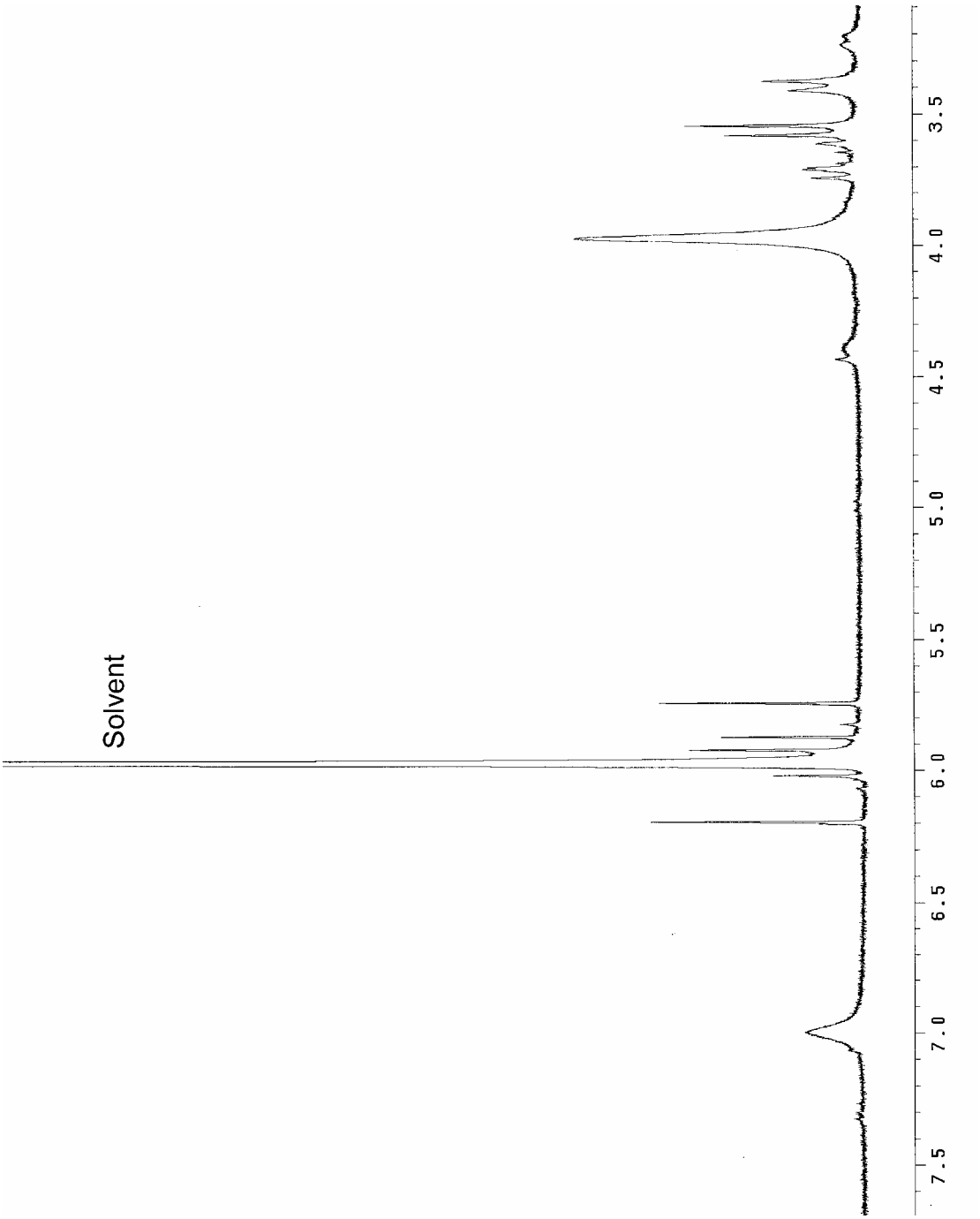

Figure 3.16. 100 MHz ^{13}C NMR spectrum of ^{13}C-labeled $Sc_3N@C_{80}$ mono-adduct **4**.

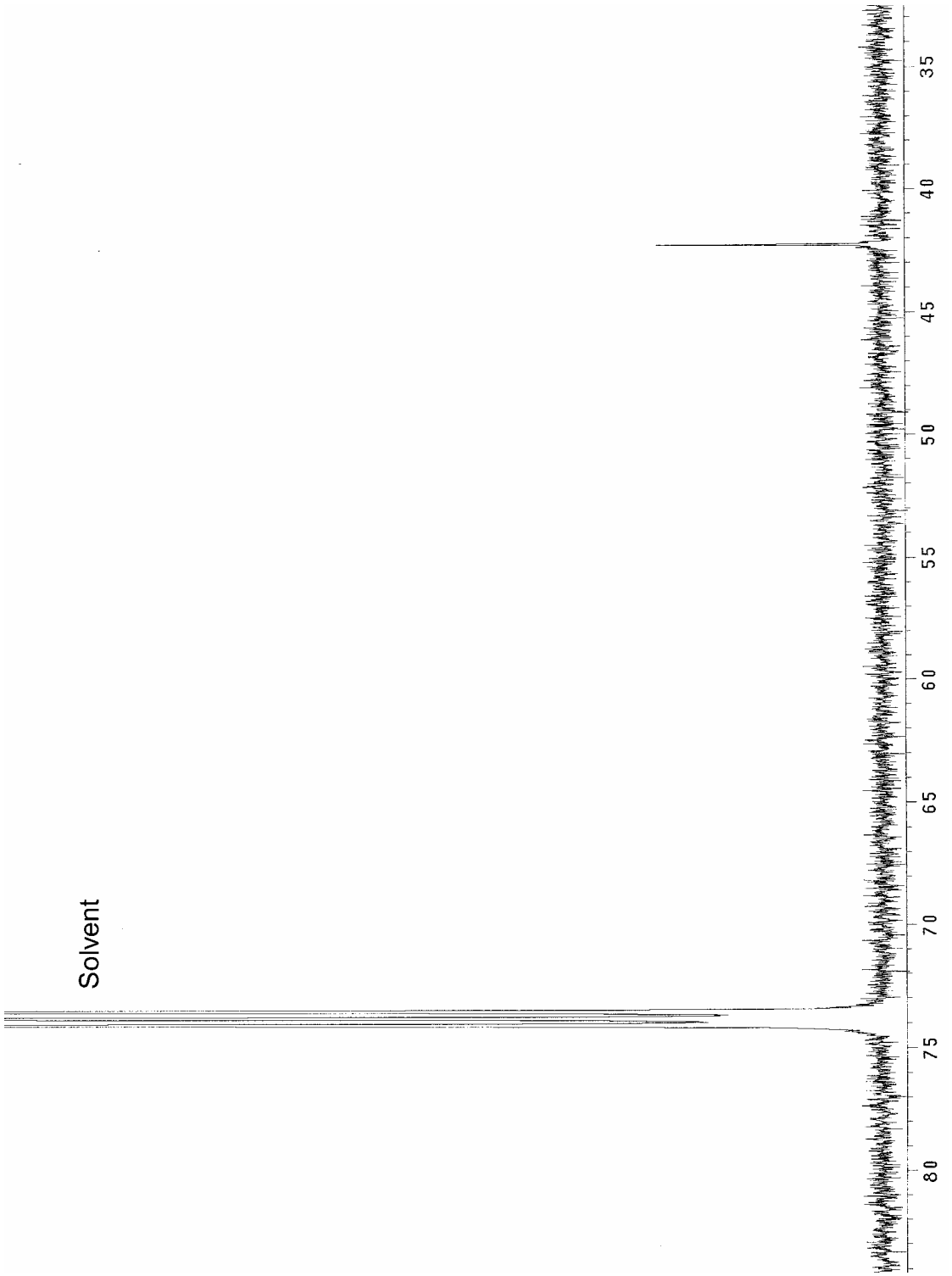

Figure 3.17. 500 MHz COSY spectrum of ^{13}C-labeled $Sc_3N@C_{80}$ mono-adduct **4**.

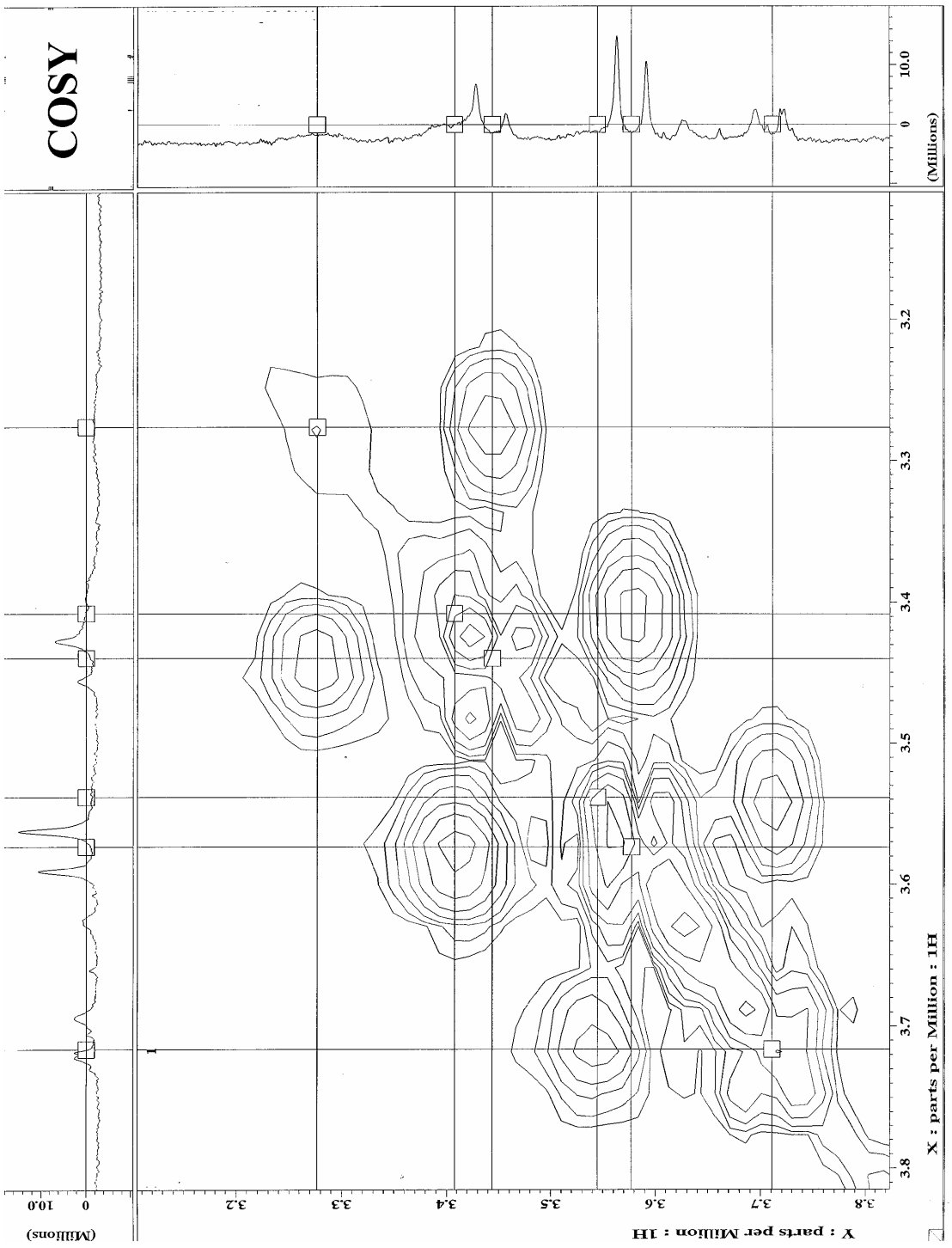

Figure 3.18. 400 MHz ^{1}H NMR spectrum at 90 ºC of ^{13}C-labeled $Sc_3N@C_{80}$ mono-adduct **4** in 1,1,2,2-tetrachloroethane-d_2.

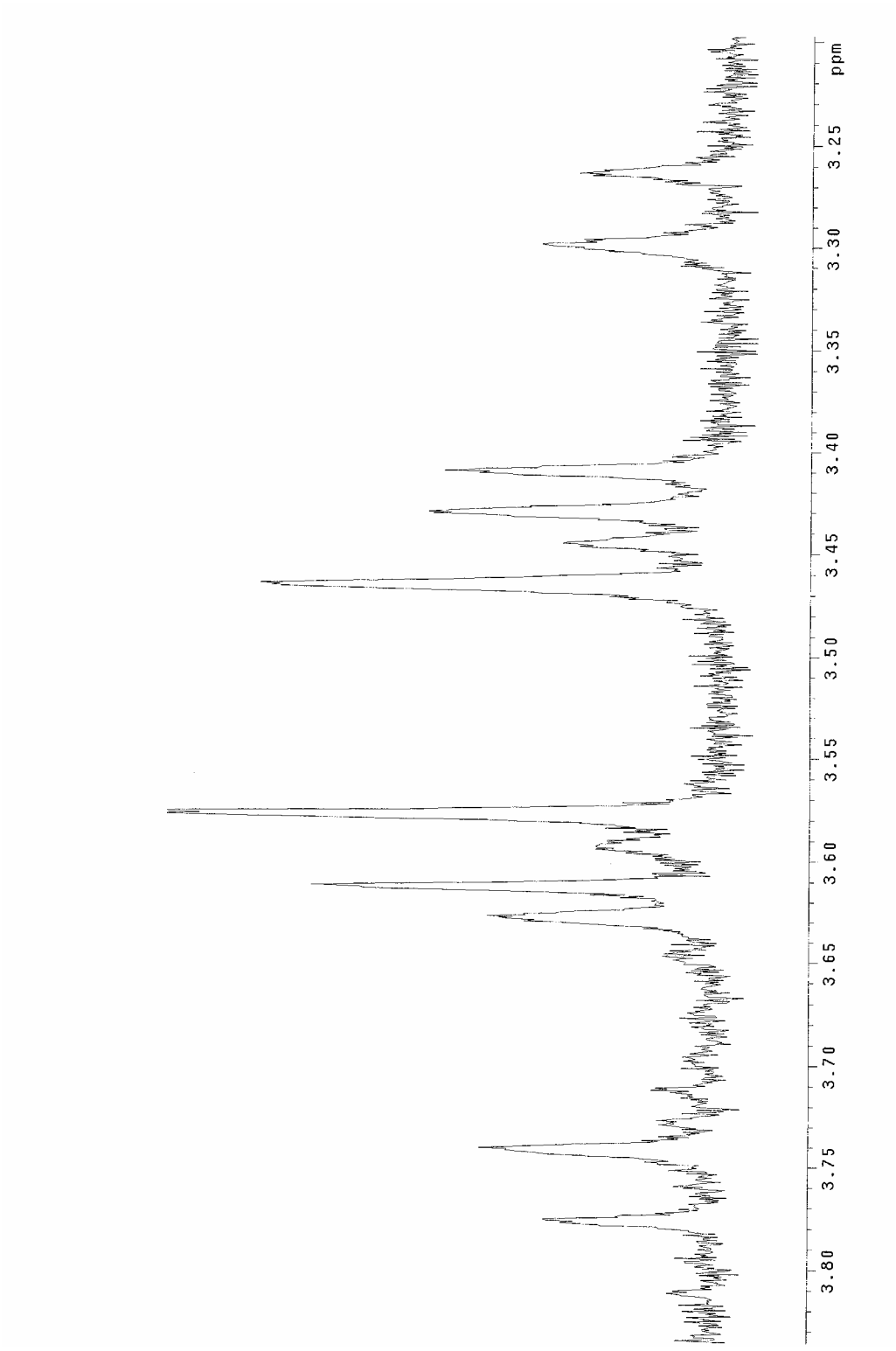

Figure 3.19. 500 MHz HMQC spectrum of ^{13}C-labeled $Sc_3N@C_{80}$ mono-adduct **4**.

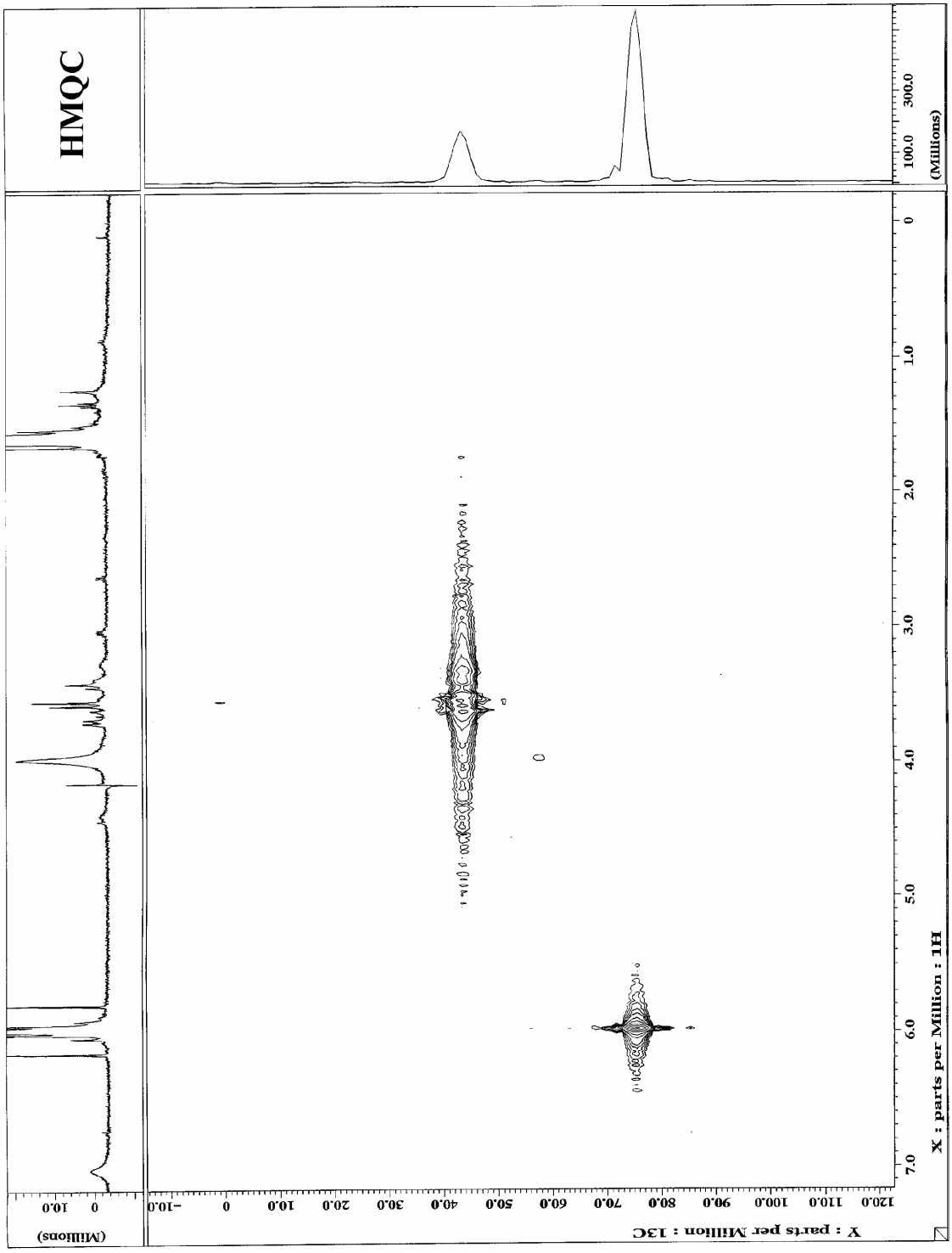

Figure 3.20. 500 MHz HMBC spectrum of ^{13}C-labeled $Sc_3N@C_{80}$ mono-adduct **4**.

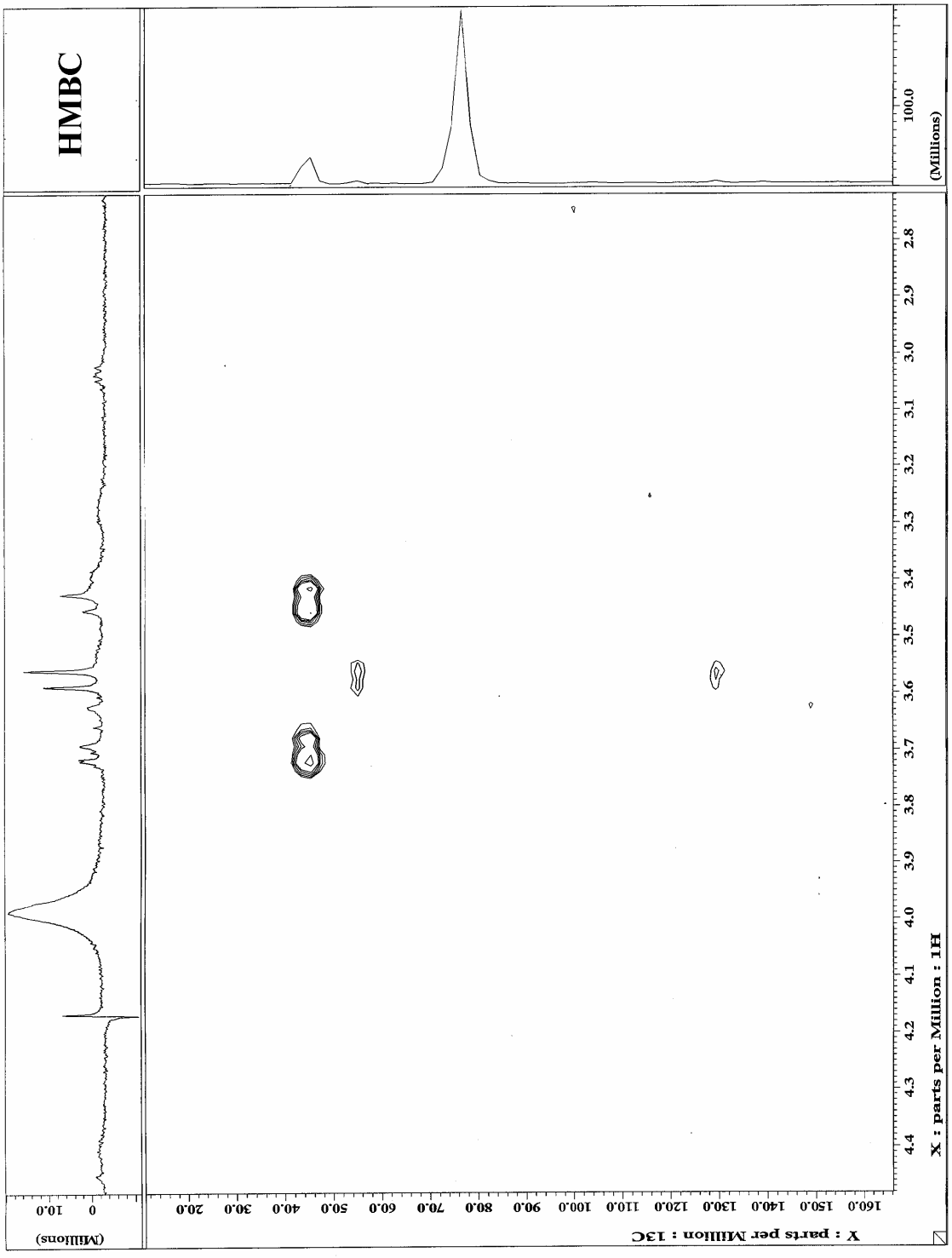

Figure 3.21. UV-Visible spectrum of ^{13}C-labeled $Sc_3N@C_{80}$ mono-adduct **4** in chloroform.

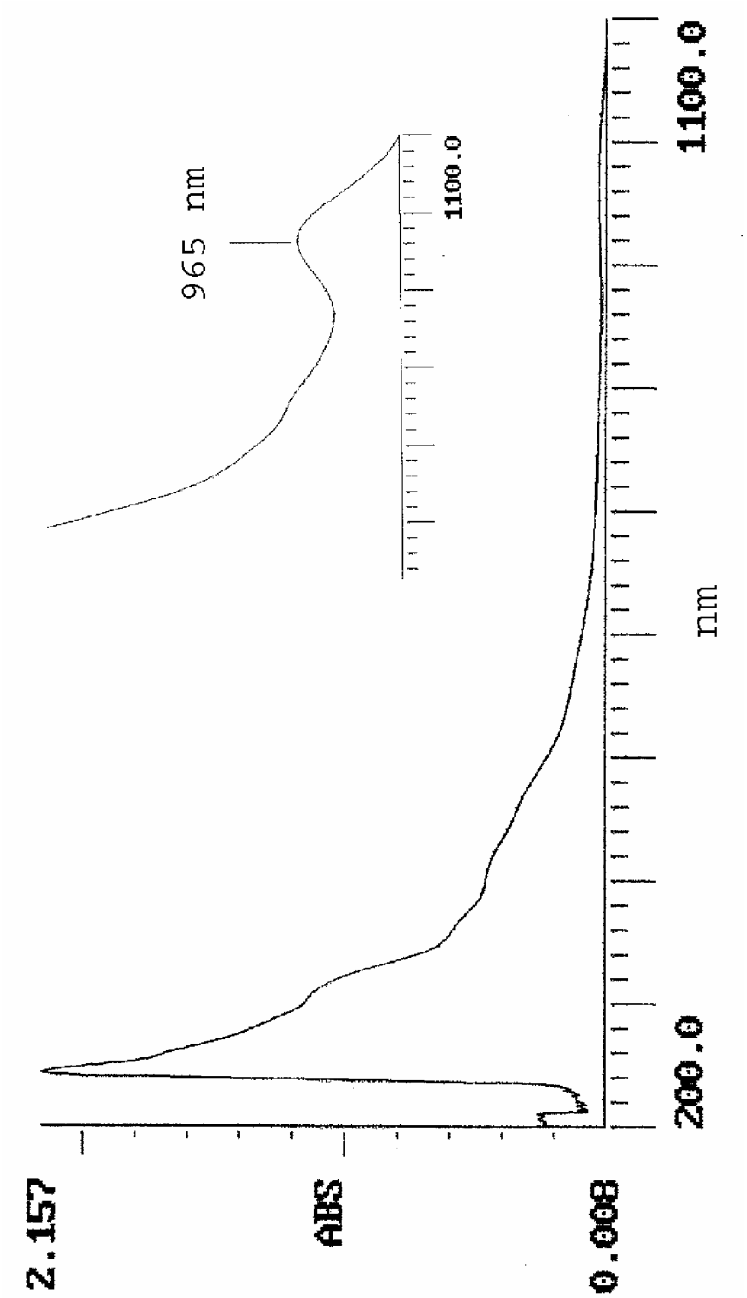

3.3.5. Synthesis of ^{13}C-labeled diethyl malonate adduct of $Sc_3N@C_{80}$ (6)

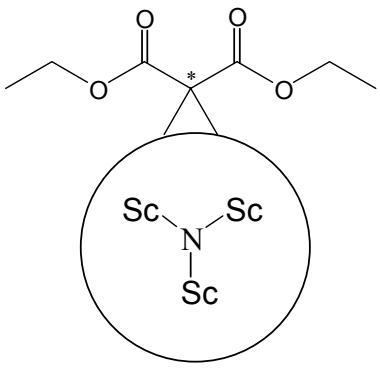

7.81 mg (7.04 μmol) of $Sc_3N@C_{80}$ **3** and 4.48 mg (14.47 μmol) CBr_4 were added to a 25 ml round bottom flask along with *ca.* 15 ml dry toluene. The solution was sonicated for 20 minutes to dissolve all of the metallofullerene. Then, 1.62 μl (10.56 μmol) of diethyl malonate (2-^{13}C) **5** and 3.2 μl (21.2 μmol) DBU were added, and the solution was stirred at room temperature for 20 hours. Flash chromatography with silica gel and toluene (eluent) were used to remove the unreacted $Sc_3N@C_{80}$, followed by a CH_2Cl_2/MeOH (1:1) solvent mixture to remove a golden-colored spot. The solvent of the second fraction was removed to reveal a brown-colored product. No products were observed by HPLC purification. Weight of product was <0.5 mg. ^{1}H NMR: peaks not discernable due to solvent impurities. ^{13}C NMR (100 MHz, $CDCl_3$, 5 s delay, 5600 scans): δ 49.64 (quaternary carbon). MALDI-TOF MS: no peaks observed.

Figure 3.22. 100 MHz ^{13}C NMR spectrum of ^{13}C-labeled diethyl malonate adduct of $Sc_3N@C_{80}$ **6**.

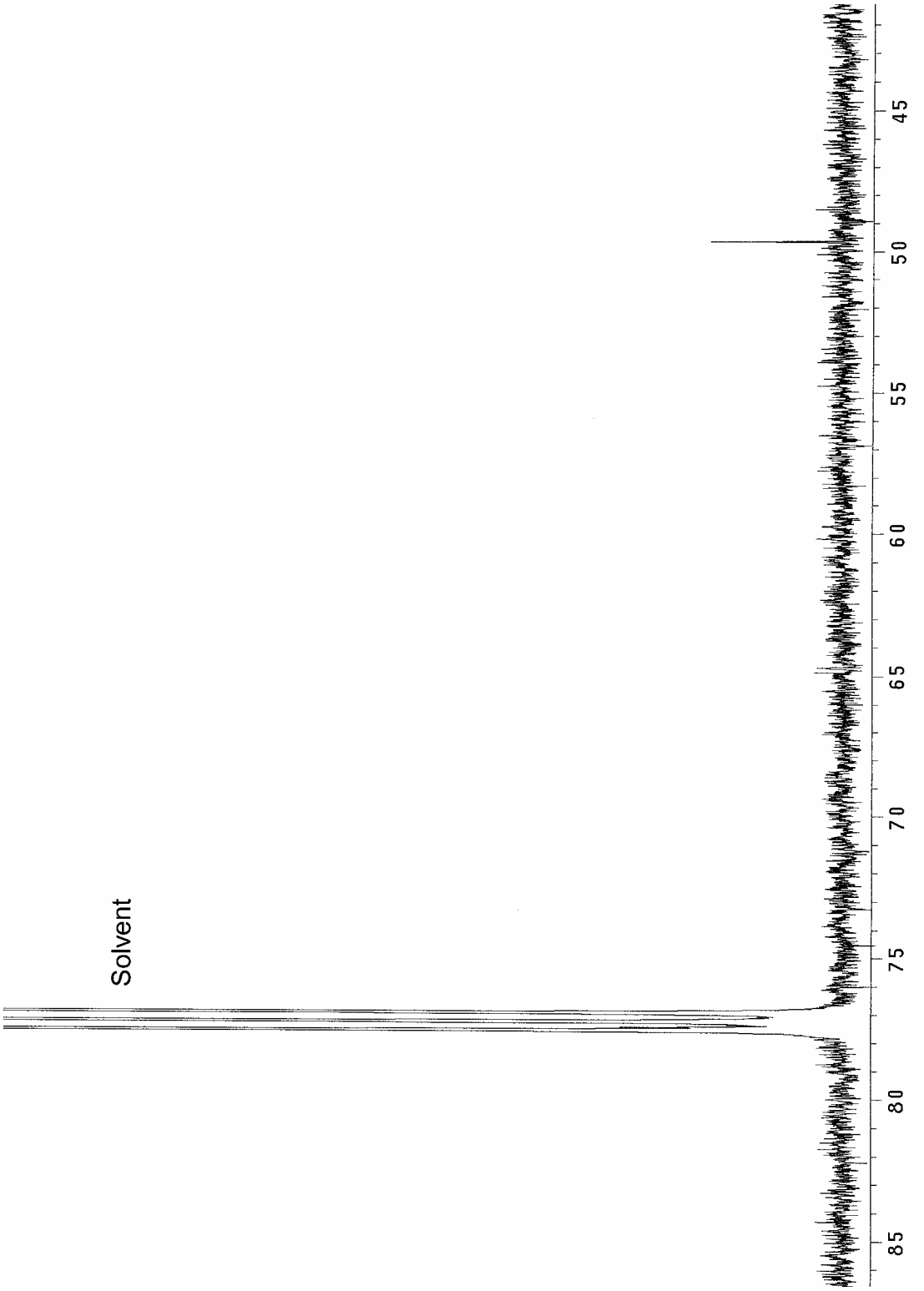

3.3.6. Synthesis of dibenzyl malonate adduct of $Sc_3N@C_{80}$ (8)

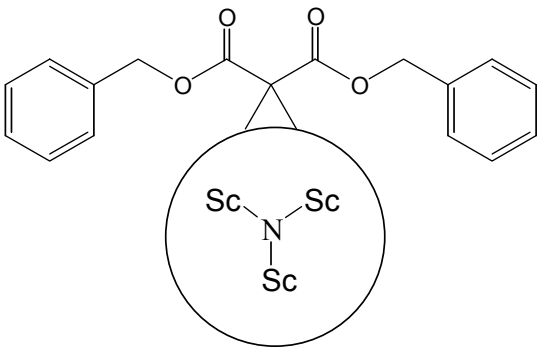

15.21 mg (13.71 μmol) of $Sc_3N@C_{80}$ **3** and 11.64 mg (35.09 μmol) CBr_4 were added to a 50 ml round bottom flask along with *ca.* 30 ml dry toluene. The solution was sonicated for 20 minutes to dissolve the metallofullerene. 5.2 μl (20.56 μmol) of dibenzyl malonate **7** and 6.2 μl (41.2 μmol) DBU were then added to the solution, and the solution was stirred at room temperature for 20 hours. The solution was filtered through pipets that contained a small amount of glass wool, to remove any insoluble metallofullerenes, and the solvent was removed with low heat and nitrogen. Chloroform was added to the brown-black crude product, the solution was sonicated for a few minutes, and then separated by HPLC (Buckyclutcher column) to yield three product peaks and a peak for the non-functionalized (parent) metallofullerene. All products were brown-colored. Weights of products were *ca.* 0.5 mg for peak 3 (*ca.* 3% conc. from HPLC), and <0.5 mg for peaks 1 and 2 (*ca.* 0.55% and *ca.* 0.82% conc. from HPLC). The ^{1}H NMR spectra of peaks 1,2 and 3 were nearly identical. ^{1}H NMR (500 MHz, CD_2Cl_2): δ 5.32 (s, 4H, CH_2) and 7.31-7.36 (m, 10H, aromatic CHs). ^{13}C NMR: no peaks observed due to lack of a ^{13}C-label. MALDI-TOF MS (positive ionization): Calcd. mass of mono-adduct is 1391.31, and found 1390, 1393.2 and 1391.8 for peak 1, 2 and 3 (three products), respectively.

Figure 3.23. 500 MHz ^{1}H NMR spectrum of dibenzyl malonate adduct of $Sc_3N@C_{80}$ **8**.

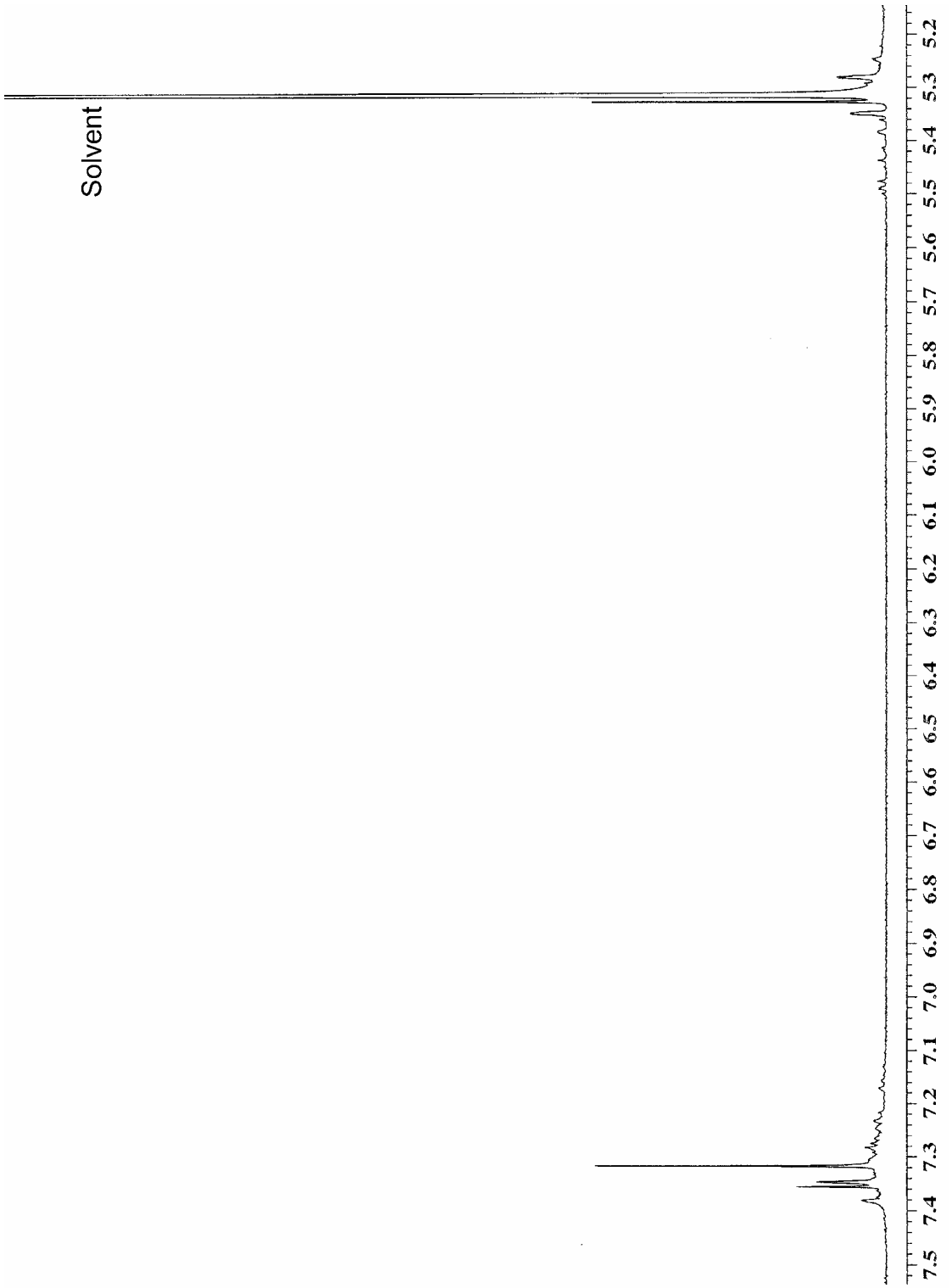

3.3.7. Synthesis of 1,3-dihydrobenzo[c]thiophene (10)

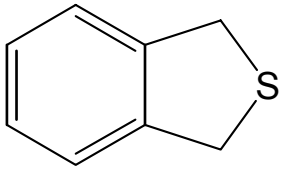

200 ml of absolute ethanol was added to a 1 L round bottom flask, followed by the addition of 9.2 g (0.4 mol) of sodium metal (dry, stick). The round bottom was submerged in an ice bath as the sodium and ethanol reacted. 200 ml ethanol (absolute) and 9.2 g sodium metal (dry, stick) were added to a separate 500 ml round bottom flask. The 1 L round bottom was submerged in the ice bath, and H_2S was bubbled through the solution for 1.5 hours while stirring. The solution became yellow and cloudy over time. Once finished, the contents from the 500 ml round bottom were slowly added to the 1 L solution while stirring, and then 105.2 g (0.4 mol) α,α'-dibromo-*o*-xylene **9** was added over a period of 45 minutes (needed a large stirring bar for the latter part). The suspension was stirred for 13 hours, and 200 ml H_2O was added to the 1 L round bottom. The golden/brown precipitate was filtered with a large Buchner funnel and 1 L filter flask. The filtrate was added to a 2 L separatory funnel, and extracted 5 times with 400 ml portions of petroleum ether (38-60 °C b.p.). The solvent was removed via rotavap to yield a yellowish-colored oil. The product was distilled from the crude oil using a high vacuum line and low heat (*ca.* 70 °C). The clear distilled oil was placed in the freezer to solidify. Weight of product was 12.037 g (22.17% yield). ^{1}H NMR (400 MHz, $CDCl_3$): δ 4.28 (s, 4H, CH_2) and 7.21-7.27 (m, 4H, aromatic CH). ^{13}C NMR (100 MHz, $CDCl_3$): δ 38.28, 124.92, 126.94 and 140.48. FAB MS (positive ionization): Calcd. mass is 136.20, and found 135.02 [M – 1].

Figure 3.24. 400 MHz ^{1}H NMR spectrum of 1,3-dihydrobenzo[c]thiophene **10**.

Figure 3.25. 100 MHz ^{13}C NMR spectrum of 1,3-dihydrobenzo[c]thiophene **10**.

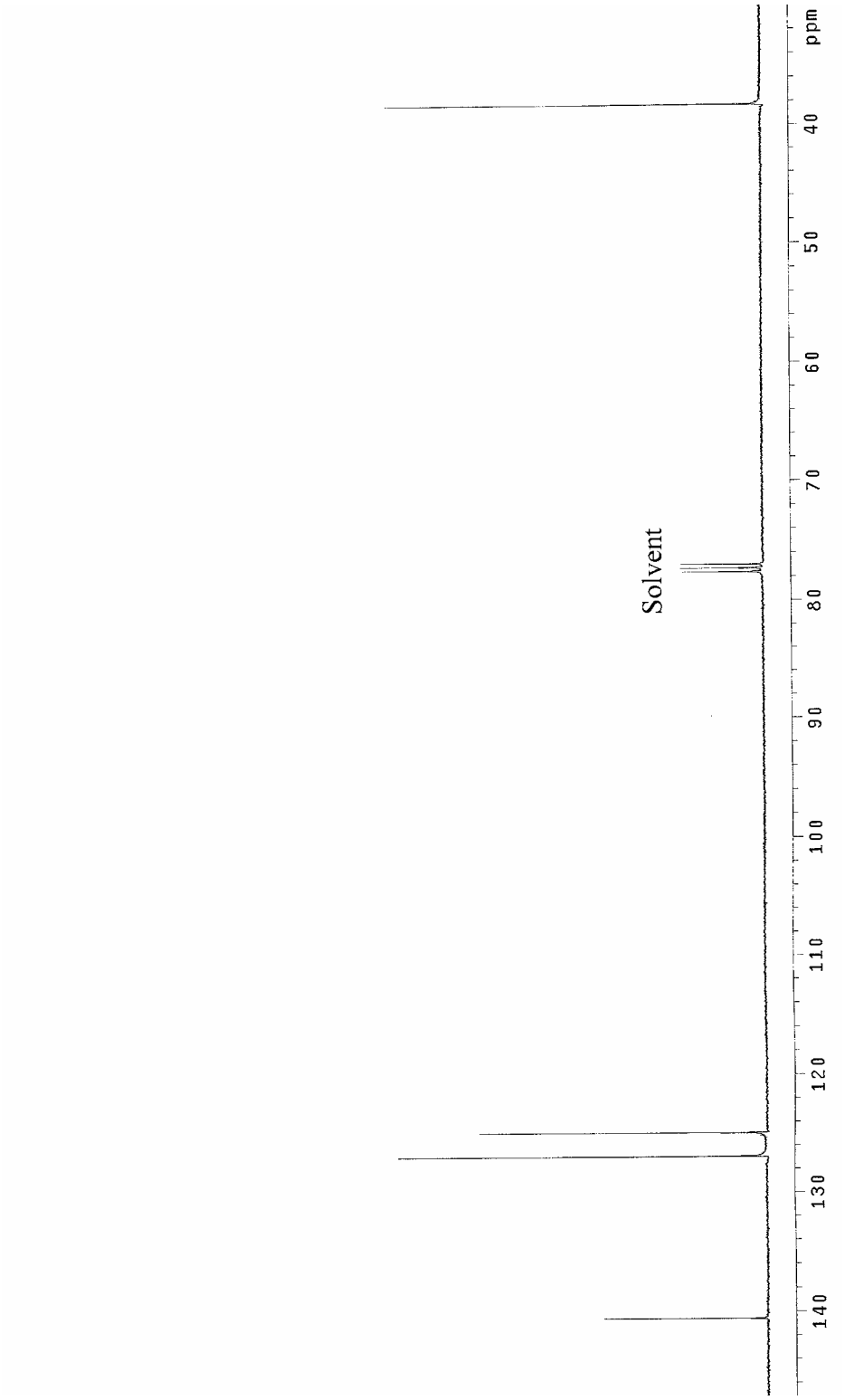

3.3.8. Synthesis of 1,3-dihydrobenzo[c]thiophene-2,2-dioxide (11)

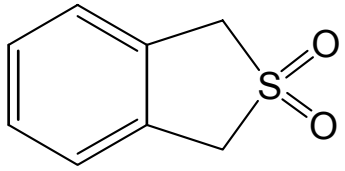

8.3 ml of glacial acetic acid was added to a 100 ml round bottom flask that contained 12.037 g (0.088 mol) of 1,3-dihydrobenzo[c]thiophene **10**. The flask was swirled to dissolve all material. 40.8 ml (0.194 mol) of peracetic acid (32 wt.% in AcOH) was added to a separate 100 ml round bottom flask. The second round bottom was submerged in an ice bath (5-10 °C), and portions of the glacial acetic acid solution were slowly added, via pipet, over a three hour period. The bath temperature was kept below 10 °C. Once the addition was completed, the solution was warmed to room temperature and stirred for 72 hours. 35 ml H_2O were added to precipitate a white product, which was vacuum filter and washed with H_2O. The mother liquor was concentrated to recover additional product. The product was vacuum dried for 6 hours and air dried overnight. Weight of product was 13.58 g (91.39% yield). ^{1}H NMR (500 MHz, $CDCl_3$): δ 4.37 (s, 4H, CH_2) and 7.28-7.38 (m, 4H, aromatic CH). ^{13}C NMR (100 MHz, $CDCl_3$): δ 57.16, 126.28, 129.07 and 131.48. FAB MS (positive ionization): Calcd. mass is 168.20, and found 169.03 [M + 1]. Melting point: 146–148 °C.

Figure 3.26. 500 MHz ^{1}H NMR spectrum of 1,3-dihydrobenzo[c]thiophene-2,2-dioxide **11**.

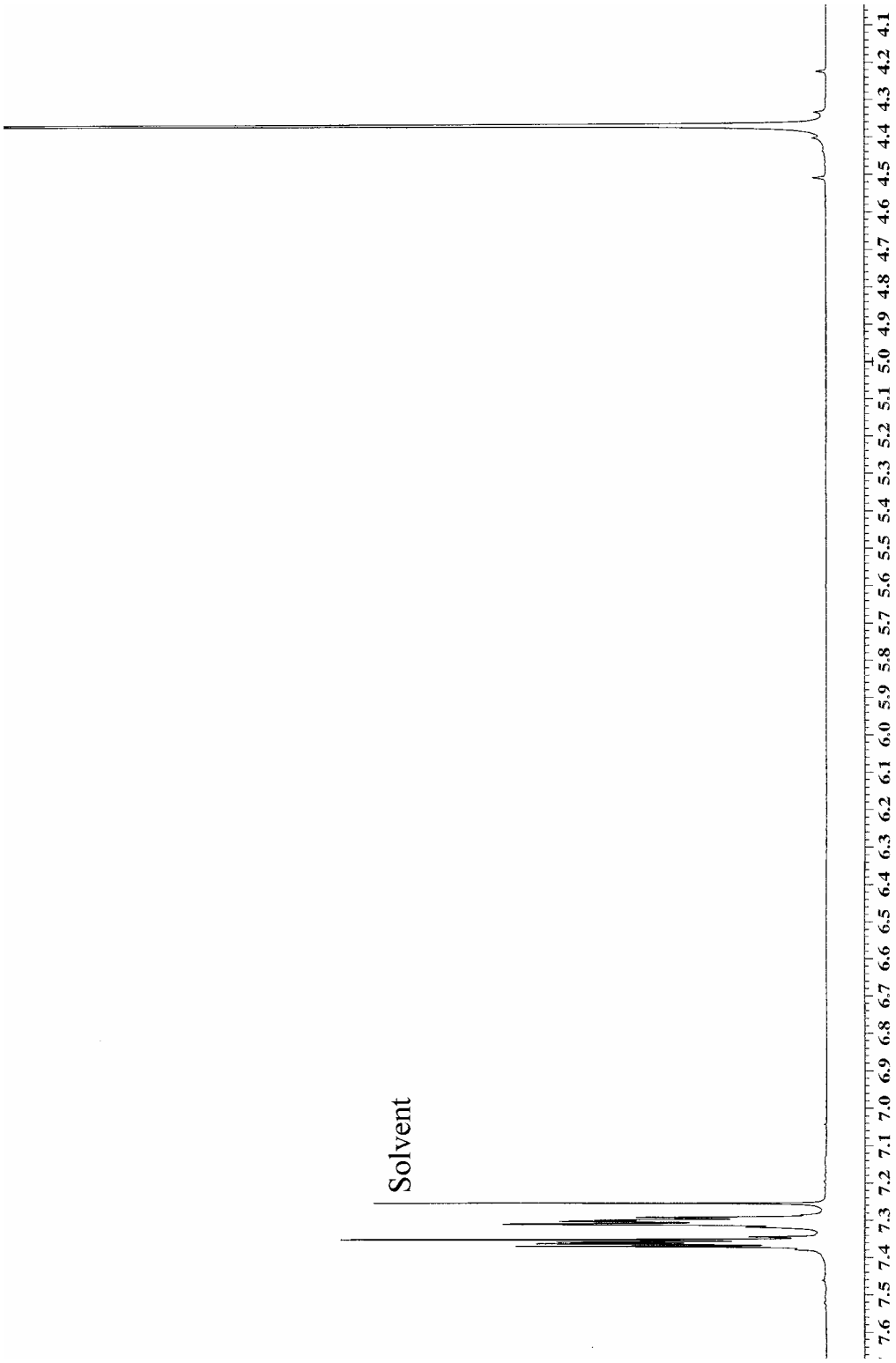

Figure 3.27. 100 MHz ^{1}H NMR spectrum of 1,3-dihydrobenzo[c]thiophene-2,2-dioxide **11**.

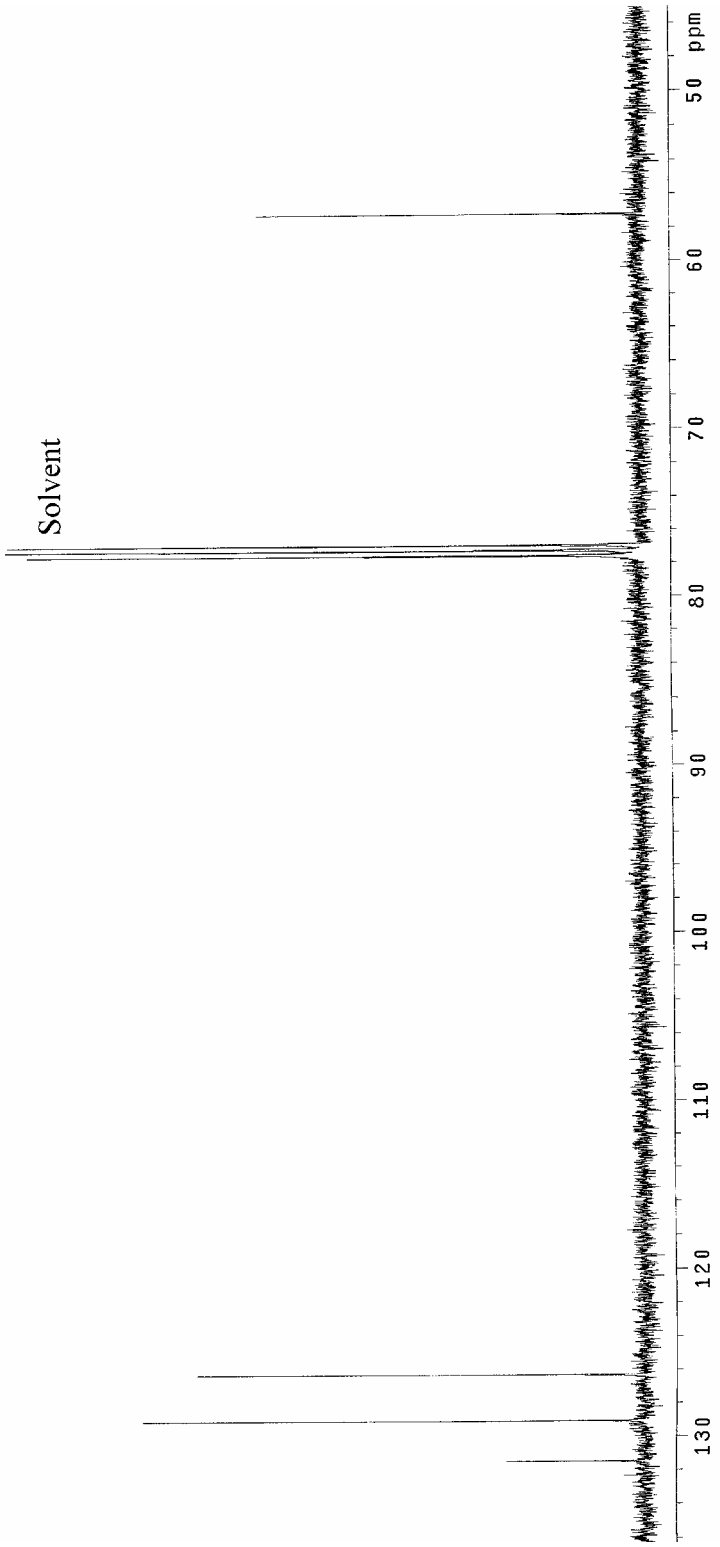

3.3.9. Synthesis of ^{15}N-labeled 1,3-dihydro-5-nitrobenzo[c]thiophene-2,2-dioxide (12)

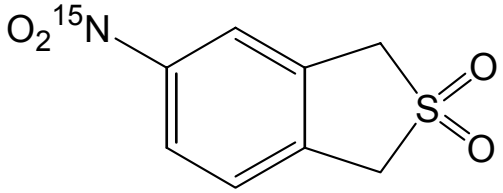

1.48 ml (0.027 mol) H_2SO_4 (97%) were added to a 10 ml round bottom flask that was submerged in an ice bath (<5 °C). While stirring, 1.27 ml (0.018 mol) of $H^{15}NO_3$ (99% ^{15}N) were added to the round bottom. The temperature was kept below 5 °C, add 500 mg (3 mmol) of 1,3-dihydrobenzo[c]thiophene-2,2-dioxide **11** was added in small portions. Each portion was allowed to dissolve before adding the next. Once addition was completed, the solution was warmed to room temperature and stirred for 5 hours. The solution was poured over 30 ml of crushed ice to yield a white precipitate. The precipitate was vacuum filtered and wash with 50 ml cold H_2O. The product was vacuum dried for 1 hour and allowed to air dried overnight. The product was not recrystallized. Weight of product was 0.6004 g (93.8% yield). ^{1}H NMR (500 MHz, $CDCl_3$): δ 4.45 (s, 2H, CH_2), 4.48 (s, 2H, CH_2), 7.54 (d, 1H, aromatic CH), 8.24 (s, 1H, aromatic CH) and 8.26 (d, 1H, aromatic CH). ^{13}C NMR (100 MHz, $CDCl_3$, 1.5 hr scan): δ 56.82, 56.86, 121.70, 124.23, 127.52, 133.32, 138.50 and 148.33 (d, J_{NC} = 15.2 Hz). HR-FAB MS (negative ionization): Calcd. mass is 214.0066, and found 213.9071.

Figure 3.28. 500 MHz ^{1}H NMR spectrum of ^{15}N-labeled 1,3-dihydro-5-nitrobenzo[c]thiophene-2,2-dioxide **12** (x = impurity).

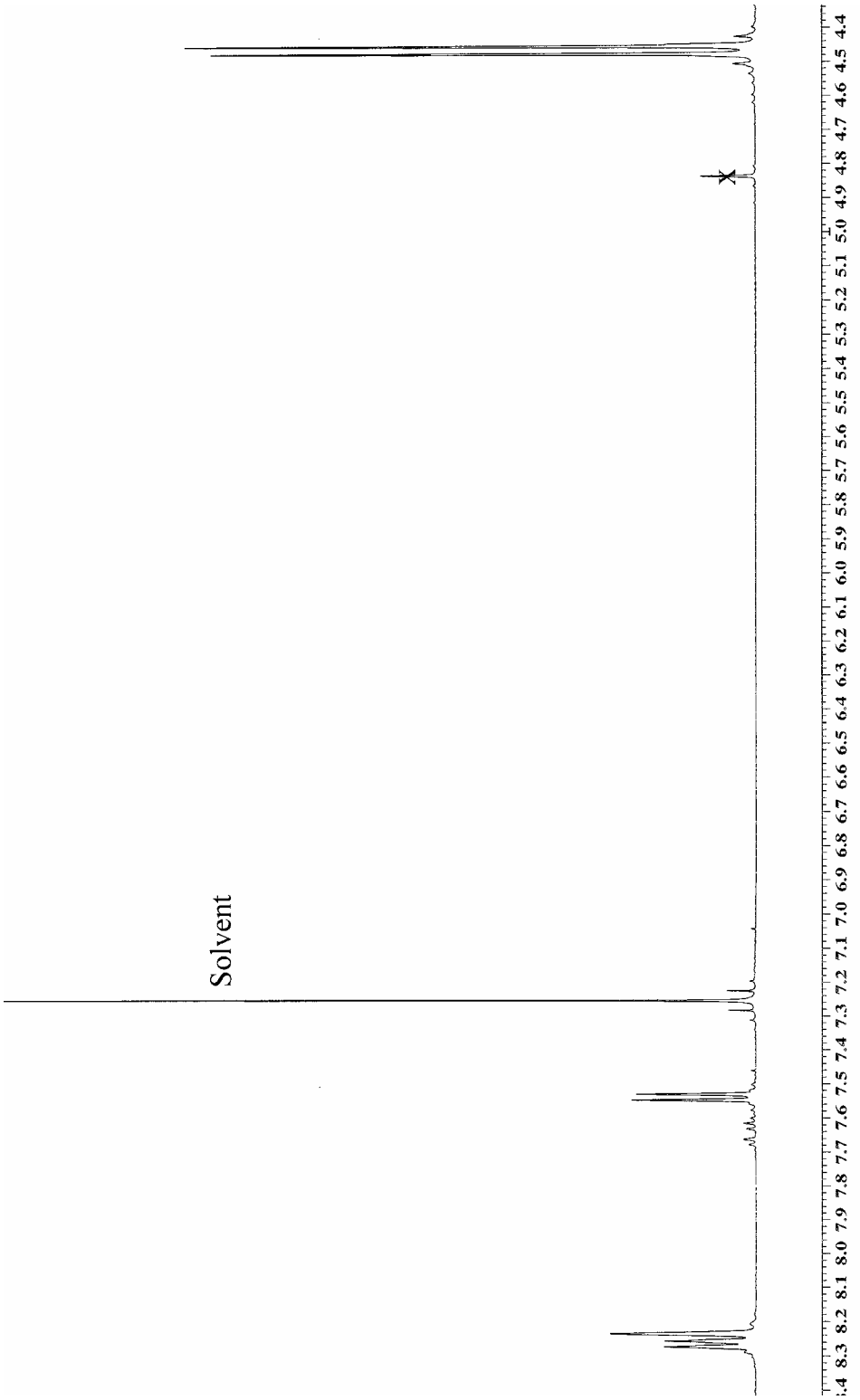

Figure 3.29. 100 MHz ^{13}C NMR spectrum of ^{15}N-labeled 1,3-dihydro-5-nitrobenzo[c]thiophene-2,2-dioxide **12** (x = impurity).

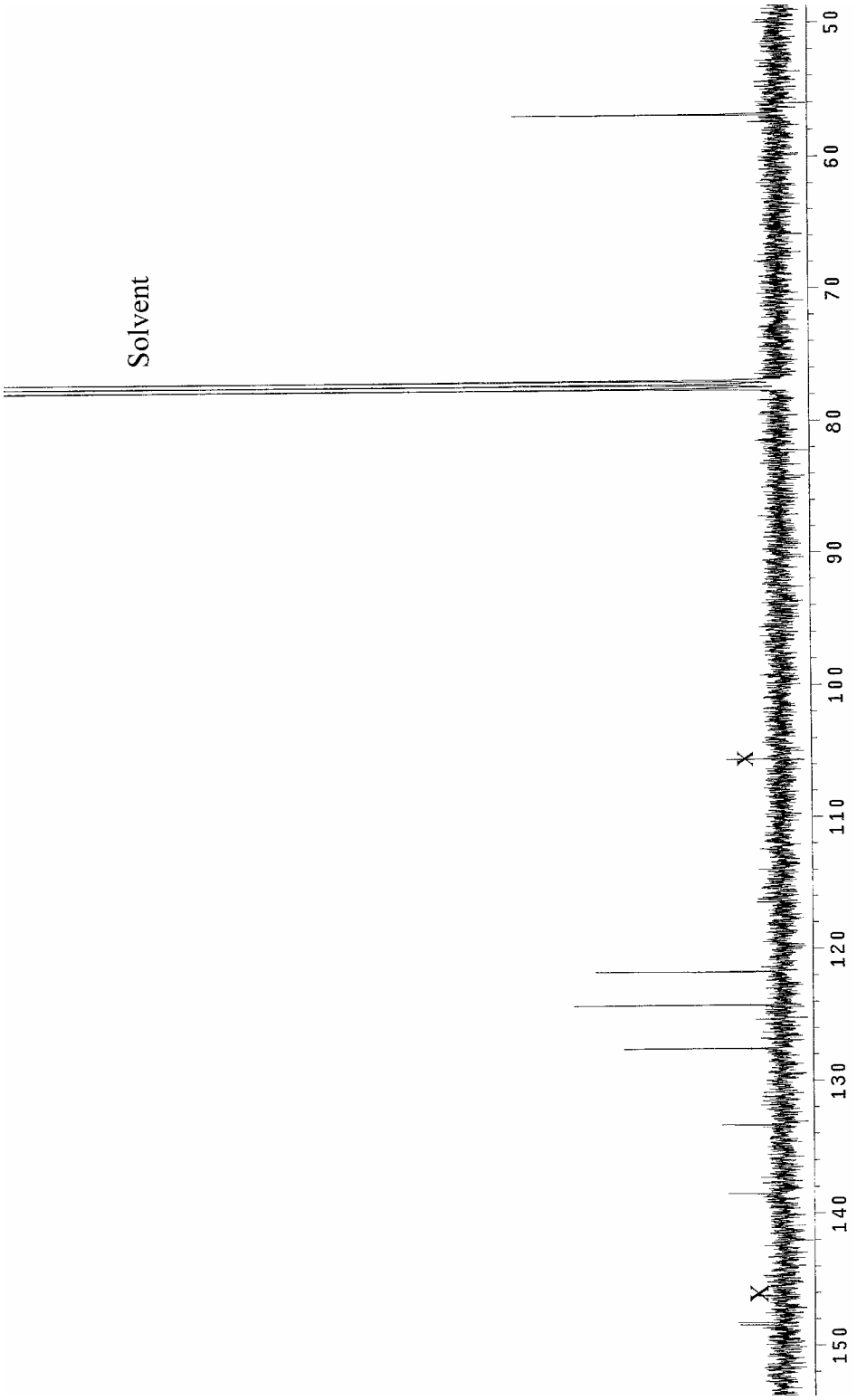

3.3.10. Synthesis of ^{15}N-labeled 5-amino-1,3-dihydrobenzo[c]thiophene-2,2-dioxide (13)

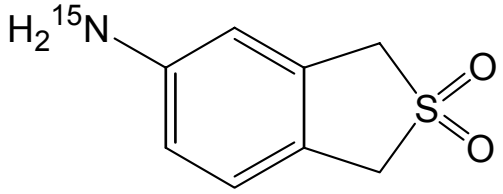

1.504 g (8.17 mmol) of 1,3-dihydro-5-nitrobenzo[c]thiophene-2,2-dioxide (15N-labeled) **12** was added to a 50 ml round bottom flask, followed by the addition of 10 ml trifluoroacetic acid (TFA). The solution was heated to 70 °C (reflux). 0.53 g (8.17 mmol) zinc metal was then added to the flask. The solution turned an orange/red color. After 5 minutes, 0.53 g of zinc was added. The solution was then refluxed for an additional 10 minutes. The hot solution (50 ml r.b.) was vacuum filtered to remove unreacted zinc and any insoluble materials. TFA was removed, via rotavap, to yield a reddish-colored oil. 10 ml H_2O was added and the flask was submerge in an ice bath. Small portions of a 25 wt.% NaOH solution were added, while stirring, until the solution was neutralized. As the solution became less acidic a mustard-colored precipitate formed. The precipitate was vacuum filtered and washed with H_2O. The crude product was vacuum dried for 2 hours, then placed in a hot oven (110 °C) for 3 hours to remove a large amount of H_2O. The crude product (*ca.* 3 g) was extracted with hot H_2O to yield a bright yellow material (desired product). Removal of yellow color was unsuccessful. Weight of product was 0.345 g (26.7% yield). ^{1}H NMR (400 MHz, DMSO-d_6): δ 4.22 (s, 2H, CH_2), 4.28 (s, 2H, CH_2), 5.25 (d, 2H, J_{HN} = 84 Hz), 6.48 (s, 1H, aromatic CH), 6.52 (d, 1H, aromatic CH) and 6.96 (d, 1H, aromatic CH). ^{13}C NMR (100 MHz, DMSO-d_6): δ 56.39, 57.03, 110.94, 114.56, 118.79, 127.03, 133.29 and 149.43. ^{15}N NMR (50 MHz, DMSO-d_6, 601 scans): δ 57.30. EI MS (positive ionization): Calcd. mass is 184.231, and found mass at 184.

Figure 3.30. 400 MHz ^{1}H NMR spectrum of ^{15}N-labeled 5-amino-1,3-dihydrobenzo[c]thiophene-2,2-dioxide **13**.

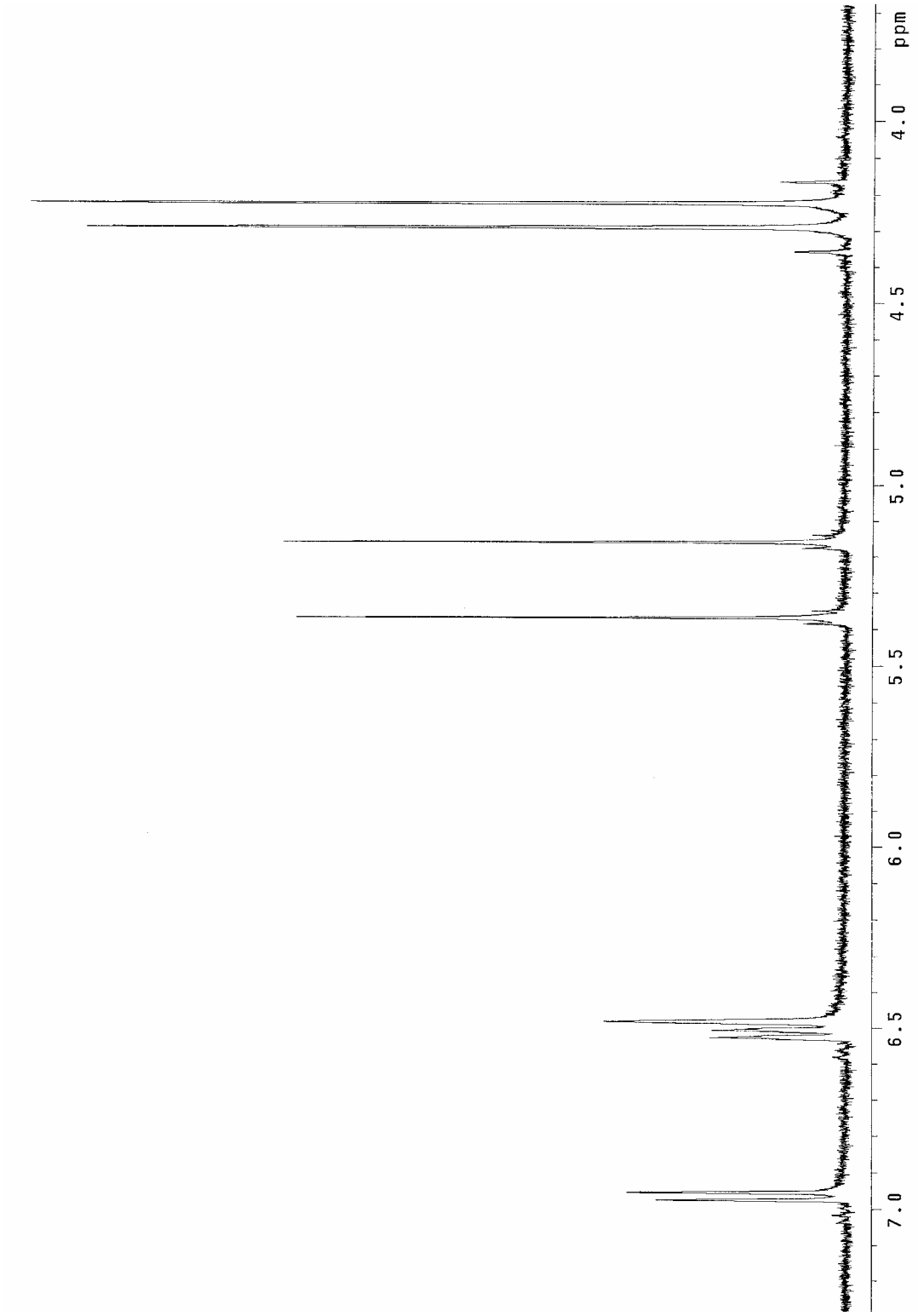

Figure 3.31. 100 MHz ^{13}C NMR spectrum of ^{15}N-labeled 5-amino-1,3-dihydrobenzo[c]thiophene-2,2-dioxide **13** (x = impurity).

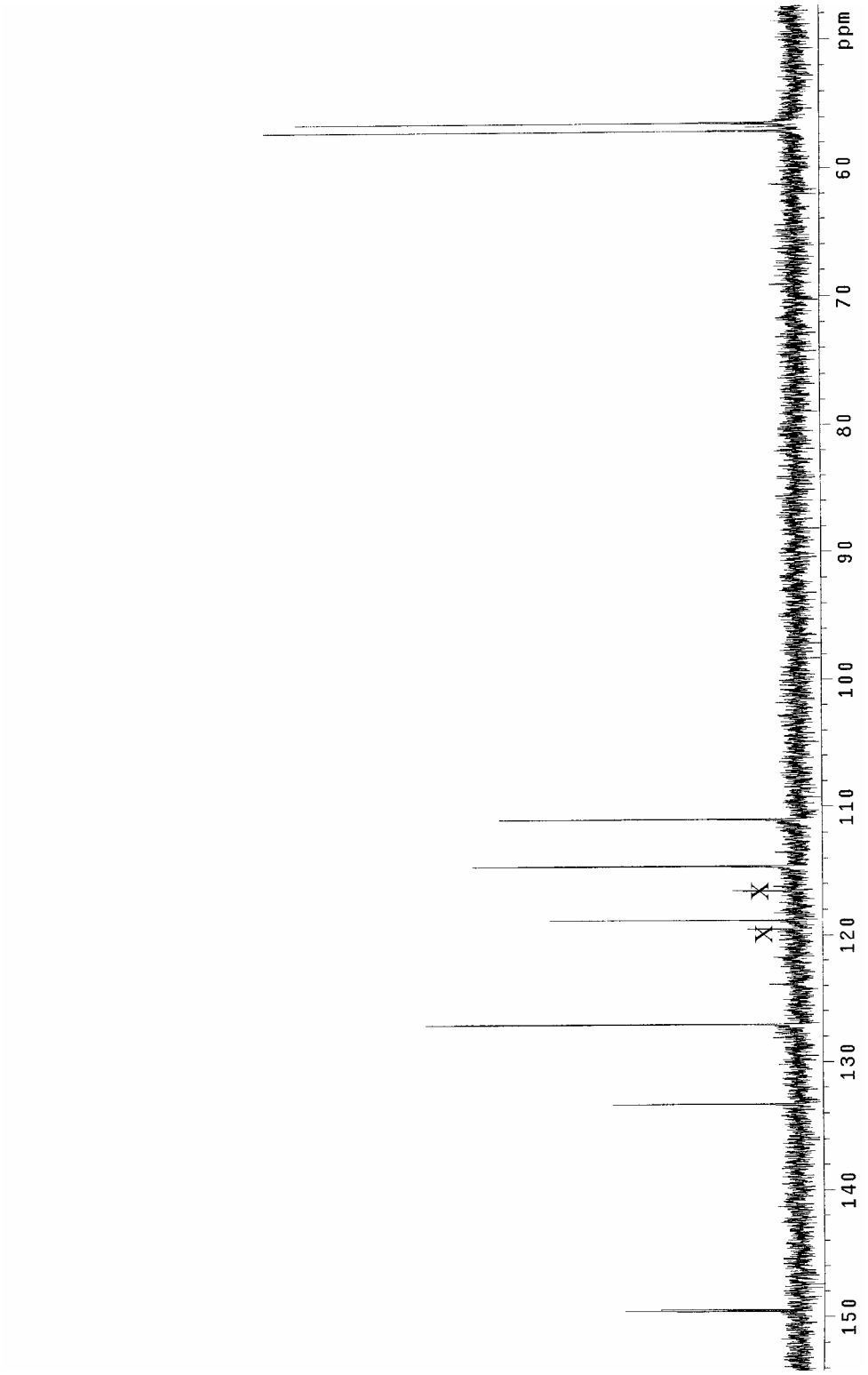

Figure 3.32. 50 MHz ^{15}N NMR spectrum of ^{15}N-labeled 5-amino-1,3-dihydrobenzo[c]thiophene-2,2-dioxide **13**.

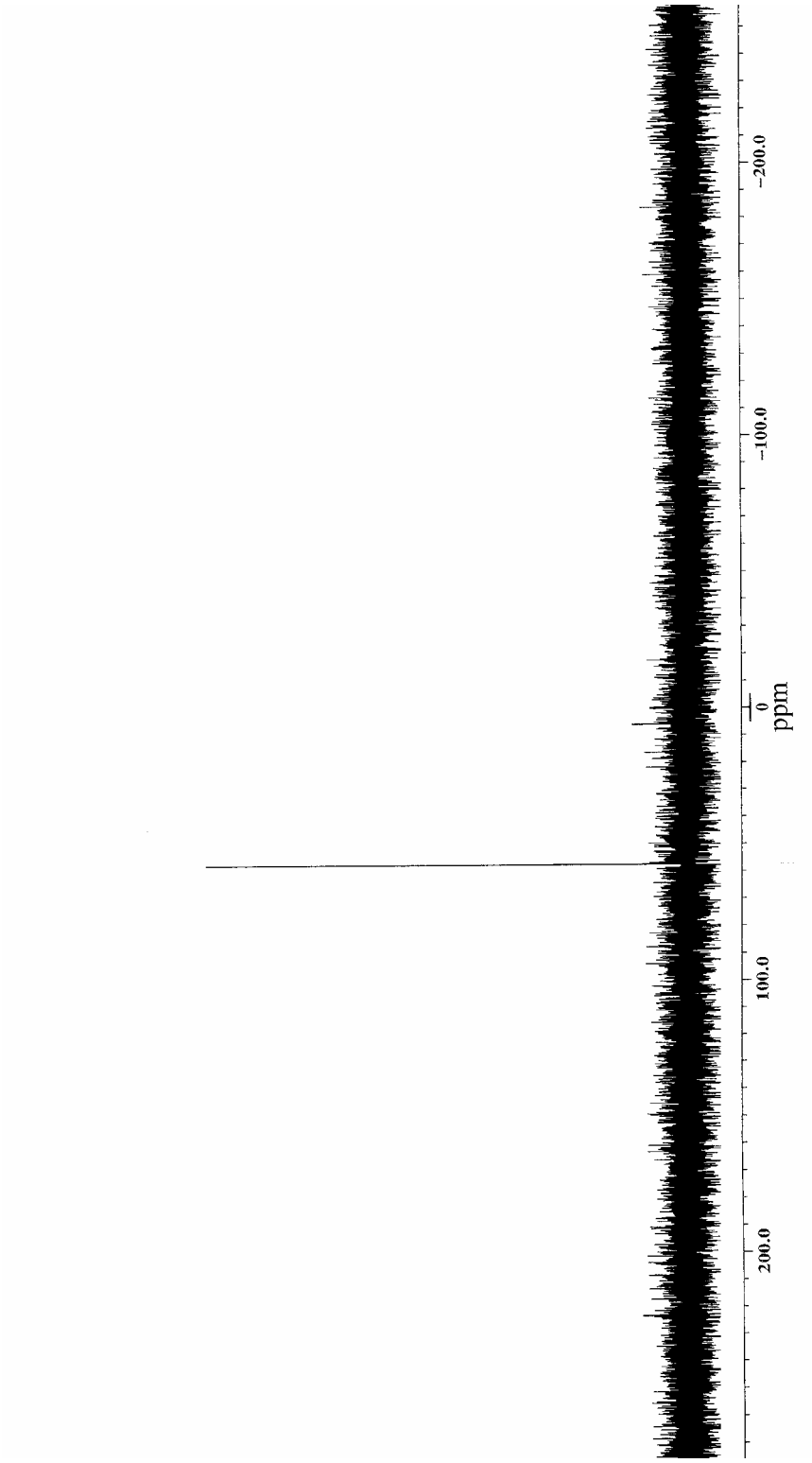

3.3.11. Synthesis of a ^{15}N-labeled $Sc_3N@C_{80}$–terminal amine derivative (14)

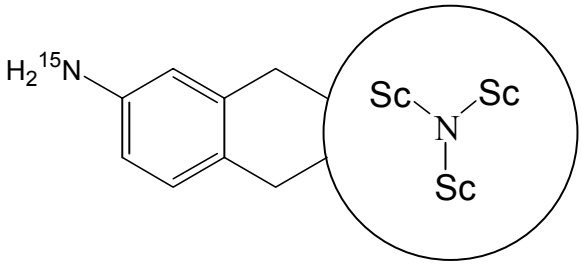

57.41 mg (51.76 μmol) $Sc_3N@C_{80}$ (*ca.* 98%) **3** and 25 ml 1,2,4-trichlorobenzene (TCB) were added to a 50 ml round bottom flask. The flask was sonicated for 20 minutes to dissolve the metallofullerene. 98.71 mg (0.53 mmol) of 5-amino-1,3-dihydrobenzo[c]thiophene-2,2-dioxide (^{15}N-labeled) **13** were then added to the flask, and the solution was refluxed under argon for 13 hours. Once finished, the solvent was removed via reduced pressure (high vacuum line) and low heat to reveal a brown/black crude product mixture. Chloroform was added to the flask, it was sonicated to dissolve the crude product, then purified with HPLC using the Buckyclutcher column. Four peaks were observed from the chromatogram and all were collected. Peak 1 was non-functionalized $Sc_3N@C_{80}$ **3** (59.15% conc. from HPLC). Peak 2, 3 and 4 were all product peaks (2 & 3 are *ca.* 5% conc. from HPLC, while peak 4 is 29% conc. from HPLC). Yield of peak 3 was *ca.* 16 mgs. ^{1}H NMR of peak 4 (400 MHz, $C_2D_2Cl_4$): δ 3.33-3.56 (m, br, 4H, CH_2), 3.65-4.00 (d, br, NH_2) and 6.56-7.00 (m, br, 3H, aromatic CH). MALDI-TOF MS (positive ionization): Calcd. mass for mono-adduct is *ca.* 1229, and found 1228.6 for peaks 2, 3 and 4. ^{13}C NMR of peak 4: no resonances observed. ^{15}N NMR of peak 4: no resonances observed.

Figure 3.33. 400 MHz ^{1}H NMR spectrum of ^{15}N-labeled $Sc_3N@C_{80}$–terminal amine **14**.

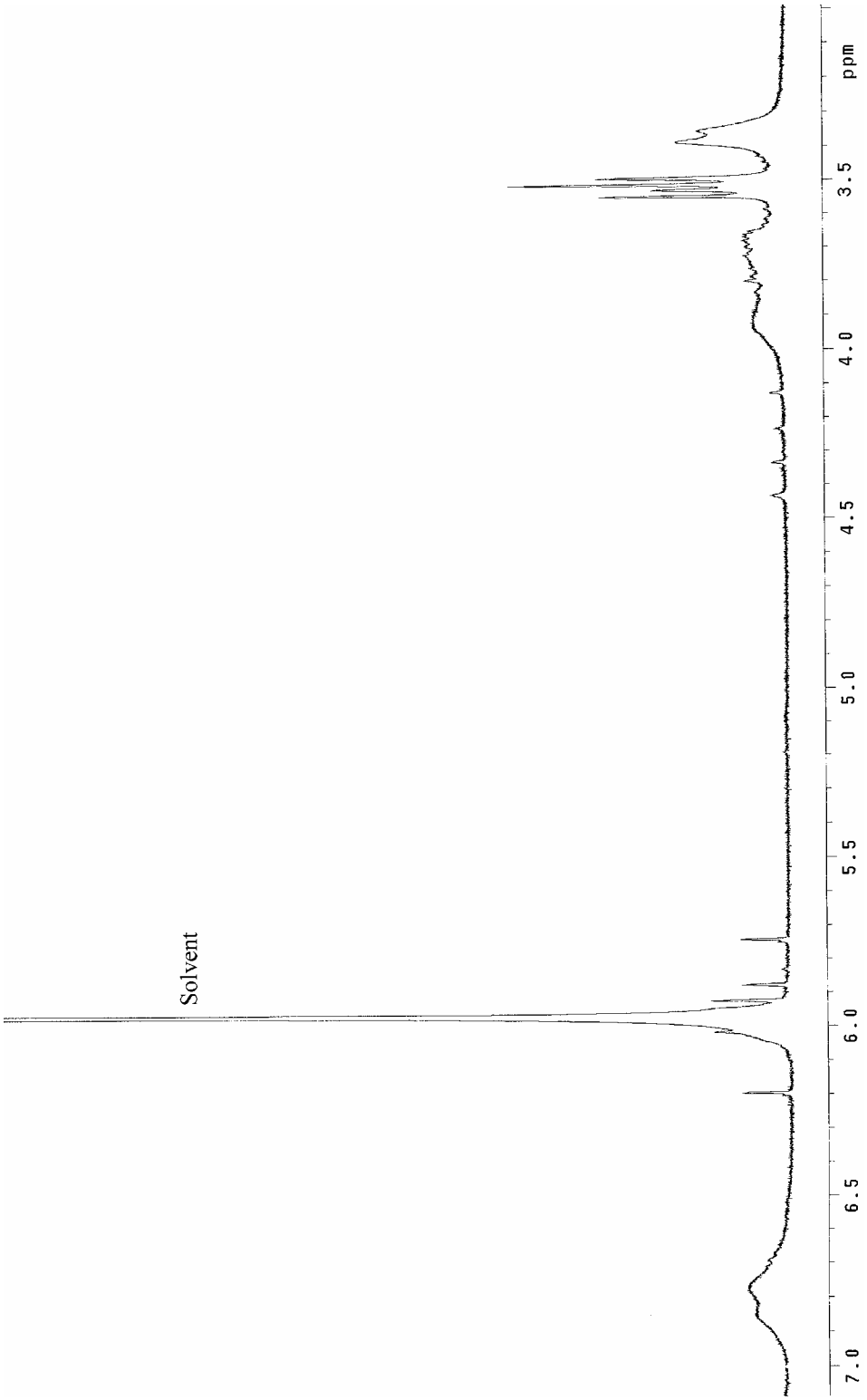

3.3.12. Synthesis of $Sc_3N@C_{80}(OH)_{\sim 10}(O)_{\sim 10}$ metallofullerenols (15)

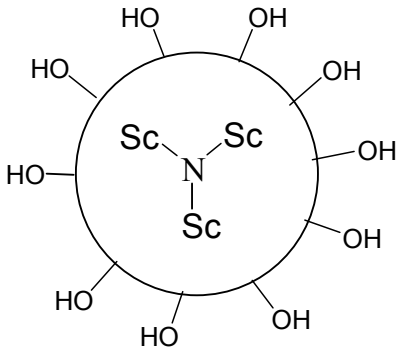

25 ml of toluene (dry) were added to a 50 ml round bottom flask containing *ca.* 4 mg $Sc_3N@C_{80}$ **3** (99%) (Dorn laboratory, Virginia Tech), and sonicated until all material was dissolved. The solution was then brought to reflux under an argon atmosphere, and 3-4 small pieces of sodium metal (*ca.* 10 mg each) were added. After 5 hours, the solution became colorless and a black precipitate was observed on the bottom of the flask. Once the flask had cooled, the precipitate was vacuum filtered and washed 4 times with dry toluene, followed by washing with methanol (3 times) to yield a brown crude material. The small silver pieces of non-reacted sodium metal were also removed. Due to the small amount of material present, the filter paper (from vacuum filtration) was added to 5 ml of water in a 10 ml round bottom and sonicated to dissolve the material. The aqueous solution was stirred (open to air) overnight to produce a golden-colored aqueous solution (pH = 7). The solution was filtered through 0.20 μm PTFE syringe filters to remove any unreacted material, and methanol was added to precipitate the material from solution. A centrifuge was used to recover the small amount of material. FT-IR (cm^{-1}, polyethylene card): 3384.6 (v br, O-H), 1629.0 (s, C=C), 1323.1 (shoulder, O-H bend), 1107.7 (s, br, C-O), 1028.1 (shoulder, br, C-O) and 615.4 (s, Sc-N). LD-TOF MS: mass at 1109 ($Sc_3N@C_{80}$). UV-Vis. (H_2O): No peaks observed. XPS (on gold foil): 284.94 eV (C=C), 286.80 eV (-C-OH) and 288.69 eV.

Figure 3.34. FT-IR spectrum of $Sc_3N@C_{80}(OH)_{\sim 10}(O)_{\sim 10}$ metallofullerenols **15** on a 3M™ polyethylene card.

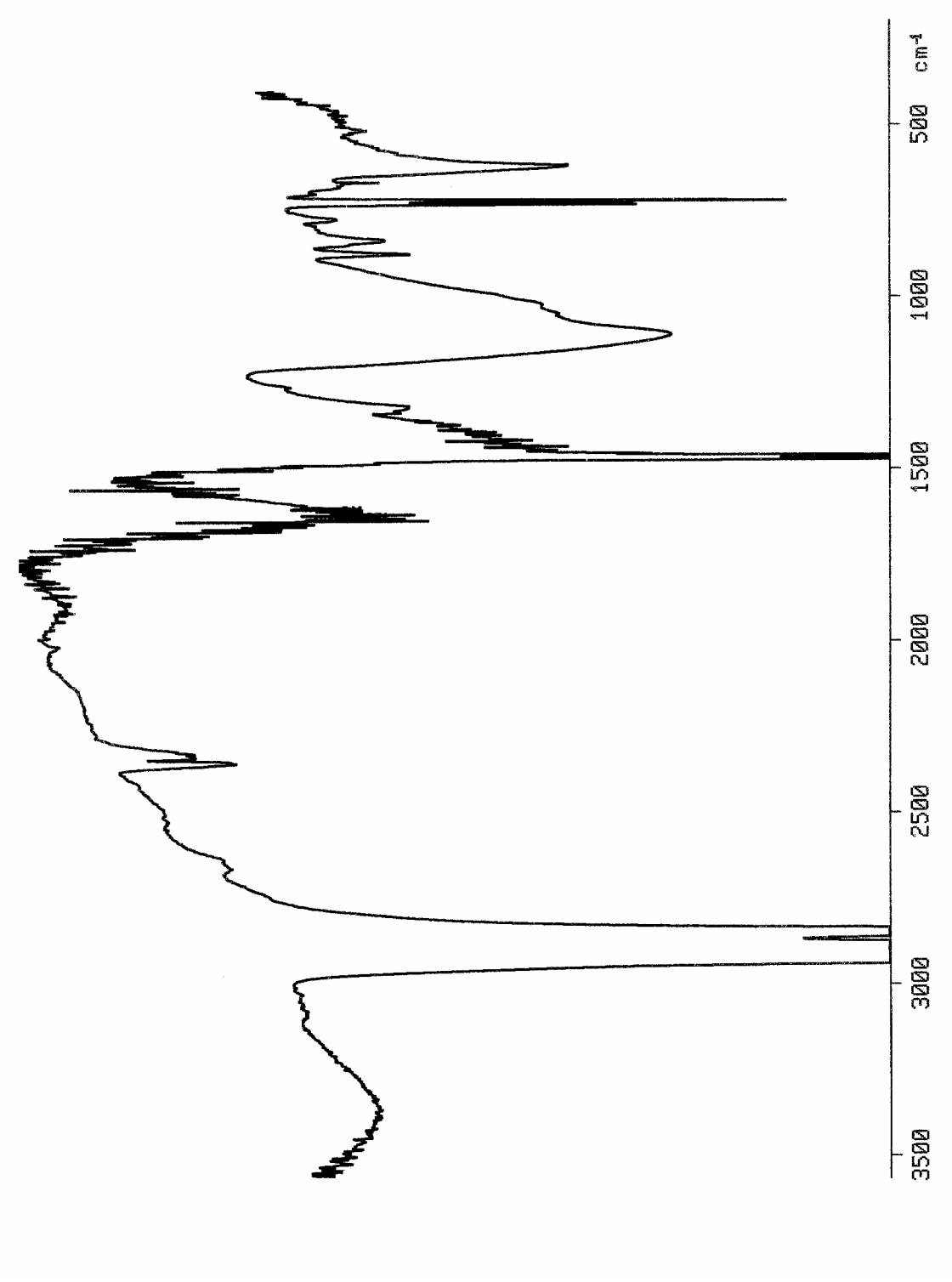

Figure 3.35. FT-IR spectrum of 3M™ polyethylene card (blank).

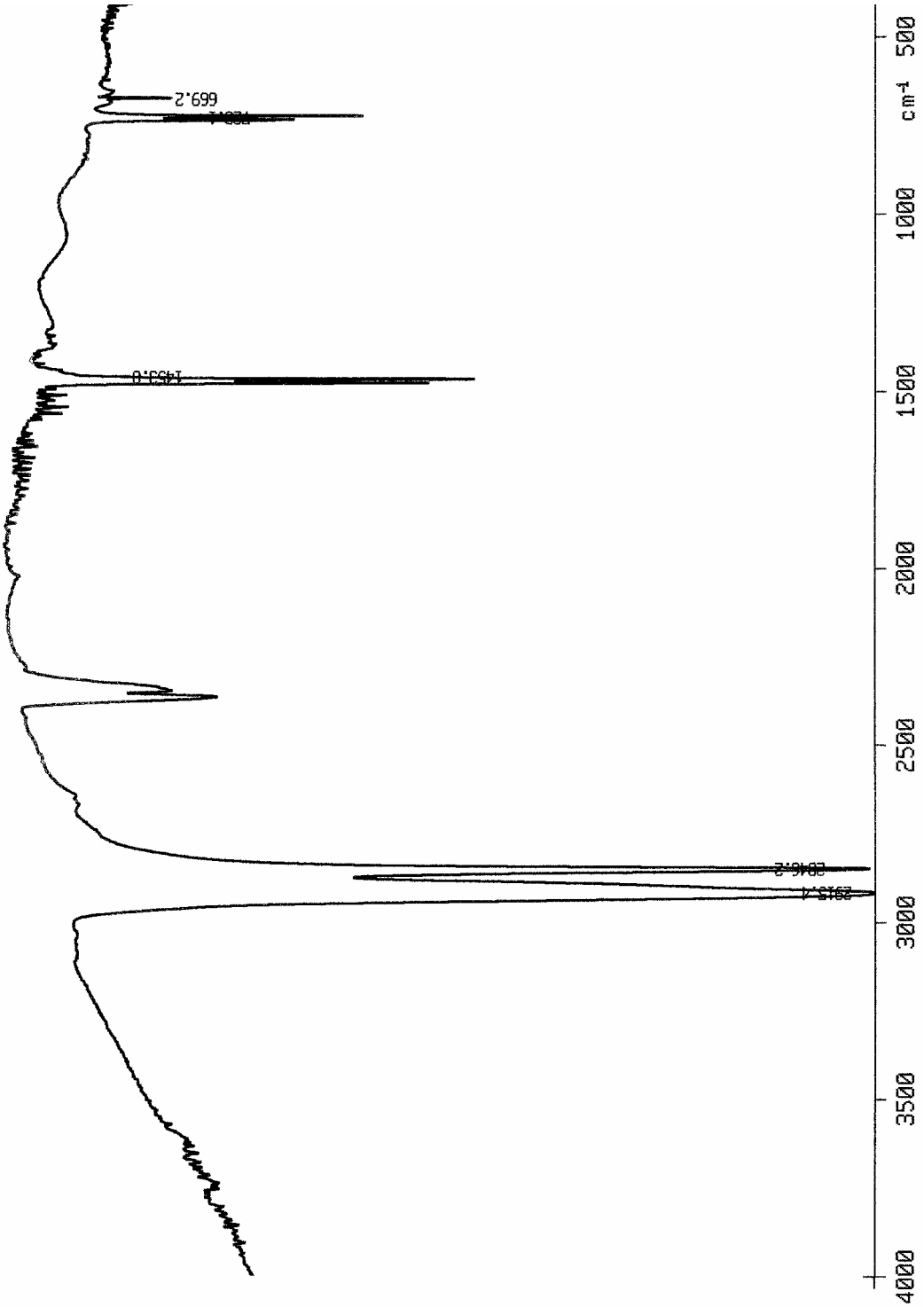

CHAPTER 4 – Functionalization of $Sc_3N@C_{78}$

4.1. Introduction

There are five isomers of the empty C_{78} cage that obey the isolated pentagon rule (IPR).[1] These isomers are: D_3 (78:1), C_{2v} (78:2), $C_{2v'}$ (78:3), D_{3h} (78:4) and $D_{3h'}$ (78:5). The first three isomers, D_3, C_{2v} and $C_{2v'}$, have all been isolated and characterized by their ^{13}C NMR spectra,[2-4] whereas the remaining two isomers (both similar in structure) are the least stable of the group, as predicted by theory,[5,6] and have not yet been found in soluble fullerene extract.

The cage of the $Sc_3N@C_{78}$ metallofullerene (Chapter 1, Figure 1.3) corresponds to the $D_{3h'}$ (78:5) isomer, which is the second least stable of the five isomers.[7] The C_{78} cage is composed of eight different carbon atoms (5 x 12 and 3 x 6), as observed from the ^{13}C NMR spectrum of $Sc_3N@C_{78}$ (CS_2/10% acetone-d_6 (9:1) with [$Cr(acac)_3$]),[7b] and contains three pyracylene-type units (two hexagons with abutted pentagons) that reside in the horizontal mirror plane. As stated in Chapter 3, these pyracylene-type units (Chapter 1, Figure 1.12) are the reactive units on C_{60} fullerene, thereby leading to a functionalization of the cage across the [6,6] bond-junctures.

---

[1] Fowler, P. W.; Manoloupoulos, D. E. In *An Atlas of Fullerene;,* Rowlinson, J. S., Ed.; International Series of Monographs on Chemistry – 30; Oxford University Press: New York, NY, 1995; pp 254–255.

[2] Diederich, F.; Whetten, R. L.; Thilgen, C.; Ettl, R.; Chao, I.; Alvarez, M. M. Fullerene Isomerism – Isolation of C_2-Nu-C_{78} and D_3-C_{78}. *Science* **1991**, *254*, 1768–1770.

[3] Kikuchi, K.; Nakahara, N.; Wakabayashi, T.; Suzuki, S.; Shiromaru, H.; Miyaki, Y.; Saito, K.; Ikemoto, I.; Kainosho, M.; Achiba, Y. NMR Characterization of Isomers of C_{78}, C_{82} and C_{84} Fullerenes. *Nature* **1992**, *357*, 142–145.

[4] Taylor, R.; Langley, G. J.; Dennis, T. J. S.; Kroto, H. W.; Walton, D. R. M. A Mass-Spectrometric NMR-Study of Fullerene-78 Isomers. *J. Chem. Soc., Chem. Commun.* **1992**, 1043–1046.

[5] Slanina, Z.; Francois, J.-P.; Bakowies, D.; Thiel, W. Fullerene C-78 Isomers – Temperature-dependence of their Calculated Relative Stabilities. *J. Mol. Struct. (THEOCHEM)* **1993**, *98*, 213–216.

[6] Ōsawa, E.; Ueno, H.; Yoshida, M.; Slanina, Z.; Zhao, X.; Nishiyama, M.; Saito, H. Combined topological and energy analysis of the annealing process in fullerene formation. Stone-Wales interconversion pathways among IPR isomers of higher fullerenes. *J. Chem. Soc., Perkin Trans. 2* **1998**, 943–950.

[7] (a) Campanera, J. M.; Bo, C.; Olmstead, M. M.; Balch, A. L.; Poblet, J. M. Bonding within the Endohedral Fullerenes $Sc_3N@C_{78}$ and $Sc_3N@C_{80}$ as Determined by Density Functional Calculations and Reexamination of the Crystal Structure of {{$Sc_3N@C_{78}$}•Co(OEP)}•1.5(C_6H_6)•0.3($CHCl_3$). *J. Phys. Chem. A* **2002**, *106*, 12356–12364. (b) Olmstead, M. M.; de Bettencourt-Dias, A.; Duchamp, J. C.; Stevenson, S.; Marciu, D.; Dorn, H. C.; Balch, A. L. Isolation and Structural Characterization of the Endohedral Fullerene $Sc_3N@C_{78}$. *Angew. Chem. Int. Ed.* **2001**, *40*, 1223–1225.

In the X-ray crystal structure (110 K) of $Sc_3N@C_{78}$,[7] the scandium atoms are localized over the three pyracylene patches; however, calculations have recently shown that the most stable position of the metal atoms, regardless of temperature, is when they are localized over the [6,6] bond-junctures of these patches.[7a] Therefore, it is not known if the reactive sites on $Sc_3N@C_{78}$ would be these pyracylene-type units, or if another site would be responsible for functionalizing the molecule.

Similar to $Sc_3N@C_{80}$, only small amounts (milligrams) of the $Sc_3N@C_{78}$ metallofullerene were available for chemical reactions. Furthermore, in fullerene soot, $Sc_3N@C_{78}$ is eight times less abundant than $Sc_3N@C_{80}$.[7b]

4.2. Results and Discussion

4.2.1. ^{13}C-labeled cycloadducts of the $Sc_3N@C_{78}$ metallofullerene (3)

The functionalization chemistry of $Sc_3N@C_{78}$, which is also a member of the novel trimetallic nitride endohedral metallofullerene family, has not been explored until now. As with the $Sc_3N@C_{80}$ member, only milligram amounts of $Sc_3N@C_{78}$ material were available for chemical functionalization. However, although $Sc_3N@C_{78}$ contains pyracylene-type units, it was not known if these units would be reactive when attempting to functionalize the molecule. Therefore, an NMR active label was needed to achieve structural data from small amounts of potentially reactive products.

Possible reactive sites on the cage of $Sc_3N@C_{78}$ were considered, using a ball and stick structure, before a chemical reaction was attempted. For instance, if the three pyracylene-type units on $Sc_3N@C_{78}$ were the *only* reactive sites on the molecule, and each unit was functionalized across the [6,6] bond-juncture with a symmetric addend, then the newly functionalized molecule would also possess D_{3h} symmetry (Scheme 4.1).

Scheme 4.1

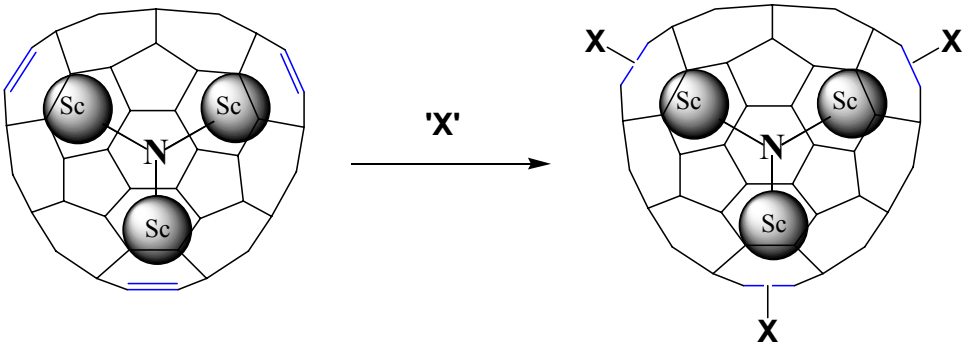

$D_{3h'}$ (78:5) D_{3h}

Furthermore, if each of the addends were labeled (i.e., ^{13}C), then a *single* signal would be present in the product's NMR spectrum. Elements of symmetry would also remain present if only one or two addends were attached to the cage.

To evaluate the aforementioned ideas of cage reactivity, a 1,2,4-trichlorobenzene (TCB) solution containing 5 mg of $Sc_3N@C_{78}$ (95%) **1** was refluxed (214 °C) with three equivalences of ^{13}C-labeled 6,7-dimethoxyisochroman-3-one **2**. During the high temperature reflux, carbon dioxide was thermally extruded from **2** to generate the highly reactive *o*-quinodimethane intermediate that reacted with $Sc_3N@C_{78}$, in a [4 + 2] cycloaddition fashion, to yield $Sc_3N@C_{78}$–$(C_{10}H_{12}O_2)_n$ **3** (Scheme 4.2). Only 3.3 equiv.

Scheme 4.2

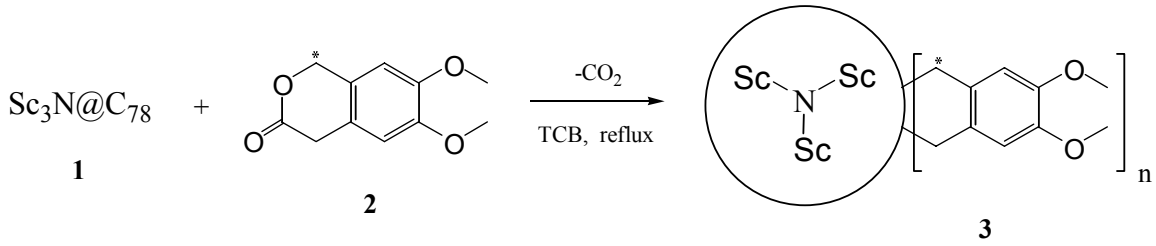

of **2** were used in the reaction, due to the fear that a complicated ^{13}C NMR spectrum would result if more than three reactive sites were present on the molecule's cage and all were functionalized.

The crude reaction solution, which was purified by column chromatography with silica gel, revealed that several reaction products of **3** were present. The mono-adduct of **3** (n = 1) was purified using toluene as the eluent, whereas the di- (n = 2) and tri-adducts (n = 3) were eluted from the column with toluene/ethyl acetate (1:1) and toluene/methanol (4:1) mixtures, respectively. However, when the *isomeric* purity of the three products were evaluated by injecting each product into the HPLC system (Buckyclutcher column, 1 ml/min. in chloroform), only the mono-adduct (n = 1) of **3** contained a single structural isomer, whereas the other two adducts contained from 4-6 structural isomers.

The mass spectrum (MALDI-TOF) of the crude solution (Figure 4.1) shows masses that range from one to three adducts of **3** (n = 1,2,3), in addition to the parent $Sc_3N@C_{78}$ metallofullerene. However, even when the adducts were purified, the parent $Sc_3N@C_{78}$ molecule (*m/z* = 1085) was still observed as a decomposition product in the mass

spectrum. Furthermore, the di- (n = 2, *m/z* = 1416.5) and tri-adducts (n = 3, *m/z* = 1580.6) of **3** decompose to show the mono-adduct (n = 1, *m/z* = 1251.4) and mono- plus di-adducts, respectively. Similar to the derivatives of $Sc_3N@C_{80}$, mass spectra of **3** were not observed unless 9-nitroanthracene was used as the matrix. It should also be noted that additions of four and five addends to the metallofullerene cage were observed from the brown-colored material that was desorbed off the silica gel.

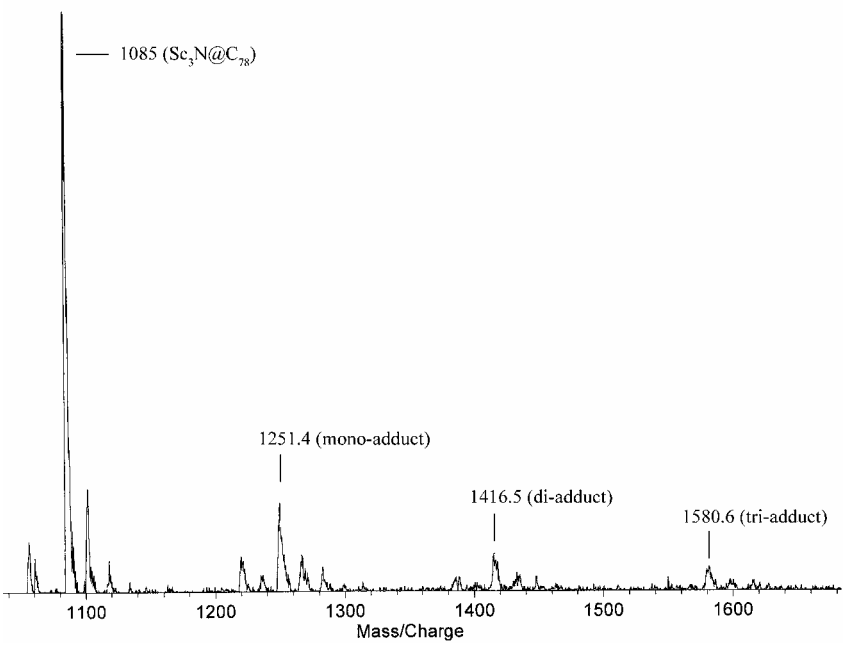

Figure 4.1. MALDI-TOF MS of tri-adduct **3** showing decomposition to mono-, di- and parent. Small amounts of the oxide and C_{88} adducts are also present.

The mono-adduct of **3** was the only product that could be purified in sufficient amounts (*ca.* 1 mg) to achieve structural data by NMR spectrometry. Unfortunately, the adduct is not highly soluble in chloroform-d, and 1,1,2,2-tetrachloroethane-d_2 was needed as a solvent to obtain the ^1H and ^{13}C NMR spectra.

In the ^1H NMR spectrum of the mono-adduct **3** at 60 °C (Figure 4.6) the methylene protons (3.84-3.94 ppm) are observed as broad multiplets due to motion within the six-membered ring of the adduct. This thermally active motion, known as ring inversion, was also observed for the mono-adduct of $Sc_3N@C_{80}$ (Chapter 3, section 3.2.1). A 60 °C temperature was employed to sharpen the linewidths of the methylene signals in the

spectrum, which appear extremely broad at room temperature (23 °C). By raising the temperature, the ring inversion occurs more rapidly, thereby yielding an averaged signal for the position of the methylene protons. The linewidths of the two separate methoxy group signals (3.98 and 4.00 ppm) are also sharpened slightly by the elevation in temperature, which most likely results from less of a dipolar interaction between the methoxy groups of one adduct and the neighboring cage of another. The two aromatic protons are found at 6.94 and 7.13 ppm. If the temperature were lowered (i.e., –60 °C), then motions within the adduct would be frozen, and the signals for the methylene protons would be better resolved. However, a spectrum cannot be acquired at this temperature due the high freezing point of 1,1,2,2-tetrachloroethane-d_2 (–43 ºC). Chloroform-d is preferred for this experiment because of its higher freezing point (–64 ºC), yet the mono-adduct is not soluble enough in the latter solvent to acquire structural data. Spectra were not recorded above 60 ºC for fear that the mono-adduct would decompose.

The ^{13}C NMR spectrum for the mono-adduct of **3** (Figure 4.7) shows signals of equal intensity at 45.27 and 47.75 ppm, which correspond to the two methylene carbons of the adduct. With this result, and from analysis of the previously discussed ^{1}H NMR spectra, it is ostensible that the mono-adduct of **3** is *asymmetric*, thereby lacking a mirror plane of symmetry that is present in the similar ^{13}C-labeled mono-adduct of $Sc_3N@C_{80}$ (Chapter 3, section 3.2.1).

The formation of an asymmetric mono-adduct is *not consistent* with the assumption that the reactive sites on $Sc_3N@C_{78}$ are the three pyracylene-type units, because additions at these sites (across a [6,6] bond-juncture) would produce adducts with mirror planes of symmetry as long as the internal cluster remained dynamic. However, changes in temperature for the ^{1}H NMR spectra of mono-adduct **3** (Figure 4.2) reveal that the linewidths of the two methoxy and two aromatic signals vary slightly with temperature, yet the two peaks *do not* coalesce. Therefore, if the internal cluster is dynamic, then varying the temperature, which consequently would change the rate of cluster rotation, does not have an affect on the positions of the proton signals. This means that mono-

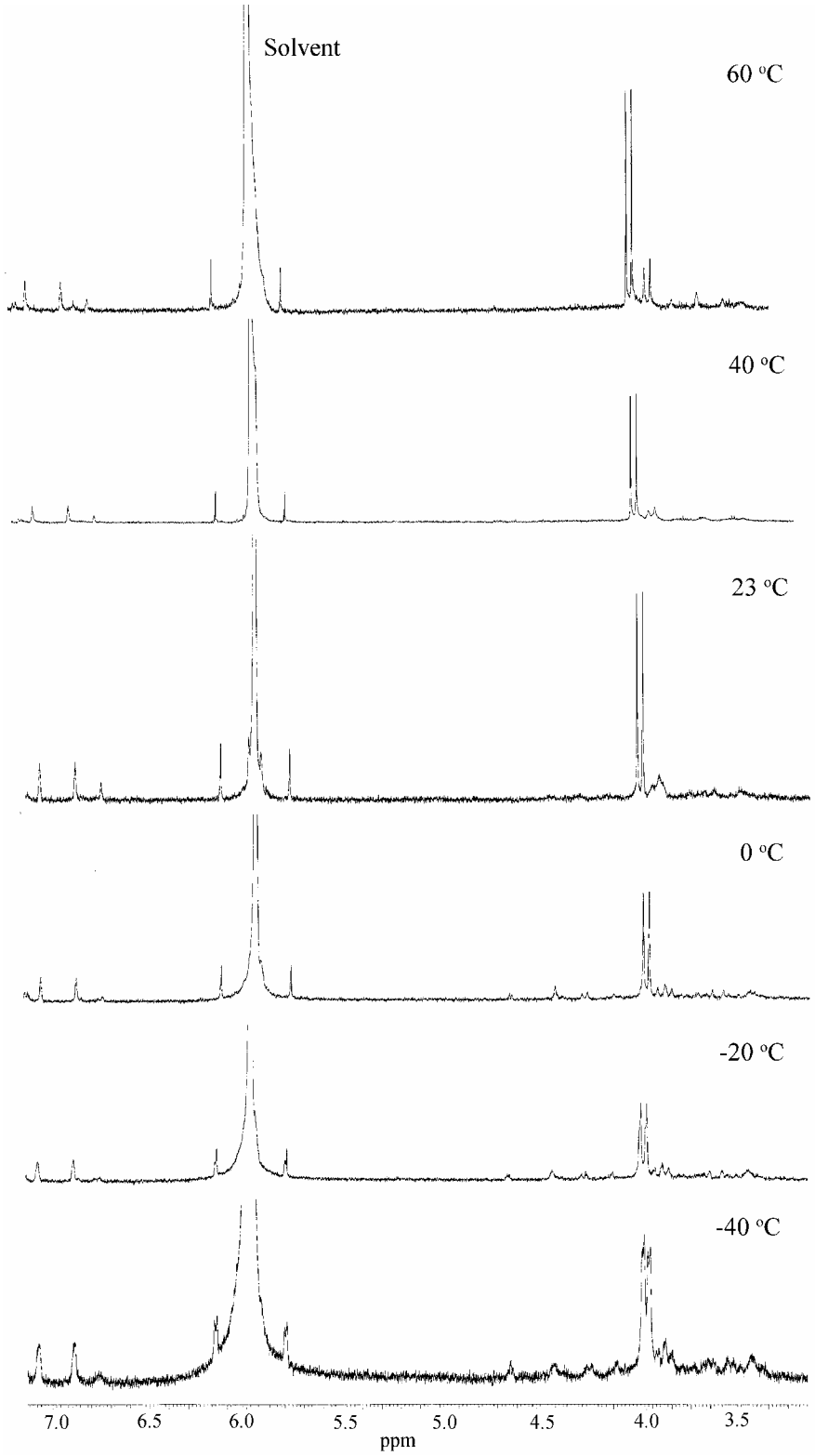

Figure 4.2. Non-coalescence of peaks in the ^{1}H NMR spectra of mono-adduct **3** with variation of temperature.

adduct **3** is asymmetric. Yet, if the Sc atoms of the internal cluster are localized at specific positions within the cage, and not located directly over the three pyracylene patches, then addend addition to the $Sc_3N@C_{78}$ molecule could have occurred at one of the [6,6] bond-junctures to produce an asymmetric adduct as depicted in Figure 4.3.

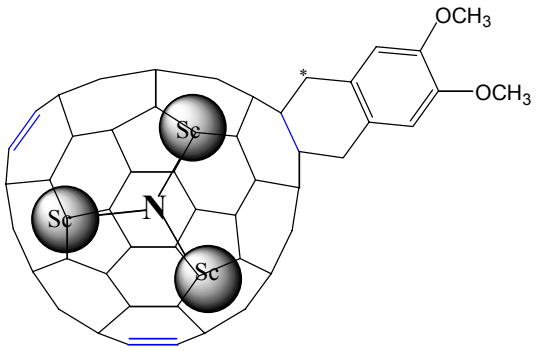

Figure 4.3. An example of an asymmetric mono-adduct **3** when addition has occurred across a [6,6] bond-juncture and the internal cluster is localized.

Utilizing this latter explanation, changes in temperature would have no affect on the proton signal positions of mono-adduct **3**. Furthermore, the latter explanation also holds true if addition occurred at the main symmetry axis (C_3) of the $Sc_3N@C_{78}$ ($D_{3h'}$ (78:5))

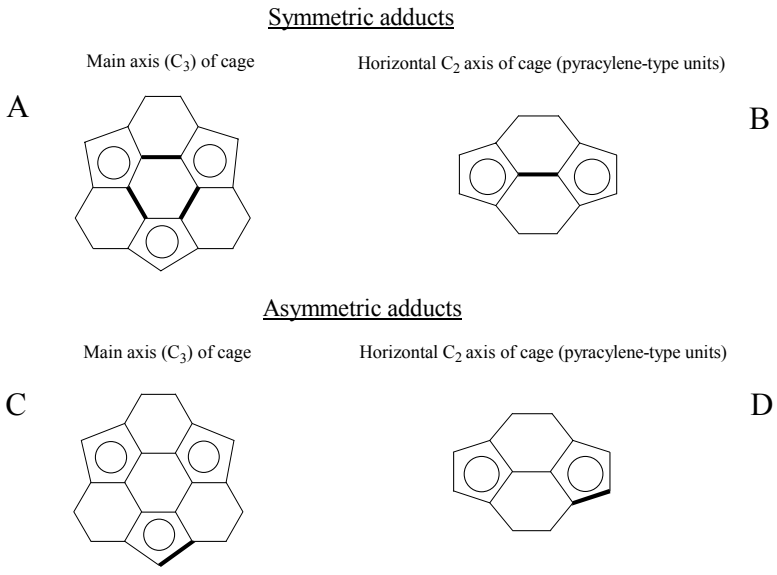

Figure 4.4. Plausible reactive sites (dark bonds) on $Sc_3N@C_{78}$ ($D_{3h'}$ (78:5)) that yield a symmetric or asymmetric mono-adduct when internal cluster is dynamic.

molecule (Figure 4.4a), since these sites would yield a symmetric product if the internal cluster were dynamic.

Another plausible explanation for the observed NMR data is that the reactive site on cage is not a pyracylene-type unit, but rather at a site that directly yields an asymmetric product if the internal cluster is dynamic. The site may be present at an adjacent position to either the main symmetry axis (C_3) (Figure 4.4c) or the three pyracylene patches (Figure 4.4d) of the molecule. The Schlegel diagram of $D_{3h'}$ (78:5) $Sc_3N@C_{78}$ (Appendix IIb) can also be used to understand this explanation.

All previous explanations for the NMR data of mono-adduct **3** have assumed that the cage of $Sc_3N@C_{78}$ is the $D_{3h'}$ (78:5) isomer, because the X-ray crystallographic data[7] yields a better correspondence to the latter. Yet, the experimental ^{13}C NMR data for $Sc_3N@C_{78}$ can be explained in a way that corroborates the D_{3h} (78:4) structural isomer. For instance, the ^{13}C NMR spectrum[7b] of pure $Sc_3N@C_{78}$ (Figure 4.5) yields eight lines (5 at 1.0 intensity and 3 at 0.5 intensity) that correspond to the calculated NMR pattern of 5x12 and 3x6 (total of 78 carbon atoms).[1] Five of these signals (142.48, 143.16, 150.50, 151.23 and 155.60) are located within the range of 142–150+ ppm, which typically signifies the existence of corannulene (intersection of a five-membered ring and two six-membered rings) and/or pyracylene-type (fused hexagons with abutted pentagons) carbon atoms. These two types of carbon atoms are more strained than the pyrene-type (intersection of three six-membered rings); hence, the former are shifted downfield, due to different ring currents,[8] as demonstrated in the NMR spectra of

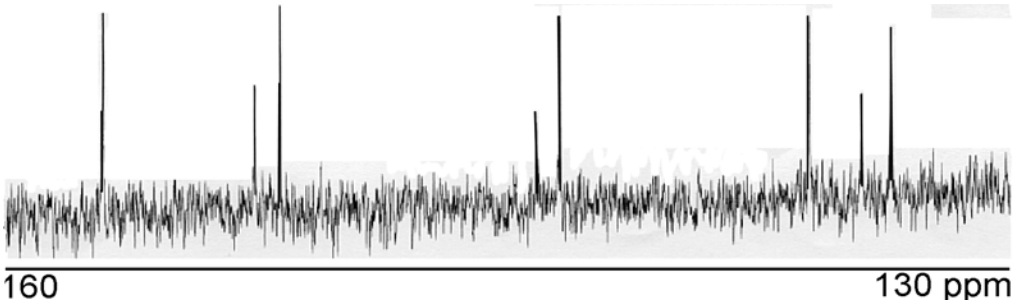

Figure 4.5. 125 MHz ^{13}C NMR spectrum (5x12, 3x6) of $Sc_3N@C_{78}$.[7b]

[8] Pasquarello, A.; Schluter, M.; Haddon, R. C. Ring Currents in Icosahedral C_{60}. *Nature* **1992**, *257*, 1660–1661.

C_{60},[8] C_{70},[9] $Sc_3N@C_{80}$ (Chapter 1, section 1.1.2.2) and numerous other fullerene/metallofullerene species.

If one observes the Schlegel diagram for the D_{3h} (78:4) cage isomer of $Sc_3N@C_{78}$ (Appendix IIa), two non-equivalent corannulene-type and four non-equivalent pyracylene-type carbons are found above the horizontal mirror plane. One of the pyracylene-type carbons is located at the highly strained polar cap (main axis, C_3) of the molecule, and is likely responsible for a full intensity signal above 150 ppm in Figure 4.5. Two of the less strained pyracylene carbons are located midway between the polar cap and the horizontal mirror plane (equatorial belt), and each of these should yield a signal of full intensity above 140 ppm, although the more strained carbon (closer to the polar cap) is likely to reside above 150 ppm. The final pyracylene-type carbon is located on the perpendicular C_2 axes of the cage, and is likely to yield a signal of 1/2 intensity (Figure 4.5) that resides above 150 ppm. As for the corannulene-type carbons, one is located near the strained polar cap and should yield a signal of 1/2 intensity above 140 ppm. On the other hand, the second corannulene-type carbon atom, which is located at the midway point, must then reside as a full intensity signal below 140 ppm.

The $D_{3h'}$ (78:5) cage isomer (Appendix IIb) possesses two non-equivalent pyracylene-type and four non-equivalent corannulene-type carbons that are located on or above the horizontal mirror plane. However, of these six carbon atoms, only the two pyracylene-type carbons (found at the polar cap (main axis, C_3) and perpendicular C_2 axes) are likely to yield signals above 150 ppm. Hence, the experiment NMR data lends more credence to a $Sc_3N@C_{78}$ molecule that possesses a D_{3h} (78:4) cage isomer, as opposed to a molecule with a $D_{3h'}$ (78:5) cage isomer.

As discussed previously, the mono-adduct of **3** appears to be an asymmetric adduct. Yet, if the cage of $Sc_3N@C_{78}$ is really the D_{3h} (78:4) isomer, and *not* the published $D_{3h'}$ (78:5) isomer,[7] then addend addition across the [6,6] bond-juncture of a mid-level pyracylene-type unit (of the D_{3h} isomer) would automatically yield an asymmetric

[9] (a) Taylor, R.; Hare, J. P.; Abdul-Sada, A. K.; Kroto, H. W. Isolation, Separation and Characterization of the Fullerene C_{60} and C_{70}: The Third Form of Carbon. *J. Chem. Soc., Chem. Commun.* **1990**, 1423–1425. (b) Johnson, R. D.; Meijer, G.; Salem, J. R.; Bethune, D. S. 2D Nuclear Magnetic Resonance Study of the Structure of the Fullerene C_{70}. *J. Am. Chem. Soc*. **1991**, *113*, 3619–3621.

product, regardless of whether the scandium atoms of the internal metal-nitride cluster were dynamic or localized.

To evaluate the veracity of the previous discussion, the true D_{3h} isomer of $Sc_3N@C_{78}$ needs to first be elucidated. This can be accomplished by synthesizing a sample of ^{13}C-labeled (*ca.* 10% labeled) $Sc_3N@C_{78}$, then obtaining a 2D NMR INADEQUATE to show the connectivity of carbons throughout the molecule.

4.3. Experimental

4.3.1. Materials and purification

HPLC grade solvents were used unless stated otherwise. Anhydrous solvents were obtained by distillation from appropriate drying agents. Toluene was refluxed with sodium metal and distilling at a reduced pressure. 1,2,4-trichlorobenzene (TCB) was obtained from Aldrich chemical company as anhydrous.

Solvents for extraction and chromatography were HPLC grade unless otherwise specified. All HPLC separations were performed with an Acuflow Series III pump and Applied Biosystems 757 Absorbance Detector (λ = 390 nm). Data was recorded on a Hitachi D-2500 Chromato-Integrator. $Sc_3N@C_{78}$ was purified from soluble fullerene extract using a two-stage HPLC process. The first stage required a 5-PBB (pentabromobenzyl) column (5 μm, 250 mm x 20 mm ID: Phenomenex) with carbon disulfide (CS_2) as eluent. The flow rate was 2 ml/min. The second stage required a Trident-Tri-DNP (Buckyclutcher) column (5 μm, 250 mm x 10 mm ID: Regis Chemical) with toluene as eluent. The flow rate was 2 ml/min. HPLC purification of functionalized $Sc_3N@C_{78}$ was performed using the Buckyclutcher column with chloroform as eluent (1.00 ml/min.) unless stated otherwise. Flash chromatography purification of the functionalized $Sc_3N@C_{78}$ metallofullerene was performed using Silica gel (200–400 Mesh, 60Å) from Aldrich chemical company.

1,1,2,2-Tetrachloroethane-d_2 (from Cambridge Isotope Laboratory) was dried with molecular sieves.

Suppliers of reagents were as follows: Luna nanoMaterials – $Sc_3N@C_{78}$ (*ca.* 80% pure); Aldrich – 1,8-diazabicyclo[5.4.0]undec-7-ene (DBU, 98%), CBr_4 (99%); Cambridge Isotope Laboratory – diethyl malonate (2-^{13}C 99%).

$Sc_3N@C_{78}$ was purified at Virginia Tech using the previously discussed dual stage HPLC separation technique. All other reagents were used as received from the vendor. 6,7-dimethoxyisochroman-3-one (^{13}C-labeled, 99%) was synthesized and purified at Virginia Tech (Chapter 3, section 3.2.3).

4.3.2. Analytical methods

^{1}H and ^{13}C NMR spectra were obtained with a JEOL Eclipse+ 500 spectrometer. ^{13}C NMR spectra of functionalized metallofullerenes were recorded using a 5 second delay between pulses. The external standard was tetramethylsilane (TMS).

Mass spectra of functionalized metallofullerenes were obtained with a Kratos Kompact SEQ matrix-assisted laser-desorption ionization time-of-flight (MALDI-TOF) mass spectrometer using 9-nitroanthracene as a matrix. Mass spectra of non-functionalized metallofullerenes were obtained with a Fisons VG Quattro mass spectrometer using a desorption chemical-ionization (DCI) probe and negative ionization.

4.3.3. Synthesis of ^{13}C-labeled $Sc_3N@C_{78}$–$(C_{10}H_{12}O_2)_n$ cycloadducts (3)

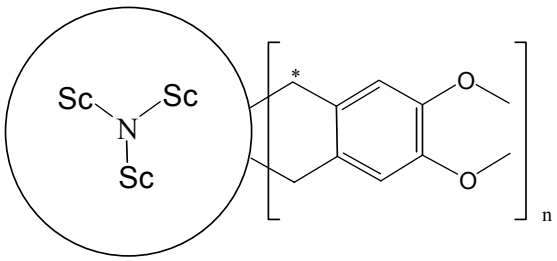

5 mg (4.61 μmol) of $Sc_3N@C_{78}$ **1** (*ca.* 95%) was added to a 10 ml round bottom flask, along with 3.5 mg (16.73 μmol, *ca.* 3.3 equiv.) 6,7-dimethoxyisochroman-3-one **2** (^{13}C-labeled, 99%) and 7 ml 1,2,4-trichlorobenzene (TCB). The flask was sonicated for 20 minutes to dissolve all reagents, then refluxed under Argon, while stirring, for 20 hours. The solvent was removed via high vacuum and low heat (*ca.* 50 °C) to reveal a black/brown colored product. The product was dissolved in toluene and separated on silica gel. First, toluene was used to remove unreacted $Sc_3N@C_{78}$ **1** (R_f = 0.99), which is a dark green colored. Toluene also elutes a reddish/brown colored product (R_f = 0.50) that had a mass of 1251.4 (mono-adduct) from MALDI-TOF MS (positive ionization). Next, a toluene/ethyl acetate mixture (1:1) was used to remove a golden/brown colored product that had a mass of 1416.5 (di-adduct). Finally, a toluene/methanol mixture (4:1) was used to elute another golden/brown colored product that corresponded to a mass of 1580.6 (tri-adduct) using MALDI-TOF MS. A brown colored material would not elute from the column, and was desorbed from the silica gel with water and chloroform. This material showed masses at 1746.8 (tetra-adduct) and 1910.0 (penta-adduct). The parent metallofullerene **1** (*m/z* 1085) was observed in all spectra. Weight of the mono-adduct was *ca.* 1 mg. ^{1}H NMR (500 MHz, $C_2D_2Cl_4$, 60 °C): δ 3.38-3.94 (m, br, 4H, CH_2), 3.98 (s, 3H, OCH_3), 4.00 (s, 3H, OCH_3), 6.94 (s, 1H, aromatic CH) and 7.13 (s, 1H, aromatic CH). ^{13}C NMR (125 MHz, $C_2D_2Cl_4$, 5 s delay, 5587 scans): δ 45.27 and 47.75.

Figure 4.6. 500 MHz ^{1}H NMR spectrum at 60 ºC of ^{13}C-labeled $Sc_3N@C_{78}$–$(C_{10}H_{12}O_2)_1$ adduct **3**.

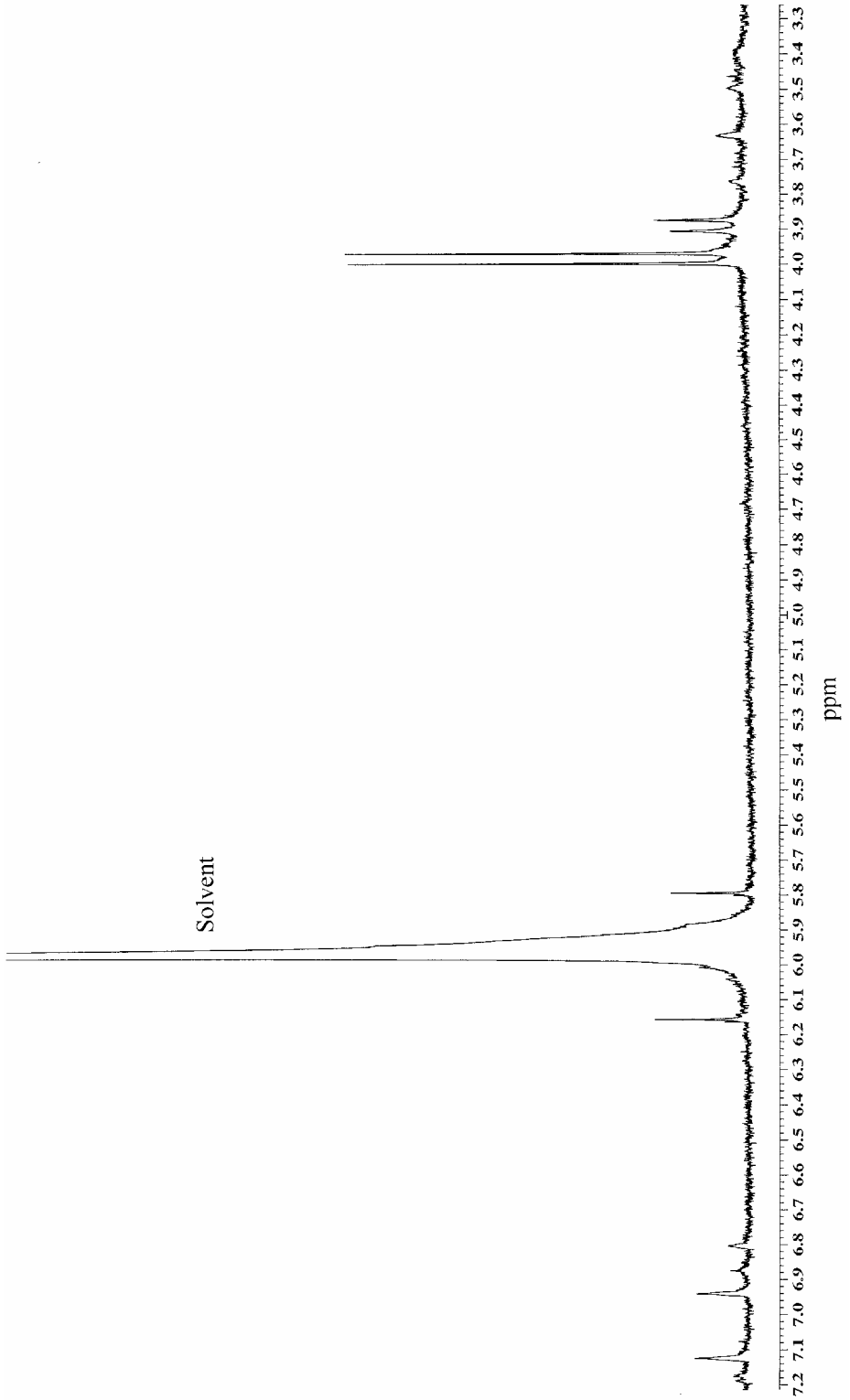

Figure 4.7. 125 MHz ^{13}C NMR spectrum of ^{13}C-labeled $Sc_3N@C_{78}$–$(C_{10}H_{12}O_2)_1$ adduct **3** (x = impurity).

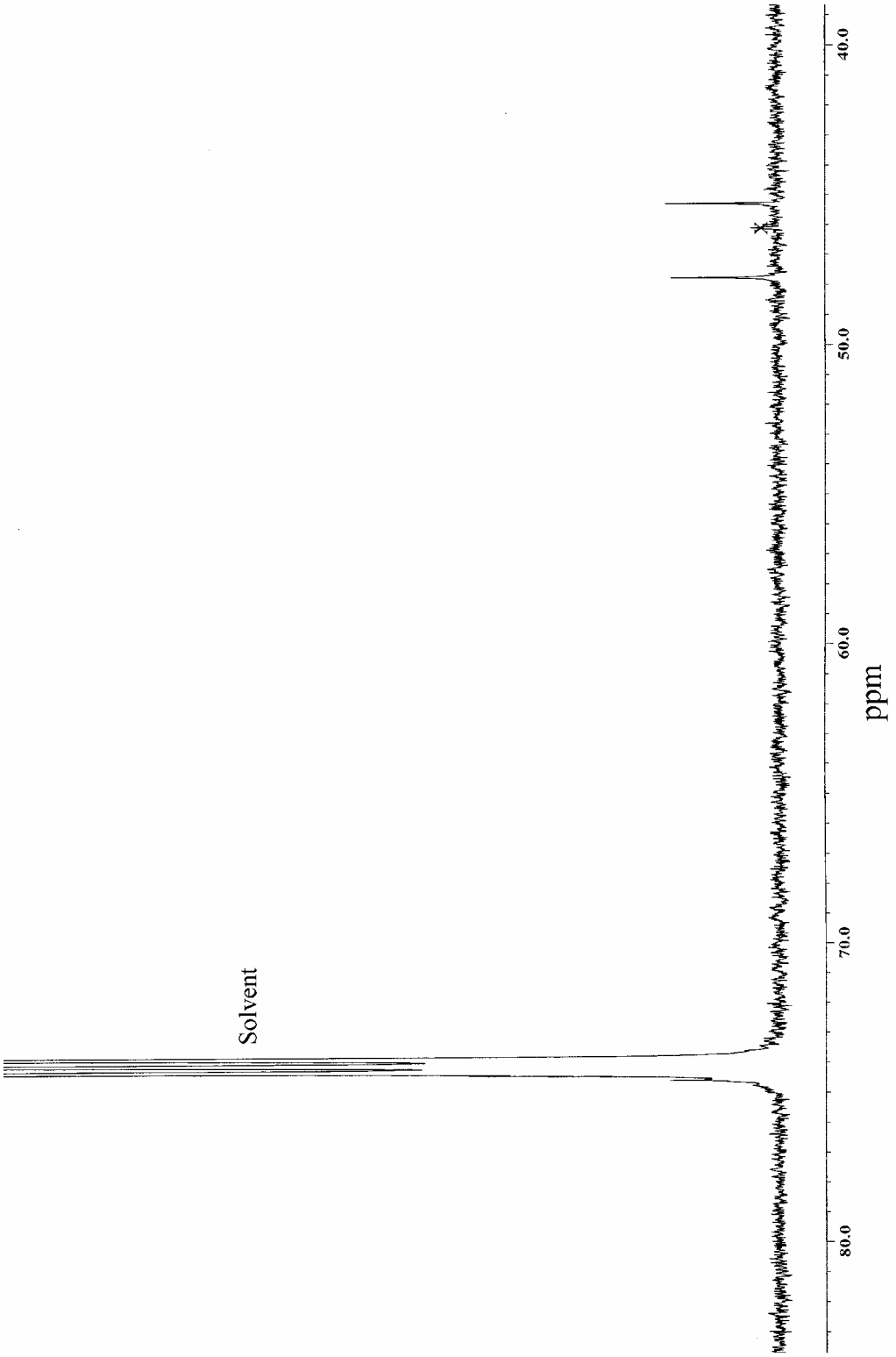

CHAPTER 5 – X-ray Contrast, a D_{5h} Isomer and ^{15}N-labeling of the Internal Metal-Nitride Cluster

5.1. Introduction

Chapter 5 discusses three separate miscellaneous studies. The first part of the chapter describes the generation of a new X-ray contrast agent, $Lu_3N@C_{80}$,[1] the second details the discovery and separation of a second isomer (D_{5h}) of $Sc_3N@C_{80}$,[2] and finally, a ^{15}N-labeling experiment of the internal Sc_3N cluster of $Sc_3N@C_{80}$ is discussed.

The ability to encapsulate lanthanide atoms into fullerene cages continues to excite scientists throughout the world. Cerium, praseodymium, terbium, gadolinium, neodymium, lanthanum, erbium, holmium, dysprosium, lutetium, thulium, samarium, europium and ytterbium have all been encapsulated to form either a mono- or dimetallofullerene species via the electric-arc process, and are listed in consecutive order of decreasing yields ($M@C_{82}$).[1,3] Interestingly, when encapsulated inside a C_{82} cage, the lanthanide metals typically exhibit a trivalent oxidation state in order to partially fill the lowest unoccupied molecular orbitals (LUMOs) of the cage and create an open-shell electronic state.[4,5] Only a few lanthanide elements, cerium and praseodymium for example, have been observed as higher symmetry (I_h) C_{80} cage encapsulates, forming $[Ce_2]^{+6}@[C_{80}]^{-6}$ and $[Pr_2]^{+6}@[C_{80}]^{-6}$, respectively.[6] Recently, a dimetallic species of

---

[1] Iezzi, E. B.; Duchamp, J. C.; Fletcher, K. R.; Glass, T. E.; Dorn, H. C. Lutetium-based Trimetallic Nitride Endohedral Metallofullerenes: New Contrast Agents. *Nano Lett.* **2002**, *2*, 1187–1190.

[2] Duchamp, J. C.; Demortier, A.; Fletcher, K. R.; Dorn, D.; Iezzi, E. B.; Glass, T.; Dorn, H. C. An Isomer of the Endohedral Metallofullerene $Sc_3N@C_{80}$ with D_{5h} Symmetry. *Chem. Phys. Lett.* **2003**, *375*, 655–659.

[3] Houjin, H.; Shihe, Y. Relative Yields of Endohedral Lanthanide Metallofullerenes by Arc Synthesis and their Correlation with the Elution Behavior. *J. Phys. Chem. B* **1998**, *102*, 10196–10200.

[4] Liu, S. Y.; Sun, S. Q. Recent progress in the studies of endohedral metallofullerenes. *J. Organomet. Chem.* **2000**, *599*, 74–86.

[5] Kikuchi, K.; Sueki, K.; Akiyama, K.; Kodama, T.; Nakahara, H.; Ikemoto, I. *Fullerenes: Recent Advances in the Chemistry and Physics of Fullerenes and Related Materials*; The Electrochemical Society, Inc.: Pennington, NJ, 1997; Vol 4, p. 408.

[6] (a) Ding, J.-Q; Yang, S.-H. Isolation and Characterization of the Dimetallofullerene $Ce_2@C_{80}$. *Angew. Chem. Int. Ed. Engl.* **1996**, *35*, 2234–2235. (b) Ding, J.; Yang, S. Isolation and Characterization of $Pr@C_{82}$ and $Pr_2@C_{80}$. *J. Am. Chem. Soc.* **1996**, *118*, 11254–11257.

titanium, $[Ti_2]^{+6}@[C_{80}]^{-6}$, was incorporated into a C_{80} cage.[7] Until now, the size selectivity of a hollow C_{80} or C_{82} cage was believed to prohibit imprisonment of more than one or two large lanthanide elements (i.e., La, Gd or Lu).

This work focuses on the development of a new generation of imaging contrast agents that are designed at the nanoscale level with improved contrast as well as multi-modal imaging potential (X-ray and MRI). Specifically, most X-ray contrast agents contain large *Z* (atomic number) elements (i.e., iodine or barium) for high contrast, such as the commercially available Iohexol (Figure 5.1), although gadolinium MRI agents have also been employed as contrast agents.[8] Here, a lutetium-based series of mixed-metal species of gadolinium/lutetium and holmium/lutetium, $Lu_{3-x}A_xN@C_{80}$ (x = 0-2) endohedral metallofullerenes, is discussed. The archetypal species is the endohedral metallofullerene, $Lu_3N@C_{80}$, synthesized by the trimetallic nitride template (TNT) process that provides a stable high symmetry (I_h) cage, $[Lu_3N]^{+6}@[C_{80}]^{-6}$.[9-16]

---

[7] Cao, B. P.; Hasegawa, M.; Okada, K.; Tomiyama, T.; Okazaki, T.; Suenaga, K.; Shinohara, H. EELS and C-13 NMR characterization of pure $Ti_2@C_{80}$ metallofullerene. *J. Am. Chem. Soc.* **2001**, *123*, 9679–9680.

[8] Yu, S.-H.; Watson, A. D. Metal-based X-ray Contrast Media. *Chem. Rev.* **1999**, *99*, 2353–2377.

[9] Stevenson, S.; Rice, G.; Glass, T.; Harich, K.; Cromer, F.; Jordan, M. R.; Craft, J.; Hadju, E.; Bible, R.; Olmstead, M. M.; Maitra, K.; Fisher, A. J.; Balch, A. L.; Dorn, H. C. Small-bandgap endohedral metallofullerenes in high yield and purity. *Nature* **1999**, *401*, 55–57.

[10] Olmstead, M. M.; de Bettencourt-Dias, A.; Duchamp, J. C.; Stevenson, S.; Dorn, H. C.; Balch, A. L. Isolation and crystallographic characterization of $ErSc_2N@C_{80}$: an endohedral fullerene which crystallizes with remarkable internal order. *J. Am. Chem. Soc.* **2000**, *122*, 12220–12226.

[11] Dunsch, L.; Bartl, A.; Georgi, P.; Georgi, P.; Kuran, P. New metallofullerenes in the size gap of C_{70} to C_{82}: From $La_2@C_{72}$ to $Sc_3N@C_{80}$. *Synth. Met.* **2001**, *121*, 1113–1114.

[12] Macfarlane, R. M.; Bethune, D. S.; Stevenson, S.; Dorn, H. C. Fluorescence spectroscopy and emission lifetimes of Er^{3+} in $Er_xSc_{3-x}N@C_{80}$ (x = 1-3). *Chem. Phys. Lett.* **2001**, *343*, 229–234.

[13] Kobayashi, K.; Sano, Y.; Nagase, S. Theoretical study of endohedral metallofullerenes: $Sc_{3-n}La_nN@C_{80}$ (n = 0-3). *J. Comput. Chem.* **2001**, *22*, 1353–1358.

[14] Jakes, P.; Dinse, K. P. Chemically induced spin transfer to an encased molecular cluster: an EPR study of $Sc_3N@C_{80}$ radical anions. *J. Am. Chem. Soc.* **2001**, *123*, 8854–8855.

[15] Larade, B.; Taylor, J.; Zheng, Q. R.; Mehrez, H.; Pomorski, P.; Guo, H. Renormalized molecular levels in a $Sc_3N@C_{80}$ molecular electronic device. *Phys. Rev. B* **2001**, *64*: art. no. 195402.

[16] Ioffe, I. N.; Ievlev, A. S.; Boltalina, O. V.; Sidorov, L. N.; Dorn, H. C.; Stevenson, S.; Rice, G. Electron affinity of some trimetallic nitride and conventional metallofullerenes. *Int. J. Mass. Spectrom*. **2002**, *213*, 183–189.

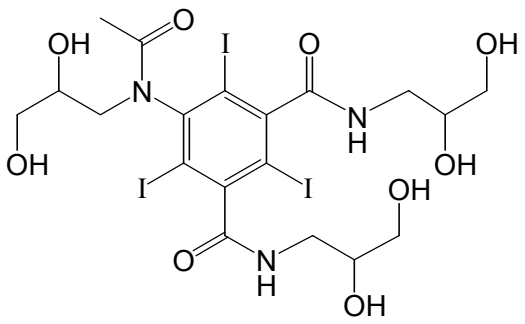

Figure 5.1. Iohexol (a commercially available X-ray contrast agent).

Numerous papers have presented theoretical data concerning the seven possible isolated pentagon rule (IPR) isomers of C_{80}.[17] The isomers of the empty-cage C_{80} fullerenes with D_{5h} and I_h symmetries are found to be the least stable of the seven, thus explaining the presence of these molecules in fullerene extract. However, several papers present calculations demonstrating the enhanced stability of the I_h C_{80} cage ($[C_{80}]^{6-}$).[18-22] For endohedral metallofullerenes, the presence of metal clusters that transfer significant charge to the fullerene cage leads to stable, neutral molecules. An example would be $Sc_3N@C_{80}$, which is formed by the trimetallic nitride template (TNT) process in high yields (5-10 % of the soluble extract).[9]

^{13}C NMR has proven to be a powerful probe for isomer identification of the fullerene cages.[23,24] For example, high field ^{13}C NMR spectra of $Sc_3N@C_{68}$,[25] $Sc_3N@C_{78}$,[26] and

---

17 Wang, C. R.; Sugai, T.; Kai, T.; Tomiyama, T.; Shinohara, H. Production and isolation of an ellipsoidal C_{80} fullerene. *Chem. Commun.* **2000**, 557–558.

18 Nakao, K.; Kurita, N.; Fujita, M. Ab-inito Molecular-orbital Calculation for C_{70} and 7 Isomers of C_{80}. *Phys. R*ev. *B* **1994**, 49, 11415–11420.

19 Furche, F.; Ahlrichs, R. Fullerene C_{80}: are there still more isomers? *J. Chem. Phys.* **2001**, *114*, 10362–10367.

20 Fowler, P. W.; Zerbetto, F. Charging and Equilibration of Fullerene Isomers. *Chem. Phys. Lett.* **1995**, *243*, 36–41.

21 Kobayashi, K.; Nagase, S.; Akasaka, T. A Theoretical Study of C_{80} and $La_2@C_{80}$. *Chem. Phys. Lett.* **1995**, *245*, 230–236.

22 Slanina, Z.; Lee, S. L.; Adamowicz, L. C_{80}, C_{86}, C_{88}: Semi-empirical and ab initio SCF calculations. *Int. J. Quantum Chem.* **1997**, *63*, 529–535.

23 Slanina, Z.; Uhlk, F.; Lee, S. L.; Osawa, E. Geometrical and thermodynamic approaches to the relative stabilities of fullerene isomers. *Match-Commun. Math Co.* **2001**, 335–348.

24 Nagase, S.; Kobayashi, K. In *Fullerenes: Recent Advances in the Chemistry and Physics of Fullerenes and Related Materials*; Kadish, K. M., Ruoff, R. S., Eds.; The Electrochemical Society, Inc.: Pennington, NJ, 1997; 4*,* pp 438–447.

$Sc_3N@C_{80}$,[9] yielded 12, 8, and 2 lines, respectively, consistent with D_3, D_{3h}, and I_h symmetries for these representative TNT members. This work reports on the discovery and characterization of a minor isomer of $Sc_3N@C_{80}$ with D_{5h} symmetry. The D_{5h} symmetry isomer appears to be *ca.* 10% of $Sc_3N@C_{80}$ formed during the electric-arc synthesis and may have been present in previously characterized samples of $Sc_3N@C_{80}$.

Early fullerene studies have demonstrated a cornucopia of motions for the different cages, although little is known regarding the cage and clusters dynamics (Figure 5.2) of the trimetallic nitride endohedral metallofullerenes. Recent ^{45}Sc solution NMR studies by Dorn and Duchamp[27] have provided insight into the symmetry and motion of the Sc_3N cluster inside the I_h $[C_{80}]^{-6}$ carbonaceous cage. For instance, the ^{45}Sc NMR spectrum for $Sc_3N@C_{80}$ exhibited a single symmetric peak at temperatures above room temperature,

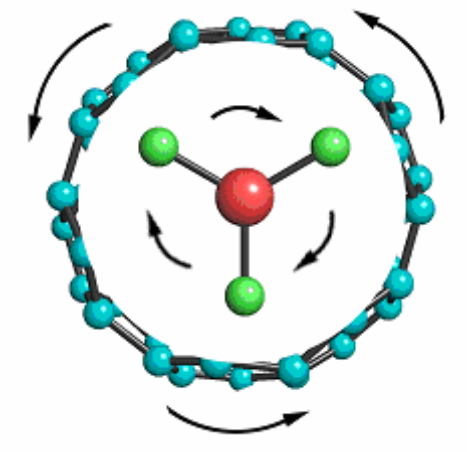

Figure 5.2. A simple representation of metal-nitride cluster and carbon cage motions.

and the linewidth is not dependent on the viscosity of the solvent. At 295 K, the ^{45}Sc NMR linewidth for $Sc_3N@C_{80}$ in carbon disulfide and decalin are *ca.* 3440 and *ca.* 3200 Hz, respectively.[27] These results suggest that the Sc atom reorientation motion is

---

[25] Stevenson, S.; Fowler, P. W.; Heine, T.; Duchamp, J. C.; Rice, G.; Glass, T.; Harich, K.; Hadju, E.; Bible, R.; Dorn, H. C. Materials science - A stable non-classical metallofullerene family. *Nature* **2000**, *408*, 427–428.

[26] Olmstead, M. M.; de Bettencourt-Dias, A.; Duchamp, J. C.; Stevenson, S.; Marciu, D.; Dorn, H. C.; Balch, A. L. Isolation and structural characterization of the endohedral fullerene $Sc_3N@C_{78}$. *Angew. Chem. Int. Ed. Engl.* **2001**, *40*, 1223–1225.

[27] Dorn, H. C.; Duchamp, J. C. Unpublished data.

independent of the solution viscosity, and also reflects the motional averaged electronic environment for the three internal Sc atoms. Therefore, with the *assumption* that the correlation time (τ_c) (motion through 2π radians, i.e., 360º) can be expressed as:

$$\tau_c = \tau_o \exp(E_a/kT)$$

where τ_o is a constant, k is the rate (linewidth) of motion (Hz = cycle/second) for the quadrupolar Sc atoms (cluster), and E_a represents an activation energy (barrier), the data could be fitted to yield activation energies of 0.080 and 0.062 eV for the internal cluster (Sc_3N) of $Sc_3N@C_{80}$ in solvents of carbon disulfide and decalin, respectively. This range of barriers is somewhat lower than the 0.088 eV barrier reported by Miyake and co-workers[28] for $Sc_2@C_{84}$ (isomer III) in carbon disulfide and *o*-dichlorobenzene. However, the relatively low Sc atom reorientation barrier (presumably dominated by motion internal to the cage) is consistent with calculations (Hartree-Fock level) for the electrostatic map of the I_h $[C_{80}]^{-6}$ cage and corresponding low internal barrier of *ca.* 5 kcal/mol (*ca.* 0.217 eV).[29]

^{15}N-labeling of the internal Sc_3N cluster of $Sc_3N@C_{80}$ would present an additional independent means for probing the cluster motional behavior. Analysis of both ^{15}N (dipolar nucleus, *S = 1/2*) and ^{45}Sc (quadrupolar nucleus, *S = 7/2*) NMR linewidths and relaxation would provide detailed information about the motion, in addition to interactions between the cluster and the cage. Therefore, after characterizing the motion of the cage, via solid state ^{13}C NMR (*S = 1/2*), the contribution due to the motion of the cage could be subtracted, thereby obtaining a correlation for the motion of the cluster that is independent of the motion of the external cage.

Understanding the cage and cluster motions of the trimetallic nitride endohedral metallofullerenes are crucial if the molecules are to be utilized in future applications,

---

[28] Miyake, Y.; Suzuki, S.; Kojima, Y.; Kikuchi, K.; Kobayashi, K.; Maniwa, Y.; Fisher, K. Motion of Scandium Ions in Sc_2C_{84} Observed by ^{45}Sc Solution NMR. *J. Phys. Chem.* **1996**, *100*, 9579–9581.

[29] Kobayashi, K.; Nagase, S.; Akasaka, T. Endohedral dimetallofullerenes $Sc_2@C_{84}$ and $La_2@C_{80}$. Are the metal atoms still inside the fullerene cages? *Chem. Phys. Lett.* **1996**, *261*, 502–506; Recent Advances in the Structural Determination of Endohedral Metallofullerenes. *J. Comput. Chem.* **1998**, *19*, 232–239.

such as of quantum computing, molecular gyroscopes, imaging agents and opto-electronic devices.

5.2. Results and Discussion

5.2.1. A lutetium-based contrast agent

The HPLC trace (Buckyclutcher column) of purified $Lu_3N@C_{80}$, which was synthesized in a Krätschmer-Huffman generator,[30] depicts a pure substance with a retention time of 13.62 minutes (Figure 5.3a). The retention time of $Lu_3N@C_{80}$ on the Buckyclutcher column is similar to the $Sc_3N@C_{80}$ metallofullerene, with a small difference only at a low flow rate (0.75 ml/min., retention times of 36.35 min. for $Lu_3N@C_{80}$ and 37.34 min. for $Sc_3N@C_{80}$). However, when both molecules are injected into the 5-PBB column (0.75 ml/min. flow rate), $Sc_3N@C_{80}$ eluted first at 35.0 minutes, while $Lu_3N@C_{80}$ appeared second at 35.66 minutes. The former column (Buckyclutcher) demonstrates that $Lu_3N@C_{80}$ possesses a slightly lower internal dipole moment, thereby interacting less with the polar stationary phase of the Buckyclutcher column (Figure 1.7). On the other hand, a greater amount of electron density in $Lu_3N@C_{80}$ is donated from the internal cluster to the cage, which explains why the molecule has a slightly longer retention time on the 5-PBB column (Figure 1.6). The ionic radii of Lu^{+3} (0.848 Å) is larger than that of Sc^{+3} (0.68 Å), although the cage and internal cluster in the X-ray

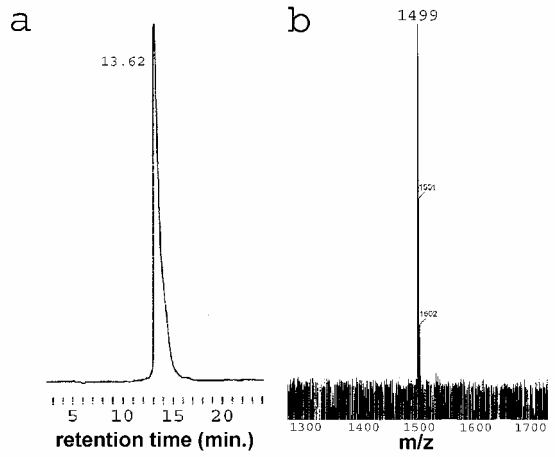

Figure 5.3. (a) HPLC trace (Buckyclutcher column, toluene, 2 ml/min. flow rate) and (b) Neg-DCI mass spectrum of pure $Lu_3N@C_{80}$.

[30] Krätschmer, W.; Lamb, L. D.; Fostiropoulos, K.; Huffman, D. R. Solid C_{60}: A New Form of Carbon. *Nature* **1990**, *347*, 354–358.

crystal structures of $Lu_3N@C_{80}$ and $Sc_3N@C_{80}$ are nearly identical.[31]

A Neg-DCI mass spectrum (Figure 5.3b) reveals a single species for purified $Lu_3N@C_{80}$ with a parent peak at *m/z* 1499. The former suggests that the C_{80} cage bond structure and number of pi-electrons transferred to the cage is similar to $Sc_3N@C_{80}$, otherwise the retention time would be significantly altered.

The ^{13}C NMR spectrum provides additional information that corroborates the structure in Figure 5.4. Of the seven isolated pentagon rule IPR isomers of C_{80}, only the I_h isomer yields a ^{13}C NMR spectrum containing two lines with a 3:1 ratio. Furthermore, the ^{13}C NMR spectrum of $Lu_3N@C_{80}$ (Figure 5.15) supports an electronic distribution of $[Lu_3N]^{+6}@[C_{80}]^{-6}$, because the pyrene-type carbon atoms (intersection of three six-membered rings, δ = 137.4 ppm) and corannulene-type carbon atoms (intersection of a five-membered and two six-membered rings, δ = 144.0 ppm) of the icosahedral cage

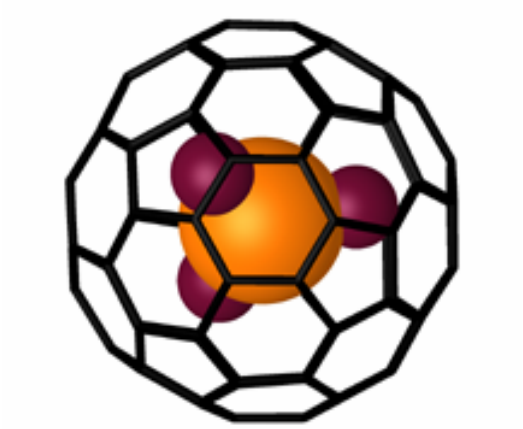

Figure 5.4. Gauss View structure of $Lu_3N@C_{80}$.

demonstrate resonances similar to those of $Sc_3N@C_{80}$ (137.2 ppm and 144.6 ppm), respectively.[9] The ^{13}C NMR spectrum at ambient temperatures is also consistent with motional averaging of the Lu_3N cluster inside the I_h cage in similar fashion to the

[31] Stevenson, S.; Lee, H. M.; Olmstead, M. M.; Kozikowski, C.; Stevenson, P.; Balch, A. L. Preparation and Crystallographic Characterization of a New Endohedral, $Lu_3N@C_{80}$•5(*o*-xylene), and Comparison with $Sc_3N@C_{80}$•5(*o*-xylene). *Chem. Eur. J.* **2002**, *8*, 4528–4535.

situation found for the Sc_3N cluster in $Sc_3N@C_{80}$. Without motional averaging, symmetry lowering would yield a greater number of lines in the ^{13}C NMR spectrum.

A comparison of the UV-Visible absorption spectra for $Lu_3N@C_{80}$ and $Sc_3N@C_{80}$ metallofullerenes are provided in Figure 5.5. While both molecules show similar absorptions, the lutetium species possesses an additional shoulder around 668 nm. Lanthanide containing monometallofullerenes of $M@C_{82}$ give similar UV-Visible maxima, suggesting that the cages accept comparable amounts of electron density from each metal atom.[32,33] Although the ^{13}C NMR for $Lu_3N@C_{80}$ indicates that this metallofullerene is diamagnetic, this is not the case for $Lu@C_{82}$,[33] which exhibits a single broad EPR peak at both room and liquid nitrogen temperatures, in addition to eight unresolved hyperfine lines from coupling to the ^{175}Lu ($I = 7/2$) nucleus. The diamagnetic nature of the $Lu_3N@C_{80}$ species results from a complete *f-subshell* filling of each lutetium atom, while donating one electron to the central nitrogen and two electrons to the fullerene cage.

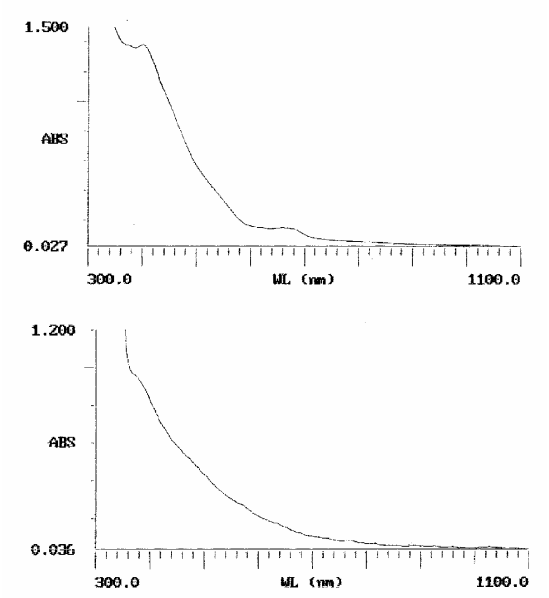

Figure 5.5. UV-Visible spectra comparison between $Lu_3N@C_{80}$ (top) and $Sc_3N@C_{80}$ (bottom).

---

[32] Ding, J.-Q.; Yang, S.-H. Systematic isolation of endohedral fullerenes containing lanthanide atoms and their characterization. *J. Phys. Chem. Solids* **1997**, *58*, 1661–1667.

[33] Houjin, H.; Shihe, Y. Preparation and Characterization of the Endohedral Metallofullerene $Lu@C_{82}$. *J. Phys. Chem. Solids* **2000**, *61*, 1105–1110.

An exciting feature of lutetium is the ability to produce families of species containing other lanthanide metals. Mass spectral data from the arc-vaporization of gadolinium oxide/lutetium oxide ($Lu_2GdN@C_{80}$) (Figure 5.6) and holmium oxide/lutetium oxide ($HoLu_2N@C_{80}$ and $Ho_2LuN@C_{80}$) (Figure 5.7) packed graphite rods demonstrate the efficacious nature of the lutetium to participate in several mixed metal-nitride clusters. These experiments demonstrate that in some cases, formation of the mixed-metal Lu species provide *higher yields* (Figure 5.8) than the $Lu_3N@C_{80}$ species. This result is similar to experiments involving scandium, in which the yield for $Sc_3N@C_{80}$ is less than that of the mixed-metal Sc species.[9]

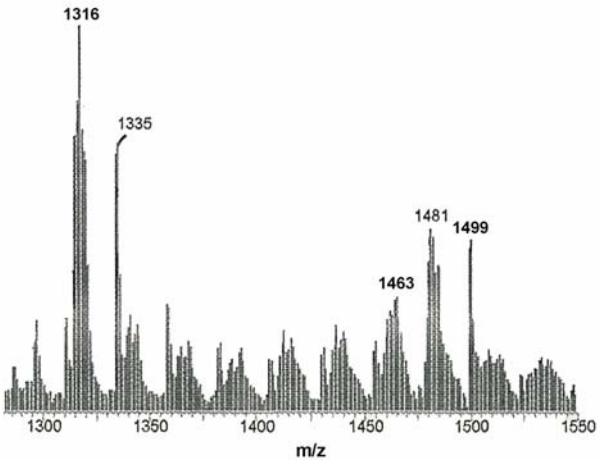

Figure 5.6. Negative DCI mass spectrum showing $Lu_3N@C_{80}$ (*m/z* = 1499), $GdLu_2N@C_{80}$ (*m/z* = 1481) and $Gd_2LuN@C_{80}$ (*m/z* = 1463). $Lu_2@C_{82}$ (*m/z* = 1335) and $LuGd@C_{82}$ (*m/z* = 1316) are also present.

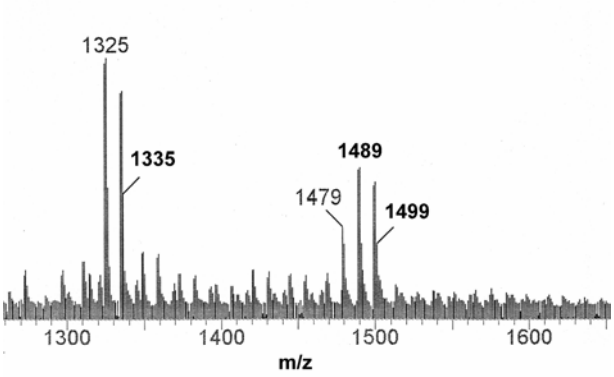

Figure 5.7. Negative DCI mass spectrum showing $Lu_3N@C_{80}$ (*m/z* = 1499), $HoLu_2N@C_{80}$ (*m/z* = 1489) and $Ho_2LuN@C_{80}$ (*m/z* = 1479). $Lu_2@C_{82}$ (*m/z* = 1335) and $LuHo@C_{82}$ (*m/z* = 1325) are also present.

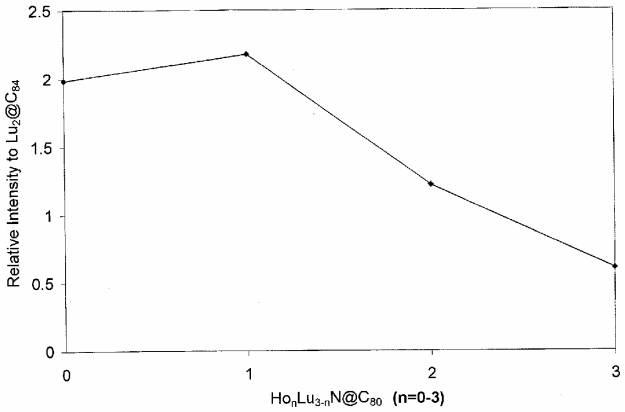

Figure 5.8. Yields for $Ho_nLu_{3-n}@C_{80}$ soluble extracts (carbon disulfide) relative to $Lu_2@C_{84}$ based on negative DCI mass spectroscopy.

A unique quality that $Lu_3N@C_{80}$ possesses over $Sc_3N@C_{80}$ is the ability to provide X-ray contrast. This is attributed to the large atom number (*Z*) of the lutetium atoms.[8] In Figure 5.9, $Lu_3N@C_{80}$ demonstrates X-ray contrast (Figure 5.9a) when distributed onto a non-absorbing Teflon block and irradiated with X-rays. As one can see (where the arrows point), the Teflon blocks that lack the lutetium species (Figure 5.9b,c) do not

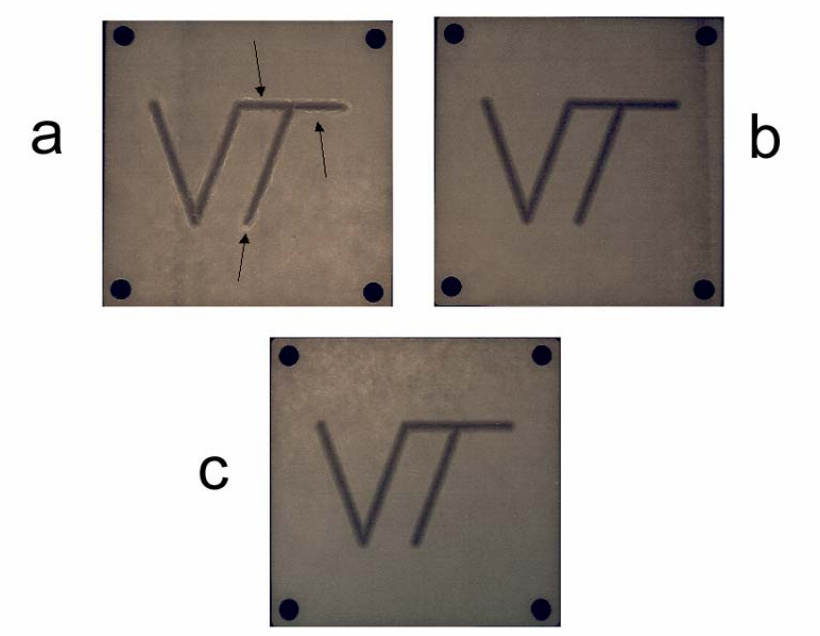

Figure 5.9. X-ray photograph of: (a) contrast (arrows point to bright areas) provided by $Lu_3N@C_{80}$ on a Teflon block, (b) C_{60} fullerene on a Teflon block and (c) a blank Teflon block. The samples were exposed for 3.5 minutes at 30 kV.

exhibit contrast. Furthermore, the C_{60} containing block (Figure 5.9b) provides evidence that contrast cannot be attributed to the carbon cage of the metallofullerene.

Endohedral metallofullerenes that contain gadolinium and/or holmium have been mentioned as potential replacements for commercial MRI contrast agents, although a mixed metal species may prove useful as a multi-modality contrast agent (e.g., X-ray and MRI). In addition, utilization of a contrast agent that provides enhancements for a variety of spectroscopic methods would simultaneously provide directly comparable images with minimal exposure to the patient.

5.2.2. A D_{5h} isomer of the $Sc_3N@C_{80}$ metallofullerene

Figure 5.10 (top) is a chromatographic trace, from the purification of $Sc_3N@C_{80}$, which shows a peak with a trailing shoulder. This peak was collected in two cuts. Both cuts contained $Sc_3N@C_{80}$ (^{13}C-enriched) as characterized by mass spectroscopy (Figure 5.10 bottom). NMR spectra of each fraction allowed the first fraction to be assigned to the I_h symmetry isomer, while the second fraction contained a mixture of both I_h and D_{5h} isomers.

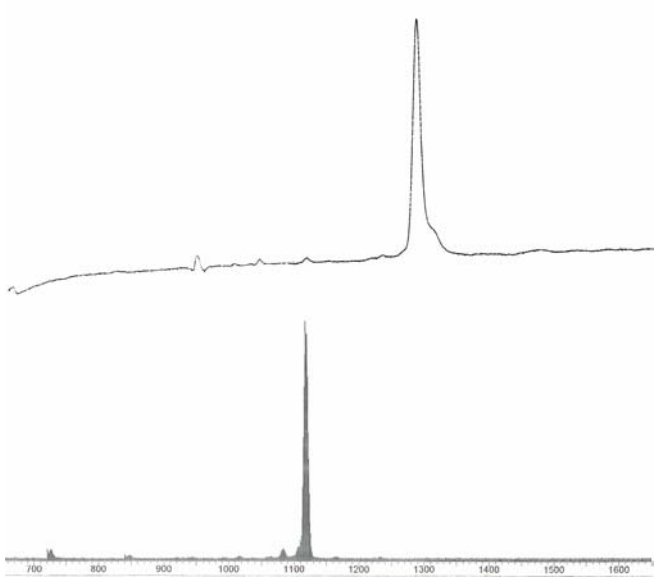

Figure 5.10. HPLC chromatogram and mass spectrum of $Sc_3N@C_{80}$ (both isomers, *ca.* 9% ^{13}C- labeled). Top: HPLC peak with shoulder (toluene, 1 ml/min, 28.3 min. retention time) on a Trident Tri-DNP (Buckyclutcher) column. Bottom: Neg-DCI mass spectrum with highest peak at m/z = 1117.

The NMR spectrum for the second fraction (Figure 5.16) shows the two signals of I_h $Sc_3N@C_{80}$,[9] but also shows six additional signals that are representative of the D_{5h} isomer. Previous work by Fowler and Manolopoulos[34] show the various NMR patterns that are expected for different structural isolated pentagon rule (IPR) isomers of C_{80}. In addition, it is worth noting that an NMR spectrum for an individual isomer may contain at most *three* different heights.[34] The reported intensity ratios for the D_{5h} isomer (2×20, 4×10) match the six line pattern and allow unambiguous assignment as the D_{5h} isomer (number of NMR lines × relative intensity).

The six lines and their intensities confirm the presence of the D_{5h} isomer. The ^{13}C NMR spectrum (Figure 5.16) also demonstrates that the Sc_3N cluster is moving isotropically inside the C_{80} cage on the NMR timescale. This was also discovered to be the case for the I_h isomer,[9] although it should be noted that several dimetallic C_{80} cage endohedrals do not possess dynamic internal metals.[7]

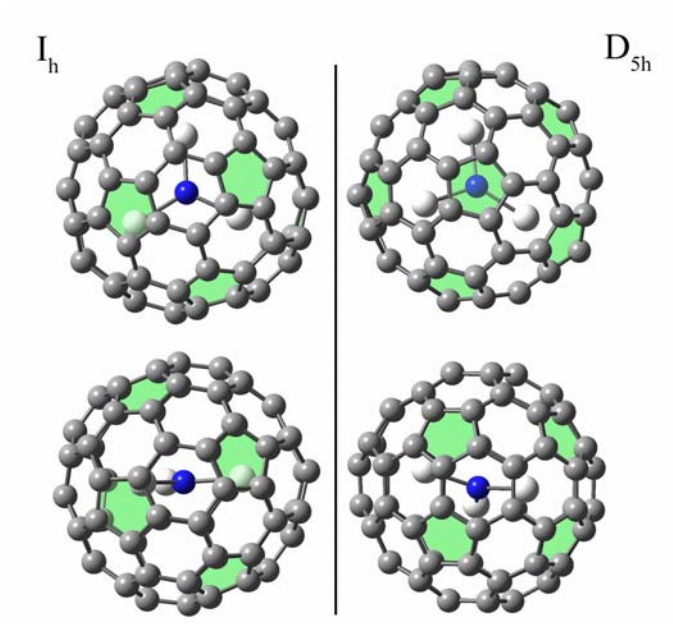

Figure 5.11. $Sc_3N@C_{80}$ structures (Gauss View) of the I_h isomer (left) and the D_{5h} isomer (right). The top and bottom views are rotated 90˚ from each other. All five-membered rings are colored green.

[34] Fowler, P. W.; Manolopoulos, D. E. In *An Atlas of Fullerene;* Rowlinson, J. S., Ed.; International Series of Monographs on Chemistry – 30; Oxford University Press Inc.: New York, NY, 1995; pp 254–255.

The structures of the two isomers are very similar (Figure 5.11). If one slices the D_{5h} isomer at the horizontal mirror plane, rotates the top half by 36˚, and reattaches the top to the bottom, then the I_h isomer of $Sc_3N@C_{80}$ is obtained. The similar structures of the two isomers are responsible for the nearly identical HPLC retention times.

Derivatization studies have not been carried out with the D_{5h} isomer due to the inability to fully separate it from the I_h isomer. Yet, the reactivity of the D_{5h} may be different from the more abundant I_h isomer, because the D_{5h} cage contains pyracylene-type units (five of these units are present on D_{5h} $Sc_3N@C_{80}$). As discussed in Chapter 1, these pyracylene-type units (two hexagons abutted by two pentagons) (Figure 1.12) are the reactive sites on the C_{60} fullerene, where functionalization occurs across the [6,6] ring-juncture of the units. Therefore, the presence of an addition isomer in the $Sc_3N@C_{80}$ starting material may explain why additional products are collected during HPLC purification of several reactions (Chapter 3, sections 3.2.3 and 3.2.4).

5.2.3. ^{15}N-labeling of internal cluster in the $Sc_3N@C_{80}$ metallofullerene

The ^{15}N-labeled metallofullerene, $Sc_3{}^{15}N@C_{80}$, was purified with HPLC using a Trident Tri-DNP column (a.k.a. Buckyclutcher) with toluene as the eluent at a low flow rate of 0.5-1 ml/min. The yield of this metallofullerene was abnormally high (due to the static process), and therefore a low flow rate and a single column was sufficient for purifying the novel trimetallic nitride endohedral metallofullerene. Normally, the two phase column system is employed because the yields of $Sc_3N@C_{80}$ are small compared to C_{60} and C_{70}, and separation with a single column at a low flow rate would require an extremely long period of time. Figure 5.12 shows the HPLC chromatogram during purification of $Sc_3{}^{15}N@C_{80}$. Found in all soluble fullerene extract, the C_{60} and C_{70} fullerenes eluted from the column at 30.48 and 34.11 minutes, respectively, while several other empty-cage and endohedral species eluted between the times of 36 and 55 minutes. The material of interest, $Sc_3{}^{15}N@C_{80}$, eluted last from the column at 56.38 minutes.

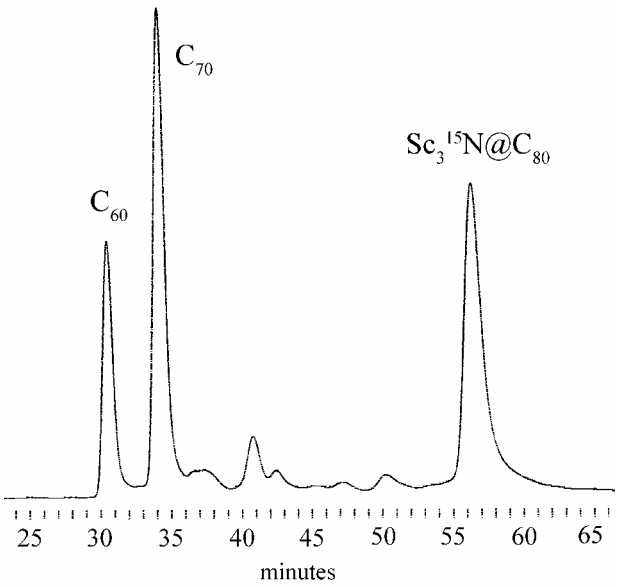

Figure 5.12. HPLC chromatographic purification of $Sc_3{}^{15}N@C_{80}$ (38% conc.) at 0.5 ml/min. flow rate in toluene.

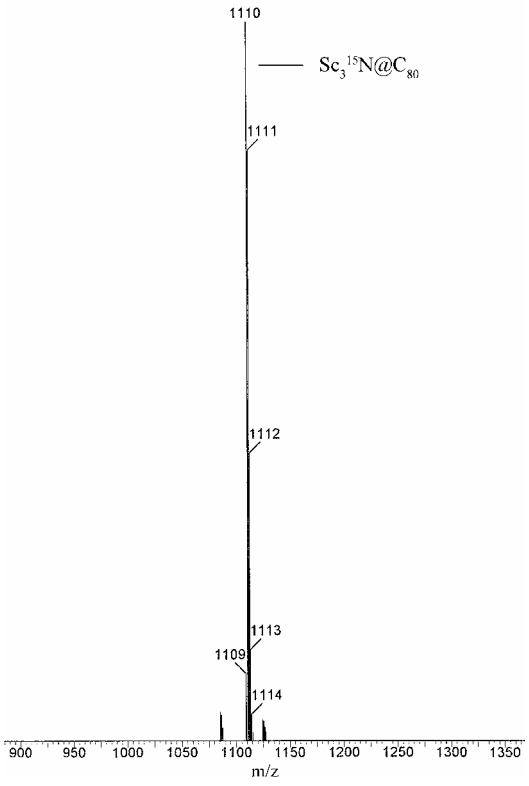

Figure 5.13. Neg-DCI mass spectrum of pure $Sc_3{}^{15}N@C_{80}$.

A Neg-DCI mass spectrum of pure $Sc_3{}^{15}N@C_{80}$ is shown in Figure 5.13. The isotope pattern provides unambiguous evidence that a ^{15}N-label is present within molecule, because the isotope pattern matches a molecule with 80 carbon atoms. A high resolution fast atom bombardment (HR-FAB) spectrum was also confirmed the mass (*m/z* 1110.8739) of the labeled metallofullerene.

Figure 5.17 shows the ^{13}C NMR spectrum of $Sc_3{}^{15}N@C_{80}$. The 20 pyrene-type carbon atoms of the I_h symmetry cage are located at 137.0 ppm, while the 60 corannulene-type carbon atoms are found at 144.23 ppm. These ^{13}C NMR signals for $Sc_3{}^{15}N@C_{80}$ are identical to those of $Sc_3N@C_{80}$ (137.24 and 144.57 ppm at 150 MHz).[9] The appearance of only two lines represents an average on the NMR timescale, which is due to the isotropic environment of the internally rotating metal-nitride cluster. Spin-coupling between the ^{13}C atoms (*S = 1/2*) of the cage and the ^{15}N atom (*S = 1/2*) of the internal cluster did not appear to occur, since the linewidths of the carbon signals were not broadened with respect to the signals from the non-labeled $Sc_3N@C_{80}$ molecule. A ^{15}N atom (dipolar nucleus, *S = 1/2*), which has a smaller linewidth and slightly greater sensitivity than a ^{14}N atom (quadrupolar nucleus, *S = 1*), should yield significant details as to the motion(s) of the cluster within the cage if a temperature study is performed.

The Neg-DCI mass spectrum of non-purified $Sc_3{}^{15}N@C_{80}$ (Figure 5.14a) indicates that a marked improvement in the yield of the latter trimetallic nitride endohedral metallofullerene (relative to C_{60}, C_{70} and C_{84}) has occurred as a result of the modified generation procedure. For instance, metal-oxide packed graphite rods are normally vaporized inside the Krätschmer-Huffmann generator (see Appendix III) under a dynamic flow of helium and nitrogen gas. However, due to the high cost ($1000/L) of the ^{15}N-labeled nitrogen gas ($^{15}N_2$), the rods were vaporized under a static environment of the two gasses. Figure 5.14 depicts the Neg-DCI mass spectra of fullerene extracts that were synthesized under a dynamic or static gas (helium and nitrogen) environment. When rods were vaporized under the static environment (Figure 5.14a,b), the yields of the trimetallic nitride endohedral metallofullerenes (*m/z* 1110 and 1109) were *significantly enhanced* with respect to C_{84} (*m/z* 1008) and other empty-cages. Yet, with the normal method (dynamic) of gas flow (Figure 5.14c), the labeled trimetallic nitride endohedral

metallofullerene, $Sc_3{}^{15}N@C_{80}$ (*m/z* 1110), is relegated to a yield that is comparable to C_{84}. The increased yields could be due to either the larger amount of nitrogen that is present inside the generator during the static burns (*ca.* 150 Torr with static versus *ca.* 30 Torr with dynamic), or the ratio of nitrogen to helium gas (*ca.* 1:1 with static versus *ca.* 1:12 with dynamic) within the generator. Furthermore, it should be noted that the higher

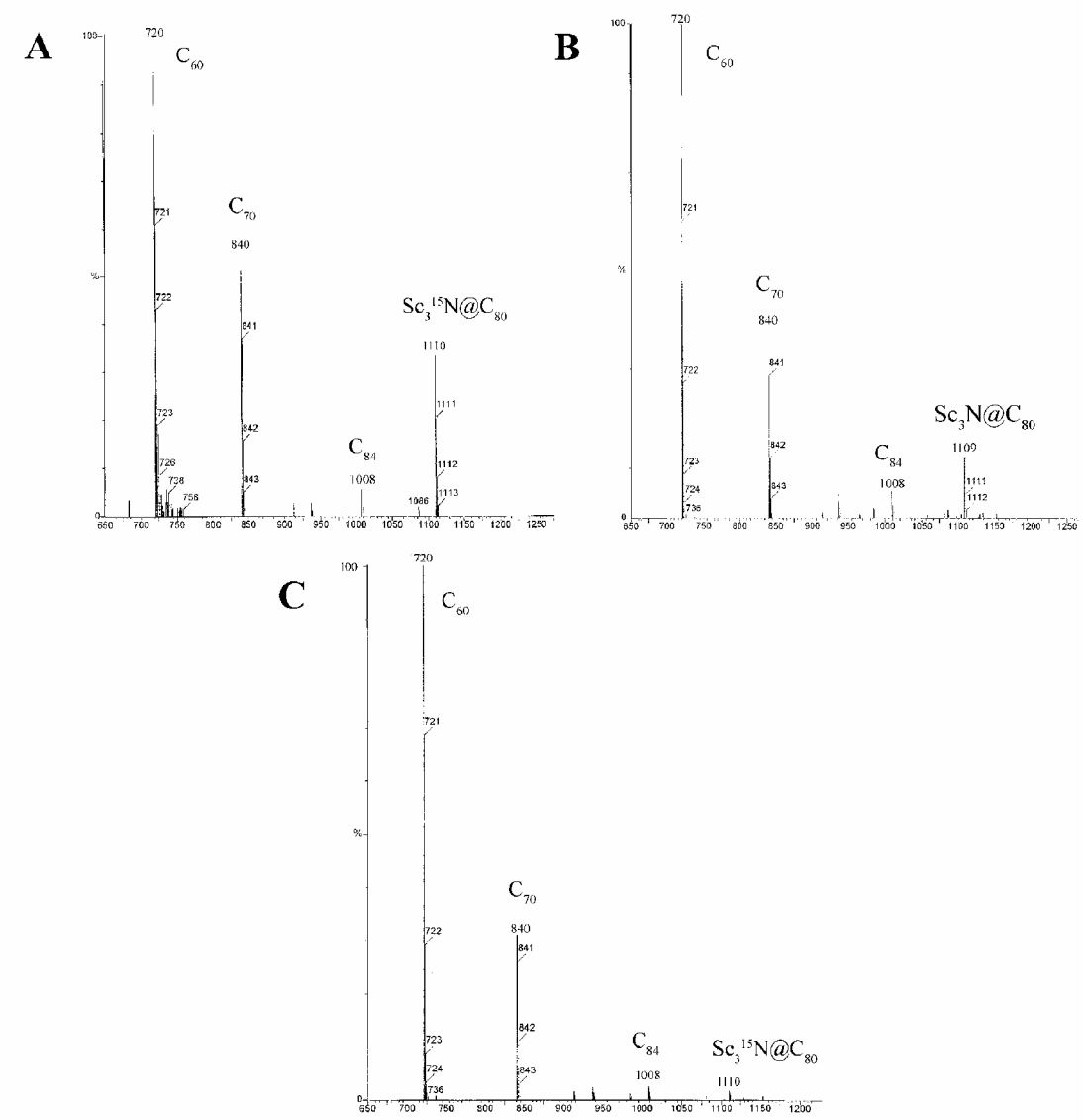

Figure 5.14. Neg-DCI mass spectra of fullerene extract from vaporization under (a) a static environment of $^{15}N_2$ and He gas, (b) a static environment of $^{14}N_2$ and He gas, and (c) a dynamic environment of $^{15}N_2$ and He gas.

overall pressure inside the generator during the static burns (*ca.* 450 Torr, Figure 5.14a & b), as compared to during the dynamic burns (*ca.* 300 Torr, Figure 5.14c), may also be responsible for the increased yields.

Previous work by Dorn and co-workers[35] found only a *small increase* in the yields of the trimetallic nitride endohedral metallofullerenes (i.e., $Sc_3N@C_{80}$) when a larger amount of nitrogen gas, and less helium gas, was used for the dynamic process. In addition, they discovered that higher gas pressures during the dynamic burns caused only a *slightly increase* in the yields of the trimetallic nitride endohedral metallofullerenes.

Metal-oxide/graphite rods are normally packed with iron nitride (FeN_x), which is purported to act as a catalyst for the formation of the trimetallic nitride endohedral metallofullerenes.[35] However, we show, for the first time, that the FeN_x does not appear to be involved in the formation process. This is because the mass spectrum of purified $Sc_3{}^{15}N@C_{80}$ (Figure 5.13) shows a large mass at 1110 for inclusion of a ^{15}N atom (from the $^{15}N_2$ gas), but only a very small mass at 1109 for the same metallofullerene when it contains a ^{14}N atom. This small mass at 1109 can be formed from small amounts of atmospheric nitrogen that seep into the generator during vaporization of the packed rods.

[35] Dorn, H. C.; Duchamp, J. C.; Stevenson, S. Unpublished data.

5.3. Experimental

5.3.1. Materials and purification

Solvents for extraction and chromatography were HPLC grade unless otherwise specified. HPLC separations of were performed with an Acuflow Series III pump and Applied Biosystems 757 Absorbance Detector (λ = 390 nm). Data was recorded on a Hitachi D-2500 Chromato-Integrator. $Lu_3N@C_{80}$ was purified from soluble fullerene extract by employing a two-stage HPLC process. The first stage required a 5-PBB (pentabromobenzyloxy) column (5 μm, 250 mm x 20 mm ID: Phenomenex) with carbon disulfide (CS_2) as eluent. The flow rate was 2 ml/min. The second stage required a Trident-Tri-DNP (Buckyclutcher) column (5 μm, 250 mm x 10 mm ID: Regis Chemical) with toluene as eluent. The flow rate was 2 ml/min., unless stated otherwise. The ^{13}C-labeled D_{5h} isomer $Sc_3N@C_{80}$ was purified by using the same tandem HPLC separation as previously noted, in addition to a Buckyprep column (250 mm x 10 mm ID: Phenomenex). The flow rate for purification of the latter ranged from *ca.* 0.5-2 ml/min.

Suppliers of reagents were as follows: Lu_2O_3 – Alfa Aesar; Sc_2O_3, ^{12}C amorphous carbon – Stanford Materials Corporation; Fe_xN – Cerac; ^{13}C amorphous carbon (99%, ^{13}C) – Cambridge Isotope Laboratory; graphite rods (6.15 mm dia. x 152 mm long) – Alfa Aesar; ^{15}N-labeled nitrogen gas ($^{15}N_2$, 99%) – Icon Isotopes.

1,2-Dichlorobenzene-d_4 was used as received from Cambridge Isotope Laboratory.

5.3.2. Analytical methods

^{13}C NMR spectra were obtained with either a JEOL Eclipse+ 500 or Varian Unity 400 spectrometer using a 5 mm or 10 mm NMR sample tubes. Sample were solubilized in either CS_2 (with acetone-d_6 to lock) or 1,2-dichlorobenzene-d_4. When noted, samples were doped with chromium acetylacetonate ($Cr(acac)_3$). Tetramethylsilane (TMS) was used as the external standard.

Mass spectra of fullerenes were obtained with either a Fisons VG Quattro mass spectrometer using a desorption chemical-ionization probe (DCI) and negative ionization,

or a JEOL HX-110 Dual Focusing mass spectrometer using high resolution fast atom bombardment (HR-FAB).

UV-Visible spectra were measured using quartz cuvettes and a Spectronic GenSys 5 Spectrometer (Emory and Henry College).

X-ray photographs of samples on Teflon blocks (0.25 in x 0.25 in x 1 in) were obtained with a Hewlett-Packard Faxitron Series X-ray System (Veterinary School, Virginia Tech).

5.3.3. Synthesis of $Lu_3N@C_{80}$

1.50 g amorphous carbon, 2.11 g Lu_2O_3 (2 mol% metal) and 0.60 g Fe_xN (catalyst) were ground with a mortar and pestle, then packed into a cored graphite rod. The rod was placed in a Krätschmer-Huffman generator and vaporized under a dynamic nitrogen/helium atmosphere (1:12) at 300 Torr (see Appendix III, How to operate Krätschmer-Huffman generator at Virginia Tech). The rod was completely vaporized in *ca.* 45 minutes. Next, the black soot was swept from inside the generator and extracted with carbon disulfide (CS_2) to remove all soluble fullerene and metallofullerene material. $Lu_3N@C_{80}$ was purified using a 5-PBB (pentabromobenzyl) column with CS_2 as the eluent, followed by further purification on a Trident Tri-DNP (Buckyclutcher) column with toluene as the eluent. Flow rate for both columns was 2 ml/min. Yields of $Lu_3N@C_{80}$ (*ca.* 1-2 mg from 5 packed rods) were generally lower than $Sc_3N@C_{80}$.[9] ^{13}C NMR (125 MHz, CS_2, $Cr(acac)_3$, 19,456 scans): δ 137.45 (pyrene-type carbons) and 144.01 (corannulene-type carbons). Neg-DCI MS: Calcd. mass is 1499.708, and found mass at 1499 ($Lu_3N@C_{80}$). UV-Vis (CS_2): peak at 668 nm.

Figure 5.15. 125 MHz ^{13}C NMR spectrum of $Lu_3N@C_{80}$.

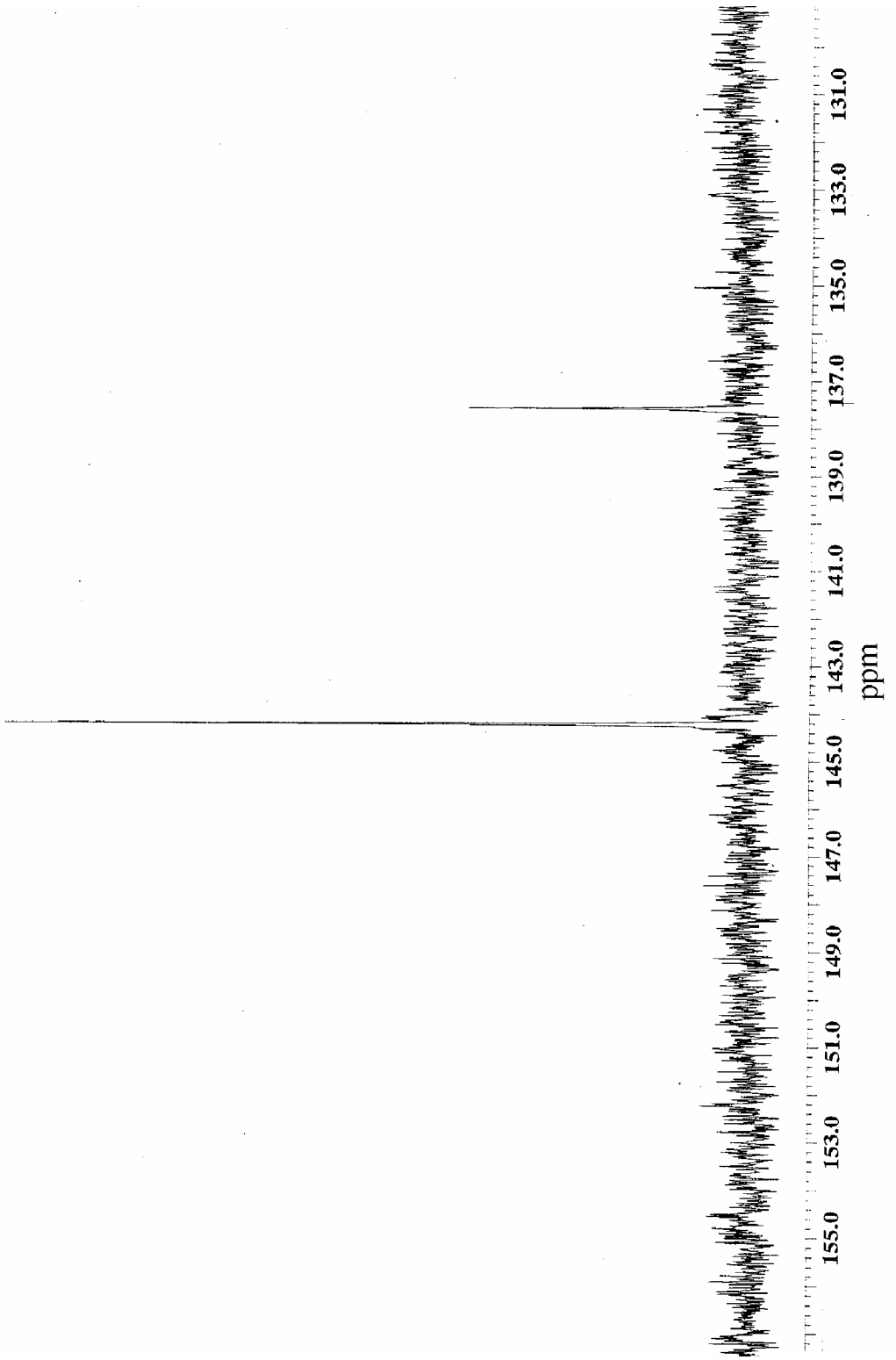

5.3.4. Synthesis of D_{5h} $Sc_3N@C_{80}$

1.00 g ^{13}C amorphous carbon, 0.73 g Sc_2O_3 (3 mol% metal) and 0.40 g Fe_xN (catalyst) were ground with a mortar and pestle, then packed into a cored graphite rod. The rod was placed in the Krätschmer-Huffman generator[30] and vaporized under a dynamic nitrogen/helium atmosphere (1:25) at 300 Torr (see Appendix III, How to operate Krätschmer-Huffman generator at Virginia Tech). The rod was completely vaporized in *ca.* 30 minutes. Next, the black soot was swept from inside the generator and extracted with carbon disulfide (CS_2) to remove all soluble fullerene and metallofullerene material. The D_{5h} isomer of $Sc_3N@C_{80}$ was *partially* purified using a 5-PBB (pentabromobenzyl) column with CS_2 as the eluent, followed by further purification with a Buckyprep column then a Trident Tri-DNP (Buckyclutcher) column using toluene as the eluent. Fractions were collected using a home-built fraction collector constructed primarily from LEGO™ blocks. Flow rate ranged from 0.5-2 ml/min. ^{13}C NMR (100 MHz, CS_2, $Cr(acac)_3$, 1 s delay, 25,000 scans): δ 135.2 (pyrene-type carbon), 138.5 (pyrene-type carbon), 139.3 (corannulene-type carbon), 143.9 (pyracylene-type carbon), 145.0 (corannulene-type carbon) and 149.8 (corannulene-type carbon). Neg-DCI MS: range of masses found between 1109 and 1125, due to ^{13}C-label, with highest mass at 1117 (10% labeled cage).

Figure 5.16. 100 MHz ^{13}C NMR spectrum of D_{5h} (◆) and I_h (*) isomers of $Sc_3N@C_{80}$.

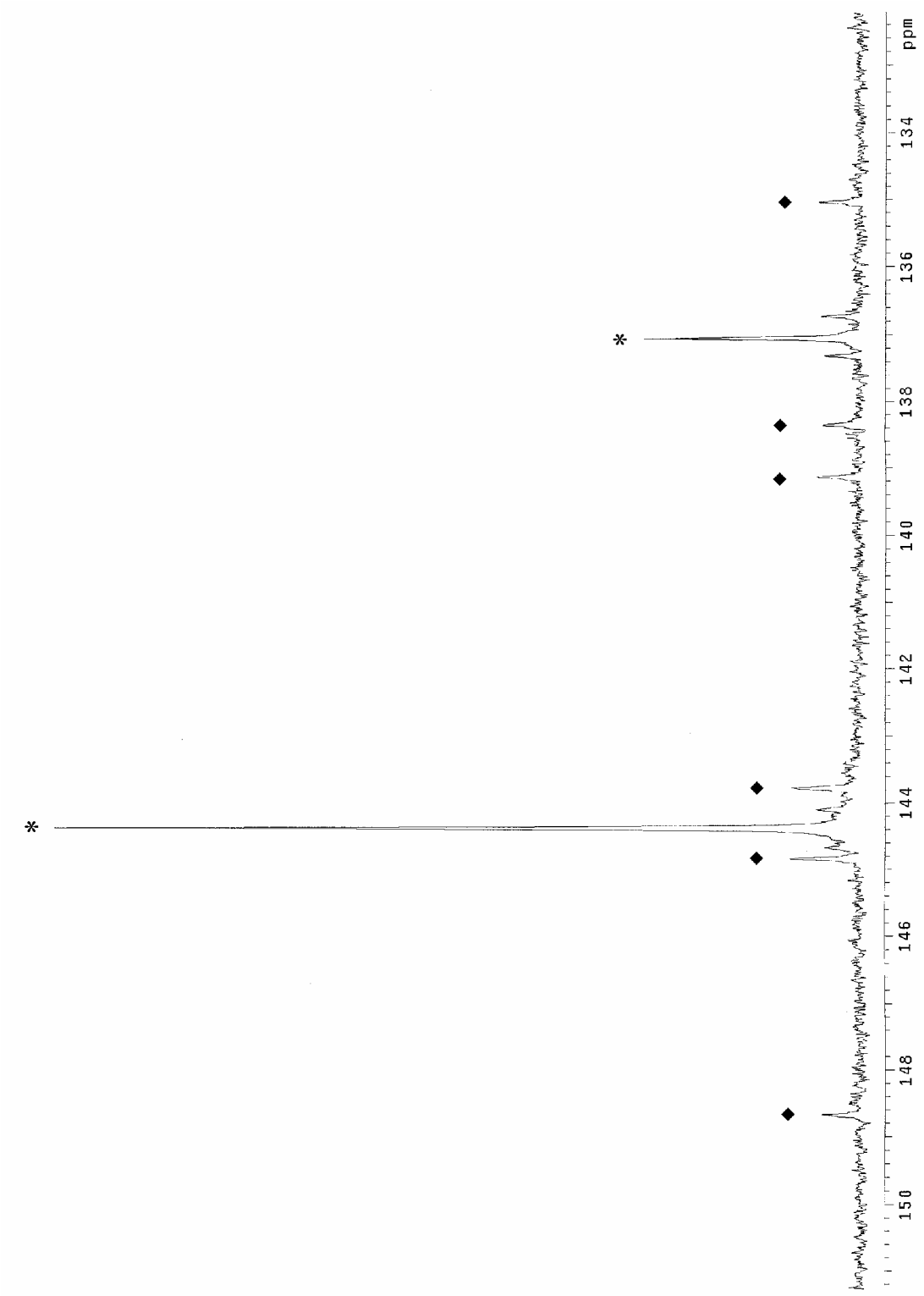

5.3.5. Synthesis of $Sc_3{}^{15}N@C_{80}$

2.07 g ^{12}C amorphous carbon, 1.45 g Sc_2O_3 (3 mol% metal) and 0.81 g Fe_xN (catalyst) were ground with a mortar and pestle, then packed into a cored graphite rod. The rod was placed in a Krätschmer-Huffman generator,[30] and filled to 150 Torr with ^{15}N-labeled nitrogen gas ($^{15}N_2$, 99%). The chamber was then backfilled to 280 Torr with helium. When vaporization of the rod began, the pressure ranged between 430 and 560 Torr. The rod was completely vaporized within 50 minutes. A total of three were vaporized. $Sc_3{}^{15}N@C_{80}$ was purified using the Buckyclutcher column with toluene as the eluent (0.5-1.0 ml/min. flow rate). Product yield was 1-2 mgs. ^{13}C NMR (100 MHz, $C_6Cl_2D_4$, $Cr(acac)_3$, 2 s delay, 12,532 scans): δ 137.0 (pyrene-type carbons) and 144.23 (corannulene-type carbons). Neg-DCI MS: Found mass at 1110 ($Sc_3{}^{15}N@C_{80}$). HR-FAB MS (positive ionization): Calcd. mass is 1110.8757, and found mass at 1110.8739 ($Sc_3{}^{15}N@C_{80}$).

Figure 5.17. 100 MHz ^{13}C NMR spectrum of $Sc_3{}^{15}N@C_{80}$.

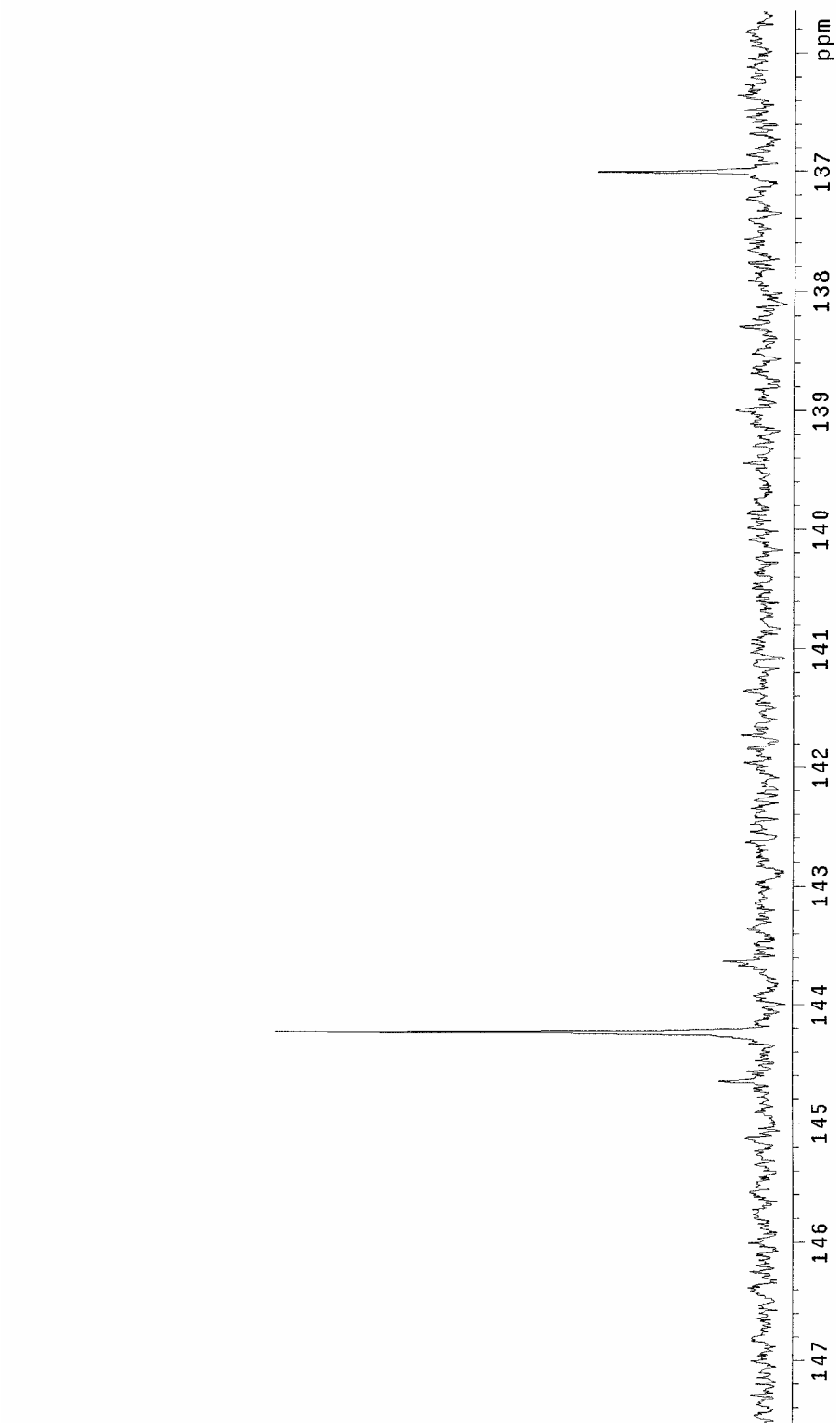

CHAPTER 6 – Summary, Conclusions and Future Work

6.1. Summary and conclusions

The first organic derivative of a trimetallic nitride endohedral metallofullerene (Chapter 3) has been successfully synthesized and characterized. HPLC data indicates that 4,5-dimethoxy-*o*-quinodimethane–$Sc_3N@C_{80}$ is the major product, and ^{13}C NMR spectroscopy (time-averaged) shows that the novel mono-adduct possesses a plane of symmetry that runs through the center of the addend and cage. 2D NMR studies were utilized to understand the complex proton couplings and broadened signals that occur within the adduct due to addend motion. The X-ray crystal structure verified that a [4 + 2] cycloaddition occurred across a [5,6] ring-juncture of the cage, and that the C1–C2 bond is elongated and pulled out from the metallofullerene cage. The Sc_3N cluster is positioned away from the site of addition, and causes the carbon atoms immediately neighboring the scandium atoms to protrude slightly from the surface of the metallofullerene cage. In addition, the adducts in the X-ray crystal structure are packed in a head-to-tail fashion, likely due to pi-stacking, while two scandium atoms of the internal cluster are directed towards the polar methoxy groups of the adduct. The directed cluster may create a dipole moment through the adduct, thus explaining why the adduct possesses a longer HPLC retention time (with the Buckyclutcher column) than the non-functionalized (parent) metallofullerene.

The most abundant trimetallic nitride endohedral metallofullerene, $Sc_3N@C_{80}$, has been functionalized with two different malonate reagents (Chapter 3). One of these reagents, diethyl malonate, contained a ^{13}C-labeled at the 2-position of the molecule, and was discovered to engender a mono-adduct that could be monitored via ^{13}C NMR spectroscopy. However, a crystal structure has not been achieved with this adduct, which may result from the lack of aryl functionality to provide pi-stacking. Therefore, a dibenzyl malonate reagent was reacted with the $Sc_3N@C_{80}$ metallofullerene in hopes of achieving a crystal structure. This reagent was not ^{13}C-labeled, although a larger amount of product was synthesized so that ^{1}H NMR data could be achieved. Three structural

isomers of the latter adduct were separated via HPLC, yet only one is purported to result from functionalization of the I_h C_{80} cage isomer of the metallofullerene. The other two products may have resulted from the presence of the recently discovered D_{5h} C_{80} cage isomer. Unfortunately, X-ray crystal structures of the three adducts have not yet been obtained.

A ^{15}N-labeled terminal derivative of $Sc_3N@C_{80}$ (Chapter 3) was synthesized for coupling with peptides and/or water-soluble dendrimers. In the case of large peptides, the ^{15}N atom could be monitored with ^{15}N NMR spectroscopy to determine whether the peptide has either reacted with the terminal amine group or solely wrapped around the adduct to provide metallofullerene water-solubility. Three structurally isomeric products were also observed during HPLC purification of the amine adduct, although only one of the three is believed to have resulted from the I_h C_{80} cage isomer of $Sc_3N@C_{80}$. Due to the small quantities of product and their low solubility in NMR solvents, a ^{15}N NMR spectrum of the $Sc_3N@C_{80}$ adduct could not be achieved. Yet, when the metallofullerene portion of the adduct was replaced with C_{60}, the adduct yielded greater solubility in several NMR solvents, and a signal for the ^{15}N-labeled atom was finally observed.

The first water-soluble metallofullerenols of a trimetallic nitride endohedral metallofullerene, $Sc_3N@C_{80}(OH)_{\sim10}(O)_{\sim10}$, were achieved via a reduction and subsequent oxidation procedure (Chapter 3). The adducts were characterized using FT-IR, XPS, and LD-TOF MS. These novel adducts demonstrate characteristics similar to other metallofullerols; however, the trimetallic nitride endohedral metallofullerenes are produced in much larger quantities than the traditional metallofullerenes, thus making them a more viable source for studies of biological applications.

^{13}C-labeled adducts of the $Sc_3N@C_{78}$ metallofullerene (Chapter 4) were synthesized in effort to discover both the placement and number of reactive sites upon the cage. The ^{1}H and ^{13}C NMR spectral data of the mono-adduct lends credence to an addend that is asymmetric with respect to the cage. However, several factors must be taken into consideration when observing the NMR data, such as: 1) does the internal Sc_3N cluster remain dynamic or become localized when the cage is derivatized and 2) is the published X-ray crystal structure of $Sc_3N@C_{78}$ the correct cage isomer, especially when the

experimental ^{13}C NMR data lends argument for a different isomer? The crystal structure of the mono-adduct has not yet been obtained.

The remarkable similarities between $Sc_3N@C_{80}$ and $Lu_3N@C_{80}$ (Chapter 5) with respect to HPLC retention times, UV-Visible and ^{13}C NMR data suggests a relatively *minor* influence of the internal trimetallic nitride cluster on "exohedral" cage properties of these two endohedral metallofullerenes. Yet, this minor difference is most pronounced by HPLC at extremely low flow rates. $Sc_3N@C_{80}$ has a slightly longer retention time than $Lu_3N@C_{80}$ when using the Trident-Tri DNP (Buckyclutcher) column, thus demonstrating that the former metallofullerene possess a greater dipole moment within the cage. On the other hand, the reverse is true ($Lu_3N@C_{80}$ has a slightly longer retention time) if the 5-PBB (pentabromobenzyl) column is used, demonstrating that more electrons are transferred to the C_{80} carbon cage from the three lutetium atoms than from the three scandium atoms. In addition, we have shown that $Lu_3N@C_{80}$ (Chapter 5) provides a small level of contrast when irradiated with X-ray radiation. The contrast results from the large X-ray absorbing nuclei of the encapsulated lutetium atoms.

A newly discovered isomer of $Sc_3N@C_{80}$, the D_{5h} isomer, has been partially isolated and characterized (Chapter 5). The ^{13}C NMR spectrum of the isomer shows six signals (2 at full intensity and 4 at 1/2 intensity) that match a calculated NMR patter of 2 x 20 and 4 x 10 for a total of 80 carbon atoms. Furthermore, the NMR spectrum demonstrates that the internal cluster is moving isotropically inside the cage on the NMR timescale. The HPLC retention time of the new isomer is nearly identical to the I_h $Sc_3N@C_{80}$ isomer, and complete separation could not be achieved at even extremely low flow rates. Cage reactivity of the D_{5h} isomer may be entirely different from the I_h isomer, since the D_{5h} isomer contains the pyracylene-type units that are routinely used to functionalize C_{60} and empty-cage fullerenes. The presence of this isomer during organic functionalization of $Sc_3N@C_{80}$ is likely the reason why three reactive products, as opposed to one, were found during HPLC purification of several crude product mixtures.

Finally, the internal cluster of $Sc_3N@C_{80}$ was labeled with a ^{15}N atom (Chapter 5) for studying the motion of the cluster and possible pyramidalization within the cage. Amazingly, rod vaporization under a static atmosphere of gasses (helium and nitrogen)

showed a marked increase in the yields of $Sc_3N@C_{80}$, as opposed to when using the traditional dynamic flow of gasses. At the current time, it is unclear as to the reason for the observed increase in yields when vaporizing packed rods with the static method.

6.2. Future work

The ^{15}N-labeled terminal amine derivative $Sc_3N@C_{80}$ shows promise for being coupled to water-soluble and/or biologically active peptides, such as a human epidermal growth factor (EGF) (Figure 6.1), and utilized for specific medicinal applications (i.e., MRI or X-ray contrasting agents). As stated previously, the ^{15}N atom would provide evidence that the peptide is actually coupled to the amine of the metallofullerene adduct and not just wrapped around the molecule. Furthermore, as discussed at the end of Chapter 3, the metallofullerene cage of the derivative could be polyhydroxyated to provide additional water-solubility.

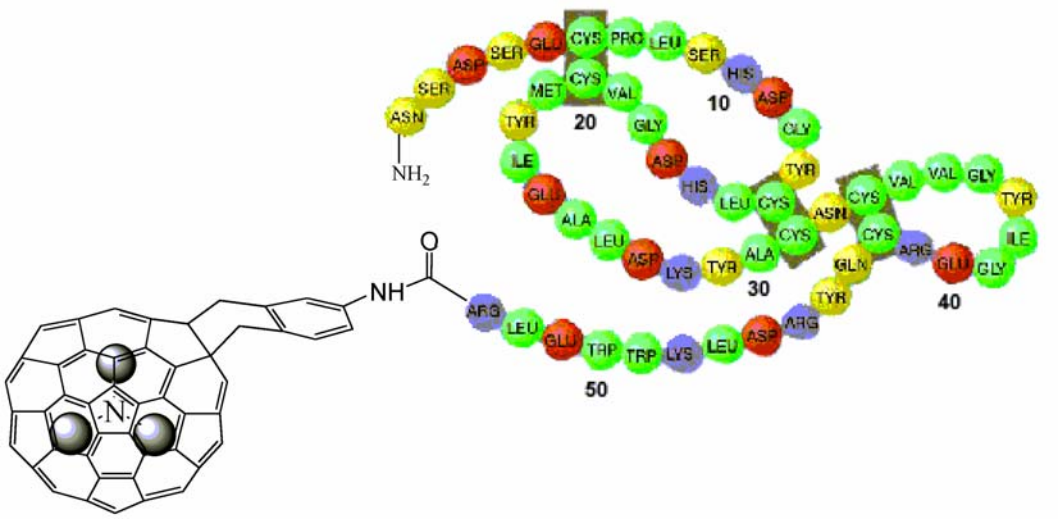

Figure 6.1. Conceptual drawing of a metallofullerene derivative that is coupled to a human epidermal growth factor (EGF) peptide. The EGF peptide binds to the epidermal growth factor receptor (EGFR) that is overexpressed in certain types of cancer cells (i.e., breast cancer).

The exact cage isomer (D_{3h} (78:4) or $D_{3h'}$ (78:5)) of the $Sc_3N@C_{78}$ metallofullerene must be determined before additional functionalization studies can be undertaken. Isomer determination can be accomplished by synthesizing a ^{13}C-labeled (*ca.* 10%) sample of $Sc_3N@C_{78}$ and acquiring a 2D INADEQUATE (Incredible Natural Abundance Double Quantum Transfer Experiment) spectrum to determine the $^{13}C–^{13}C$ connectivity.

The $Sc_3N@C_{80}$ metallofullerene was labeled with a ^{15}N-labeled atom (dipolar nuclei, $S = 1/2$) because it provides a greater NMR sensitivity and smaller signal linewidth than that of a ^{14}N atom (quadrupolar nucleus, $S = 1$). As a result, the linewidth of the signal for the internal cluster of $Sc_3{}^{15}N@C_{80}$ should change if the temperature is varied. This in turn would provide invaluable information as to the motion(s) of the cluster within the carbon cage, which thereby would lead to experimentally calculating the cluster's rotational activation barrier. Variations in peak linewidth, via an NMR temperature study of the normal ^{14}N atom cluster in $Sc_3N@C_{80}$, would not lead to an effective interpretation of cluster motion due to the multiple pathways of relaxation that can occur in a quadrupolar nucleus.

Appendix I. Schlegel diagram of $Sc_3N@C_{80}$ carbon cage

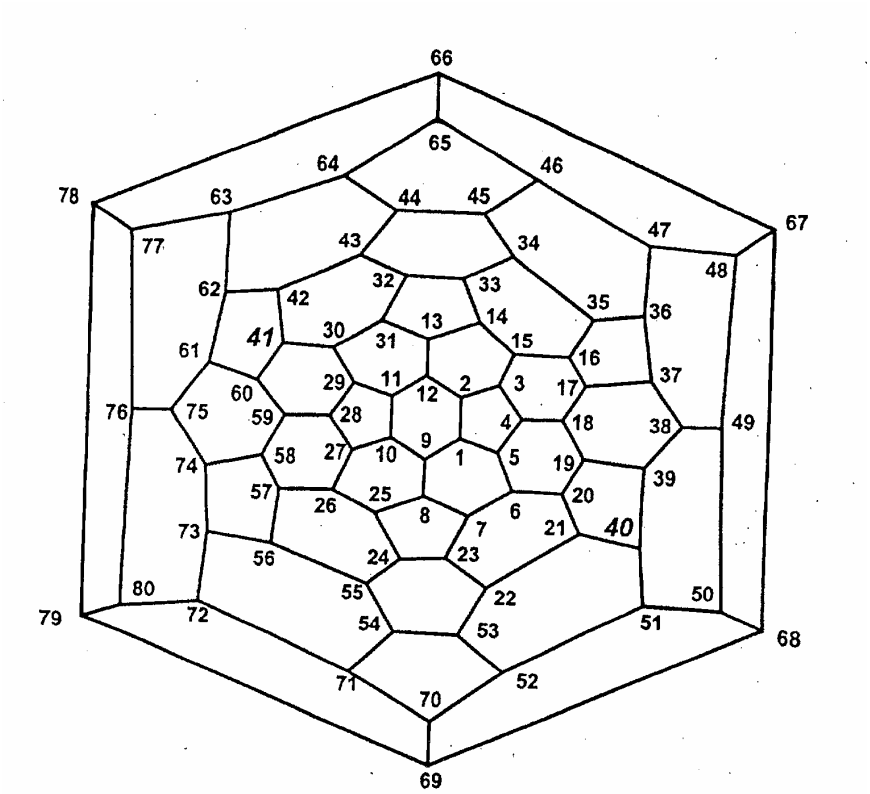

Numbering scheme for I_h isomer

Appendix II. Schlegel diagrams of $Sc_3N@C_{78}$ carbon cage

A

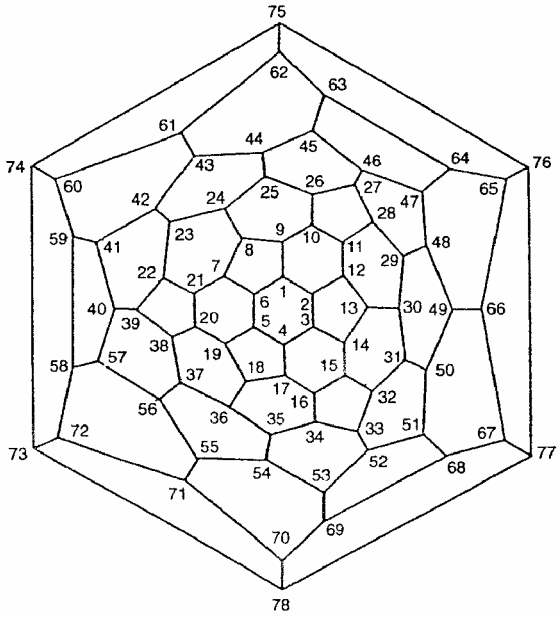

Numbering scheme for D_{3h} (78:4) isomer

B

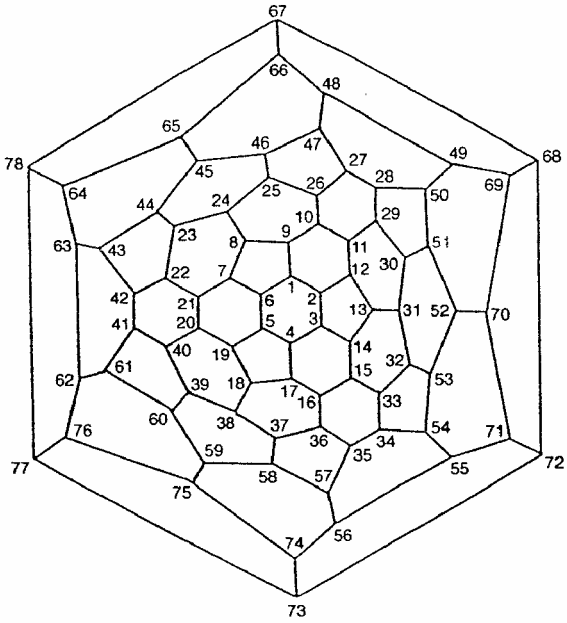

Numbering scheme for $D_{3h'}$ (78:5) isomer

Appendix III. How to operate the Krätchmer-Huffman generator at Virginia Tech

To synthesize trimetallic nitride endohedral metallofullerenes, a metal oxide/graphite rod is placed inside the generator at point 'D' (Figure 1) once the pressure of the generator has equalized to room pressure. The cover is then closed, and the pressure inside the generator is reduced by opening valve 'A' (Figure 1). If metallofullerene soot is not already present inside the generator from a previous arc-vaporization, then valve 'B' (Figure 1) can also be opened to reduce the pressure at a faster rate. However, unlike valve 'A', valve 'B' is not connected to filter 'C' (Figure 1), and soot will be sucked into the vacuum pump if valve 'B' is opened when soot is present inside the generator.

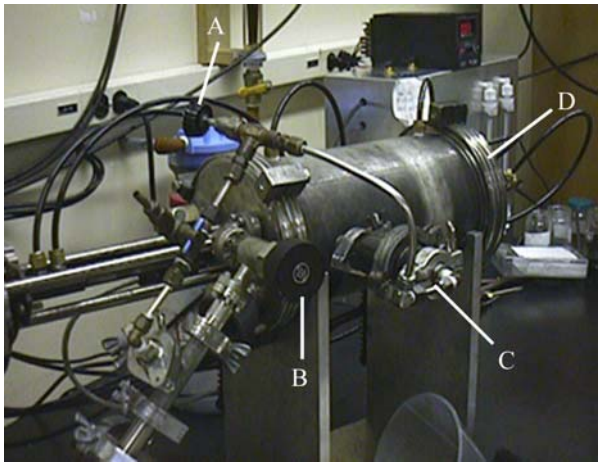

Figure 1. Krätchmer-Huffman generator at Virginia Tech.

When the pressure inside the generator reaches *ca.* 0 Torr, as indicated by the digital pressure reader 'F' (Figure 2), then the chamber must be evacuated and refilled with helium and nitrogen gas three times to remove any oxygen that is present. To accomplish this, lift up valve 'H' (Figure 2) to allow gas flow to the chamber. Once digital pressure indicator 'F' reads 400 Torr, then close valve 'H', and let the vacuum pump reduce the pressure back to 0 Torr. This step is then repeated two more times. Now, set the gas flows of helium and nitrogen to *ca.* 500 ml/min. and *ca.* 40 ml/min., respectively, by adjusting the flow valves (black dials) of 'G' (Figure 2), so that when valve 'H' and vacuum valve 'A' are both open, the pressure indicator reads *ca.* 300 Torr.

Figure 2. Pressure, voltage and gas flow indicators for generator at Virginia Tech.

Turn on the cold water at a flow rate of 1 gallon per minute (GPM). This meter is located directly behind the generator and on the wall. Turn on the voltage indicator by lifting switch 'E' (Figure 2). Indicator 'E' is powered by three AAA batteries that are located inside the aluminum control box. Turn on the arc-welder (Figure 3a), and the voltage indicator 'E' should jump to 50+ Volts. Turn generator motor control power to

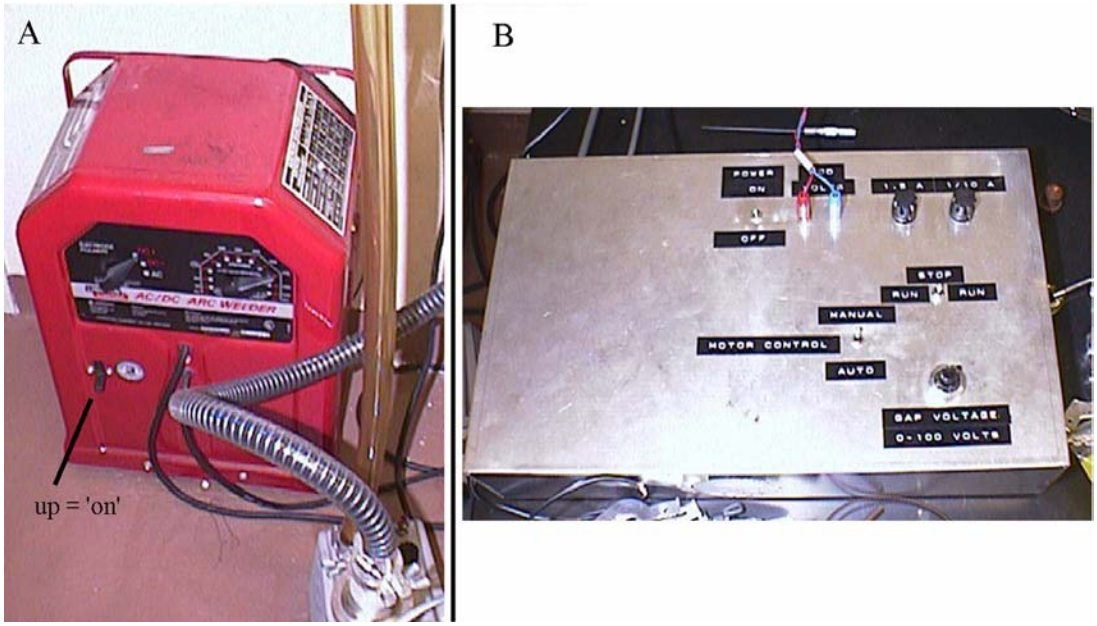

Figure 3. (a) Arc-welder (DC+ current) and (b) motor controls for generator.

'on' (Figure 3b), and turn the motor control switch to 'manual'. Next, flip the 'run' switch (Figure 3b) of the motor controls to the right. This will move an internal graphite rod (for arcing) towards the internal metal-oxide/graphite packed rod that is intended to be vaporized. *When the two rods come in contact with each other they begin to arc, and a humming sound can then be heard.* Once arcing begins, flip the 'run' switch of the motor controls to the left, and pull the arcing rod back slightly. Now, turn the motor control switch to 'auto', and flip the 'run' control switch back to the right. The controls are set to keep the voltage of vaporization at *ca.* 31.3 Volts. The pressure will rise slightly due to the vaporization. **DO NOT TOUCH THE GENERATOR WHEN THE ACR-WELDER IS 'ON'!** The time of complete rod vaporization takes from 30 minutes to 1 hour.

Once the rod is completely vaporized, the voltage indicator ('E') will jump to 50+ Volts. Turn off the arc-welder (Figure 3a), and let the internal soot cool for at least 5 hours. Close vacuum valve 'A', and let the chamber fill with gas until the pressure reaches 700 Torr. The generator can now be opened at point 'D' (Figure 1). Soot inside the chamber is removed with a small brush and placed inside a cellulose extraction thimble (43 mm ID x 123 mm ED: Whatman). The soot can also be removed by placing one of the thimbles on an attachment of the vacuum cleaner. Fullerenes and metallofullerenes are then extracted with carbon disulfide. Individual species are purified by methods that are outlined in the chapters of this dissertation.

Appendix IV. Determination of symmetry

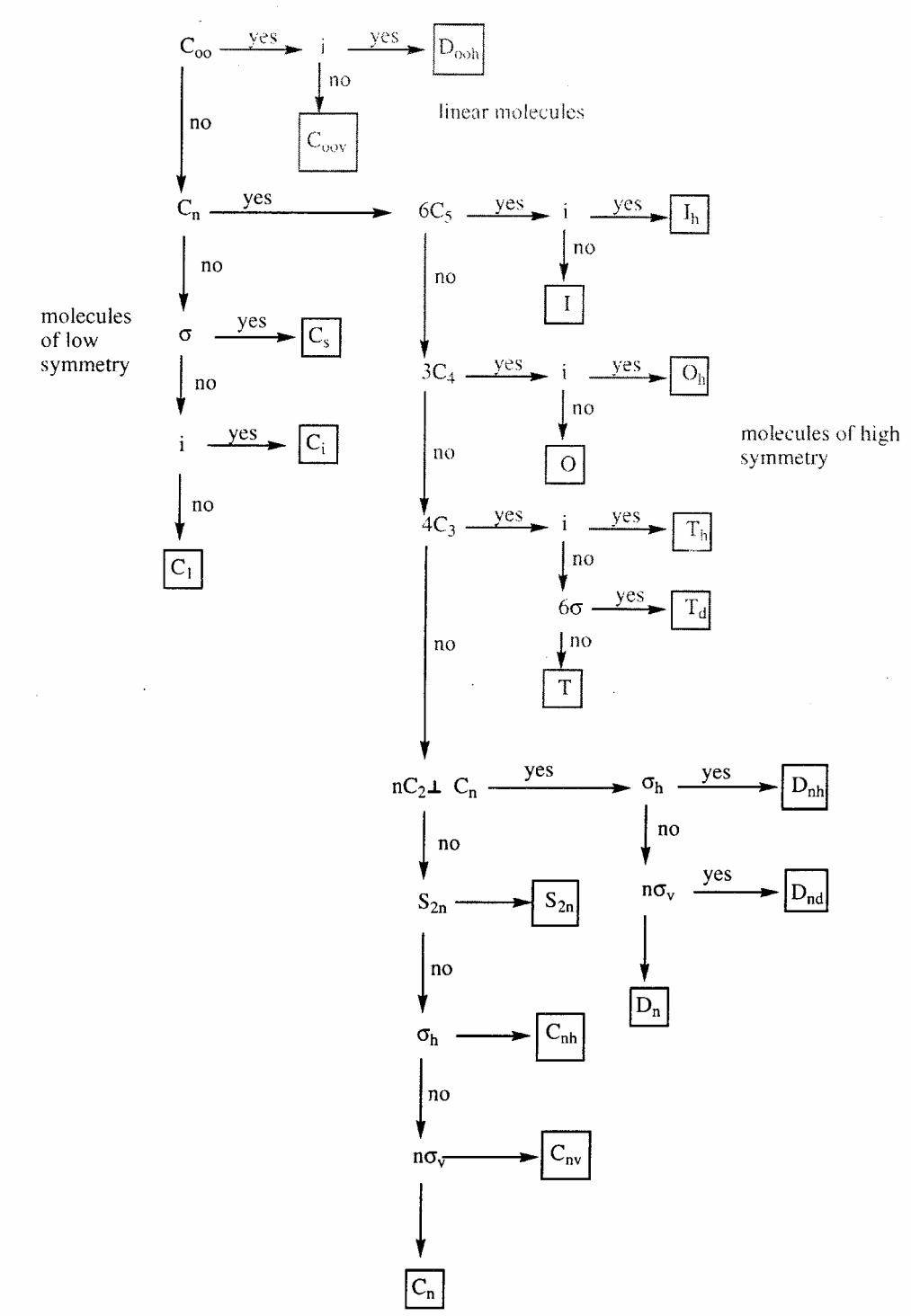

Appendix V. X-ray crystal structure coordinates of 4,5-dimethoxy-*o*-quinodimethane–$Sc_3N@C_{80}$ (4).

* This data can be downloaded from the Journal of the American Chemical Society's website as a .cif file. Lee, H.-M.; Olmstead, M. M.; Iezzi, E.; Duchamp, J. C.; Dorn, H. C.; Balch, A. L. *J. Am. Chem. Soc.*, **2002**, *124*, 3494–3495.

```
data_hml02

_audit_creation_method            SHELXL-97
_chemical_name_systematic
;
 ?
;
_chemical_name_common        '4,5-dimethoxyl-o-quinodimethane-Sc3N@C80'
_chemical_melting_point           ?
_chemical_formula_moiety          ?
_chemical_formula_sum
 'C102 H24 N O2 Sc3'
_chemical_formula_weight          1430.10

loop_
 _atom_type_symbol
 _atom_type_description
 _atom_type_scat_dispersion_real
 _atom_type_scat_dispersion_imag
 _atom_type_scat_source
 'C'  'C'   0.0033   0.0016
 'International Tables Vol C Tables 4.2.6.8 and 6.1.1.4'
 'H'  'H'   0.0000   0.0000
 'International Tables Vol C Tables 4.2.6.8 and 6.1.1.4'
 'N'  'N'   0.0061   0.0033
 'International Tables Vol C Tables 4.2.6.8 and 6.1.1.4'
 'O'  'O'   0.0106   0.0060
 'International Tables Vol C Tables 4.2.6.8 and 6.1.1.4'
 'Sc'  'Sc'   0.2519   0.3716
 'International Tables Vol C Tables 4.2.6.8 and 6.1.1.4'

_symmetry_cell_setting            monoclinic
_symmetry_space_group_name_H-M    'P 21/n'

loop_
 _symmetry_equiv_pos_as_xyz
 'x, y, z'
 '-x+1/2, y+1/2, -z+1/2'
 '-x, -y, -z'
 'x-1/2, -y-1/2, z-1/2'

_cell_length_a                    19.972(7)
_cell_length_b                    14.196(5)
_cell_length_c                    20.986(8)
```

```
_cell_angle_alpha                 90.00
_cell_angle_beta                  117.548(11)
_cell_angle_gamma                 90.00
_cell_volume                      5275(3)
_cell_formula_units_Z             4
_cell_measurement_temperature     91(2)
_cell_measurement_reflns_used     819
_cell_measurement_theta_min       2.188
_cell_measurement_theta_max       24.295

_exptl_crystal_description        bipyramid
_exptl_crystal_colour             black
_exptl_crystal_size_max           0.11
_exptl_crystal_size_mid           0.10
_exptl_crystal_size_min           0.06
_exptl_crystal_density_meas       ?
_exptl_crystal_density_diffrn     1.801
_exptl_crystal_density_method     'not measured'
_exptl_crystal_F_000              2888
_exptl_absorpt_coefficient_mu     0.451
_exptl_absorpt_correction_type    none
_exptl_absorpt_correction_T_min   0.9520
_exptl_absorpt_correction_T_max   0.9734
_exptl_absorpt_process_details    ?

_exptl_special_details
;
 ?
;

_diffrn_ambient_temperature       91(2)
_diffrn_radiation_wavelength      0.71073
_diffrn_radiation_type            MoK\a
_diffrn_radiation_source          'normal-focus sealed tube'
_diffrn_radiation_monochromator   graphite
_diffrn_measurement_device_type   'Bruker SMART 1000'
_diffrn_measurement_method        \W
_diffrn_detector_area_resol_mean  8.3
_diffrn_standards_number          ?
_diffrn_standards_interval_count  ?
_diffrn_standards_interval_time   ?
_diffrn_standards_decay_%         ?
_diffrn_reflns_number             70657
_diffrn_reflns_av_R_equivalents   0.2438
_diffrn_reflns_av_sigmaI/netI     0.2536
_diffrn_reflns_limit_h_min        -28
_diffrn_reflns_limit_h_max        26
_diffrn_reflns_limit_k_min        -20
_diffrn_reflns_limit_k_max        20
_diffrn_reflns_limit_l_min        -30
_diffrn_reflns_limit_l_max        30
_diffrn_reflns_theta_min          1.80
_diffrn_reflns_theta_max          31.51
_reflns_number_total              16838
_reflns_number_gt                 6304
```

```
_reflns_threshold_expression      I>2\s(I)
_computing_data_collection        'SMART (Bruker, 2000)'
_computing_cell_refinement        'SMART (Bruker, 2000)'
_computing_data_reduction         'SAINT (Bruker, 1999)'
_computing_structure_solution     'SHELXS-97 (Sheldrick, 1990)'
_computing_structure_refinement   'SHELXL-97 (Sheldrick, 1997)'
_computing_molecular_graphics     'SHELXL 5.1 (Sheldrick, 1994)'
_computing_publication_material   'SHELXL-97 (Sheldrick, 1997)'

_refine_special_details
;
 Refinement of F^2^ against ALL reflections.  The weighted R-factor wR
and
 goodness of fit S are based on F^2^, conventional R-factors R are
based
 on F, with F set to zero for negative F^2^. The threshold expression
of
 F^2^ > 2sigma(F^2^) is used only for calculating R-factors(gt) etc.
and is
 not relevant to the choice of reflections for refinement.  R-factors
based
 on F^2^ are statistically about twice as large as those based on F,
and R-
 factors based on ALL data will be even larger.
;

_refine_ls_structure_factor_coef  Fsqd
_refine_ls_matrix_type            full
_refine_ls_weighting_scheme       calc
_refine_ls_weighting_details
 'calc w=1/[\s^2^(Fo^2^)+(0.0511P)^2^+0.0000P] where
P=(Fo^2^+2Fc^2^)/3'
_atom_sites_solution_primary      direct
_atom_sites_solution_secondary    difmap
_atom_sites_solution_hydrogens    geom
_refine_ls_hydrogen_treatment     constr
_refine_ls_extinction_method      none
_refine_ls_extinction_coef        ?
_refine_ls_number_reflns          16838
_refine_ls_number_parameters      985
_refine_ls_number_restraints      0
_refine_ls_R_factor_all           0.2161
_refine_ls_R_factor_gt            0.0643
_refine_ls_wR_factor_ref          0.1513
_refine_ls_wR_factor_gt           0.1098
_refine_ls_goodness_of_fit_ref    0.848
_refine_ls_restrained_S_all       0.848
_refine_ls_shift/su_max           0.001
_refine_ls_shift/su_mean          0.000

loop_
 _atom_site_label
 _atom_site_type_symbol
 _atom_site_fract_x
 _atom_site_fract_y
```

```
 _atom_site_fract_z
 _atom_site_U_iso_or_equiv
 _atom_site_adp_type
 _atom_site_occupancy
 _atom_site_symmetry_multiplicity
 _atom_site_calc_flag
 _atom_site_refinement_flags
 _atom_site_disorder_assembly
 _atom_site_disorder_group
N1 N 1.03910(15) 0.8626(2) 0.26165(15) 0.0168(7) Uani 1 1 d . . .
Sc1 Sc 0.95836(4) 0.92464(6) 0.17161(4) 0.01785(19) Uani 0.9507(12) 1 d
P A 1
Sc2 Sc 1.07428(4) 0.94064(6) 0.35199(4) 0.01950(19) Uani 0.9507(12) 1 d
P A 1
Sc3 Sc 1.07207(4) 0.72890(6) 0.25652(5) 0.0246(2) Uani 0.9507(12) 1 d P
A 1
Sc1B Sc 0.9342(12) 0.8807(17) 0.1861(12) 0.050 Uiso 0.0493(12) 1 d P A
2
Sc2B Sc 1.0482(12) 0.8959(17) 0.3640(12) 0.050 Uiso 0.0493(12) 1 d P A
2
Sc3B Sc 1.1299(11) 0.8410(15) 0.2408(11) 0.050 Uiso 0.0493(12) 1 d P A
2
O1 O 0.79131(13) 1.48196(18) 0.20444(12) 0.0200(6) Uani 1 1 d . A .
O2 O 0.86075(13) 1.48770(18) 0.34279(12) 0.0215(6) Uani 1 1 d . . .
C1 C 0.91198(19) 1.0713(3) 0.31899(18) 0.0170(8) Uani 1 1 d . A .
C2 C 0.85799(18) 1.0641(3) 0.23276(18) 0.0177(8) Uani 1 1 d . A .
C3 C 0.90887(19) 1.0939(3) 0.20039(18) 0.0176(8) Uani 1 1 d . . .
C4 C 0.97938(19) 1.1276(3) 0.2552(2) 0.0182(8) Uani 1 1 d . A .
C5 C 0.98654(19) 1.1072(3) 0.32470(18) 0.0165(8) Uani 1 1 d . . .
C6 C 1.0590(2) 1.0955(3) 0.38503(19) 0.0234(9) Uani 1 1 d . A .
C7 C 1.0666(2) 1.0283(3) 0.43893(19) 0.0234(9) Uani 1 1 d . . .
C8 C 1.0023(2) 0.9672(3) 0.4208(2) 0.0248(9) Uani 1 1 d . A .
C9 C 0.9297(2) 0.9790(3) 0.3590(2) 0.0205(8) Uani 1 1 d . . .
C10 C 0.8873(2) 0.8995(3) 0.3297(2) 0.0233(9) Uani 1 1 d . A .
C11 C 0.83855(19) 0.8916(3) 0.2525(2) 0.0227(9) Uani 1 1 d . . .
C12 C 0.83344(18) 0.9637(3) 0.2063(2) 0.0214(9) Uani 1 1 d . A .
C13 C 0.82267(19) 0.9380(3) 0.1367(2) 0.0237(9) Uani 1 1 d . . .
C14 C 0.8488(2) 0.9928(3) 0.09395(19) 0.0237(9) Uani 1 1 d . A .
C15 C 0.8990(2) 1.0702(3) 0.13125(18) 0.0216(9) Uani 1 1 d . A .
C16 C 0.9642(2) 1.0817(3) 0.1194(2) 0.0238(9) Uani 1 1 d . . .
C17 C 1.0332(2) 1.1206(3) 0.1742(2) 0.0239(9) Uani 1 1 d . A .
C18 C 1.0427(2) 1.1431(3) 0.2425(2) 0.0232(9) Uani 1 1 d . . .
C19 C 1.1144(2) 1.1342(3) 0.3024(2) 0.0247(9) Uani 1 1 d . A .
C20 C 1.1230(2) 1.1083(3) 0.3714(2) 0.0228(9) Uani 1 1 d . . .
C21 C 1.1898(2) 1.0521(3) 0.4057(2) 0.0301(11) Uani 1 1 d . A .
C22 C 1.1960(2) 0.9786(3) 0.4553(2) 0.0297(11) Uani 1 1 d . . .
C23 C 1.1348(2) 0.9683(3) 0.4722(2) 0.0291(10) Uani 1 1 d . A .
C24 C 1.1100(2) 0.8742(3) 0.47616(19) 0.0284(10) Uani 1 1 d . . .
C25 C 1.0293(2) 0.8731(3) 0.4460(2) 0.0271(10) Uani 1 1 d . A .
C26 C 0.9853(2) 0.7926(3) 0.4150(2) 0.0300(10) Uani 1 1 d . . .
C27 C 0.9130(2) 0.8055(3) 0.3576(2) 0.0282(10) Uani 1 1 d . A .
C28 C 0.8810(2) 0.7422(3) 0.2985(2) 0.0285(10) Uani 1 1 d . . .
C29 C 0.8360(2) 0.7933(3) 0.2344(2) 0.0254(9) Uani 1 1 d . A .
C30 C 0.8299(2) 0.7673(3) 0.1679(2) 0.0296(10) Uani 1 1 d . . .
C31 C 0.8241(2) 0.8398(3) 0.1195(2) 0.0291(11) Uani 1 1 d . A .
```

```
C32 C 0.8542(2) 0.8315(3) 0.0703(2) 0.0285(10) Uani 1 1 d . . .
C33 C 0.8700(2) 0.9239(3) 0.05360(19) 0.0279(10) Uani 1 1 d . A .
C34 C 0.9378(2) 0.9345(3) 0.04673(19) 0.0299(10) Uani 1 1 d . . .
C35 C 0.9827(2) 1.0171(3) 0.0780(2) 0.0287(10) Uani 1 1 d . A .
C36 C 1.0637(2) 1.0170(3) 0.1061(2) 0.0286(10) Uani 1 1 d . . .
C37 C 1.0950(2) 1.0815(3) 0.1646(2) 0.0285(10) Uani 1 1 d . A .
C38 C 1.1659(2) 1.0645(3) 0.2256(2) 0.0292(10) Uani 1 1 d . . .
C39 C 1.1767(2) 1.0951(3) 0.2935(2) 0.0307(10) Uani 1 1 d . A .
C40 C 1.2225(2) 1.0447(3) 0.3584(2) 0.0303(11) Uani 1 1 d . . .
C41 C 0.8672(2) 0.6814(3) 0.1650(2) 0.0274(10) Uani 1 1 d . A .
C42 C 0.8989(2) 0.6741(3) 0.1165(2) 0.0302(11) Uani 1 1 d . . .
C43 C 0.8958(2) 0.7485(3) 0.0700(2) 0.0271(10) Uani 1 1 d . A .
C44 C 0.9566(2) 0.7615(3) 0.05542(19) 0.0272(10) Uani 1 1 d . . .
C45 C 0.9789(2) 0.8532(3) 0.04537(19) 0.0291(10) Uani 1 1 d . A .
C46 C 1.0593(2) 0.8536(3) 0.0728(2) 0.0302(10) Uani 1 1 d . . .
C47 C 1.1039(2) 0.9335(3) 0.1060(2) 0.0296(10) Uani 1 1 d . A .
C48 C 1.1771(2) 0.9213(3) 0.1645(2) 0.0311(10) Uani 1 1 d . . .
C49 C 1.2075(2) 0.9853(3) 0.2228(2) 0.0294(10) Uani 1 1 d . A .
C50 C 1.2544(2) 0.9351(3) 0.2876(2) 0.0308(10) Uani 1 1 d . . .
C51 C 1.2605(2) 0.9597(3) 0.3552(2) 0.0312(11) Uani 1 1 d . A .
C52 C 1.2688(2) 0.8883(3) 0.4048(2) 0.0300(10) Uani 1 1 d . . .
C53 C 1.2355(2) 0.8960(3) 0.4523(2) 0.0313(11) Uani 1 1 d . A .
C54 C 1.2136(2) 0.8044(3) 0.4630(2) 0.0293(10) Uani 1 1 d . . .
C55 C 1.1494(2) 0.7897(3) 0.47293(19) 0.0285(10) Uani 1 1 d . A .
C56 C 1.1050(2) 0.7074(3) 0.4450(2) 0.0296(10) Uani 1 1 d . . .
C57 C 1.0251(2) 0.7073(3) 0.4168(2) 0.0275(10) Uani 1 1 d . A .
C58 C 0.9934(2) 0.6443(3) 0.3578(2) 0.0286(10) Uani 1 1 d . . .
C59 C 0.9226(2) 0.6616(3) 0.2965(2) 0.0293(10) Uani 1 1 d . A .
C60 C 0.9125(2) 0.6317(3) 0.2291(2) 0.0312(11) Uani 1 1 d . . .
C61 C 0.9751(2) 0.5899(3) 0.2212(2) 0.0258(10) Uani 1 1 d . A .
C62 C 0.9651(2) 0.6175(3) 0.1509(2) 0.0268(10) Uani 1 1 d . A .
C63 C 1.0291(2) 0.6324(3) 0.1386(2) 0.0259(10) Uani 1 1 d . . .
C64 C 1.0242(2) 0.7041(3) 0.0909(2) 0.0263(10) Uani 1 1 d . A .
C65 C 1.0871(2) 0.7613(3) 0.1007(2) 0.0276(10) Uani 1 1 d . A .
C66 C 1.1579(2) 0.7489(3) 0.1625(2) 0.0250(9) Uani 1 1 d . . .
C67 C 1.2042(2) 0.8285(3) 0.1921(2) 0.0262(9) Uani 1 1 d . A .
C68 C 1.2517(2) 0.8366(3) 0.2675(2) 0.0286(10) Uani 1 1 d . A .
C69 C 1.25475(19) 0.7659(3) 0.3154(2) 0.0226(9) Uani 1 1 d . . .
C70 C 1.26663(19) 0.7909(3) 0.3855(2) 0.0290(11) Uani 1 1 d . A .
C71 C 1.2325(2) 0.7391(3) 0.42120(19) 0.0281(10) Uani 1 1 d . A .
C72 C 1.1864(2) 0.6597(3) 0.3896(2) 0.0282(10) Uani 1 1 d . . .
C73 C 1.1235(2) 0.6436(3) 0.4027(2) 0.0286(10) Uani 1 1 d . A .
C74 C 1.0554(2) 0.6034(3) 0.3486(2) 0.0278(10) Uani 1 1 d . A .
C75 C 1.0467(2) 0.5736(3) 0.2807(2) 0.0254(9) Uani 1 1 d . . .
C76 C 1.1120(2) 0.5792(3) 0.2673(2) 0.0247(9) Uani 1 1 d . A .
C77 C 1.1024(2) 0.6117(3) 0.1981(2) 0.0215(9) Uani 1 1 d . A .
C78 C 1.1632(2) 0.6739(3) 0.2098(2) 0.0212(9) Uani 1 1 d . A .
C79 C 1.21059(19) 0.6827(3) 0.2857(2) 0.0202(8) Uani 1 1 d . A .
C80 C 1.17926(19) 0.6271(3) 0.3219(2) 0.0216(9) Uani 1 1 d . A .
C81 C 0.8777(2) 1.1379(3) 0.35449(18) 0.0183(8) Uani 1 1 d . . .
H81A H 0.8330 1.1075 0.3543 0.022 Uiso 1 1 calc R A .
H81B H 0.9152 1.1491 0.4051 0.022 Uiso 1 1 calc R . .
C82 C 0.78939(18) 1.1306(2) 0.20893(19) 0.0183(8) Uani 1 1 d . . .
H82A H 0.7640 1.1362 0.1559 0.022 Uiso 1 1 calc R A .
H82B H 0.7528 1.1032 0.2233 0.022 Uiso 1 1 calc R . .
```

```
C83 C 0.85463(18) 1.2309(3) 0.31569(19) 0.0171(8) Uani 1 1 d . A .
C84 C 0.87211(19) 1.3169(3) 0.35138(19) 0.0182(8) Uani 1 1 d . . .
H84 H 0.8999 1.3186 0.4023 0.022 Uiso 1 1 calc R A .
C85 C 0.84928(18) 1.3998(3) 0.31312(18) 0.0161(8) Uani 1 1 d . A .
C86 C 0.80999(18) 1.3965(3) 0.23800(18) 0.0164(8) Uani 1 1 d . . .
C87 C 0.79191(18) 1.3105(3) 0.20292(18) 0.0164(8) Uani 1 1 d . A .
H87 H 0.7653 1.3085 0.1519 0.020 Uiso 1 1 calc R . .
C88 C 0.81246(18) 1.2271(3) 0.24177(18) 0.0153(8) Uani 1 1 d . A .
C89 C 0.7592(2) 1.4816(3) 0.12809(18) 0.0215(9) Uani 1 1 d . . .
H89A H 0.7926 1.4473 0.1137 0.032 Uiso 1 1 calc R A .
H89B H 0.7531 1.5465 0.1105 0.032 Uiso 1 1 calc R . .
H89C H 0.7098 1.4505 0.1076 0.032 Uiso 1 1 calc R . .
C90 C 0.8962(2) 1.4927(3) 0.41931(19) 0.0275(10) Uani 1 1 d . . .
H90A H 0.8647 1.4604 0.4371 0.041 Uiso 1 1 calc R . .
H90B H 0.9024 1.5588 0.4344 0.041 Uiso 1 1 calc R . .
H90C H 0.9458 1.4622 0.4391 0.041 Uiso 1 1 calc R . .
C91 C 0.5880(2) 1.1877(3) -0.0507(2) 0.0302(10) Uani 1 1 d . . .
H91 H 0.5413 1.1972 -0.0499 0.036 Uiso 1 1 calc R . .
C92 C 0.6539(2) 1.2156(3) 0.0064(2) 0.0299(10) Uani 1 1 d . . .
H92 H 0.6530 1.2434 0.0472 0.036 Uiso 1 1 calc R . .
C93 C 0.7223(2) 1.2033(3) 0.0051(2) 0.0320(11) Uani 1 1 d . . .
H93 H 0.7682 1.2227 0.0447 0.038 Uiso 1 1 calc R . .
C94 C 0.7226(2) 1.1620(3) -0.0552(2) 0.0376(11) Uani 1 1 d . . .
H94 H 0.7689 1.1528 -0.0567 0.045 Uiso 1 1 calc R . .
C95 C 0.6567(3) 1.1351(3) -0.1115(2) 0.0406(12) Uani 1 1 d . . .
H95 H 0.6572 1.1085 -0.1528 0.049 Uiso 1 1 calc R . .
C96 C 0.5891(3) 1.1456(3) -0.1097(2) 0.0387(12) Uani 1 1 d . . .
H96 H 0.5435 1.1241 -0.1487 0.046 Uiso 1 1 calc R . .
C97 C 1.0066(3) 1.4057(4) 0.0626(3) 0.0480(13) Uani 1 1 d . . .
H97 H 1.0344 1.4237 0.0381 0.058 Uiso 1 1 calc R . .
C98 C 0.9295(3) 1.4026(4) 0.0256(3) 0.0479(14) Uani 1 1 d . . .
H98 H 0.9041 1.4197 -0.0238 0.057 Uiso 1 1 calc R . .
C99 C 1.0443(2) 1.3837(3) 0.1334(3) 0.0426(13) Uani 1 1 d . . .
H99 H 1.0979 1.3864 0.1582 0.051 Uiso 1 1 calc R . .
C100 C 0.8898(3) 1.3750(3) 0.0597(3) 0.0430(13) Uani 1 1 d . . .
H100 H 0.8363 1.3721 0.0338 0.052 Uiso 1 1 calc R . .
C101 C 1.0038(3) 1.3569(3) 0.1697(3) 0.0442(13) Uani 1 1 d . . .
H101 H 1.0291 1.3431 0.2197 0.053 Uiso 1 1 calc R . .
C102 C 0.9254(3) 1.3510(3) 0.1310(3) 0.0464(13) Uani 1 1 d . . .
H102 H 0.8967 1.3303 0.1540 0.056 Uiso 1 1 calc R . .

loop_
 _atom_site_aniso_label
 _atom_site_aniso_U_11
 _atom_site_aniso_U_22
 _atom_site_aniso_U_33
 _atom_site_aniso_U_23
 _atom_site_aniso_U_13
 _atom_site_aniso_U_12
N1 0.0135(14) 0.0217(17) 0.0136(15) -0.0012(13) 0.0050(12) 0.0006(12)
Sc1 0.0170(4) 0.0216(4) 0.0092(3) 0.0012(3) 0.0012(3) 0.0038(3)
Sc2 0.0188(4) 0.0251(5) 0.0098(3) -0.0035(3) 0.0025(3) 0.0012(3)
Sc3 0.0218(4) 0.0181(4) 0.0367(5) -0.0001(4) 0.0160(4) 0.0025(3)
O1 0.0231(13) 0.0191(14) 0.0126(13) 0.0015(11) 0.0037(11) 0.0012(11)
O2 0.0220(13) 0.0209(15) 0.0138(13) -0.0034(11) 0.0016(11) 0.0001(11)
```

C1 0.0182(17) 0.018(2) 0.0124(17) 0.0042(15) 0.0053(14) 0.0045(15)
C2 0.0146(16) 0.018(2) 0.0163(18) -0.0004(16) 0.0036(14) -0.0011(15)
C3 0.0218(18) 0.015(2) 0.0151(18) 0.0013(15) 0.0074(15) 0.0062(15)
C4 0.0194(18) 0.0126(19) 0.024(2) -0.0014(15) 0.0110(16) 0.0032(15)
C5 0.0199(18) 0.0142(19) 0.0131(17) -0.0020(15) 0.0057(14) 0.0018(15)
C6 0.0196(19) 0.025(2) 0.0158(19) -0.0082(16) -0.0005(15) 0.0024(16)
C7 0.024(2) 0.030(2) 0.0110(18) -0.0068(16) 0.0040(15) 0.0062(17)
C8 0.038(2) 0.026(2) 0.018(2) 0.0039(17) 0.0188(18) 0.0101(18)
C9 0.027(2) 0.021(2) 0.021(2) 0.0009(17) 0.0183(17) 0.0058(17)
C10 0.0205(19) 0.023(2) 0.033(2) 0.0015(18) 0.0179(18) 0.0019(16)
C11 0.0148(17) 0.020(2) 0.039(2) 0.0017(18) 0.0172(17) 0.0038(15)
C12 0.0088(16) 0.021(2) 0.029(2) -0.0032(17) 0.0037(15) 0.0024(14)
C13 0.0139(17) 0.025(2) 0.0216(19) -0.0069(17) -0.0012(15) 0.0054(16)
C14 0.023(2) 0.029(2) 0.0115(18) 0.0033(17) 0.0022(16) 0.0123(17)
C15 0.0251(19) 0.022(2) 0.0133(17) 0.0071(16) 0.0055(15) 0.0100(17)
C16 0.037(2) 0.019(2) 0.0187(19) 0.0085(17) 0.0161(17) 0.0115(18)
C17 0.034(2) 0.020(2) 0.025(2) 0.0062(17) 0.0204(18) 0.0017(18)
C18 0.031(2) 0.015(2) 0.027(2) -0.0014(17) 0.0159(18) -0.0020(17)
C19 0.022(2) 0.019(2) 0.031(2) -0.0040(17) 0.0094(18) -0.0085(16)
C20 0.0180(18) 0.019(2) 0.023(2) -0.0093(17) 0.0026(16) -0.0029(16)
C21 0.0166(18) 0.029(2) 0.028(2) -0.0162(19) -0.0036(17) -0.0034(17)
C22 0.021(2) 0.034(3) 0.017(2) -0.0119(18) -0.0054(16) 0.0037(18)
C23 0.031(2) 0.032(3) 0.0113(19) -0.0061(17) -0.0017(17) 0.0105(19)
C24 0.029(2) 0.043(3) 0.0079(18) 0.0045(17) 0.0041(16) 0.012(2)
C25 0.042(2) 0.034(3) 0.0146(19) 0.0075(18) 0.0206(18) 0.013(2)
C26 0.043(3) 0.032(3) 0.027(2) 0.0111(19) 0.026(2) 0.009(2)
C27 0.031(2) 0.030(3) 0.038(3) 0.007(2) 0.028(2) -0.0010(19)
C28 0.023(2) 0.026(2) 0.045(3) 0.008(2) 0.023(2) 0.0019(17)
C29 0.0165(18) 0.024(2) 0.038(2) -0.0066(19) 0.0152(18) -0.0045(16)
C30 0.0124(17) 0.024(2) 0.041(3) -0.009(2) 0.0032(17) -0.0067(17)
C31 0.0129(18) 0.025(2) 0.030(2) -0.0085(19) -0.0063(17) 0.0020(16)
C32 0.0183(19) 0.036(3) 0.0157(19) -0.0063(18) -0.0050(16) 0.0023(18)
C33 0.026(2) 0.034(3) 0.0096(17) 0.0004(17) -0.0034(15) 0.0110(19)
C34 0.043(2) 0.026(2) 0.0117(18) 0.0032(18) 0.0052(17) 0.006(2)
C35 0.039(2) 0.034(3) 0.018(2) 0.0108(18) 0.0176(19) 0.011(2)
C36 0.044(3) 0.030(3) 0.023(2) 0.0133(19) 0.026(2) 0.011(2)
C37 0.036(2) 0.026(2) 0.036(2) 0.008(2) 0.028(2) -0.0031(19)
C38 0.034(2) 0.022(2) 0.042(3) -0.001(2) 0.027(2) -0.0111(19)
C39 0.026(2) 0.021(2) 0.045(3) -0.005(2) 0.016(2) -0.0106(18)
C40 0.0144(18) 0.029(2) 0.044(3) -0.016(2) 0.0104(18) -0.0086(17)
C41 0.0174(19) 0.022(2) 0.036(2) -0.0067(19) 0.0069(18) -0.0065(17)
C42 0.019(2) 0.022(2) 0.033(2) -0.0126(19) -0.0012(18) -0.0056(17)
C43 0.022(2) 0.026(2) 0.018(2) -0.0127(17) -0.0024(16) 0.0008(17)
C44 0.031(2) 0.030(2) 0.0097(18) -0.0094(17) -0.0001(16) 0.0091(19)
C45 0.036(2) 0.037(3) 0.0084(18) 0.0016(17) 0.0050(17) 0.011(2)
C46 0.044(3) 0.033(3) 0.022(2) 0.0023(19) 0.023(2) 0.011(2)
C47 0.046(3) 0.033(3) 0.027(2) 0.003(2) 0.032(2) 0.002(2)
C48 0.035(2) 0.034(3) 0.040(3) 0.006(2) 0.030(2) -0.002(2)
C49 0.027(2) 0.027(2) 0.047(3) -0.001(2) 0.028(2) -0.0064(18)
C50 0.0148(18) 0.035(3) 0.047(3) -0.006(2) 0.0181(19) -0.0045(18)
C51 0.0117(18) 0.034(3) 0.041(3) -0.012(2) 0.0059(18) -0.0075(17)
C52 0.0116(18) 0.037(3) 0.028(2) -0.010(2) -0.0023(17) 0.0024(17)
C53 0.0177(19) 0.041(3) 0.017(2) -0.0082(19) -0.0076(16) 0.0045(19)
C54 0.024(2) 0.040(3) 0.0103(18) 0.0004(18) -0.0031(16) 0.0146(19)
C55 0.039(2) 0.034(3) 0.0089(18) 0.0078(17) 0.0079(17) 0.015(2)

```
C56 0.040(2) 0.035(3) 0.019(2) 0.0145(19) 0.0182(19) 0.016(2)
C57 0.035(2) 0.031(3) 0.026(2) 0.0139(19) 0.0216(19) 0.0078(19)
C58 0.035(2) 0.021(2) 0.042(3) 0.015(2) 0.028(2) 0.0015(18)
C59 0.030(2) 0.020(2) 0.048(3) 0.003(2) 0.026(2) -0.0055(18)
C60 0.027(2) 0.017(2) 0.050(3) -0.003(2) 0.018(2) -0.0069(17)
C61 0.023(2) 0.015(2) 0.037(2) -0.0007(18) 0.0114(19) -0.0004(16)
C62 0.025(2) 0.019(2) 0.030(2) -0.0105(18) 0.0077(18) -0.0037(17)
C63 0.028(2) 0.022(2) 0.021(2) -0.0093(17) 0.0056(17) 0.0022(18)
C64 0.026(2) 0.032(2) 0.0160(19) -0.0094(18) 0.0055(16) 0.0044(18)
C65 0.042(2) 0.029(2) 0.018(2) 0.0048(18) 0.0190(19) 0.013(2)
C66 0.032(2) 0.024(2) 0.029(2) -0.0017(18) 0.0226(19) 0.0059(17)
C67 0.029(2) 0.027(2) 0.035(2) 0.0028(19) 0.0252(19) 0.0059(18)
C68 0.0154(18) 0.030(3) 0.045(3) -0.005(2) 0.0178(19) -0.0021(17)
C69 0.0131(17) 0.026(2) 0.027(2) -0.0075(18) 0.0073(16) 0.0020(16)
C70 0.0087(17) 0.035(3) 0.030(2) -0.0085(19) -0.0028(16) 0.0067(17)
C71 0.0202(19) 0.039(3) 0.0121(18) 0.0006(18) -0.0036(15) 0.0177(19)
C72 0.026(2) 0.033(3) 0.021(2) 0.0111(19) 0.0073(17) 0.0142(19)
C73 0.037(2) 0.026(2) 0.026(2) 0.0119(18) 0.0167(19) 0.0138(19)
C74 0.037(2) 0.020(2) 0.034(2) 0.0099(19) 0.023(2) 0.0071(18)
C75 0.026(2) 0.015(2) 0.036(2) 0.0034(18) 0.0147(18) 0.0030(17)
C76 0.026(2) 0.017(2) 0.032(2) 0.0020(18) 0.0149(18) 0.0043(17)
C77 0.0219(19) 0.019(2) 0.021(2) -0.0034(16) 0.0078(16) 0.0045(16)
C78 0.0204(18) 0.021(2) 0.020(2) -0.0019(16) 0.0081(16) 0.0060(16)
C79 0.0164(18) 0.022(2) 0.024(2) 0.0035(17) 0.0107(16) 0.0068(16)
C80 0.0177(18) 0.023(2) 0.022(2) 0.0032(17) 0.0074(16) 0.0076(16)
C81 0.0211(18) 0.023(2) 0.0117(17) 0.0019(15) 0.0080(15) 0.0035(16)
C82 0.0129(17) 0.019(2) 0.0183(19) -0.0003(15) 0.0029(15) 0.0031(15)
C83 0.0141(16) 0.0167(19) 0.0197(19) 0.0029(16) 0.0072(15) 0.0004(15)
C84 0.0148(17) 0.024(2) 0.0139(18) 0.0017(16) 0.0046(14) 0.0017(15)
C85 0.0124(16) 0.020(2) 0.0149(18) -0.0041(15) 0.0058(14) -0.0016(14)
C86 0.0131(16) 0.020(2) 0.0149(18) 0.0060(15) 0.0058(14) 0.0005(15)
C87 0.0124(16) 0.023(2) 0.0108(17) -0.0019(15) 0.0028(14) 0.0002(15)
C88 0.0109(15) 0.0167(19) 0.0177(18) 0.0002(16) 0.0061(14) 0.0014(14)
C89 0.0212(18) 0.027(2) 0.0121(18) 0.0037(16) 0.0044(15) 0.0024(16)
C90 0.037(2) 0.024(2) 0.0150(19) -0.0039(17) 0.0065(17) -0.0008(19)
C91 0.029(2) 0.031(3) 0.029(2) 0.005(2) 0.0119(19) 0.0003(19)
C92 0.032(2) 0.035(3) 0.022(2) 0.0012(19) 0.0121(18) 0.0007(19)
C93 0.024(2) 0.044(3) 0.024(2) 0.002(2) 0.0076(18) 0.0031(19)
C94 0.034(2) 0.044(3) 0.040(3) -0.002(2) 0.022(2) 0.008(2)
C95 0.055(3) 0.041(3) 0.030(3) -0.009(2) 0.024(2) 0.002(2)
C96 0.047(3) 0.026(3) 0.034(3) -0.003(2) 0.011(2) -0.009(2)
C97 0.043(3) 0.053(4) 0.059(4) -0.010(3) 0.033(3) -0.001(3)
C98 0.049(3) 0.057(4) 0.034(3) -0.018(2) 0.016(2) 0.005(3)
C99 0.023(2) 0.027(3) 0.065(4) -0.012(2) 0.010(2) -0.001(2)
C100 0.028(2) 0.051(3) 0.046(3) -0.003(3) 0.013(2) 0.003(2)
C101 0.048(3) 0.024(3) 0.043(3) 0.002(2) 0.006(2) 0.009(2)
C102 0.045(3) 0.042(3) 0.071(4) 0.013(3) 0.043(3) 0.010(2)

_geom_special_details
;
 All esds (except the esd in the dihedral angle between two l.s.
planes)
 are estimated using the full covariance matrix.  The cell esds are
taken
```

```
 into account individually in the estimation of esds in distances,
angles
 and torsion angles; correlations between esds in cell parameters are
only
 used when they are defined by crystal symmetry.  An approximate
(isotropic)
 treatment of cell esds is used for estimating esds involving l.s.
planes.
;

loop_
 _geom_bond_atom_site_label_1
 _geom_bond_atom_site_label_2
 _geom_bond_distance
 _geom_bond_site_symmetry_2
 _geom_bond_publ_flag
N1 Sc1B 1.97(2) . ?
N1 Sc2 2.020(3) . ?
N1 Sc3 2.029(3) . ?
N1 Sc1 2.032(3) . ?
N1 Sc3B 2.08(2) . ?
N1 Sc2B 2.12(2) . ?
Sc1 C14 2.255(3) . ?
Sc1 C33 2.282(3) . ?
Sc1 C15 2.337(4) . ?
Sc1 C34 2.462(4) . ?
Sc1 C13 2.466(4) . ?
Sc1 C16 2.511(4) . ?
Sc1 C32 2.550(4) . ?
Sc1 C35 2.589(4) . ?
Sc1 C31 2.669(4) . ?
Sc1 C3 2.769(4) . ?
Sc1 Sc2 3.4111(16) . ?
Sc2 C23 2.272(4) . ?
Sc2 C7 2.272(4) . ?
Sc2 C6 2.367(4) . ?
Sc2 C22 2.454(4) . ?
Sc2 C8 2.494(4) . ?
Sc2 C20 2.532(4) . ?
Sc2 C24 2.543(4) . ?
Sc2 C21 2.586(4) . ?
Sc2 C25 2.694(4) . ?
Sc2 C5 2.839(4) . ?
Sc3 C76 2.243(4) . ?
Sc3 C77 2.307(4) . ?
Sc3 C75 2.369(4) . ?
Sc3 C80 2.416(4) . ?
Sc3 C78 2.556(4) . ?
Sc3 C63 2.603(4) . ?
Sc3 C61 2.620(4) . ?
Sc3 C79 2.625(4) . ?
Sc3 C62 2.756(4) . ?
Sc3 C74 2.759(4) . ?
Sc3 C72 2.843(4) . ?
Sc1B C31 2.07(2) . ?
Sc1B C13 2.14(2) . ?
Sc1B C32 2.31(2) . ?
Sc1B C14 2.48(2) . ?
Sc1B C33 2.54(2) . ?
Sc1B C30 2.52(3) . ?
Sc1B C12 2.53(2) . ?
Sc1B C11 2.84(2) . ?
Sc1B C15 2.88(2) . ?
Sc1B Sc2B 3.36(3) . ?
Sc1B Sc3B 3.57(3) . ?
Sc2B C25 1.95(2) . ?
Sc2B C8 2.07(2) . ?
Sc2B C24 2.11(2) . ?
Sc2B C23 2.36(2) . ?
Sc2B C7 2.37(2) . ?
Sc2B C26 2.47(3) . ?
Sc2B C9 2.60(2) . ?
Sc2B C55 2.70(2) . ?
Sc2B C6 2.86(2) . ?
Sc2B Sc3B 3.72(3) . ?
Sc3B C67 2.16(2) . ?
Sc3B C68 2.23(2) . ?
Sc3B C66 2.36(2) . ?
Sc3B C48 2.48(2) . ?
Sc3B C69 2.49(2) . ?
Sc3B C50 2.58(2) . ?
Sc3B C78 2.63(2) . ?
Sc3B C79 2.67(2) . ?
Sc3B C49 2.70(2) . ?
O1 C86 1.365(4) . ?
O1 C89 1.424(4) . ?
O2 C85 1.366(4) . ?
O2 C90 1.426(4) . ?
C1 C9 1.507(5) . ?
C1 C5 1.525(5) . ?
C1 C81 1.547(5) . ?
C1 C2 1.626(5) . ?
C2 C3 1.520(5) . ?
C2 C12 1.525(5) . ?
C2 C82 1.544(5) . ?
C3 C15 1.412(5) . ?
C3 C4 1.427(5) . ?
C4 C5 1.428(5) . ?
C4 C18 1.425(5) . ?
C5 C6 1.425(5) . ?
```

C6 C7 1.433(6) . ?
C6 C20 1.444(6) . ?
C7 C8 1.448(6) . ?
C7 C23 1.479(5) . ?
C8 C9 1.440(5) . ?
C8 C25 1.446(5) . ?
C9 C10 1.374(5) . ?
C10 C27 1.452(6) . ?
C10 C11 1.457(5) . ?
C11 C12 1.380(5) . ?
C11 C29 1.442(5) . ?
C12 C13 1.422(5) . ?
C13 C31 1.444(5) . ?
C13 C14 1.454(6) . ?
C14 C15 1.450(5) . ?
C14 C33 1.478(5) . ?
C15 C16 1.443(5) . ?
C16 C35 1.425(6) . ?
C16 C17 1.436(5) . ?
C17 C18 1.393(5) . ?
C17 C37 1.450(5) . ?
C18 C19 1.408(5) . ?
C19 C20 1.425(6) . ?
C19 C39 1.450(6) . ?
C20 C21 1.429(5) . ?
C21 C22 1.437(6) . ?
C21 C40 1.425(6) . ?
C22 C53 1.430(6) . ?
C22 C23 1.430(6) . ?
C23 C24 1.439(6) . ?
C24 C25 1.433(6) . ?
C24 C55 1.453(6) . ?
C25 C26 1.404(6) . ?
C26 C27 1.400(6) . ?
C26 C57 1.439(6) . ?
C27 C28 1.422(6) . ?
C28 C59 1.425(6) . ?
C28 C29 1.423(6) . ?
C29 C30 1.392(6) . ?
C30 C31 1.412(6) . ?
C30 C41 1.445(6) . ?
C31 C32 1.420(6) . ?
C32 C33 1.429(6) . ?
C32 C43 1.443(6) . ?
C33 C34 1.435(6) . ?
C34 C45 1.425(6) . ?
C34 C35 1.437(6) . ?
C35 C36 1.442(6) . ?
C36 C37 1.423(6) . ?
C36 C47 1.432(6) . ?
C37 C38 1.423(6) . ?
C38 C49 1.415(6) . ?
C38 C39 1.409(6) . ?
C39 C40 1.432(6) . ?
C40 C51 1.442(6) . ?
C41 C60 1.415(6) . ?
C41 C42 1.429(6) . ?
C42 C43 1.420(6) . ?
C42 C62 1.425(5) . ?
C43 C44 1.396(6) . ?
C44 C45 1.423(6) . ?
C44 C64 1.453(5) . ?
C45 C46 1.433(6) . ?
C46 C47 1.411(6) . ?
C46 C65 1.438(6) . ?
C47 C48 1.419(6) . ?
C48 C49 1.415(6) . ?
C48 C67 1.440(6) . ?
C49 C50 1.433(6) . ?
C50 C51 1.412(6) . ?
C50 C68 1.455(6) . ?
C51 C52 1.405(6) . ?
C52 C53 1.437(6) . ?
C52 C70 1.436(6) . ?
C53 C54 1.423(6) . ?
C54 C55 1.407(6) . ?
C54 C71 1.442(6) . ?
C55 C56 1.420(6) . ?
C56 C57 1.422(6) . ?
C56 C73 1.432(6) . ?
C57 C58 1.418(6) . ?
C58 C59 1.426(6) . ?
C58 C74 1.458(6) . ?
C59 C60 1.399(6) . ?
C60 C61 1.463(6) . ?
C61 C75 1.415(5) . ?
C61 C62 1.448(6) . ?
C62 C63 1.432(6) . ?
C63 C64 1.399(6) . ?
C63 C77 1.448(5) . ?
C64 C65 1.428(6) . ?
C65 C66 1.420(5) . ?
C66 C67 1.410(6) . ?
C66 C78 1.426(5) . ?
C67 C68 1.424(6) . ?
C68 C69 1.403(6) . ?
C69 C70 1.421(6) . ?
C69 C79 1.433(5) . ?
C70 C71 1.428(6) . ?
C71 C72 1.412(6) . ?
C72 C73 1.421(6) . ?
C72 C80 1.439(6) . ?
C73 C74 1.427(6) . ?
C74 C75 1.419(6) . ?
C75 C76 1.457(6) . ?
C76 C77 1.450(5) . ?
C76 C80 1.467(5) . ?
C77 C78 1.428(5) . ?
C78 C79 1.432(5) . ?
C79 C80 1.425(5) . ?

```
C81 C83 1.506(5) . ?
C82 C88 1.507(5) . ?
C83 C88 1.382(5) . ?
C83 C84 1.390(5) . ?
C84 C85 1.378(5) . ?
C85 C86 1.400(5) . ?
C86 C87 1.385(5) . ?
C87 C88 1.387(5) . ?
C91 C92 1.367(5) . ?
C91 C96 1.384(6) . ?
C92 C93 1.390(6) . ?
C93 C94 1.396(6) . ?
C94 C95 1.355(6) . ?
C95 C96 1.376(6) . ?
C97 C98 1.367(6) . ?
C97 C99 1.357(7) . ?
C98 C100 1.348(7) . ?
C99 C101 1.395(7) . ?
C100 C102 1.371(7) . ?
C101 C102 1.394(6) . ?

loop_
 _geom_angle_atom_site_label_1
 _geom_angle_atom_site_label_2
 _geom_angle_atom_site_label_3
 _geom_angle
 _geom_angle_site_symmetry_1
 _geom_angle_site_symmetry_3
 _geom_angle_publ_flag
Sc1B N1 Sc2 117.5(7) . . ?
Sc1B N1 Sc3 109.2(7) . . ?
Sc2 N1 Sc3 125.60(14) . . ?
Sc2 N1 Sc1 114.66(15) . . ?
Sc3 N1 Sc1 119.58(14) . . ?
Sc1B N1 Sc3B 123.8(9) . . ?
Sc2 N1 Sc3B 108.7(6) . . ?
Sc3 N1 Sc3B 60.9(6) . . ?
Sc1 N1 Sc3B 105.2(6) . . ?
Sc1B N1 Sc2B 110.3(9) . . ?
Sc3 N1 Sc2B 112.6(6) . . ?
Sc1 N1 Sc2B 120.3(6) . . ?
Sc3B N1 Sc2B 124.9(8) . . ?
N1 Sc1 C14 161.05(14) . . ?
N1 Sc1 C33 152.93(14) . . ?
C14 Sc1 C33 38.02(14) . . ?
N1 Sc1 C15 140.48(13) . . ?
C14 Sc1 C15 36.76(13) . . ?
C33 Sc1 C15 66.59(14) . . ?
N1 Sc1 C34 133.22(14) . . ?
C14 Sc1 C34 65.03(14) . . ?
C33 Sc1 C34 34.95(14) . . ?
C15 Sc1 C34 75.93(14) . . ?
N1 Sc1 C13 126.86(13) . . ?
C14 Sc1 C13 35.53(14) . . ?
C33 Sc1 C13 59.06(14) . . ?
C15 Sc1 C13 61.39(14) . . ?
C34 Sc1 C13 93.46(14) . . ?
N1 Sc1 C16 127.87(13) . . ?
C14 Sc1 C16 61.89(14) . . ?
C33 Sc1 C16 72.47(14) . . ?
C15 Sc1 C16 34.38(13) . . ?
C34 Sc1 C16 60.21(13) . . ?
C13 Sc1 C16 93.92(13) . . ?
N1 Sc1 C32 122.78(14) . . ?
C14 Sc1 C32 58.33(14) . . ?
C33 Sc1 C32 33.84(14) . . ?
C15 Sc1 C32 94.29(13) . . ?
C34 Sc1 C32 58.11(15) . . ?
C13 Sc1 C32 55.38(13) . . ?
C16 Sc1 C32 106.30(13) . . ?
N1 Sc1 C35 125.35(13) . . ?
C14 Sc1 C35 72.21(14) . . ?
C33 Sc1 C35 60.09(15) . . ?
C15 Sc1 C35 61.23(14) . . ?
C34 Sc1 C35 32.94(13) . . ?
C13 Sc1 C35 107.60(13) . . ?
C16 Sc1 C35 32.41(13) . . ?
C32 Sc1 C35 89.83(14) . . ?
N1 Sc1 C31 113.59(13) . . ?
C14 Sc1 C31 56.08(14) . . ?
C33 Sc1 C31 55.04(15) . . ?
C15 Sc1 C31 90.33(13) . . ?
C34 Sc1 C31 87.03(14) . . ?
C13 Sc1 C31 32.36(12) . . ?
C16 Sc1 C31 117.54(13) . . ?
C32 Sc1 C31 31.48(13) . . ?
C35 Sc1 C31 115.07(14) . . ?
N1 Sc1 C3 112.51(11) . . ?
C14 Sc1 C3 57.33(12) . . ?
C33 Sc1 C3 93.77(13) . . ?
C15 Sc1 C3 30.64(11) . . ?
C34 Sc1 C3 106.39(12) . . ?
C13 Sc1 C3 62.86(12) . . ?
C16 Sc1 C3 54.40(12) . . ?
C32 Sc1 C3 113.32(12) . . ?
C35 Sc1 C3 86.39(13) . . ?
C31 Sc1 C3 95.09(12) . . ?
N1 Sc1 Sc2 32.57(9) . . ?
C14 Sc1 Sc2 135.02(10) . . ?
C33 Sc1 Sc2 172.84(11) . . ?
C15 Sc1 Sc2 108.26(9) . . ?
C34 Sc1 Sc2 150.58(11) . . ?
C13 Sc1 Sc2 114.39(10) . . ?
C16 Sc1 Sc2 106.30(9) . . ?
C32 Sc1 Sc2 146.42(11) . . ?
C35 Sc1 Sc2 122.61(10) . . ?
C31 Sc1 Sc2 121.49(10) . . ?
C3 Sc1 Sc2 80.08(7) . . ?
N1 Sc2 C23 155.84(14) . . ?
N1 Sc2 C7 158.53(13) . . ?
```

```
C23 Sc2 C7 38.00(13) . . ?
N1 Sc2 C6 138.41(13) . . ?
C23 Sc2 C6 65.70(14) . . ?
C7 Sc2 C6 35.91(14) . . ?
N1 Sc2 C22 136.19(13) . . ?
C23 Sc2 C22 34.95(15) . . ?
C7 Sc2 C22 65.01(14) . . ?
C6 Sc2 C22 75.33(13) . . ?
N1 Sc2 C8 125.65(13) . . ?
C23 Sc2 C8 58.89(14) . . ?
C7 Sc2 C8 34.99(13) . . ?
C6 Sc2 C8 60.20(14) . . ?
C22 Sc2 C8 93.22(15) . . ?
N1 Sc2 C20 127.40(13) . . ?
C23 Sc2 C20 72.02(15) . . ?
C7 Sc2 C20 61.26(15) . . ?
C6 Sc2 C20 34.09(13) . . ?
C22 Sc2 C20 60.10(13) . . ?
C8 Sc2 C20 92.66(14) . . ?
N1 Sc2 C24 124.69(14) . . ?
C23 Sc2 C24 34.20(14) . . ?
C7 Sc2 C24 58.10(14) . . ?
C6 Sc2 C24 93.29(14) . . ?
C22 Sc2 C24 58.82(15) . . ?
C8 Sc2 C24 54.99(13) . . ?
C20 Sc2 C24 106.17(14) . . ?
N1 Sc2 C21 126.70(14) . . ?
C23 Sc2 C21 60.06(16) . . ?
C7 Sc2 C21 72.07(15) . . ?
C6 Sc2 C21 60.90(13) . . ?
C22 Sc2 C21 33.01(14) . . ?
C8 Sc2 C21 106.96(14) . . ?
C20 Sc2 C21 32.41(12) . . ?
C24 Sc2 C21 90.50(14) . . ?
N1 Sc2 C25 113.76(14) . . ?
C23 Sc2 C25 55.54(15) . . ?
C7 Sc2 C25 55.80(14) . . ?
C6 Sc2 C25 89.12(14) . . ?
C22 Sc2 C25 87.74(15) . . ?
C8 Sc2 C25 32.09(12) . . ?
C20 Sc2 C25 116.76(13) . . ?
C24 Sc2 C25 31.60(12) . . ?
C21 Sc2 C25 115.49(14) . . ?
N1 Sc2 C5 110.66(11) . . ?
C23 Sc2 C5 92.39(12) . . ?
C7 Sc2 C5 56.02(12) . . ?
C6 Sc2 C5 30.06(10) . . ?
C22 Sc2 C5 105.21(12) . . ?
C8 Sc2 C5 61.55(12) . . ?
C20 Sc2 C5 53.51(11) . . ?
C24 Sc2 C5 111.72(12) . . ?
C21 Sc2 C5 85.48(12) . . ?
C25 Sc2 C5 93.48(12) . . ?
N1 Sc2 Sc1 32.77(8) . . ?
C23 Sc2 Sc1 169.58(11) . . ?
C7 Sc2 Sc1 131.65(10) . . ?
C6 Sc2 Sc1 105.88(9) . . ?
C22 Sc2 Sc1 151.82(12) . . ?
C8 Sc2 Sc1 112.07(10) . . ?
C20 Sc2 Sc1 104.75(9) . . ?
C24 Sc2 Sc1 146.85(11) . . ?
C21 Sc2 Sc1 122.38(11) . . ?
C25 Sc2 Sc1 120.27(10) . . ?
C5 Sc2 Sc1 78.04(7) . . ?
N1 Sc3 C76 171.79(14) . . ?
N1 Sc3 C77 150.96(14) . . ?
C76 Sc3 C77 37.14(14) . . ?
N1 Sc3 C75 138.83(14) . . ?
C76 Sc3 C75 36.69(14) . . ?
C77 Sc3 C75 65.00(15) . . ?
N1 Sc3 C80 138.94(13) . . ?
C76 Sc3 C80 36.48(13) . . ?
C77 Sc3 C80 59.27(13) . . ?
C75 Sc3 C80 62.80(13) . . ?
N1 Sc3 C78 127.77(13) . . ?
C76 Sc3 C78 57.78(14) . . ?
C77 Sc3 C78 33.67(12) . . ?
C75 Sc3 C78 93.35(14) . . ?
C80 Sc3 C78 55.50(13) . . ?
N1 Sc3 C63 124.79(12) . . ?
C76 Sc3 C63 62.83(13) . . ?
C77 Sc3 C63 33.62(12) . . ?
C75 Sc3 C63 72.82(14) . . ?
C80 Sc3 C63 92.34(13) . . ?
C78 Sc3 C63 56.96(12) . . ?
N1 Sc3 C61 120.29(12) . . ?
C76 Sc3 C61 59.78(13) . . ?
C77 Sc3 C61 69.37(14) . . ?
C75 Sc3 C61 32.46(12) . . ?
C80 Sc3 C61 93.13(13) . . ?
C78 Sc3 C61 103.03(13) . . ?
C63 Sc3 C61 57.25(14) . . ?
N1 Sc3 C79 123.68(12) . . ?
C76 Sc3 C79 56.84(13) . . ?
C77 Sc3 C79 55.71(12) . . ?
C75 Sc3 C79 91.39(13) . . ?
C80 Sc3 C79 32.51(12) . . ?
C78 Sc3 C79 32.05(11) . . ?
C63 Sc3 C79 86.48(12) . . ?
C61 Sc3 C79 116.03(13) . . ?
N1 Sc3 C62 115.44(12) . . ?
C76 Sc3 C62 69.22(13) . . ?
C77 Sc3 C62 56.99(13) . . ?
C75 Sc3 C62 58.35(13) . . ?
C80 Sc3 C62 105.49(13) . . ?
C78 Sc3 C62 86.63(13) . . ?
C63 Sc3 C62 30.83(12) . . ?
C61 Sc3 C62 31.13(13) . . ?
C79 Sc3 C62 112.67(12) . . ?
N1 Sc3 C74 114.81(13) . . ?
```

```
C76 Sc3 C74 58.00(14) . . ?
C77 Sc3 C74 93.05(14) . . ?
C75 Sc3 C74 30.95(13) . . ?
C80 Sc3 C74 65.07(13) . . ?
C78 Sc3 C74 114.16(13) . . ?
C63 Sc3 C74 103.46(14) . . ?
C61 Sc3 C74 53.07(13) . . ?
C79 Sc3 C74 97.53(12) . . ?
C62 Sc3 C74 83.87(13) . . ?
N1 Sc3 C72 113.84(12) . . ?
C76 Sc3 C72 59.14(13) . . ?
C77 Sc3 C72 89.11(13) . . ?
C75 Sc3 C72 67.80(13) . . ?
C80 Sc3 C72 30.40(12) . . ?
C78 Sc3 C72 83.14(12) . . ?
C63 Sc3 C72 120.96(13) . . ?
C61 Sc3 C72 99.79(13) . . ?
C79 Sc3 C72 53.41(12) . . ?
C62 Sc3 C72 124.30(13) . . ?
C74 Sc3 C72 52.47(13) . . ?
N1 Sc1B C31 155.2(14) . . ?
N1 Sc1B C13 156.9(13) . . ?
C31 Sc1B C13 40.1(4) . . ?
N1 Sc1B C32 140.0(12) . . ?
C31 Sc1B C32 37.3(4) . . ?
C13 Sc1B C32 63.1(6) . . ?
N1 Sc1B C14 143.4(13) . . ?
C31 Sc1B C14 61.3(6) . . ?
C13 Sc1B C14 35.8(4) . . ?
C32 Sc1B C14 58.8(5) . . ?
N1 Sc1B C33 136.2(12) . . ?
C31 Sc1B C33 59.2(6) . . ?
C13 Sc1B C33 59.5(6) . . ?
C32 Sc1B C33 33.8(3) . . ?
C14 Sc1B C33 34.2(3) . . ?
N1 Sc1B C30 122.3(11) . . ?
C31 Sc1B C30 34.1(4) . . ?
C13 Sc1B C30 64.3(6) . . ?
C32 Sc1B C30 61.8(6) . . ?
C14 Sc1B C30 94.0(7) . . ?
C33 Sc1B C30 91.4(7) . . ?
N1 Sc1B C12 123.8(10) . . ?
C31 Sc1B C12 64.2(6) . . ?
C13 Sc1B C12 34.1(4) . . ?
C32 Sc1B C12 95.8(8) . . ?
C14 Sc1B C12 61.2(5) . . ?
C33 Sc1B C12 91.9(7) . . ?
C30 Sc1B C12 69.9(6) . . ?
N1 Sc1B C11 108.5(10) . . ?
C31 Sc1B C11 66.5(7) . . ?
C13 Sc1B C11 55.3(6) . . ?
C32 Sc1B C11 103.7(8) . . ?
C14 Sc1B C11 88.3(7) . . ?
C33 Sc1B C11 114.2(8) . . ?
C30 Sc1B C11 54.0(5) . . ?
C12 Sc1B C11 29.0(3) . . ?
N1 Sc1B C15 114.5(10) . . ?
C31 Sc1B C15 90.3(8) . . ?
C13 Sc1B C15 56.2(5) . . ?
C32 Sc1B C15 86.6(7) . . ?
C14 Sc1B C15 30.2(3) . . ?
C33 Sc1B C15 55.3(5) . . ?
C30 Sc1B C15 120.3(8) . . ?
C12 Sc1B C15 64.3(5) . . ?
C11 Sc1B C15 92.8(7) . . ?
N1 Sc1B Sc2B 36.3(6) . . ?
C31 Sc1B Sc2B 136.9(11) . . ?
C13 Sc1B Sc2B 122.2(10) . . ?
C32 Sc1B Sc2B 165.8(11) . . ?
C14 Sc1B Sc2B 133.9(9) . . ?
C33 Sc1B Sc2B 160.0(10) . . ?
C30 Sc1B Sc2B 107.3(9) . . ?
C12 Sc1B Sc2B 88.1(8) . . ?
C11 Sc1B Sc2B 73.5(7) . . ?
C15 Sc1B Sc2B 107.3(8) . . ?
N1 Sc1B Sc3B 28.9(5) . . ?
C31 Sc1B Sc3B 146.7(10) . . ?
C13 Sc1B Sc3B 163.1(12) . . ?
C32 Sc1B Sc3B 114.3(9) . . ?
C14 Sc1B Sc3B 127.5(10) . . ?
C33 Sc1B Sc3B 108.3(9) . . ?
C30 Sc1B Sc3B 130.8(9) . . ?
C12 Sc1B Sc3B 148.8(9) . . ?
C11 Sc1B Sc3B 137.3(8) . . ?
C15 Sc1B Sc3B 107.7(8) . . ?
Sc2B Sc1B Sc3B 64.8(6) . . ?
C25 Sc2B N1 153.4(14) . . ?
C25 Sc2B C8 42.0(5) . . ?
N1 Sc2B C8 146.8(11) . . ?
C25 Sc2B C24 41.0(5) . . ?
N1 Sc2B C24 145.7(11) . . ?
C8 Sc2B C24 67.5(7) . . ?
C25 Sc2B C23 65.0(7) . . ?
N1 Sc2B C23 138.8(12) . . ?
C8 Sc2B C23 63.6(6) . . ?
C24 Sc2B C23 37.0(4) . . ?
C25 Sc2B C7 65.2(7) . . ?
N1 Sc2B C7 139.7(12) . . ?
C8 Sc2B C7 37.3(4) . . ?
C24 Sc2B C7 62.9(6) . . ?
C23 Sc2B C7 36.5(4) . . ?
C25 Sc2B C26 34.5(5) . . ?
N1 Sc2B C26 118.9(10) . . ?
C8 Sc2B C26 65.9(7) . . ?
C24 Sc2B C26 65.4(7) . . ?
C23 Sc2B C26 97.7(9) . . ?
C7 Sc2B C26 97.9(9) . . ?
C25 Sc2B C9 64.4(7) . . ?
N1 Sc2B C9 114.1(9) . . ?
C8 Sc2B C9 33.5(4) . . ?
```

```
C24 Sc2B C9 99.4(9) . . ?
C23 Sc2B C9 95.1(8) . . ?
C7 Sc2B C9 61.7(6) . . ?
C26 Sc2B C9 69.6(6) . . ?
C25 Sc2B C55 62.3(6) . . ?
N1 Sc2B C55 114.4(9) . . ?
C8 Sc2B C55 98.2(9) . . ?
C24 Sc2B C55 32.2(3) . . ?
C23 Sc2B C55 60.0(5) . . ?
C7 Sc2B C55 93.2(7) . . ?
C26 Sc2B C55 68.5(6) . . ?
C9 Sc2B C55 126.6(10) . . ?
C25 Sc2B C6 93.4(8) . . ?
N1 Sc2B C6 110.0(10) . . ?
C8 Sc2B C6 56.6(6) . . ?
C24 Sc2B C6 90.5(8) . . ?
C23 Sc2B C6 56.7(5) . . ?
C7 Sc2B C6 30.0(3) . . ?
C26 Sc2B C6 122.5(9) . . ?
C9 Sc2B C6 63.9(5) . . ?
C55 Sc2B C6 116.6(8) . . ?
C25 Sc2B Sc1B 131.4(11) . . ?
N1 Sc2B Sc1B 33.4(5) . . ?
C8 Sc2B Sc1B 114.7(9) . . ?
C24 Sc2B Sc1B 166.8(12) . . ?
C23 Sc2B Sc1B 156.2(11) . . ?
C7 Sc2B Sc1B 127.3(9) . . ?
C26 Sc2B Sc1B 102.9(8) . . ?
C9 Sc2B Sc1B 81.3(7) . . ?
C55 Sc2B Sc1B 139.5(9) . . ?
C6 Sc2B Sc1B 101.5(8) . . ?
C25 Sc2B Sc3B 154.6(11) . . ?
N1 Sc2B Sc3B 27.2(5) . . ?
C8 Sc2B Sc3B 162.6(11) . . ?
C24 Sc2B Sc3B 121.7(9) . . ?
C23 Sc2B Sc3B 113.5(9) . . ?
C7 Sc2B Sc3B 130.1(10) . . ?
C26 Sc2B Sc3B 130.6(9) . . ?
C9 Sc2B Sc3B 138.5(8) . . ?
C55 Sc2B Sc3B 94.3(7) . . ?
C6 Sc2B Sc3B 106.8(8) . . ?
Sc1B Sc2B Sc3B 60.3(6) . . ?
N1 Sc3B C67 165.6(11) . . ?
N1 Sc3B C68 155.4(11) . . ?
C67 Sc3B C68 37.8(4) . . ?
N1 Sc3B C66 137.7(10) . . ?
C67 Sc3B C66 36.0(4) . . ?
C68 Sc3B C66 65.0(6) . . ?
N1 Sc3B C48 134.3(10) . . ?
C67 Sc3B C48 35.3(4) . . ?
C68 Sc3B C48 58.6(5) . . ?
C66 Sc3B C48 61.5(6) . . ?
N1 Sc3B C69 130.5(10) . . ?
C67 Sc3B C69 63.7(6) . . ?
C68 Sc3B C69 34.0(3) . . ?
C66 Sc3B C69 73.2(6) . . ?
C48 Sc3B C69 92.0(7) . . ?
N1 Sc3B C50 128.7(10) . . ?
C67 Sc3B C50 58.1(5) . . ?
C68 Sc3B C50 34.2(3) . . ?
C66 Sc3B C50 93.2(7) . . ?
C48 Sc3B C50 54.6(5) . . ?
C69 Sc3B C50 58.3(5) . . ?
N1 Sc3B C78 122.1(9) . . ?
C67 Sc3B C78 60.1(6) . . ?
C68 Sc3B C78 70.4(6) . . ?
C66 Sc3B C78 32.7(3) . . ?
C48 Sc3B C78 92.3(7) . . ?
C69 Sc3B C78 58.3(5) . . ?
C50 Sc3B C78 104.6(7) . . ?
N1 Sc3B C79 119.6(9) . . ?
C67 Sc3B C79 70.4(6) . . ?
C68 Sc3B C79 58.5(5) . . ?
C66 Sc3B C79 58.7(5) . . ?
C48 Sc3B C79 105.5(8) . . ?
C69 Sc3B C79 32.0(3) . . ?
C50 Sc3B C79 89.1(6) . . ?
C78 Sc3B C79 31.4(3) . . ?
N1 Sc3B C49 122.1(9) . . ?
C67 Sc3B C49 55.4(5) . . ?
C68 Sc3B C49 55.0(5) . . ?
C66 Sc3B C49 89.3(7) . . ?
C48 Sc3B C49 31.4(3) . . ?
C69 Sc3B C49 86.6(6) . . ?
C50 Sc3B C49 31.4(3) . . ?
C78 Sc3B C49 115.1(8) . . ?
C79 Sc3B C49 113.4(8) . . ?
N1 Sc3B Sc1B 27.3(5) . . ?
C67 Sc3B Sc1B 138.4(9) . . ?
C68 Sc3B Sc1B 171.6(10) . . ?
C66 Sc3B Sc1B 116.0(8) . . ?
C48 Sc3B Sc1B 113.9(8) . . ?
C69 Sc3B Sc1B 154.0(9) . . ?
C50 Sc3B Sc1B 139.3(9) . . ?
C78 Sc3B Sc1B 115.3(8) . . ?
C79 Sc3B Sc1B 129.6(8) . . ?
C49 Sc3B Sc1B 116.7(8) . . ?
N1 Sc3B Sc2B 27.9(5) . . ?
C67 Sc3B Sc2B 164.2(9) . . ?
C68 Sc3B Sc2B 127.5(8) . . ?
C66 Sc3B Sc2B 157.0(9) . . ?
C48 Sc3B Sc2B 140.5(9) . . ?
C69 Sc3B Sc2B 106.6(7) . . ?
C50 Sc3B Sc2B 106.4(7) . . ?
C78 Sc3B Sc2B 127.1(8) . . ?
C79 Sc3B Sc2B 108.5(8) . . ?
C49 Sc3B Sc2B 113.8(8) . . ?
Sc1B Sc3B Sc2B 54.9(6) . . ?
C86 O1 C89 116.8(3) . . ?
C85 O2 C90 116.7(3) . . ?
```

```
C9 C1 C5 106.1(3) . . ?
C9 C1 C81 107.8(3) . . ?
C5 C1 C81 113.0(3) . . ?
C9 C1 C2 115.4(3) . . ?
C5 C1 C2 103.3(3) . . ?
C81 C1 C2 111.2(3) . . ?
C3 C2 C12 105.5(3) . . ?
C3 C2 C82 111.2(3) . . ?
C12 C2 C82 111.4(3) . . ?
C3 C2 C1 104.1(3) . . ?
C12 C2 C1 113.6(3) . . ?
C82 C2 C1 110.8(3) . . ?
C15 C3 C4 121.6(4) . . ?
C15 C3 C2 126.1(3) . . ?
C4 C3 C2 110.3(3) . . ?
C15 C3 Sc1 57.53(19) . . ?
C4 C3 Sc1 98.5(2) . . ?
C2 C3 Sc1 103.6(2) . . ?
C5 C4 C3 110.5(3) . . ?
C5 C4 C18 123.0(3) . . ?
C3 C4 C18 122.1(4) . . ?
C6 C5 C4 120.8(3) . . ?
C6 C5 C1 125.8(3) . . ?
C4 C5 C1 110.8(3) . . ?
C6 C5 Sc2 56.3(2) . . ?
C4 C5 Sc2 97.8(2) . . ?
C1 C5 Sc2 103.1(2) . . ?
C5 C6 C7 118.2(4) . . ?
C5 C6 C20 116.0(3) . . ?
C7 C6 C20 117.3(3) . . ?
C5 C6 Sc2 93.7(2) . . ?
C7 C6 Sc2 68.4(2) . . ?
C20 C6 Sc2 79.2(2) . . ?
C5 C6 Sc2B 90.3(5) . . ?
C7 C6 Sc2B 55.6(5) . . ?
C20 C6 Sc2B 96.0(5) . . ?
C6 C7 C8 115.8(3) . . ?
C6 C7 C23 119.6(4) . . ?
C8 C7 C23 106.8(3) . . ?
C6 C7 Sc2 75.7(2) . . ?
C8 C7 Sc2 80.9(2) . . ?
C23 C7 Sc2 71.0(2) . . ?
C6 C7 Sc2B 94.4(6) . . ?
C8 C7 Sc2B 60.2(6) . . ?
C23 C7 Sc2B 71.5(5) . . ?
C9 C8 C25 119.1(4) . . ?
C9 C8 C7 124.6(3) . . ?
C25 C8 C7 108.8(3) . . ?
C9 C8 Sc2B 93.8(6) . . ?
C25 C8 Sc2B 64.5(7) . . ?
C7 C8 Sc2B 82.4(7) . . ?
C9 C8 Sc2 96.0(2) . . ?
C25 C8 Sc2 81.6(2) . . ?
C7 C8 Sc2 64.1(2) . . ?
C10 C9 C8 117.6(4) . . ?
C10 C9 C1 121.8(3) . . ?
C8 C9 C1 118.8(3) . . ?
C10 C9 Sc2B 90.4(6) . . ?
C8 C9 Sc2B 52.7(5) . . ?
C1 C9 Sc2B 113.1(6) . . ?
C9 C10 C27 122.9(4) . . ?
C9 C10 C11 121.2(4) . . ?
C27 C10 C11 107.9(3) . . ?
C12 C11 C29 123.4(4) . . ?
C12 C11 C10 121.2(3) . . ?
C29 C11 C10 107.0(3) . . ?
C12 C11 Sc1B 62.9(5) . . ?
C29 C11 Sc1B 76.6(5) . . ?
C10 C11 Sc1B 107.1(5) . . ?
C11 C12 C13 117.2(4) . . ?
C11 C12 C2 122.0(3) . . ?
C13 C12 C2 118.9(4) . . ?
C11 C12 Sc1B 88.1(6) . . ?
C13 C12 Sc1B 57.5(5) . . ?
C2 C12 Sc1B 110.4(6) . . ?
C12 C13 C31 119.6(4) . . ?
C12 C13 C14 124.7(4) . . ?
C31 C13 C14 107.9(4) . . ?
C12 C13 Sc1B 88.4(7) . . ?
C31 C13 Sc1B 67.4(7) . . ?
C14 C13 Sc1B 84.9(7) . . ?
C12 C13 Sc1 95.3(2) . . ?
C31 C13 Sc1 81.6(2) . . ?
C14 C13 Sc1 64.27(19) . . ?
C13 C14 C15 115.4(3) . . ?
C13 C14 C33 106.2(4) . . ?
C15 C14 C33 120.0(4) . . ?
C13 C14 Sc1 80.2(2) . . ?
C15 C14 Sc1 74.7(2) . . ?
C33 C14 Sc1 71.98(19) . . ?
C13 C14 Sc1B 59.3(6) . . ?
C15 C14 Sc1B 90.6(6) . . ?
C33 C14 Sc1B 75.2(6) . . ?
C3 C15 C16 116.3(3) . . ?
C3 C15 C14 117.9(4) . . ?
C16 C15 C14 116.6(4) . . ?
C3 C15 Sc1 91.8(2) . . ?
C16 C15 Sc1 79.4(2) . . ?
C14 C15 Sc1 68.5(2) . . ?
C3 C15 Sc1B 85.4(5) . . ?
C16 C15 Sc1B 95.9(5) . . ?
C14 C15 Sc1B 59.2(5) . . ?
C35 C16 C17 108.1(3) . . ?
C35 C16 C15 122.8(4) . . ?
C17 C16 C15 120.9(3) . . ?
C35 C16 Sc1 76.8(2) . . ?
C17 C16 Sc1 102.3(2) . . ?
C15 C16 Sc1 66.2(2) . . ?
C18 C17 C16 122.4(4) . . ?
C18 C17 C37 120.7(4) . . ?
```

```
C16 C17 C37 107.7(3) . . ?
C17 C18 C19 119.8(4) . . ?
C17 C18 C4 116.5(3) . . ?
C19 C18 C4 116.3(4) . . ?
C18 C19 C20 121.7(4) . . ?
C18 C19 C39 119.8(4) . . ?
C20 C19 C39 109.0(3) . . ?
C21 C20 C19 107.6(4) . . ?
C21 C20 C6 122.3(4) . . ?
C19 C20 C6 122.1(3) . . ?
C21 C20 Sc2 75.9(2) . . ?
C19 C20 Sc2 102.8(2) . . ?
C6 C20 Sc2 66.7(2) . . ?
C20 C21 C22 121.2(4) . . ?
C20 C21 C40 108.2(4) . . ?
C22 C21 C40 122.5(4) . . ?
C20 C21 Sc2 71.7(2) . . ?
C22 C21 Sc2 68.5(2) . . ?
C40 C21 Sc2 104.8(2) . . ?
C53 C22 C21 115.4(4) . . ?
C53 C22 C23 118.7(4) . . ?
C21 C22 C23 117.1(4) . . ?
C53 C22 Sc2 97.0(2) . . ?
C21 C22 Sc2 78.5(2) . . ?
C23 C22 Sc2 65.5(2) . . ?
C22 C23 C24 117.7(4) . . ?
C22 C23 C7 122.0(4) . . ?
C24 C23 C7 107.2(4) . . ?
C22 C23 Sc2 79.5(2) . . ?
C24 C23 Sc2 83.3(2) . . ?
C7 C23 Sc2 71.0(2) . . ?
C22 C23 Sc2B 97.8(7) . . ?
C24 C23 Sc2B 62.2(6) . . ?
C7 C23 Sc2B 72.1(6) . . ?
C25 C24 C23 109.3(4) . . ?
C25 C24 C55 119.5(4) . . ?
C23 C24 C55 123.8(4) . . ?
C25 C24 Sc2B 63.4(7) . . ?
C23 C24 Sc2B 80.8(7) . . ?
C55 C24 Sc2B 96.8(7) . . ?
C25 C24 Sc2 80.0(2) . . ?
C23 C24 Sc2 62.5(2) . . ?
C55 C24 Sc2 99.2(2) . . ?
C26 C25 C24 123.3(4) . . ?
C26 C25 C8 122.3(4) . . ?
C24 C25 C8 107.7(4) . . ?
C26 C25 Sc2B 93.5(7) . . ?
C24 C25 Sc2B 75.6(7) . . ?
C8 C25 Sc2B 73.5(7) . . ?
C26 C25 Sc2 107.4(3) . . ?
C24 C25 Sc2 68.4(2) . . ?
C8 C25 Sc2 66.3(2) . . ?
C25 C26 C27 117.9(4) . . ?
C25 C26 C57 116.9(4) . . ?
C27 C26 C57 118.0(4) . . ?
C25 C26 Sc2B 52.0(6) . . ?
C27 C26 Sc2B 94.5(5) . . ?
C57 C26 Sc2B 97.2(6) . . ?
C26 C27 C28 122.4(4) . . ?
C26 C27 C10 120.0(4) . . ?
C28 C27 C10 107.2(4) . . ?
C27 C28 C59 120.0(4) . . ?
C27 C28 C29 109.6(4) . . ?
C59 C28 C29 120.3(4) . . ?
C30 C29 C28 122.4(4) . . ?
C30 C29 C11 119.8(4) . . ?
C28 C29 C11 108.3(4) . . ?
C29 C30 C31 118.0(4) . . ?
C29 C30 C41 117.3(4) . . ?
C31 C30 C41 117.1(4) . . ?
C29 C30 Sc1B 89.8(6) . . ?
C31 C30 Sc1B 55.3(5) . . ?
C41 C30 Sc1B 98.0(6) . . ?
C30 C31 C32 122.8(4) . . ?
C30 C31 C13 121.8(4) . . ?
C32 C31 C13 109.0(4) . . ?
C30 C31 Sc1B 90.6(7) . . ?
C32 C31 Sc1B 80.7(7) . . ?
C13 C31 Sc1B 72.4(7) . . ?
C30 C31 Sc1 107.5(2) . . ?
C32 C31 Sc1 69.6(2) . . ?
C13 C31 Sc1 66.0(2) . . ?
C31 C32 C33 108.5(4) . . ?
C31 C32 C43 120.5(4) . . ?
C33 C32 C43 123.8(4) . . ?
C31 C32 Sc1B 62.0(6) . . ?
C33 C32 Sc1B 81.8(7) . . ?
C43 C32 Sc1B 97.5(6) . . ?
C31 C32 Sc1 78.9(2) . . ?
C33 C32 Sc1 62.73(19) . . ?
C43 C32 Sc1 100.3(2) . . ?
C32 C33 C34 116.5(4) . . ?
C32 C33 C14 108.2(4) . . ?
C34 C33 C14 121.5(4) . . ?
C32 C33 Sc1 83.4(2) . . ?
C34 C33 Sc1 79.4(2) . . ?
C14 C33 Sc1 70.00(19) . . ?
C32 C33 Sc1B 64.3(6) . . ?
C34 C33 Sc1B 96.5(6) . . ?
C14 C33 Sc1B 70.5(5) . . ?
C45 C34 C33 119.8(4) . . ?
C45 C34 C35 115.2(4) . . ?
C33 C34 C35 117.3(4) . . ?
C45 C34 Sc1 99.3(2) . . ?
C33 C34 Sc1 65.6(2) . . ?
C35 C34 Sc1 78.4(2) . . ?
C16 C35 C36 108.1(4) . . ?
C16 C35 C34 121.3(4) . . ?
C36 C35 C34 122.1(4) . . ?
C16 C35 Sc1 70.8(2) . . ?
```

```
C36 C35 Sc1 105.0(2) . . ?
C34 C35 Sc1 68.7(2) . . ?
C37 C36 C47 120.7(4) . . ?
C37 C36 C35 108.3(4) . . ?
C47 C36 C35 121.5(4) . . ?
C38 C37 C36 121.6(4) . . ?
C38 C37 C17 119.8(4) . . ?
C36 C37 C17 107.7(4) . . ?
C49 C38 C39 118.0(4) . . ?
C49 C38 C37 117.2(4) . . ?
C39 C38 C37 118.7(4) . . ?
C38 C39 C40 122.6(4) . . ?
C38 C39 C19 120.7(4) . . ?
C40 C39 C19 106.1(4) . . ?
C39 C40 C21 109.2(4) . . ?
C39 C40 C51 119.6(4) . . ?
C21 C40 C51 121.0(4) . . ?
C60 C41 C42 110.0(4) . . ?
C60 C41 C30 119.7(4) . . ?
C42 C41 C30 119.9(4) . . ?
C43 C42 C62 120.1(4) . . ?
C43 C42 C41 122.8(4) . . ?
C62 C42 C41 107.1(4) . . ?
C44 C43 C42 118.9(4) . . ?
C44 C43 C32 116.9(4) . . ?
C42 C43 C32 116.6(4) . . ?
C43 C44 C45 121.2(4) . . ?
C43 C44 C64 120.7(4) . . ?
C45 C44 C64 107.9(4) . . ?
C44 C45 C34 121.0(4) . . ?
C44 C45 C46 108.3(4) . . ?
C34 C45 C46 122.5(4) . . ?
C47 C46 C65 119.6(4) . . ?
C47 C46 C45 122.4(4) . . ?
C65 C46 C45 108.0(4) . . ?
C46 C47 C48 119.5(4) . . ?
C46 C47 C36 116.1(4) . . ?
C48 C47 C36 117.0(4) . . ?
C49 C48 C47 121.9(4) . . ?
C49 C48 C67 107.9(4) . . ?
C47 C48 C67 120.3(4) . . ?
C49 C48 Sc3B 82.8(5) . . ?
C47 C48 Sc3B 93.8(5) . . ?
C67 C48 Sc3B 60.3(5) . . ?
C38 C49 C48 121.3(4) . . ?
C38 C49 C50 119.7(4) . . ?
C48 C49 C50 109.4(4) . . ?
C38 C49 Sc3B 102.2(5) . . ?
C48 C49 Sc3B 65.8(5) . . ?
C50 C49 Sc3B 69.9(5) . . ?
C51 C50 C49 123.0(4) . . ?
C51 C50 C68 120.3(4) . . ?
C49 C50 C68 106.4(4) . . ?
C51 C50 Sc3B 97.5(5) . . ?
C49 C50 Sc3B 78.7(5) . . ?
C68 C50 Sc3B 59.5(5) . . ?
C52 C51 C50 119.4(4) . . ?
C52 C51 C40 117.0(4) . . ?
C50 C51 C40 116.8(4) . . ?
C51 C52 C53 121.6(4) . . ?
C51 C52 C70 120.6(4) . . ?
C53 C52 C70 107.8(4) . . ?
C22 C53 C52 122.3(4) . . ?
C22 C53 C54 121.7(4) . . ?
C52 C53 C54 108.4(4) . . ?
C55 C54 C53 121.8(4) . . ?
C55 C54 C71 120.5(4) . . ?
C53 C54 C71 107.8(4) . . ?
C54 C55 C56 119.9(4) . . ?
C54 C55 C24 115.8(4) . . ?
C56 C55 C24 116.8(4) . . ?
C54 C55 Sc2B 99.7(6) . . ?
C56 C55 Sc2B 91.7(6) . . ?
C24 C55 Sc2B 51.0(5) . . ?
C55 C56 C57 122.6(4) . . ?
C55 C56 C73 119.1(4) . . ?
C57 C56 C73 107.7(4) . . ?
C58 C57 C56 108.9(4) . . ?
C58 C57 C26 119.3(4) . . ?
C56 C57 C26 120.7(4) . . ?
C57 C58 C59 122.3(4) . . ?
C57 C58 C74 107.7(4) . . ?
C59 C58 C74 119.9(4) . . ?
C60 C59 C58 118.6(4) . . ?
C60 C59 C28 117.3(4) . . ?
C58 C59 C28 117.4(4) . . ?
C59 C60 C41 122.7(4) . . ?
C59 C60 C61 120.5(4) . . ?
C41 C60 C61 107.3(4) . . ?
C75 C61 C62 123.4(4) . . ?
C75 C61 C60 122.3(4) . . ?
C62 C61 C60 106.4(3) . . ?
C75 C61 Sc3 64.0(2) . . ?
C62 C61 Sc3 79.6(2) . . ?
C60 C61 Sc3 102.8(2) . . ?
C42 C62 C63 121.5(4) . . ?
C42 C62 C61 109.1(4) . . ?
C63 C62 C61 120.6(3) . . ?
C42 C62 Sc3 106.1(2) . . ?
C63 C62 Sc3 68.7(2) . . ?
C61 C62 Sc3 69.2(2) . . ?
C64 C63 C62 117.6(4) . . ?
C64 C63 C77 118.2(4) . . ?
C62 C63 C77 116.4(4) . . ?
C64 C63 Sc3 100.4(2) . . ?
C62 C63 Sc3 80.5(2) . . ?
C77 C63 Sc3 61.9(2) . . ?
C63 C64 C65 123.0(3) . . ?
C63 C64 C44 121.0(4) . . ?
C65 C64 C44 107.6(4) . . ?
```

```
C66 C65 C64 119.9(4) . . ?
C66 C65 C46 121.2(4) . . ?
C64 C65 C46 108.2(4) . . ?
C67 C66 C65 118.4(4) . . ?
C67 C66 C78 118.0(4) . . ?
C65 C66 C78 116.8(4) . . ?
C67 C66 Sc3B 64.4(6) . . ?
C65 C66 Sc3B 96.4(6) . . ?
C78 C66 Sc3B 84.0(6) . . ?
C66 C67 C68 121.2(4) . . ?
C66 C67 C48 120.5(4) . . ?
C68 C67 C48 107.8(4) . . ?
C66 C67 Sc3B 79.6(6) . . ?
C68 C67 Sc3B 73.7(6) . . ?
C48 C67 Sc3B 84.4(6) . . ?
C69 C68 C67 121.7(4) . . ?
C69 C68 C50 119.8(4) . . ?
C67 C68 C50 108.4(4) . . ?
C69 C68 Sc3B 83.1(6) . . ?
C67 C68 Sc3B 68.5(6) . . ?
C50 C68 Sc3B 86.3(6) . . ?
C68 C69 C70 119.6(4) . . ?
C68 C69 C79 117.6(3) . . ?
C70 C69 C79 115.5(4) . . ?
C68 C69 Sc3B 62.9(5) . . ?
C70 C69 Sc3B 100.6(6) . . ?
C79 C69 Sc3B 81.0(5) . . ?
C71 C70 C69 121.5(4) . . ?
C71 C70 C52 107.9(4) . . ?
C69 C70 C52 120.1(4) . . ?
C72 C71 C70 122.1(4) . . ?
C72 C71 C54 120.0(4) . . ?
C70 C71 C54 108.1(4) . . ?
C71 C72 C73 118.8(4) . . ?
C71 C72 C80 117.7(4) . . ?
C73 C72 C80 116.5(4) . . ?
C71 C72 Sc3 103.8(2) . . ?
C73 C72 Sc3 82.3(2) . . ?
C80 C72 Sc3 58.17(19) . . ?
C72 C73 C56 121.5(4) . . ?
C72 C73 C74 120.9(4) . . ?
C56 C73 C74 108.7(4) . . ?
C75 C74 C73 123.2(4) . . ?
C75 C74 C58 122.3(4) . . ?
C73 C74 C58 106.9(4) . . ?
C75 C74 Sc3 59.2(2) . . ?
C73 C74 Sc3 85.4(2) . . ?
C58 C74 Sc3 102.7(2) . . ?
C74 C75 C61 116.2(4) . . ?
C74 C75 C76 118.2(4) . . ?
C61 C75 C76 116.8(4) . . ?
C74 C75 Sc3 89.9(3) . . ?
C61 C75 Sc3 83.6(2) . . ?
C76 C75 Sc3 67.0(2) . . ?
C77 C76 C75 119.6(3) . . ?
C77 C76 C80 106.5(3) . . ?
C75 C76 C80 117.0(4) . . ?
C77 C76 Sc3 73.8(2) . . ?
C75 C76 Sc3 76.4(2) . . ?
C80 C76 Sc3 78.2(2) . . ?
C78 C77 C63 117.6(3) . . ?
C78 C77 C76 108.4(3) . . ?
C63 C77 C76 122.8(4) . . ?
C78 C77 Sc3 82.8(2) . . ?
C63 C77 Sc3 84.5(2) . . ?
C76 C77 Sc3 69.0(2) . . ?
C66 C78 C79 120.5(4) . . ?
C66 C78 C77 123.9(3) . . ?
C79 C78 C77 108.5(3) . . ?
C66 C78 Sc3 101.6(2) . . ?
C79 C78 Sc3 76.6(2) . . ?
C77 C78 Sc3 63.5(2) . . ?
C66 C78 Sc3B 63.3(5) . . ?
C79 C78 Sc3B 76.0(5) . . ?
C77 C78 Sc3B 107.9(5) . . ?
C80 C79 C78 108.5(3) . . ?
C80 C79 C69 123.9(4) . . ?
C78 C79 C69 120.9(4) . . ?
C80 C79 Sc3 65.65(19) . . ?
C78 C79 Sc3 71.3(2) . . ?
C69 C79 Sc3 105.4(2) . . ?
C80 C79 Sc3B 108.2(5) . . ?
C78 C79 Sc3B 72.6(5) . . ?
C69 C79 Sc3B 67.0(5) . . ?
C79 C80 C72 118.8(4) . . ?
C79 C80 C76 108.1(3) . . ?
C72 C80 C76 123.8(4) . . ?
C79 C80 Sc3 81.8(2) . . ?
C72 C80 Sc3 91.4(2) . . ?
C76 C80 Sc3 65.34(19) . . ?
C83 C81 C1 111.6(3) . . ?
C88 C82 C2 111.7(3) . . ?
C88 C83 C84 120.6(3) . . ?
C88 C83 C81 116.6(3) . . ?
C84 C83 C81 122.7(3) . . ?
C85 C84 C83 120.2(3) . . ?
O2 C85 C84 125.0(3) . . ?
O2 C85 C86 115.6(3) . . ?
C84 C85 C86 119.4(3) . . ?
O1 C86 C87 124.6(3) . . ?
O1 C86 C85 115.4(3) . . ?
C87 C86 C85 120.0(3) . . ?
C88 C87 C86 120.4(3) . . ?
C83 C88 C87 119.2(3) . . ?
C83 C88 C82 116.6(3) . . ?
C87 C88 C82 124.2(3) . . ?
C92 C91 C96 120.1(4) . . ?
C91 C92 C93 120.2(4) . . ?
C92 C93 C94 119.1(4) . . ?
C95 C94 C93 120.0(4) . . ?
```

```
C94 C95 C96 121.0(4) . . ?
C95 C96 C91 119.5(4) . . ?
C98 C97 C99 121.6(5) . . ?
C100 C98 C97 119.4(5) . . ?
C97 C99 C101 119.5(4) . . ?
C98 C100 C102 121.2(4) . . ?
C99 C101 C102 118.5(5) . . ?
C100 C102 C101 119.8(5) . . ?

_diffrn_measured_fraction_theta_
max    0.959
_diffrn_reflns_theta_full
31.51
_diffrn_measured_fraction_theta_
full   0.959
_refine_diff_density_max
0.646
_refine_diff_density_min   -
0.787
_refine_diff_density_rms
0.094

#===END
```

Appendix VI. Cover of Science News magazine (July 13, 2002)

Vita

Erick B. Iezzi was born on March 1, 1977 in Greensburg, Pennsylvania to Deborah and Donald Iezzi. In May of 1995 he graduated with honors from Jeannette Senior High School in Jeannette, Pennsylvania, then attended Duquesne University in Pittsburgh, Pennsylvania during the fall of that same year. At Duquesne, Erick performed undergraduate research with Professor Theodore J. Weismann, where he worked with YBCO superconducting ceramics. Erick obtained a Bachelor of Science degree in Chemistry and graduated Magna Cum Laude in the spring of 1999, then enrolled during the fall of 1999 at Virginia Polytechnic Institute and State University (Virginia Tech) in Blacksburg, Virginia, where he began seeking a graduate degree in chemistry. At Virginia Tech, Erick worked for Professor Harry C. Dorn in the areas of organic synthesis and nanotechnology. His research pertained specifically to exohedral functionalization and applications of the novel trimetallic nitride endohedral metallofullerenes. Erick received a Doctor of Philosophy in Chemistry in October of 2003.

Erick began a postdoctoral research position with Professor Peter Wipf at the University of Pittsburgh in Pittsburgh, Pennsylvania during the fall of 2003.